THE UNIVERSITY OF HULL

Development of a microfluidic device with a screen printed electrode for studies on phase II metabolism

being a Thesis submitted for the Degree

of Doctor of Philosophy

in the University of Hull

by

Rafaela Vasiliadou BSc (Hons), MSc

October 2015

Abstract

Simulating human metabolism by electrochemistry (EC) and mass spectrometry (MS) provides an alternative approach to the existing *in vitro* and *in vivo* methodologies. Herein, screen printed electrodes (SPEs) were investigated as potent electrochemical tools with the aim of developing a microfluidic device with a SPE. The proposed chip could be used as a primary screening tool for phase II glutathione (GSH) adducts.

The reusability of SPEs was investigated with solvent treatment, mechanical polishing, and electrochemical activation. However, damages to the three-electrode configuration and lack of reproducibility prevented the effective removal of deposited material. Thus, SPEs were used as single-shot sensors for micking phase I and phase II metabolism.

The electrochemical reactions of dopamine, raloxifene, eugenol, and doxorubicin were examined initially on a bare SPE. Similar kinetics and reaction mechanisms were obtained as in previous studies with a glassy carbon electrode, confirming that SPEs can be used as cheaper alternatives. Controlled potential electrolysis (CPE) at the optimized potential was recorded for 30 min, in the presence of GSH, and subsequent offline MS permitted the detection of the corresponding GSH adducts of dopamine and raloxifene.

Dopaminoquinone and raloxifene di-quinone methide were generated via dehydrogenation and reacted covalently with GSH. However, the GSH adducts for eugenol and doxorubicin were not formed, leading to the generation of unconjugated metabolites. For example, eugenol was electrolysed via a single electron transfer with the addition of a proton to the corresponding phenoxyl radical. However, the oxidation reaction of GSH to form glutathione disulfide (GSSG) prevented further stabilisation to eugenol quinone methide and subsequent GSH adduct formation, mimicking only the catalytic pathway and

polymerisation process. In the case of doxorubicin, the GSH adducts were probably formed at extremely low concentrations that were below the detection limits of the mass spectrometer or the expected doxorubicin semiquinone C7 free radical was generated but its trapping was unlikely, as proposed in previous *in vitro* and *in vivo* studies, owing to its quick oxidation back to the parent drug. Also, the possibility of generating non-reactive and highly unstable electrochemical products which were not capable of forming GSH adducts was considered. Thus, dopamine and raloxifene were selected for experiments in the microfluidic device. In addition, as the behaviour of acetaminophen on SPE is well-known, it was considered suitable for investigation with the proposed chip.

A polycarbonate disposable chip was developed, in which a 32 μL SPE- electrochemical cell was integrated with a serpentine channel. The chip was coupled online to an electrospray mass spectrometer for a semi-automated methodology. At an optimized flow rate of 5 μL min^{-1}, $2.5x10^{-5}$ M solutions of dopamine and acetaminophen were allowed to electrolyse for 6.4 min in the SPE cell. The electrogenerated toxic intermediates dopaminoquinone and *N*-acetyl-p-benzoquinone imine reacted covalently with $5x10^{-5}$ M GSH and the resulting adducts were detected online by MS. Raloxifene failed to generate the GSH adduct in the microfluidic device owing to the requirement for lower flow rates that were incompatible with MS. In conclusion, a disposable and cost effective microfluidic device was developed for the simulation of phase II metabolism. This microdevice has the potential to reduce the expensive and time consuming use of the current *in vitro* and *in vivo* methodologies, in pharmaceutical industry and medical research.

Acknowledgements

Firstly, I would like to thank my first supervisor Dr Kevin Welham for his support, help and continuous guidance during my doctoral studies. Also, I would like to express my appreciation to my second supervisor Dr Jay Wadhawan.

I am very grateful to Dr Mohammad-Mehdi Nasr Esfahani for his expert advice and help in microfluidics, patience, support and encouragement.

Many thanks to the analytical research group and mass spectrometry lab (C006) at the University of Hull for their help. I am blessed to have friends and colleagues, like Nadia, Dalila, Pai and Khadijiah who encouraged me in my studies.

Last but not the least, I would like to thank my parents Antreas and Androulla for providing me financial and emotional support. I thank my grandfather Christos for funding my studies and for giving me valuable advice. I am also grateful to Geronta Athanasio, Geronta Nikodemo, Geronta Anthimo, Gerontisa Efraimia, Chrystala and Kaliopi for their continuous support, until the last minute of my doctoral studies.

This thesis is dedicated to my wonderful mother, who has always been next to me through this journey, giving me support, encouragement, help, and inspiration. Also, I would like to thank her for her great patience through the hard times. Without her, I would never have made it.

Table of contents

Abbreviations

ADE……..Adenine

AcCoA…….Acetyl coenzyme A

APAP……..Acetaminophen

Aux.....Auxiliary electrode

BAC.....Bacterial artificial chromosome

cDNA.....Complementary DNA

CPE……...Controlled potential electrolysis

cm.....Centi meter

CV…….……Cyclic voltammetry

CYP ……..…...Cytochrome

DT.....Di or triphosphopyridine nucleotide

DOPA…….Dopamine

DOXO…….……Doxorubicin

DPV……..…Differential pulse voltammetry

EC…….……Electrochemistry

EC′……..……Electrochemical step-catalytic reaction

ECE……..….Electrochemical step-chemical step-electrochemical step

ESI……..Electrospray ionization

GBP.....Great Britain pounds

GUA……Guanine

GSH…….……....Glutathione

GST……..Glutathione sulphur transferases

GSSG…….…….Glutathione disulfide

h.....Hour

HS-CoA…….Co enzyme A

IHP…….Inner Helmholtz plane

Intens……Intensity

LC……..….Liquid chromatography

m.....Meter

mA……miliAmpere

micro TAS..... micro Total Analysis

min.....Minute

MS……Mass spectrometry

m / z……...….....Mass – to- charge ratio

N-0923…….……Dopamine agonist

NADPH……..…Nicotinamide Adenine Dinucleotide Hydrogen

NAT…… Acetyl CoA-dependent *N*-acetyltransferases

ND: YAG…….……Neodymium-doped yttrium aluminium garnet

Pd/H_2……..…Palladium/hydrogen

pH.....Potential of hydrogen

R.....Resistor

Rbrush……..Rough brush

Ref.....Reference electrode

RF……..……Radio frequency

RLM……..Rat liver mitochondria

RLX…….Raloxifene

rpm.....Revolutions per minute

RSD…….…..Relative standard deviation

s……Second

Sbrush……...Soft brush

SERM……. Selective estrogen receptor modulator

SPEs……...……..Screen printed electrodes

SQRT…….square root

S9.....Product of organ tissue

TCC……Triclocarban

UGTs ……..Uridine diphosphate glucuronosyltransferases

UV-Vis.....UltraViolet-Visible

V……..Volts

Chapter 1: Introduction

1.0 Metabolism

Metabolism is a physiological process that occurs mainly within the liver, in slightly alkaline conditions (pH 7.4).[1-3] During this process, exogenous and endogenous compounds (Figure 1.1) undergo biochemical modifications and metabolites are formed[4] which are eventually eliminated from the body as urine or via bile, sweat, saliva, air, or faeces.[5, 6] The aim of metabolism is to generate more hydrophilic compounds for excretion[7]. Usually, drugs are less active after the metabolic process and their therapeutic action decreases considerably. However, this is not always the case; sometimes, the metabolites can be more active than the parent drug and the therapeutic action is initiated by the metabolites,[8, 9] for example, prodrugs.

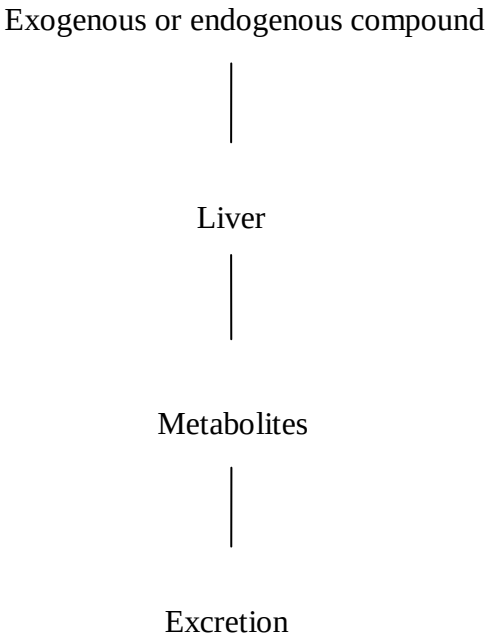

Figure 1.1 Metabolism of exogenous or endogenous compounds.

1.1 Phase I and phase II metabolic reactionns

Drugs are metabolised by phase I (functionalization) and phase II (conjugation) metabolic reactions. Phase I reactions such as oxidations, reductions, and isomerization, transform lipid-soluble drugs into water-soluble substances by incorporating polar moieties into their structures. Conjugating groups are then added to the already formed phase I metabolites, generating, in this way, adducts that are easily eliminated from the body. Examples of phase II reactions include GSH conjugation, glucuronidation, and acetylation.[10]

1.1.1 Phase I reactions

Phase I reactions are catalyzed mainly by CYP 450 enzymes, a large family of monooxygenases located in the liver. The active site is an iron-containing protoporphyrin moiety with a cysteine group and an active binding site, in its sixth coordination site.[11, 12] The catalytic cycle of CYP 450 involves a series of events that eventually lead to the formation of an oxidised product, described briefly[12-15] in (Equation 1.1). As shown in (Figure 1.2), initially, the substrate (RH) binds to the oxidised form of iron (Fe^{III}), and then the ferrous state is reduced by CYP450 reductases into Fe^{II}. Afterwards, molecular oxygen is added to the complex, which is reduced in the next stage to oxygen anion (O_2^{2-}) by cytochrome b or P450-reductases. Subsequently, two protons are gained from the surrounding environment followed by the actual oxidation of the substrate. Finally, a hydrolysis step releases the oxidised product and iron returns to its initial state (Fe^{III}). Phase I oxidations are divided into aromatic hydroxylations, heteroatom oxidations, heteroatom dealkylations, and dehydrogenations.[16]

$$\mathbf{R\text{-}H + O_2 + H^+ + NADPH \longrightarrow R\text{-}OH + H_2O + NADP} \qquad \textbf{(Equation 1.1)}^{11}$$

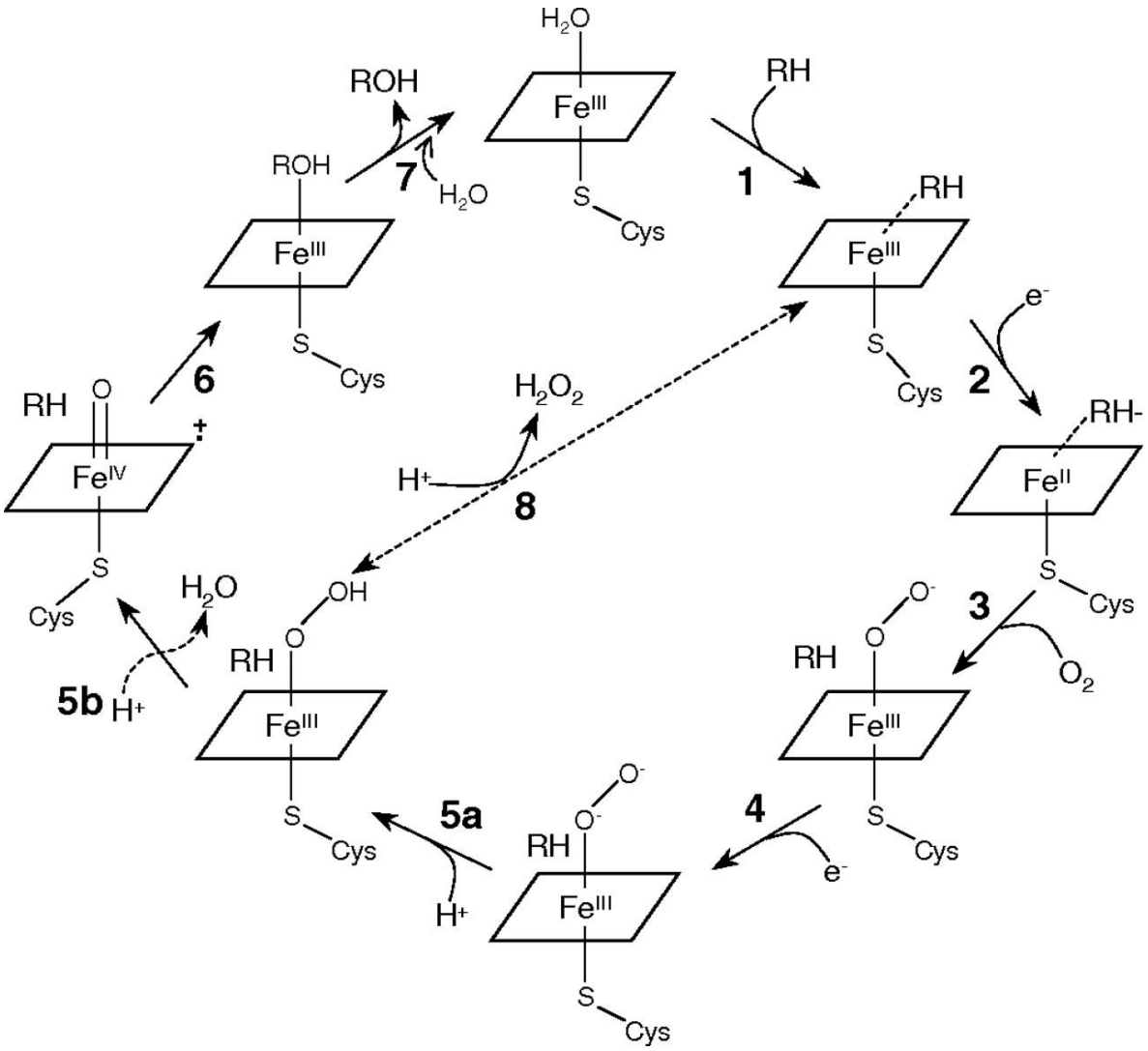

Figure 1.2 Catalytic cycle of CYP 450, reprinted with permission from Shebley *et al.*[15] 1) Substrate binding, 2) Reduction, 3) Oxygen addition, 4) Second electron reduction, 5) Protonation 6) Oxidation and 7) Product release 8) Peroxide shunt.

Rarely, reduction reactions can be catalyzed by CYP 450, the reduction process is described in (Equation 1.2). Potential targets (S=X) for reduction involve quinones, azo-, halogenated, nitro-, *N*-hydroxy-, and hydroperoxide moieties.[17] Peroxidases can also lead to reductive actiovation; however, ongoing research is focused on the catalytic action of CYP 450. In Particular, peroxidases are haeme-containing enzymes like CYP 450 and are composed of four nitrogen pyrroles that are bound to Fe^{III}. Their catalytic action is mediated through the transfer of a single electron using hydrogen peroxidase.[18]

$$\mathbf{S{=}X + NADPH + H^{+} \longrightarrow S{-}H + X{-}H + NADP^{+}} \qquad \textbf{(Equation 1.2)}^{17}$$

1.1.2 Phase II Reactions

Phase II reactions are catalyzed by a wide range of enzymes such as Glutahtiones-S-transferases (GSTs), Uridine diphosphate glucuronosyltransferases (UGTs), and acetyl transferases.[19] Each enzyme transfers a particular conjugating group into a phase I metabolite for adduct formation. For instance, GSTs aid the addition of glutathione (GSH) molecules, UGTs, the transfer of a glucuronide moiety, and acetyltransferases, the addition of an acetyl group.

1.1.2.1 GSH Conjugation

GSTs are an important class of phase II metabolising enzymes, located in subcellular compartments such as the cytosol, endoplasmic reticulum, mitochondria, plasma membrane, and nucleus.[19, 20] GSTs are capable of generating excretion products[21] and protecting the organism from reactive metabolites, through their catalytic behaviour.[22] In particular, GSTs catalyze the covalent binding of phase I electrophilic intermediates with endogenous reduced GSH,[23] a tripeptide composed of cysteine, glutamate, and glycine.[24] The conjugation reaction occurs on the thiol group of the cysteine amino acid via nucleophilic substitution (Scheme 1.1). Consequently, a thioether bond is formed, generating, in this way, a GSH adduct.[25-27]

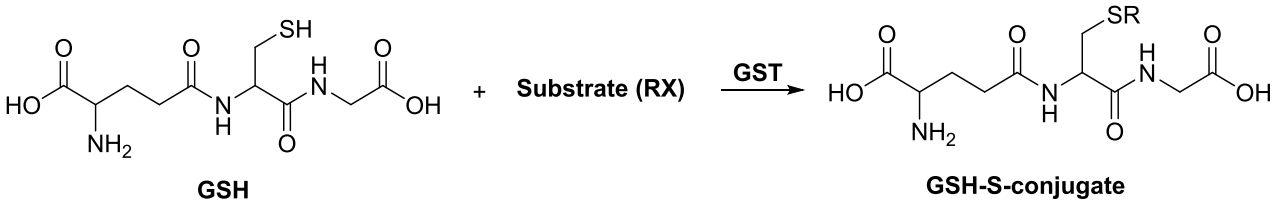

Scheme 1.1 GSH conjugation.[23] GST mediate the transfer of GSH on the substrate (RX) leading to GSH-S-conjugate formation.

1.1.2.2 Glucuronidation

UGTs are membrane-bound enzymes, found in the endoplasmic reticulum and nuclear envelope. The particular phase II enzymes, initiate the transfer of the cofactor uridine di phosphate-glucuronic acid into endogenous or exogenous compounds. [28] The reaction is initiated between a nucleophile-containing substrate with uridine diphospho-glucuronic,[23] resulting in a carbon configuration and the conversion of α glucuronic acid into β-glucuronide (Scheme 1.2). Depending on the substrate, different types of glucuronide adducts can be formed, for example, nucleophile atoms such as nitrogen, sulphur, carbon anion, or oxygen, generate N-glucuronides, S-glucuronides, C-glucuronides and O-glucuronides, respectively. On the other hand, nucleophiles that contains a hydroxyl moiety such as phenols, carboxylic acids and alcohols, from ether glucuronides since an ether bond is formed between the nucleophile and cofactor.[29]

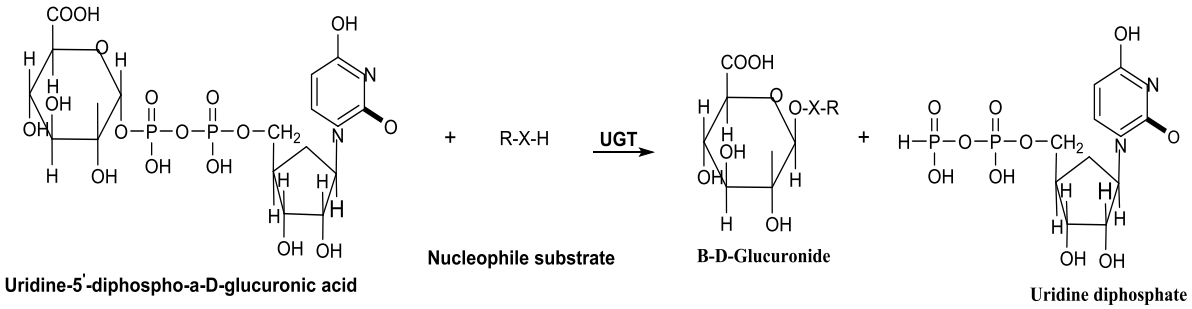

Scheme 1.2 Glucuronidation.[23] UGTs catalyze the transfer of cofactor uridine diphospho-glucuronic acid on the nucleopnile substrate.

1.1.2.3 Acetylation

Acetyltransferases are found in the cytosol[30] and their involvement in endogenous metabolism is still unclear. However, in terms of xenobiotic metabolism, they mediate a detoxification process like GSH conjugation, by the transfer of an acetyl group on electrophilic reactive intermediates.[31] Acetylation is a two-step ping-pong mechanism,[23, 32, 33, 34] involving, initially, the transfer of an acetyl moiety from acetyl co-enzyme A into the active cysteine moiety of the acetyltransferases, resulting in the formation of an acetyl enzyme intermediate. Subsequently, the conjugating group is transferred from the enzyme into the substrate (Scheme 1.3) causing the formation of an acetyl adduct. Potent substrates for N-acetylation are aromatic amines and hydrazines[35].

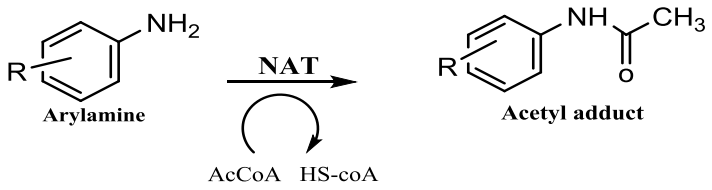

Scheme1.3 Acetylation.[23] A two step ping-pong mechanism, in which the acetyl moiety is transferred initially from co-enzyme A and then from acetyl transferases into the subtrate.

1.2 Reactive metabolites

Although metabolism is generally beneficial for humans since it allows exogenous and endogenous compounds to be eliminated from the body, reactive metabolites can be formed causing toxicity via macromolecule interactions.[36, 37] The majority of reactive metabolites are generated during phase I reactions,[38] but some types of phase II intermediates are also capable of inducing toxicity.[39]

Phase I metabolites are usually unstable and highly reactive[38] with short half-lives.[40] Reactive metabolites are classified into electrophiles and free radicals,[41] with the former further subdivided into soft and hard electrophiles,[42] as shown in (Figure 1.3).

In particular, soft electrophiles are large uncharged or partially positively charged molecules with low electrophilicity.[41-43] Characteristic examples involve quinones, quinone methides, quinone imines, epoxides, imine methides, α,β-unsaturated carbonyls, isocyanate, isothiocyanates, aziridinium, and episulfonium ions.[41, 44, 45] Soft nucleophiles such as RSH, GSH, RS^-, I^-, RSe^-, and alkenes have a high degree of polarizability and, as a consequence, react via orbital interactions with soft electrophilic macromolecules and induce toxicity via the formation of covalent adducts.[41, 43, 46]

On the other hand, hard electrophiles such as alkyl carbocation, carbonyl carbocation, and nitrenium ion are small, charged molecules with high electrophilicity that interact with hard nucleophiles such as R-NH_2, R-OH, RO^-, SO_4^{2-}, Cl^-, mainly by electrostatic interactions.[41, 46] The second classification, the free radicals have an unpaired electron capable of inducing toxicity via hydrogen abstraction or interaction with other free radicals.[41, 47] Oxygen free radicals are highly reactive and frequently obtained in metabolism studies, categorised broadly as reactive oxygen species (ROS).[48]

In general, phase II metabolism is considered a safe detoxification process; however, toxic adducts can still be formed, as an exception to the general rule. In particular, carboxylic compounds are capable of forming reactive acyl glucuronides.[49] The mechanism involves the formation of a glycosidic bond via carboxylic deprotonation between the substrate and glucuronic acid, catalyzed by the action of UGTs. Subsequently, acyl glucuronides react with nucleophilic sites on cellular proteins by transacylation, where the glucuronic group is

released, and the remaining structure is composed only of the electrophilic moiety. Acyl glucuronides can also be formed by glaciations involving the migration of acyl groups. Also, acyl thioester contains an electrophilic carbon that leads to nucleophilic acyl substitution with macromolecules.[49, 50]

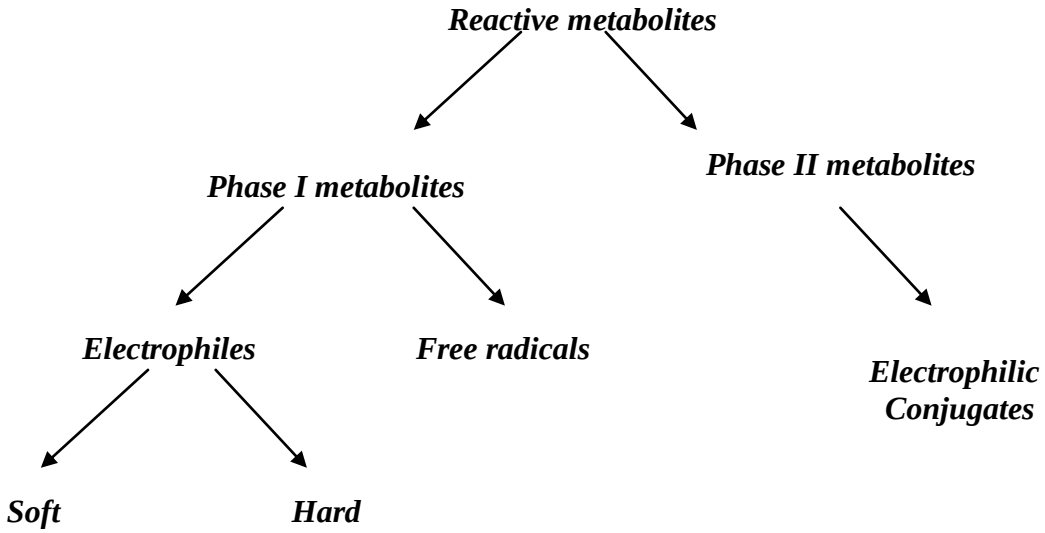

Figure 1.3 Classification of reactive metabolites.[41, 42]

1.3 Mechanism of toxicity with macromolecules

Electrophilic intermediates modify proteins through covalent binding with the lone pair of electrons on nitrogen and sulphur atoms within amino acids.[41, 43] As a consequence, the metabolite-protein adducts lead to toxicity via two mechanisms: 1) direct mechanism and 2) immune response.[51] The first mechanism affects the majority of the population and is associated with changes in the tertiary structure, gene expression, alterations in protein function, and enzyme inactivation. In the second mechanism, an immune response is

triggered since the modified proteins are now recognised as foreign compounds, leading to hypersensitivity reactions and generation of immune complexes. This particular mechanism is unpredictable using *in vivo* models and affects a small group of the population; it is also known as an idiosyncratic reaction.

Moreover, nucleic acids also have nucleophilic sites available for covalent bonding similar to proteins; this facilitates the alteration of the DNA structure, in particular, the purine and pyrimidine bases.[41, 51, 52] Additional damage involves the breaking of the double helix through the loss of bases or even unfolding of the DNA strand, consequently causing mutagenicity, carcinogenicity, and teratogenicity.

In general, free radicals have affinity for nucleophilic compounds and, specifically, carbon free radicals are capable of binding covalently with proteins, thereby altering their biological function. In addition, free radical metabolites can bind to DNA and cause damage to nucleobases.[53]

1.4 Natural detoxification

In normal conditions, reactive intermediates such as electrophiles are trapped during phase II reactions, mainly by endogenous GSH and detoxified by the mechanism previously described in section 1.1.2.1[54] However, GSH detoxification pathway is saturable and in cases of overdose, the GSH levels are depleted; therefore, reactive metabolites can react freely with macromolecules and induce toxicity.[51] Free radicals are also detoxified by GSH through covalent bonding.[55]

1.5 *In vitro* and *in vivo* studies

In order to identify reactive drug metabolites, pharmaceutical companies conduct several *in vitro* and *in vivo* studies (Figure 1.4) to exclude potential drug candidates, at the earliest opportunity.[56-58] Each year, billions of dollars are spent on these studies, reflecting their significance in drug development.[59] Endogenous metabolism is also investigated in clinical research using the same methodologies.[60, 61]

Figure 1.4 *In vitro* and *in vivo* metabolism.

1.5.1 *In vitro* studies

In vitro models are used prior to *in vivo* models in order to choose the most appropriate animals; usually, this is achieved by comparing human and animal *in vitro* models.[62] However, in vitro studies are characterised by expensive and tedious processes, implying the need of more affordable screening metbods .Herein, the main *in vitro* techniques are described.

1.5.1.1 Cellular organelles

Cellular organelles such as the hepatocytes contain all the necessary enzymes and cofactors at physiological levels and thus can successfully mimic the human organism.[62] However, hepatocyte preparations are limited to one use, have replicability problems, and cannot be obtained from higher animals or humans.[63]

1.5.1.2 Subcellular fractions

Microsomes are subcellular fractions from either liver or gut tissues.[63] They are readily available from humans, affordable and easy to handle; however, the available enzymes are limited to CYP and glucuronyl transferases. On the other hand, S9 fractions are composed of both cytosol and microsomes, so all the metabolising enzymes are present. A major limitation, in this case, is the lower enzyme activity that can hide the appearance of some intermediates.[64]

1.5.1.3 Recombinant CYP 450 enzymes

The process of creating recombinant enzymes involves the incorporation of human cDNA of a known sequence into a host like *E. coli* or yeast.[65, 66] The main advantages include simplicity of use and specificity since the metabolic activity of a particular isoform of CYP 450 can be determined. However, recombinant enzymes are expressed in different concentrations, as in the human liver microsomes, so all enzymes do not present the same native conditions.[67]

1.5.1.4 Metalloporphyrins

Synthetic metalloporphyrins are structural analogs of haeme,[68] with a catalytic role in the mimicry of oxidative metabolism.[69] An appropriate single oxygen donor such as peroxidase is added to initiate a binding with the corresponding metalloporphyrins. As a result, an oxoferryl-porphyrin-like radical is formed, as in human metabolism, that permits the binding to molecular oxygen.[70] The particular synthetic method generates relatively pure metabolites at a high yield,[71] but poor regioselectivity is obtained with hydroxylated metabolites.[12]

1.5.1.5 Fenton reaction

A Fenton reagent is a mixture containing ferrous salt and hydrogen peroxide. The oxidative metabolism is initiated through the transfer of an electron from the ferrous iron into hydrogen peroxide, causing the oxidation of ferrous iron to ferric iron and the reduction of oxygen to hydroxyl ion and hydroxyl radical release (Scheme 1.4). The oxidation reactions are initiated through the electrophilic action of hydroxyl radical with various substrates.[72] Fenton reactions are still in the primary stages of investigation; thus, further studies are required for a complete view.[12]

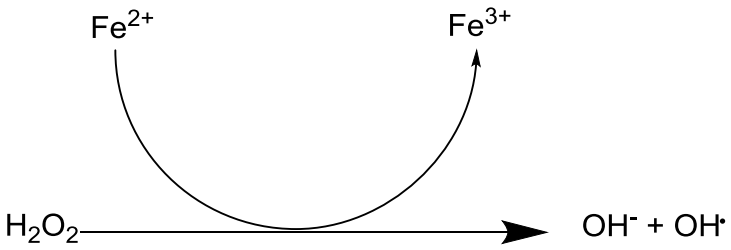

Scheme 1.4 Fenton reaction.[72] One electron is transferred from ferrous iron causing the reduction of oxygen to hydroxyl ion and hydroxyl radical release.

1.5.2 In vivo studies

Over the years, several animals have been used to provide a model for simulating human metabolic process.[73] However, ethical issues and the long duration reguired for complete metabolic profile empasized the need of an alternative system for tracking metabolism. Herein, the major animal models are discussed.

1.5.2.1 Small animals and humanised mouse models

Small animals such as rats, mice, guinea pigs, rabbits, and dogs are frequently used in animal models; however, the differences in expression and catalytic activity of CYP 450 in between different species and humans lead to poor conclusions.[73, 74] A more reliable *in vivo* animal model, known as a humanized mouse model, was developed. It involves the transfer of human genes or cDNA into mice.[75, 76] Several models were proposed involving the transplantation in human hepatocytes, [77] human receptor cDNA,[78, 79] peroxisome proliferator cDNA,[80] human BAC, and CYP 450 isomers.[81, 82] The major disadvantages of this model are long duration of time required for the generation of transgenic mice and the extremely high costs.[83]

1.5.2.2 Non-human primates

Non-human primates such as monkeys are physiologically and genetically closer to humans, and thus models using such animals provide more reliable results.[74] In addition, the gray mouse lemur (*Microcebus murinus*), a small primate, is also capable of generating successful metabolic profiles. The major limitation of using the particular species (gray mouse lemur) are the seasonal changes in their body weight that require continuous monitoring throughout the metabolism research, making the process time consuming and tedious.[84]

1.6 Electrochemical simulation

An alternative to the *in vitro* approach, in addition to the existing methodologies, is the coupling of EC with MS, which provides a pure instrumental method, with a potential to reduce the expensive and time consuming use of current *in vitro* and *in vivo* models. Metabolites are synthesised electrochemically (Figure 1.5) in a few minutes and detected by MS, without the involvement of expensive enzymes.[85, 86] As a consequence a complete metabolic profile is obtained quickly in a clean matrix, economically with solvent consumption restricted to the μmolar level and more importantly without the unethical use of animals.[87] In contrast, *in vitro* and *in vivo* methods are time consuming since the sample collection occurs at different time points. Also, suitable extraction processes such liquid-liquid extraction or solid phase extraction are conducted for removing the interfering materials prior to the investigation.[88] The only limitation of EC/MS is low metabolite yield, in the case of some metabolic reactions.[87] Thus, the possibility of using cheaper electrodes with simplier instrumental set ups in miniaturized formats would probably provide an even more economical fashion towards the mimicry of human metabolism.

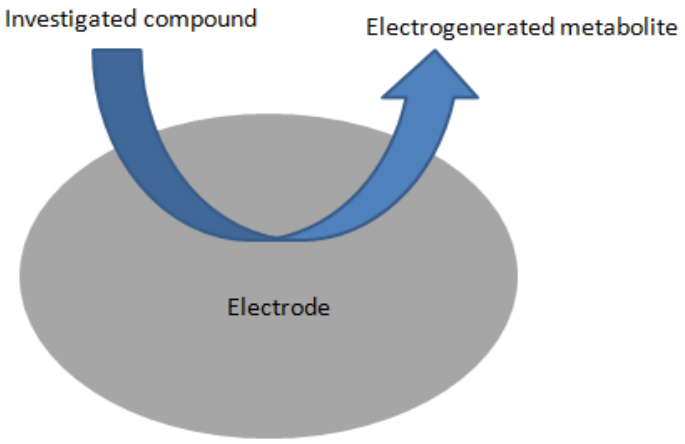

Figure 1.5 Electrochemical simulation.

1.7 Electrochemistry

Electrochemistry is a branch of chemistry associated with chemical and electrical phenomena.[89] Electrochemistry plays a dominant role in the simulation of human metabolism, and is the heart of the system, since the generation of metabolites is determined by a specific analytical method.[90] In-depth knowledge of electrochemical parameters and methodologies can provide valuable information regarding the reaction mechanisms and substrate behaviour,[91] further supporting the detection of data. Herein, the basic concepts and principles of electrochemistry are discussed.

1.7.1 Potentiostat

A potentiostat is an electrical device connected with an electrochemical cell that controls the potentials applied to the working electrode. A diagram is shown in (Figure 1.6); a potential is applied to amplifier (A1) and a current (i) is generated, which flows to the working electrode (WE) and is recorded by a second amplifier (A2).[92]

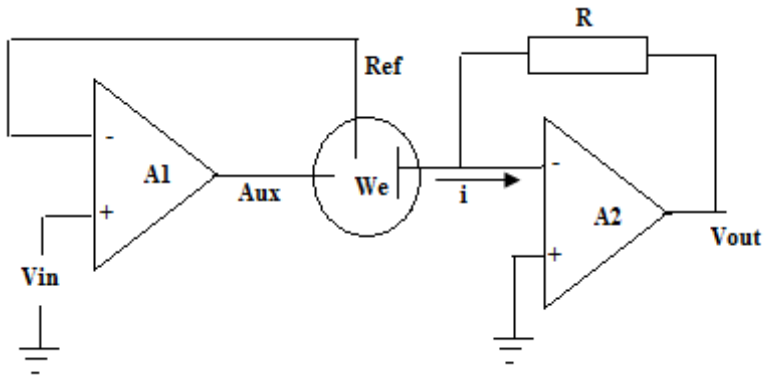

Figure 1.6 Potentiostat.[92]

1.7.2 Electrodes

Electrodes play a vital role in electroanalytical measurements.They are classified as 1) working, 2) reference, and 3) counter or auxiliary electrodes. Electrodes are placed in electrochemical cells with appropriate buffer solutions and analytes (Figure 1.7). Each type of electrode serves a specific function for successful measurement. Depending on the electrochemical technique, a two-electrode (working and reference electrodes) or three-electrode configuration (working, reference, and counter electrodes) is required.[93] Herein, the role of a three-electrode configuration is discussed.

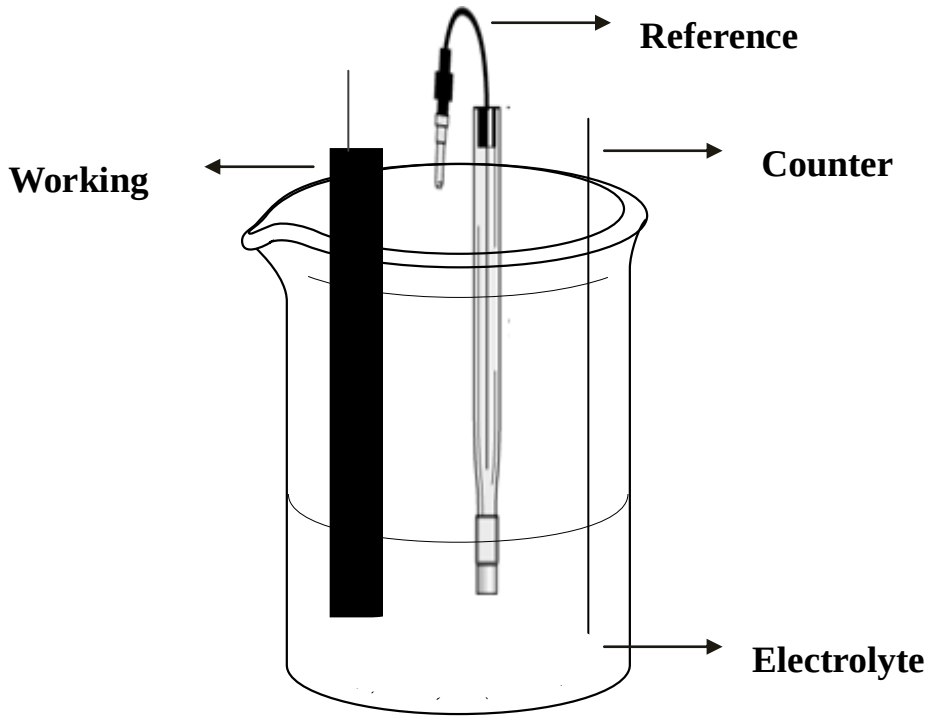

Figure 1.7 Three electrode configuration.[94]

Electrochemical reactions (oxidations or reductions) occur on the surface of the working electrode.[95] When a potential is applied on the working electrode, the analyte is transported into the electrode and either it gains or losses an electron, resulting in a generated current. Several solid electrodes such as glassy carbon, gold, platinum, carbon fibre, and epoxy-bonded graphite are extensively used as working electrodes.[96] Carbon electrodes are widely used for both oxidation and reduction process, owing to their wide potential windows.[97, 98] Reference electrodes provide a reference point with a stable and reproducible potential for the measurement of the working electrode potential. The frequently used electrodes are standard hydrogen electrode, silver/silver chloride, and pseudoreference electrodes.[97, 99, 100] The counter or auxiliary electrode completes the circuit and allows the charge to pass through the electrochemical cell.[101] Thus, its main role is to supply or remove electrons passing through the working electrode.[97]

1.7.3 Screen printed electrodes

Advances in electroanalytical chemistry have led to the development of SPEs, which have replaced the large conventional cells, with the three electrode configuration in many applications.[102] In detail, SPEs (Figure 1.8) are electrochemical sensors containing the necessary electrodes (working, reference, and counter) to drive electrochemical reactions and measurements.[103] They can be commercially obtained from various industrial companies such as DROPSENSE and Kanichi[104] or custom made with the appropriate facilities.[105] Besides the three-electrode configuration, several other types can be found including only the working electrode or both the working and reference electrodes.[106-108] The major advantages include low cost, disposability, simplicity of use, portability, integration in microfluidics, and low volume consumption.[109, 110]

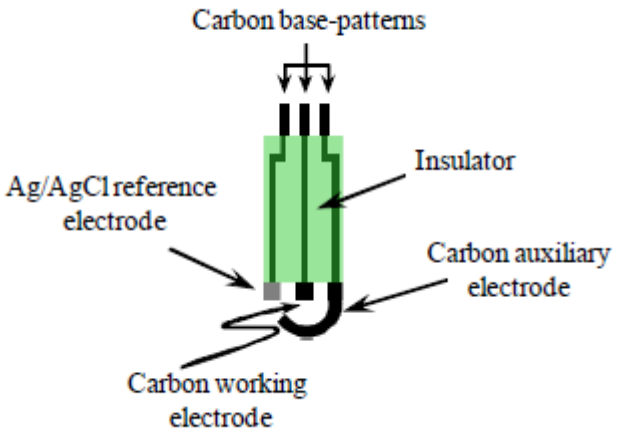

Figure 1.8 SPE, reprinted from Sanllorente-Mendez *et al.*[103]

SPEs are fabricated by depositing inks or pastes onto an insulating substrate made from glass, alumina, plastic, ceramic, alumina-ceramic composite, polyester foil, polyethylene terephthalate, and nylon.[111] Gold and carbon inks are used as working electrodes with the latter applied more frequently owing to its low cost;[108] on the other hand, the reference electrode is usually made from silver inks and the counter electrode, from the same ink as the working electrode. The fabrication process is simple: a mesh with the desired pattern is placed above the substrate; the ink passes through with the use of a roller, creating a film over the surface of the substrate. Different meshes are developed to fabricate all the parts of SPEs. The first one involves the deposition of silver paste for the formation of lines that separate the electrode area from the wire connection. Then, a second mesh is usually used for printing the working and counter parts if they are made from the same material, and a third mesh, for the silver ink of the reference electrode.[108, 111] The inks and pastes need to be solidified before the next ink deposition, so they are allowed to dry and cure. Finally, an

insulating material is used to cover the substrates besides the electrodes and wire connections.[112]

Over the years SPEs, have been used extensively for detection and kinetic studies in microbiology,[113] immunology,[114] pharmaceuticals,[109] drug metabolism,[115] forensics,[116] and environmental chemistry.[102] Several parameters have been investigated successfully such as effect of scan rate, reversibility, effect of pH, voltammetry, CPE, and detection limits. However, the main focus has been environmental chemistry, in particular, the detection of heavy metals.[108]

1.7.4 Electrode/solution interface

When an electrode is immersed into an ionic solution, an interface is created, and in this binary phase, the electrochemical reaction occurs.[117] Over the years, several models have been proposed for establishing the electrode/surface interface; however, in this section, the modified Stern model is discussed. The Stern theory combines the idea of the Helmholtz model and the diffusion layer theory.[118]

According to this model (Figure 1.9), a double electric layer consisting of the inner (IHP) and outer Helmholtz planes (OHP) is formed at a certain distance from the electrode. In the case of a negative potential, IHP dipoles such as water molecules and adsorbed anions are oriented on the surface of the working electrode. Meanwhile, the cations react with water molecules, as solvated cations and oriented in the outer plane. In the diffuse layer, the cations and anions are present in different concentrations.[119]

During redox reactions, electrons travel across the binary phase and a current is generated; in the case of reduction, electrons from the power pack travel to the electrode, pass through the electrode/solution interface, and reach the electroactive analyte in solution. In contrast, during oxidation, electrons travel from the solution containing the electroactive analyte, pass the electrode/solution interface, and are finally taken up by the electrode.[120]

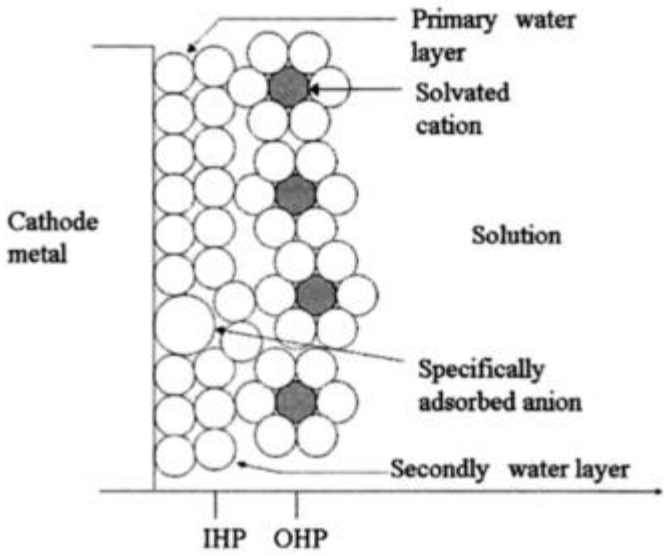

Figure 1.9 Double layer reprinted with permission from Buitrago *et al.*[119] Water molecules and specifically absorbed anion are oriented in the IHP, whereas solvated cations rely on the OHP.

1.7.5 Faradaic and non-faradaic processes

Faradaic and non-faradaic processes occur in parallel during electrode reactions, and as result, the generated current is the sum of both faradaic and non-faradaic currents. During faradaic processes, when a potential is applied, a charge is transferred between the electrode and analyte, leading to oxidation or reduction. On the other hand, in a non-faradaic process, the charge is not transferred, but a charging current is still generated owing to ion rearrangements on the electrode surface.[121]

1.7.6 Mass transport

The electroactive molecule travels from the bulk solution to the electrode surface via three different mechanisms: 1) convection, 2) migration, or 3) diffusion.[122] In the process of convection, two different modes are observed: 1) natural convection and 2) forced convection. In natural convection, the material is transported by a physical phenomenon such as density difference between the reactant and product. On the other hand, in forced convection, a mechanistic force such as stirring is applied, causing movement in the entire solution.[123] Migration refers to the movement of charged species down a potential gradient.[124] For example, if a negative potential is applied on the working electrode, electrostatic attraction is seen between the cations and repulsion between the anions in the solution. Finally, diffusion involves the movement of the electroactive species down a concentration gradient from an area of a higher concentration to an area of a lower concentration [125]. This happens because the concentration of the reactant (electroactive species) is reduced during the electrochemical reaction and products are generated continuously at the surface of the electrode. As a result, the electroactive species are diffused from the bulk solution (higher concentration) towards the electrode surface and the products, towards the bulk solution.

1.7.7 Voltammetry

Voltammetry is an electrochemical technique based on a potential-current relationship with a three-electrode configuration. The potential is applied through the potentiostat to the working electrode and a current is generated that is recorded in a voltamogram.[122] Herein, CV and DPV are described.

1.7.7.1 Cyclic voltammetry

A potential is cycled at the working electrode in unstirred solution at a constant scan rate and the generated current is measured. The resulting peaks indicate the transfer of electrons between the electrode surface and analyte. In the case of oxidation (Figure 1.10), the potential is scanned to more positive values during the forward scan. The initial potential is not capable of inducing electrolysis, but as the potential is increased, the electroactive compound approaches the optimum anode potential, leading to electrolysis and generation of anode current. In the reverse scan, the oxidised product is reduced back to the starting material. The obtained graph is called as cyclic voltammogram and represents a plot of current versus applied potential.[126-128] Valuable information is acquired from the current-potentials plots such redox behaviour, kinetics of the electroactive compound, mass transfer, and reactivity of generated products.[116, 117]

During CV, the concentration profiles vary,[127] as shown in (Figure 1.10). At point (A), the dominant mode is the electrode kinetics, where only a small amount of the reactant is oxidised, generating small currents. At (B), the maximum current is observed since the working electrode is sufficiently positive (high positive potential) to drive the reaction (oxidation). Both electron transfer and mass transport are important and compete with each other. At point (C), mass transport dominates, and the current is decreased because the concentration of the reactants is consumed and the oxidised species are diffused from the electrode surface to the bulk solution. From (C) to (F), the reverse process occurs; products are reduced back to their original form. At (D), the current is small, and the products start to reduce, but the electrode is not sufficiently negative. Herein, the dominant mode is the electrode kinetics as in (A). The electrode becomes negative enough at (E); both electrode

kinetics and diffusion are important, generating the maximum current. Finally, the oxidised product diffuses from the electrodes to the bulk solution (F).

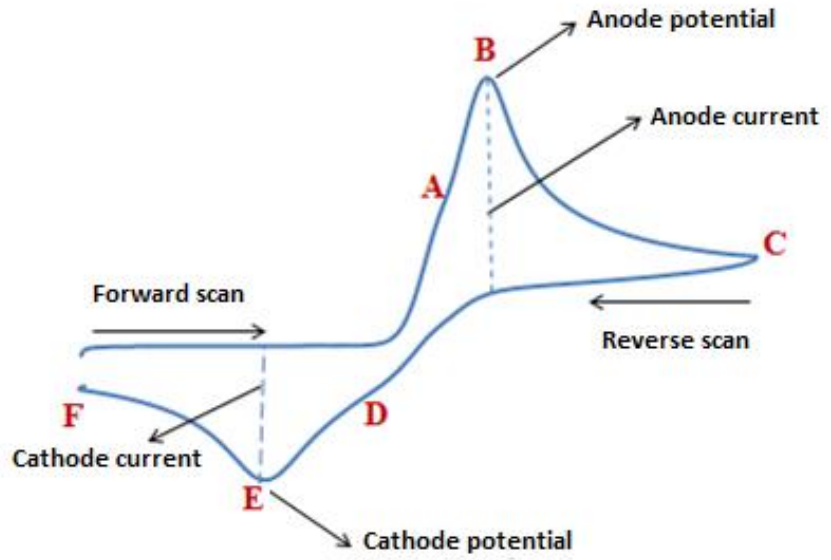

Figure 1.10 Cyclic voltammogram.

1.7.7.2 Electron transfer kinetics

Electron transfer kinetics can be reversible, irreversible, and quasi-reversible.[122,127] When the electron transfer rate is faster compared with the mass transfer, then the system is characterised as reversible and the Nernestian equilibrium is maintained, (Equation 1.3): where E: the applied potential, n: the number of electrons, F: Faraday constant, R: the gas rate constant and T: the temperature. In irreversible systems, the electron transfer rate is slower than that in mass transport and the reverse peak is not obtained. Moreover, quasi-reversible systems are dominated by both reversible and irreversible processes, creating an intermediate condition.[127, 129]

$$E = \mathrm{E_f} + \frac{\mathrm{RT}}{\mathrm{nF}} \ln\left(\frac{[\mathrm{ox}]_{\mathrm{surf}}}{[\mathrm{red}]_{\mathrm{surf}}}\right) \qquad \textbf{(Equation 1.3)}^{127}$$

Scan rate plays a critical role in determining the mode of electron transfer. In reversible systems, the peak current is proportional to the SQRT of the scan rate, as described by the Randles-Sevcik (Equation 1.4). Where ip:peak current, S:surface area, D:diffusion coeffician, all other parameters, as stated before. In addition, the peak potential is constant and independent of the scan rate [130]. While in irreversible and quasi-reversible systems, the peak potential is dependent on the scan rate and a linear but not proportional relationship is obtained between the peak current and SQRT of the scan rate[131, 132] (Table 1.1).

$$ip(ox) = -ip(red) = -0.4463\left(\frac{nF}{RT}\right)^{\frac{1}{2}} nFSD_{OX}^{\frac{1}{2}}\ [ox]_{bulk}\, V^{1/2} \qquad \textbf{(Equation 1.4)}^{127}$$

Several other parameters besides the scan rate determine the electron transfer kinetics such as the separation potential (Equation 1.5) and peak current ratio (Equation 1.6). For example, in reversible systems, the separation peak potential equals 0.057 V and peak current ratio equals unity. However, in quasi-reversible systems, larger separation peak potentials are obtained, which are varied as a function of scan rate, and the peak current ratio is less than unity.[132, 133]

Separation peak potential = Anode potential – cathode potential **(Equation 1.5)**[132]

Peak current ratio = anode current/cathode current **(Equation 1.6)**[132]

In some cases, the described electron kinetics can be coupled with chemical steps known as ECE and EC′ mechanisms. In ECE, electrochemical reactions are followed by chemical reactions, which generate electroactive products capable of undergoing further electrochemical reactions. EC′ is a catalytic system in which the electrogenerated product reacts chemically with a substrate in solution, resulting in the formation of a new product and the regeneration of the starting material.[122]

Table 1.1 Electron transfer kinetics.

Parameter	Reversible	Irreversible	Quasi-reversible
SQRT scan rate	Independent	Dependent	Dependent
Peak current	Proportional with SQRT of scan rate	Not proportional with SQRT of scan rate	Not proportional with SQRT of scan rate
Separation peak potential	0.057 V	-	>0.057 V
Peak current ratio	Unity or close to unity	-	>1

1.7.7.3 Differential pulse voltammetry

The potential is applied over a series of pulses; the generated current is measured at two points, i.e. prior to and after each pulse. The obtained voltammogram reflects the difference in currents for each pulse plotted versus the potential. DPV is an extremely helpful electroanalytical method for quantification purposes in the field of pharmaceuticals.[134]

1.7.8 Controlled potential electrolysis

In CPE, the potential is held constant over a period of time.[135, 136] The appropriate range of potentials is selected by CV; usually, the maximum electrochemical conversion is obtained at potentials controlled mainly or solely by mass transfer. CPE synthesises sufficient amounts of products usually identified by a suitable analytical method such as MS. Three electrodes are used as in CV; however, larger electrodes are required in CPE for total conversion of the analyte. During electrolysis, CV can be recorded regularly to study the consumption of the analyte.[91, 138-140] Over time, the current is decreased and at the end of the analysis, in an ideal scenario, it should approach zero, implying total analyte consumption.[136]

1.8 Electrospray ionization/ mass spectrometry

ESI/MS was introduced in 1989 by the Fenn research group,[141] as a revolutionary approach suitable for quantitative and qualitative analysis of small molecules such as nucleic acids,[142] peptides,[143] proteins,[144] drugs and their metabolites.[145,146] The main advantages include high sensitivity to the fentommolar range, slight fragmentation, suitability for thermally liable compounds, hyphenated easily with separation methods, and robust.[147,148] In general, the process involves the transformation of the sample into ions within the ionisation source and their separation to the mass analyser region, based on their mass to charge ratios (*m/z*). Subsequently, ions strike the detector and an electrical signal is generated. The mass spectrum obtained can be represented by a plot of ion abundance versus the mass to charge ratio.[149]

The sample solution is injected directly or as an effluent, using a separation method (liquid chromatography or gas chromatography), into the ESI source and, in particular, towards the heated capillary. A high potential difference is applied between the capillary and the counter electrode, creating, in this way, an electric field. If a positive potential is applied to the spraying nozzle, then the generated ions will predominantly be protonated and if a negative potential is applied, then the ions will predominantly be deprotonated. For example, if a negative potential is applied, negatively charged molecules dominate over the positively charged ones and a Taylor cone will be formed by the charged droplets (Figure 1.11). Subsequently, charged droplets containing the desired analytes are sprayed from the tip of the Taylor cone towards the counter electrode. The solvent evaporates continuously, the droplet shrinks, and the Rayleigh limit is reached because the surface tension cannot sustain the charge. As a result, the droplet bursts (Coulomb explosion) and charged analytes are formed in the gaseous phase. Multiple charged ions are formed and are emitted from the droplet as a part of the Coulomb explosion.[150, 151]

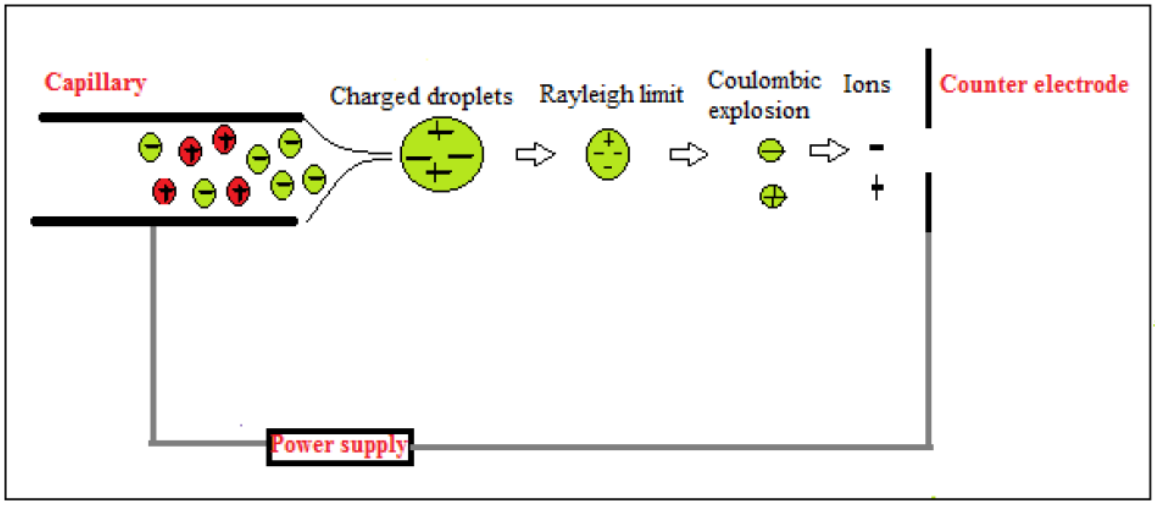

Figure 1.11 ESI process.[150, 151]

1.8.1 Ion trap mass analyser

Ion trap mass analysers are widely used in clinical, biological, and chemical research. These are relatively inexpensive as compared to other mass analysers with improved sensitivity and capable of scanning high mass ranges. An ion trap has the size of a tennis ball and consists of three hyperbolic electrodes (Figure 1.12), two endcap electrodes, and a ring electrode.[152, 153] Ions enter the instrument through a small hole at the centre of end cap electrode and become trapped as a result of the application of an RF voltage at the ring electrode. Additionally, the kinetic energy of the ions is reduced significantly through their collision with argon gas. Ions are selectively ejected by increasing the RF voltage: the heavier ions stabilise while the lighter ones destabilize and are ejected towards the detector. The RF voltage needs to be increased continuously in order to eject the heavier ions.[153- 156]

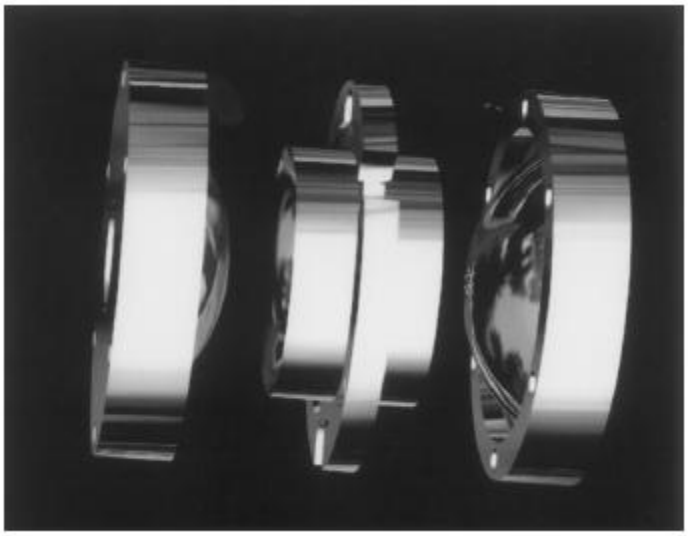

Figure 1.12 Ion trap mass analyser, reprinted with permission from Jonscher *et al*.[152]

1.8.2 ESI as an interface

One of the main features that lead to the online coupling of EC with MS is the development of the ESI source.[157] The majority of published data regarding the simulation of drug metabolism use this type of ionisation.[158] In this section, the advantages and limitations of ESI as an interface for EC/MS are discussed.

ESI is a suitable interface for EC/MS since the majority of xenobiotics are polar, so the drugs and their intermediates can be identified quickly and easily.[159- 161] Additionally, less polar drugs with poor ionisation efficiencies and low detection efficiencies in mass spectra can also provide a metabolic profile because the resultant electrogenerated metabolites are more polar and more easily detected.[162] Also, ESI is proven to be successful in endogenous metabolism for polar compounds.[163]

However, ESI has the capacity to act as a controlled–current device, so electrogenerated products on their way into ESI/MS can be oxidised or reduced further within the ionisation source. This problem can be overcome by increasing the transfer time of the electrogenerated product from the flow cell to the ESI source, by incorporating grounded metal tubing in between the potentiostat and MS.[164, 165] However, in drug metabolism, this approach creates problems for the identification of unstable and short-lived metabolites. Additionally, a limited number of electrolytes such as ammonium formate, ammonium acetate, and acetic acid are suitable for EC/MS, since non-volatile buffers such as phosphate buffer block the capillary needle.[166]

1.9 Online coupling of EC with MS

In the particular, instrumental set up the EC is connected directly to MS. The electrochemical products travel at an optimize flow rate via transfer capilarries to the mass spectrometer for detection. More than 20 years ago, Getek *et al.*[167] proposed first, the simulation of APAP metabolism via the online coupling of EC with MS.However, extensive work has been done the last decade by Karst and Bruins research groups, through the use of commercially available flow cells by Thermo scientific, Biosciences, and Antec. In general, the sample solutions are infused constantly into the flow cells and various potentials applied depending on the electrode material for a predetermined time scale. The generated metabolites are then detected by MS via transfer capillaries and a complete metabolic profile is obtained.[168]

1.9.1 Flow cells

The heart of the particular hyphenated method is the electrochemical flow cell in which the electrochemical reactions occur and metabolites are generated. A three-electrode configuration is integrated within flow cells composed of a working, reference, and counter electrodes.[169] Two main types have been extensively used for the online methods: 1) coloumetric[170] and 2) amperometric flow cells.[171] The particular cells are placed prior to the ESI source; however, source cells have also been developed for simulating human metabolism.[172]

1.9.1.1 Coulometric flow cell

The main advantage of coulometric flow cells is their large working electrode area, which provides higher conversional rates. Thermo Scientific™ works extensively with this particular type of cell. According to their design, the three-electrode set-up is composed of a working porous glassy carbon, a Pd/H_2 reference electrode, and a counter palladium electrode (Figure 1.13); the flow rate in most published data is 10 μL min^{-1}, but higher flow rates of up to 1.5 mL min^{-1} can be applied. A major limitation is the inability to polish the working electrode after the completion of each electrolysis. This creates adsorption phenomena on the working surface, especially in cases of non-polar drugs. The problem can be overcome by the use of a highly organic solvent, up to 90%, mixed with a salt buffer.[85, 168, 173]

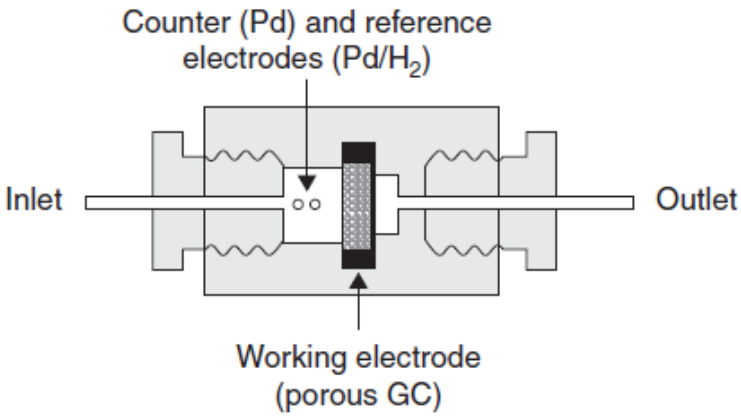

Figure 1.13 Coulometric flow cell, reprinted with permission from Baumann *et al.*[168]

1.9.1.2 Amperometric flow cell

Amperometric cells used for drug metabolism are developed exclusively by ANTEC. The working electrode has a small planar area so the conversion efficiencies are affected mainly by the flow rate. At higher flow rates of above 10 μL min^{-1}, the chemical reactants spent less time on the surface, leading to incomplete reactions, and as a consequence, maximum conversion is achieved at flow rates of below 10 μL min^{-1}. The cell is composed of three electrodes as in coulometric cells: an exchangeable working electrode that can be a glassy carbon rod, a platinum rod, or diamond rod; a Pd/H_2 reference electrode; and titanium counter electrode[168, 174] (Figure 1.14). The exchangeable electrode provides the possibility of generating a wide range of electrochemical reactions that are favoured under particular electrode materials. In addition, the working electrode (carbon and platinum) can be polished manually to reduce adsorption effects.[85, 168]

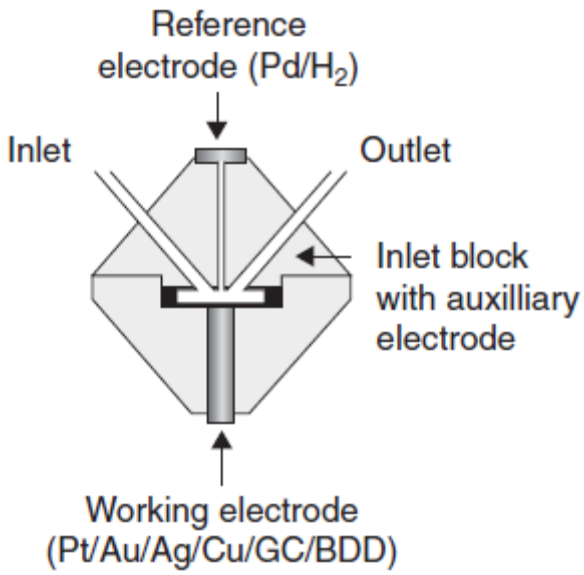

Figure 1.14 Amperometric flow cell, reprinted with permission from Baumann *et al*.[168]

1.9.1.3 In-source cells

Apart from the well-known functionality of ESI source in generating charged droplets, the interface can be used as an electrochemical cell with appropriate modifications. In particular, the ESI can act as a two-electrode cell composed of a working emitter electrode with the actual MS serving as the counter electrode.[175-177] In the field of metabolism, an excellent modification of an ESI source into a two-electrode configuration, was presented by the Bratjer-Toth research group (Figure 1.19), illustrating the detoxification of DOPA with cysteine. The ionisation interface was modified in such a way that the oxidation of DOPA occurred prior to mass spectrometric detection. As seen in (Figure 1.115), the homemade cell consisted of two capillaries which were separated by plastic tubing. The first cylindrical capillary served as the working electrode and the second as the counter, while both of them function as usual, as a capillary needle, the potentials were applied via a 9V battery. The sample solution was injected into the first tubing and the reactants were electrolysed on the surface of the working electrode; then, the obtained products were detected online by ESI/MS.[178]

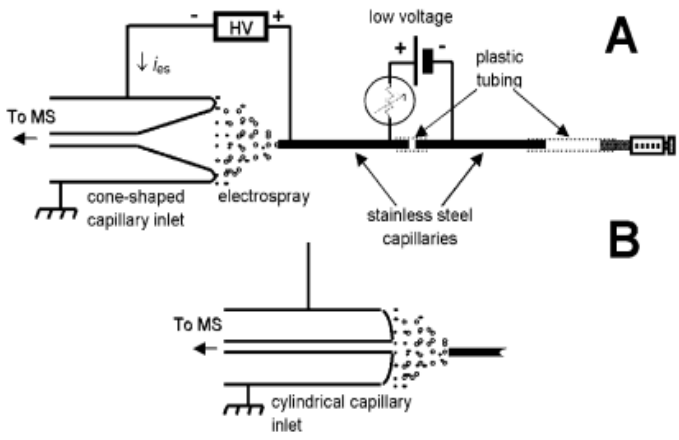

Figure 1.15 In-source cell, reprinted with permission from Mautjana *et al*.[178]

1.9.2 Instrumental set-ups

Several instrumental set-ups have been proposed for the generation of a wide range of metabolites; depending on the desired application.[168] The Bruins research group investigated extensively the direct online coupling of electrochemical flow cells with ESI-mass spectrometers via transfer capillaries (Figure 1.20A). It is a simple and quick methodology for the identification of the maximum metabolite yield at the optimum potential.[179, 180] More complicated pathways involving multiple metabolic reactions or the formation of isomers at a given potential, lead to issues regarding their identification by EC/MS. Therefore, a separation column is inserted after the electrochemical cell (Figure 1.16B). Usually, a reverse phase hydrophobic column is used owing to the hydrophobic nature of the drugs analysed.[181, 182]

The insertion of an injection valve between the electrochemical cell and separation column (Figure 1.16C) allows the independent optimisation of the electrochemical and separation conditions. In this particular instrumental set-up, the effluent from the electrochemical cell is discharged into a loop on a switching valve; then, the valve is switched over, and the electrochemical solution passes onto the column and then into the mass spectrometers.[183, 184]

The last type of instrumental set-up is suitable for the formation of phase II adducts, as seen in (Figure 1.16D). The effluent from the electrochemical solution containing the generated metabolites is mixed with GSH via a reaction coil and the adducts formed are detected by MS. The design is used for trapping highly unstable metabolites. Additionally, biomolecule adducts involving DNA and proteins as trapping agents have been reported.[185]

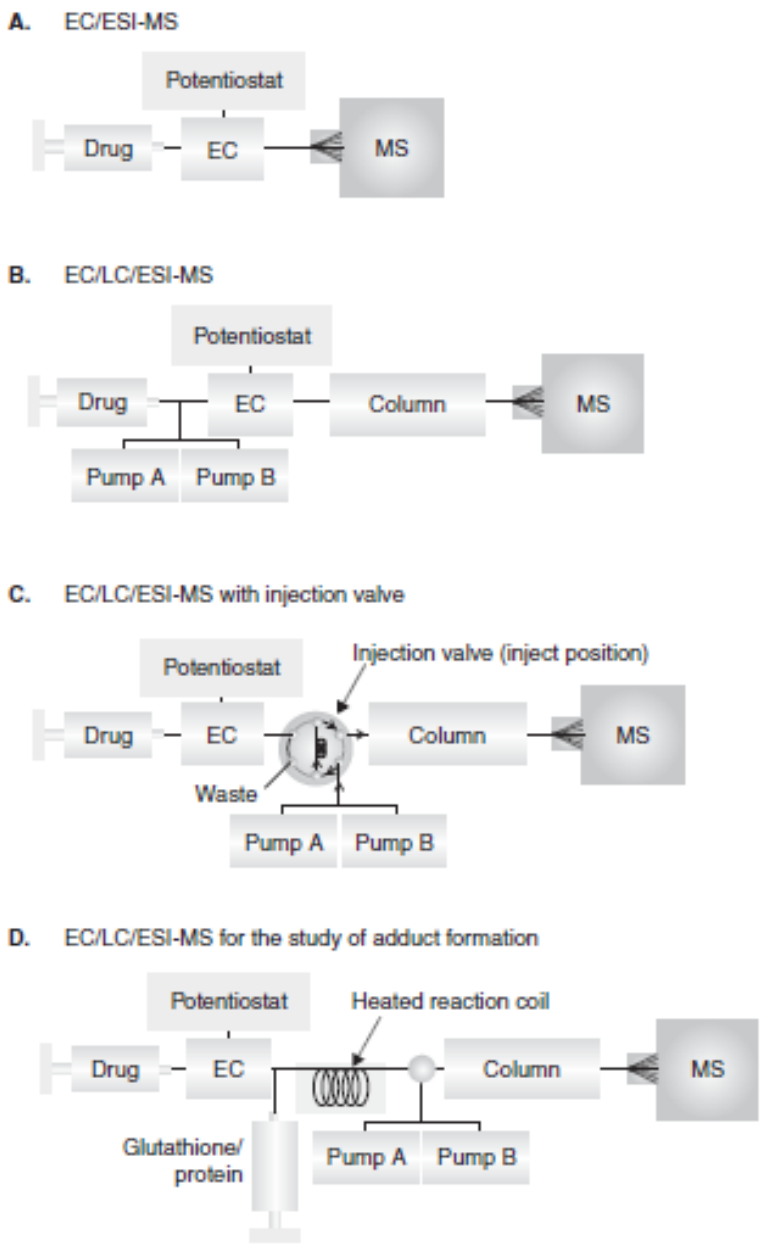

Figure 1.16 Online instrumental set-ups, reprinted with permission from Baumann *et al.*[168]

1.10 Reactions mimicked by the online coupling of EC/MS

Metabolic reactions involving a single electron transfer have been mimicked successfully with the corresponding online systems;[180] a brief summary is presented in (Table 1.2). An extensive investigation was presented by the Bruins research group using various drug probes for each metabolic reaction. In their study, a wide range of metabolic reactions have been mimicked such as dehydrogenation, aromatic hydroxylation, heteroatom dealkylation, and heteroatom oxidation.

Table 1.2 Reactions mimicked by EC/MS.

Compound	Reaction	Buffer (pH)	Potential (V)	Reference
APAP DOPA	Dehydrogenation	7 6.3	0.2	180 178
N-0923	Aromatic hydroxylation	3	0.3	179
Lidocaine	Nitrogen dealkylation	7	0.4	180
Parathion	Phosphate oxidation	3	0.6	180
S methyl thiopurines	Sulphur oxidation	3	0.85	180

1.10.1 Dehydrogenation

In particular, Acetaminophen (APAP) was dehydrogenated to yield the reactive N acetyl p benzoquinone imine (NAPQI)[180] via the initial loss of a single electron and a single proton from the hydroxyl moiety, followed by a second loss of a single electron and single proton from the amine group (Scheme 1.5).

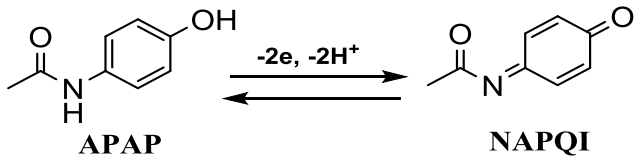

Scheme 1.5 Dehydrogenation.[180]

Also, the dehydrogenation of DOPA was described by Bratjer-Toth research group[178] using a home-made amperometric cell. The ortho hydroxyl moieties in the aromatic ring were dehydrogenated, generating an ortho quinone known as dopaminoquinone. Considering the instability of the electrogenerated metabolite subsequent reactions have lead to the nucleophilic substitution of ortho quinone with ammonia.

1.10.2 Aromatic hydroxylation

Jurva *et al.*[179] simulated the aromatic hydroxylation of dopamine (DOPA) agonist N-0923, (Scheme 1.6). The hydroxylated product reacted further via dehydrogenation at the optimised potential generating a quinone metabolite. As concluded, the substrate requires an electron donating group, e.g. a hydroxyl group, to activate the aromatic hydroxylation.

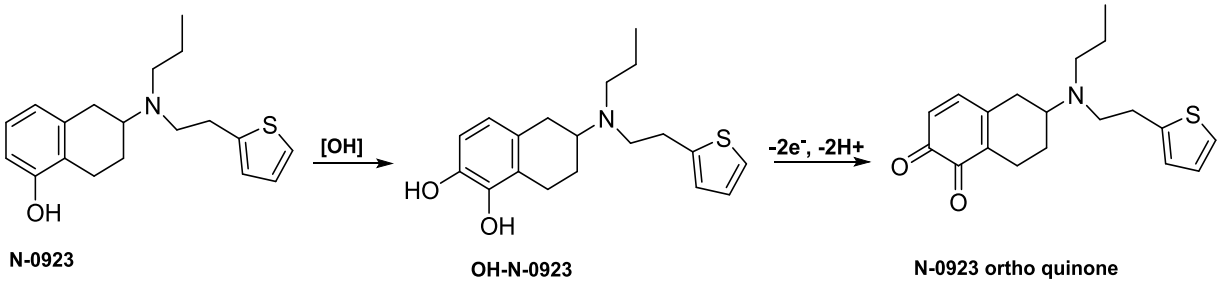

Scheme 1.6 Aromatic hydroxylation.[179]

1.10.3 Heteroatom dealkylation and oxidation

Heteroatom dealkylations and oxidations were also a subject of study for the online coupling of EC and MS. A characteristic example is the N-dealkylation of aliphatic amines such as lidocaine.[180] In general, the mechanism was initiated though a single electron transfer from the lone pair, generating an aminium radical cation, which was subsequently deprotonated and oxidised to an iminium ion and eventually hydrolysed (Scheme 1.7). A characteristic observation was the dependence of the applied potential with the length of the alkyl chains. As proposed lower oxidation potentials were required for the dealkylation of long alkyl chains.[180]

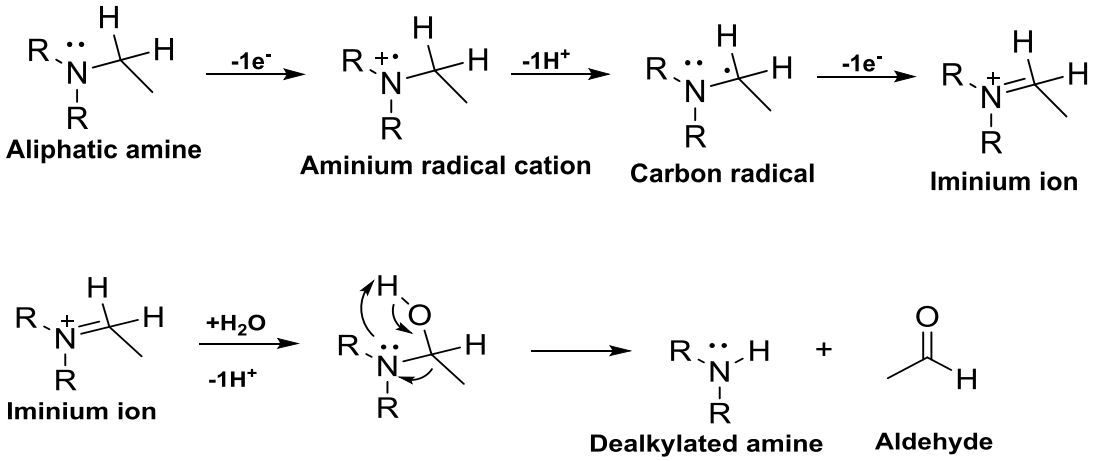

Scheme 1.7 N-dealkylation.[180]

The heteroatom oxidation of sulphur and phosphorus atoms was achieved at moderate potentials (Table1.2). In particular, sulphide-like compounds were oxidised to their corresponding sulphoxides via oxygen interaction with the lone pair and the phosphorothionate pesticide parathion was oxidised by the replacement of sulphur atom with oxygen.[180]

1.11 Reactions simulated by the online coupling of EC/Injection valve/LC-MS

As expected, the reactions that were simulated in the EC/MS were adapted successfully in EC/LC/MS or EC/Injection valve/LC-MS.[183, 186, 187] Herein, multiple metabolites were generated since several metabolic reactions were under investigation or the generated metabolite was still active and reacted further; the reactions are summarised in (Table 1.3). In addition, in most cases the formation of the multiple metabolites required extremely high potentials (> 1V), which were not seen in EC/MS, since the methodology was focused on optimum potential rather than the multiple metabolite generanation.

A characteristic example was presented by Baumann *et al.*, involving the simulation of tetrazepam (1, 4 benzodiazepine)[188] in acidic conditions (10 mM formic acid, pH 3.1) with the use of a platinum working electrode at 2 V. The drug gave raise to intermediates via dehydrogenation, demethylation, and hydroxylation. Owing to the high potential applied, the hydroxylation of alkanes and alkenes was achieved for the first time. In addition, the oxygen was inserted in five different positions on the cyclohexenyl ring, a unique mechanism which was not observed with the use of glassy carbon electrode. In general, the electrogenerated tetrazepam metabolites were in good agreement with microsomal incubations, but the demethylation products such as nitrazepam, were formed at very low yields because these type of reactions are not favoured electrochemically, so further intermediates from nitrazepam were not observed.

A series of metabolic reactions on a diamond electrode at 2 V were conducted by Jahn *et al.*[189] in this study, a wide range of metabolites and their isomers were generated and detected for the first time. Verapamil was electrolysed directly into five main intermediates

by N-dealkylation, oxygenation and demethylation, in a neutral environment (50% 20 mM ammonium formate: 50% acetonitrile, pH 7.4); all of them reacted further and generated new intermediates. For example, the N-dealkylated intermediate was either doubly oxygenated on the aromatic ring or demethylated. The hydroxylated intermediate formed dehydrogenated, oxygenated, and demethylated compounds, and finally the demethylated intermediate lost a second methyl group. Isomers were obtained from the direct hydroxylation and demethylation of verapamil and from the indirect oxidations initiated by the electrogenerated metabolites.

Another important drug that leaded to three oxidation reactions was alprenolol.[190] However, the unique feature of this drug was the mimicry of benzylic hydroxylation rather than the separation of the multiple metabolites. In the same study, the metabolism of acebutolol was also investigated, leading to the successful simulation of both O-dealkoxylation and N- dealkylation.

Platter *et a*l. simulated the interaction of APAPs reactive metabolites with genetic material in the same cell.[191] Five isomeric guanosine adducts were obtained in the potential range of 1.25 V–1.75 V, with a diamond working electrode. APAP and guanosine were oxidised via single electron and single proton transfers and reacted together subsequently.

Li *et al*. simulated the reductive metabolism of three nitro aromatic compounds[192] 3-trifluoromethyl-4-nitrophenol, niclosamide, and nilutamide. The reductive potential was held at -2.5 V using a reactor cell assembled with a diamond working electrode. The generation of metabolites was favoured in acidic conditions, involving a series of three reduction processes leading to a nitroso intermediate, a hydroxylamine, and amine via the transfer of two electrons and two protons.

Lohmann *et al*. successfully generated the phase I metabolites of boscalid (*m/z* 343)[193] in slightly alkaline conditions using a coulometric cell. The main three metabolites were obtained at 1.5 V: a hydroxylated metabolite with *m/z* of 359, a second metabolite with *m/z* of 357 generated after an aromatic hydroxylation and dehydrogenation, and, lastly, a third metabolite with a *m/z* of 323 resulted from a Cl substitution and dehydrogenation. Alternations to the above set-up and, in particular, the addition of a second cell in reductive conditions (-1 V), between the first cell and switching valve, provided information about the quinoid nature of the oxidised metabolites.

Table 1.3 Reactions simulated by EC/Injection valve/LC-MS.

Compound	Reaction	Buffer (pH)	Potential (V)	Reference
Tetrazepam	Aliphatic hydroxylation Dehydrogenation Aromatic hydroxylation	3.1	2	188
Vepamil	N-dealkylation Demethylation Oxygenation Dehydrogenation	7.4	2	189
Alprenolol	Benzylic hydroxylation	7.4	1	190
Acebutolol	O-dealkoxylation N-dealkylation	7.4	1	190
APAP	Dehydrogenation	7.3	1.75	191
Trifluoromethyl-4-Nitrophenol, Niclosamide, Nilutamide, and Boscalid	Reduction	7.4	-2.5 -1	192 193

1.12 Reactions simulated by EC/reaction coil/LC-MS

Many of the phase I metabolites generated in sections 1.10 and 1.11 were allowed to react with GSH or NAC. The quinone imine NAPQI was trapped with GSH and NAC, generating, in this way, APAP-GSH adducts (*m/z* 457) and APAP-NAC adducts (*m/z* 311).[187] In addition, acebutolol quinone methide formed during O- dealkoxylation bound covalently with GSH and generated acebutolol-GSH adducts.[190]

Baumann *et al*.[194] described the application of both instrumental set-ups (in the presence and absence of a reaction coil) and gave a complete view of the metabolic simulation of triclocarban (TCC). In the absence of a reaction coil, TCC was electrolysed on boron doped diamond at an optimised potential of 2.5 V, in a neutral environment (1 mM ammonium acetate pH 7). Ten metabolites have been identified in total: three main monohydroxylated products, which were in agreement with *in vivo* or *in vitro* studies, two dihydroxylated metabolites observed in RLM studies only, and two dechlorinated metabolites that were in very low intensities and have not been detected in *in vitro* and *in vivo* studies. Additionally, dehydrogenated metabolites were generated from the mono and dihydroxylated products, and their obtained *m/z* probably corresponded to formation of quinine methide. Further studies were conducted to investigate their toxicity, at 1.5 V, when the effluent was mixed with GSH via a reaction coil and as proven, GSH adducts were formed, suggesting the generation of the reactive quinone imines. The particular work strongly supported the great advantage of the particular instrumental set-up (EC/reaction coil/LC-MS) over the EC/LC/MS for the identification of reactive metabolites.

The successful generation of GSH adducts led to the simulation of metabolite-protein adducts and the simulation of reactive metabolic pathways. In particular, Fiber *et al.*[195] generated adducts with β-lactoglobulin, a milk protein with a thiol group in its T13 peptide, which is easily ionised in an ESI source. The drug under investigation was diclofenac (*m/z* 294), which was oxidised in a boron doped electrode at 2.4 V. As a result, owing to the high potential, hydroxyl radicals were produced, leading to the generation of two catechol metabolites (*m/z* 326, 282) that reacted further at the optimised potential and a hydroxylated metabolite (*m/z* 310) was produced that subsequently reacted with β-

lactoglobulin. Additionally, in a similar study by Lohmann *et al.*,[196] the well-known reactive metabolites of NAPQI, amodiaquine, and clozapine nitrenium ions, of APAP amodiaquine and clozapine, respectively, were allowed to interact with β-lactoglobulin and human serum albumin. The metabolite-protein adducts were identified by time-of-flight mass analyser.

1.13 Offline coupling of EC/MS

In Offline coupling, the electrochemical process is not connected to MS and both techniques operate independently. The major advantage of the offline approach relies on the separate optimization of the two porcesses and the extended reaction times.[166] However; limited studies in the literature refer to the offline approach, given the advantages of the automated online approaches. Herein, the offline approaches involving conventional electrodes, flow cells, and sensors as electrochemical tools are discussed.

1.13.1 Conventional electrodes

An offline approach was proposed by De Lima *et al.*[197] The aim of their research was to electrochemically generate the main metabolite of albendazole, a sulphur oxide intermediate known as albendazole sulfoxide, which oxidises further on the sulphur group and generates a second metabolite, albendazole sulfone. Albendazole was studied extensively both kinetically and in terms of CPE, using conventional electrodes. For the kinetic studies, a glassy carbon working electrode was used with a surface area of 0.78 cm^2, a silver reference electrode, and a platinum wire as the counter electrode. According to the obtained cyclic voltammograms, an irreversible anode peak appeared at 1 V, indicating the irreversible oxidation of albendazole. However, a second oxidative peak did not appear to prove the subsequent reaction of generated species into the second intermediate

(albendazole sulfone). Albendazole was electrolysed for 30 min at a wide range of potentials from 0.8 V to 1.20 V in 1 M HCL; at 0.8 V, a mixture of albendazole and albendazole sulfoxide was obtained, at a higher potential of 1 V, both of the metabolites were obtained, and at 1.10 V, only albendazole sulfone was obtained. In contrast, when the drug was electrolysed in acidic conditions, in trifluoroacetate, pH 3.3 between 0.85 V and 1.20 V, only albendazole sulfoxide was generated.

1.13.2 Flow cells

Limited studies in the literature involve the offline coupling of flow cells with EC or EC/LC/MS. In particular, Baumann *et al.*,[195] generated protein adducts between the β-lactoglobulin and triclocarban reactive metabolites. Triclocarban was electrolysed on a diamond electrode at 1.5 V and the generated metabolites were then collected in a glass vial containing 150 μL of the protein solution. The triclocarban quinone imines reacted non-covalently with the proteins, and the generated adducts were detected by LC/MS.

1.13.3 Sensors

Kauffmann *et al*. studied the use of SPEs as an inexpensive tool for simulating human drug metabolism.[115] In particular, APAP was electrolysed in the presence of GSH in an attempt to mimic the phase II metabolic process and it was demonstrated that the APAP-GSH adducts were generated successfully, indicating, in this way, an alternative and cost-effective approach in both *in vitro* and *in vivo* studies and existing flow cells. In particular, 50 μL of sample solution containing $3x10^{-5}$ M of APAP and $6x10^{-5}$ M of GSH in 0.1 M of ammonium acetate (pH 7.4) were loaded on the surface of the SPE and electrolysed for 10 min. Subsequently, at the end of electrolysis, the generated adducts were analysed by ESI/LC/MS. The potentials were chosen based on the voltammograms of APAP in the

presence of GSH, by increasing the potential, and additional metabolites were obtained such as di GSH-APAP adducts.

1.14 Microfluidics

Microfluidics (Figure 1.17) are miniaturised devices operating at micro- and nano-scale volume.[198-200] Depending on the required application, fluids can be mixed,[201, 202] separated, [203-205] or detected[206, 207] through their movement within the microfluidic channels. The ultimate aim is the integration of a series of processes on the same microfluidic device for a complete on-chip analysis, known as a lab-on-chip or microTAS.[208, 209] Microfluidics are widely used in pharmaceuticals,[210] forensics, [211] genetics, [212] and environmental analysis.[213] The main advantages include low volume consumption, rapid analysis, portability, mass production, and simplicity of use without the need of a highly expert operator.[214- 218]

Earlier, devices were fabricated from glass and silicon;[219, 220] however, improvements in the field led to the use of polymers,[221-224] paper,[225, 226] and fabrics.[227] Glass is a universal material in microfluidics owing to its transparency, chemical and mechanical stability, resistant in organic and inorganic solvents and high bonding strength, up to 12MPa.[228, 229] Silicon has the same advantages as glass such as surface stability and solvent compatibility[230] and was thus widely used prior to the use of other materials.[231] On the other hand, polymers are inexpensive and are fabricated faster than glass and silicon. Additionally, they are robust, optically transparent, biocompatible, and replicated quiet easily.[232, 233] Papers and fabrics are newly emerging materials in microfluidic fabrication, offering disposability and cost effectiveness.[227, 234]

Figure 1.17 Microfluidic device.[235]

1.14.1 Electrochemical cells on-a- chip

After the big expansion of EC and MS as a mimicry tool for metabolism[168], in 2009 Odjinik *et al.*[236] developed the first electrochemical cell on-a-chip. In particular a miniaturized three electrode structure was transferred into a miniaturized device. The chip was designed for cases of limited sample volume and high electrochemical conversions. The miniaturised device as shown in (Figure 1.18) was fabricated by two glass (Pyrex^{TM}) wafers bonded together by press and annealing treatment of 450 ^{o}C for 1 h.

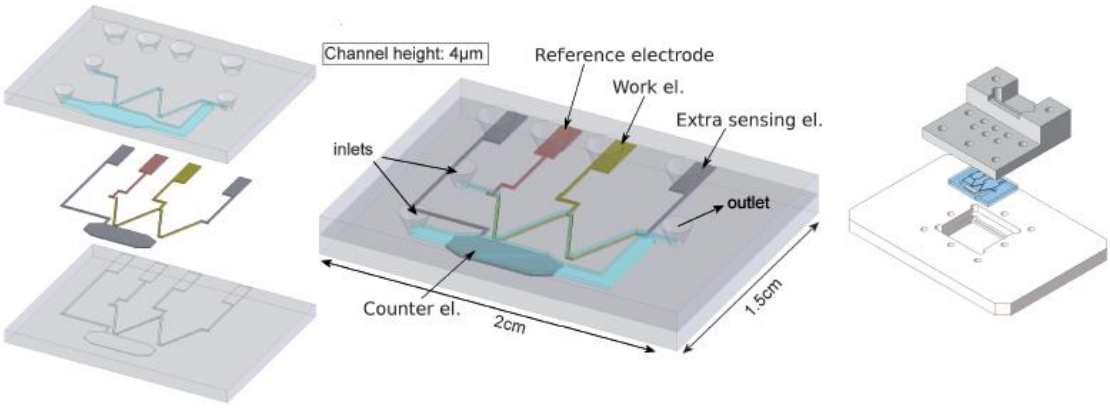

Figure 1.18 Electrochemical cell on-a-chip, reprinted with permission from Odijk *et al.*[236]

The bottom wafer was etched with four individual wells for the integration of the platinum working, palladium pseudoreference, and platinum auxiliary electrodes, which was placed in a side channel to prevent the detection of unwanted redox products. Additionally, an extra platinum sensor electrode was present for detection purposes and, in particular, for the identification of the newly synthesised metabolites. The main channel was etched in the top wafer with a volume capacity of 9.6 nL and dimensions of 4 μm × 150 μm × 16 μm (height, width, length). Also, a chip holder was developed on the basis of total dimensions of the chip for better chip connections.

The instrumental set-up was similar to the conventional approach, as described first by the Karst research group.[183, 184] Drug solutions were infused into the microfluidic device via two syringes pumps and potentials were applied by a potentiostat; then, the electrogenerated products were collected in a 10 μL loop owing to differences in the flow rates between the chip (1 μL min^{-1}) and separation column. By switching the valve, the metabolites were directed first to a separation column and then to a mass spectrometer for detection (Figure 1.19). Amodiaquine was used as a drug probe by comparing the data with the conventional methodology; the particular chip design generated comparable products in the limited volume of 9.6 nL.

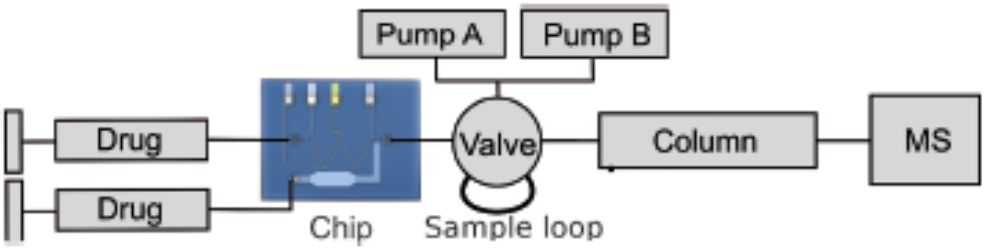

Figure 1.19 Instrumental set-up, reprinted with permission from Odijk *et al*.[236]

The second aim regarding the high conversion efficiencies was reordered using a chip and UV-Vis spectrometer at a constant flow rate of 1 μL min^{-1}. Ferrocyanide, with its well-known absorption in the UV-Vis region, was investigated with CPE in reductive and oxidative conditions. The calculated conversion efficiency was 97%, as estimated by the absorption bands of ferrocyanide and its products.

The same research group developed an improved design[237] for high conventional efficiencies, at higher flow rates up to 8 μL min^{-1}. The novelty of the design relies on the frit channels (9.4 mm length and cross sectional area of 5μm x 100μm) that were placed in between the working and counter electrode channels, thereby providing a uniform distribution of the current. In detail, the microfluidic devics, as seen in (Figure 1.20), was fabricated by Micronit (Netherlands) and composed of two glass wafers; the pseudoreference electrode was placed next to the inlet and the flow splits equally between the platinum working or platinum counter channels. The outlet of the working electrode was coupled externally with a chip ESI source.

The drug solution was infused constantly into the inlet of the chip, and the outlet of the working electrode was coupled with the ESI chip via a grounded metal capillary that

provided sufficient electrical resistant and the generated ions were detected by MS. The products formed from the counter electrode were emptied to a waste container to reduce errors from unwanted products.

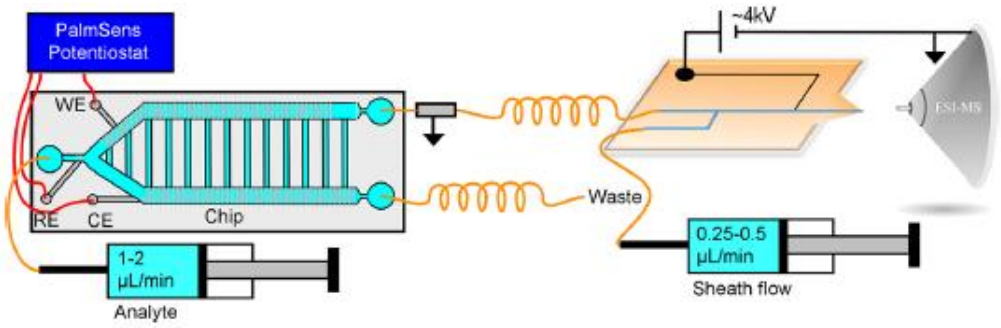

Figure 1.20 Microfluidic device connected to a microchip ESI, reprinted with permission from Odijk *et al*.[237]

Recently, the design was slightly modified by the same research group to reduce the transfer time between the electrochemical process and MS detection.[238] This was achieved by integrating a commercially available stainless steel needle via a nanoport assembly at the end of the working electrode (Figure 1.21). As a result, unstable reactive intermediates such as the short-lived chlorpromazine radical cation could be identified. The calculated transit time was very fast, between 3 s and 5 s, as compared to that of conventional flow cells using conventional capillary tubing that require 1 min. Additionally, the reactivity of the generated metabolites towards biomolecules such as endogenous thiols and proteins was investigated by a simple modification of the set-up, which involves a second infusing pump with GSH and the addition of a reaction coil.

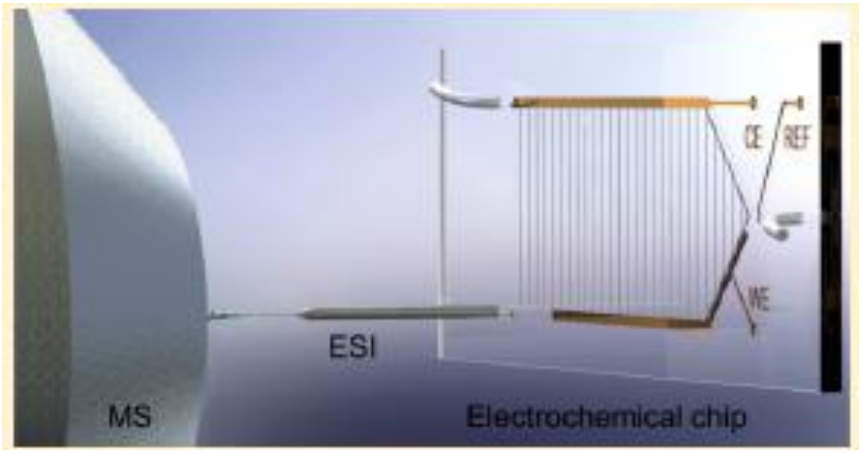

Figure 1.21 Chip/MS, reprinted with permission from Van den Brink *et al*.[238]

1.15 Aims and objectives

Aims

Development of an inexpensive and fast screening methodology for tracking metabolism based on a pure instrumental approach. The methodology would involve the hyphenation of EC with MS, aiming to reduce the expensive and time consuming use of the current *in vitro* and *in vivo* studies. In addition, it will address issues related with the unethical use of animal models, in pharmaceutical and medical research. SPEs as inexpensive sensors with a three electrode configuration can provide an ideal synthesizing tool for the electrochemical generation of various reactive intermediates. The overall aim was the development of a microfludic device for tracking reactive metabolism. Thus, chips that can fasciliate electrochemistry for the generation of reactive metabolites has been the focus of the present study rather than the metabolite quantitation. The system would target the identification of the frequently observed phase I soft electrophiles such as quinones, quinone imines, quinone methides and radicals, which are subsequently trapped by GSH during phase II metabolism. In addition, the screening methodology must have a wide range of applicability since the selected metabolites are observed in various compounds such endogenous neurotransmitters, over the counter formulations, prescribed drugs and essential oils such as dopamine (DOPA), acetaminophen (APAP), raloxifene (RLX), doxorubicin (DOXO) and eugenol, respectively.

Objectives

1) Mimicking phase I and phase II metabolic reactions of DOPA, RLX, DOXO and eugenol on a bare SPE via CPE and offline MS.
2) Integration of a SPE into a polycarbonate microfluidic device for the development of an inexpensive and reusable platform for monitoring the reactive metabolism of DOPA, RLX, DOXO and eugenol. The electrogenerated metabolites would be synthesized on the surface of the SPE and subsequently react with GSH within a serpentine channel.
3) The online hyphenation of the microfluidic device with ESI/ MS for the detection of the phase II GSH adducts, providing in this way an automated and simple methodology.

Chapter 2: Materials and methods

2.1 Instrumentation

2.1.1 Potentiostats

Calibration studies of DOPA, RLX, eugenol and DOXO were carried out in bare SPEs using an SP-50 potentiostat (Bio-Logic, France) controlled by EC-Lab V10.34 software (Bio-Logic, France). Electrochemical studies of APAP, DOPA and RLX were conducted within the polycarbonate microfludic device using a PalmSens potentiostat (PalmSens, Netherlands) controlled by PSTrace 4.0 software.

2.1.2 Electrodes

A three-electrode configuration (working electrode, reference electrode, and counter electrode) was used for all the experiments.

2.1.2.1 Screen printed electrodes

SPEs were purchased from DROPSENSE (Spain), the three electrodes (working, reference and counter) were printed into the ceramic substrate as ink patterns. The conncetions of the sensor were fabricated with a silver ink and covered with a blue insulator (Figure 2.1). DS-150 (DROPSENSE, Spain) SPEs containing a carbon working electrode of a 4 mm diameter, a silver reference electrode, and a platinum counter were used for the electrochemical studies involving the simulation of RLX. APAP, DOPA, eugenol and DOXO, were investigated with DS-110 (DROPSENS, Spain) containing a carbon working electrode of a 4 mm diameter, a silver reference electrode, and a carbon counter electrode An edge connector interface (DROPSENS, Spain) was used to connect the SPEs with the potentiostat.

.

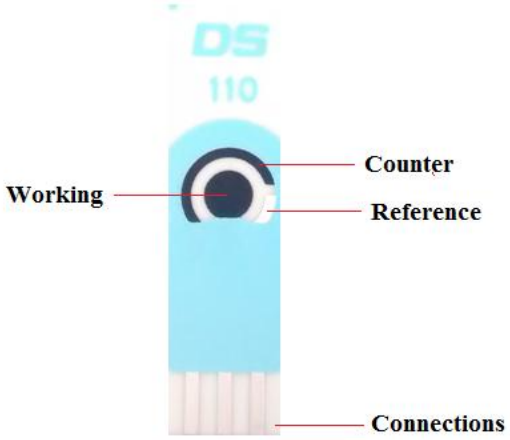

Figure 2.1 DROPSENS SPE.

2.1.2.2 Conventional electrodes

A glassy carbon electrode with a 3 mm diameter was used as the working electrode (BASi, USA), a silver/silver chloride, as the reference electrode (BASi, USA) and a platinum wire, as the counter electrode. The working electrode was maintained by mechanical polishing with a wetted rayon polishing cloth using 0.3 µm alumina slurry (Presi, France).

2.1.2.3 Conventional flow cell

The µ-PrepCell (Antec, Netherlands) as shown in (Figure 2.2) was composed of a working glassy carbon electrode, a Pd/H_2, reference electrode, and a titanium counter electrode. The total volume of the cell was 11 µL, using a 50 µm spacer. The cell was controlled by the Dialogue software and a coulochem potentiostat, all obtained from Antec (Netherlands).

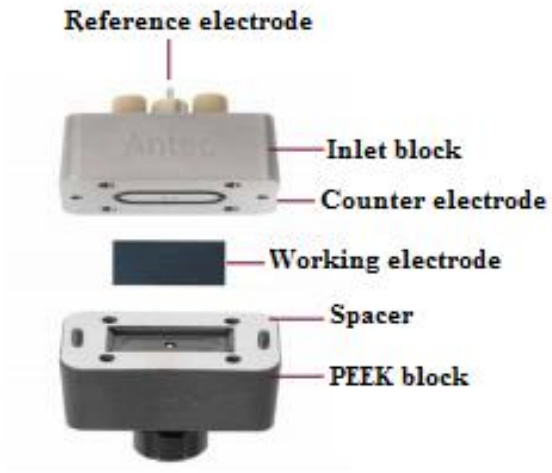

Figure 2.2 µ-PrepCell.[174]

2.1.3 Mass spectrometers

An LCQ classic ion trap mass spectrometer (Thermo Scientific, UK) was used that was coupled with an ESI and controlled by the Xcalibur 2.0. Alternatively, on a few occasions, an Esquire HCT ultra II ion trap was also used, coupled with ESI and controlled by the compass 1.4 software.

2.1.4 SPEs coupled offline to MS

In offline coupling, the electrochemical synthesis and detection were optimized indepently since the SPEs were not connected directly with the MS. SPEs were used without any treatment, and each time (n=3), a new strip was used to avoid memory effects in the carbon ink surface. The SPE was connected via an edge conncector interface to the potentiostat (Figure 2.3). The sample solution (50 µL) of either $2.5x10^{-5}$ M DOPA, RLX, eugenol, DOXO in the presence of $5x10^{-5}$ M of GSH were loaded with a pippet on the three electrode configuration and electrolyzed at a specified time, to allow the metabolic

synthesis, at the given potential, by CPE. After the completion of the electrolysis, the droplet containg the electogenerated metabolite was collected with a pippet and analysed by ESI mass spectrometry for metabolite identification. The mass spectrometric conditions are outlined below:

m/z range: 75-1400, 145-2000, 150-2000
Spray voltage [KV]: 4:05 or - 4:05
Spray current [μA]: 0.39
Sheath gas flow rate: 34.42
Auxiliary gas flow rate: 9:45
Capillary voltage: 47.72
Capillary temperature [$^{\circ}$C]: 200.30
Tube lends [U, SP]: 35.00
Flow rate: 350 μL min^{-1}

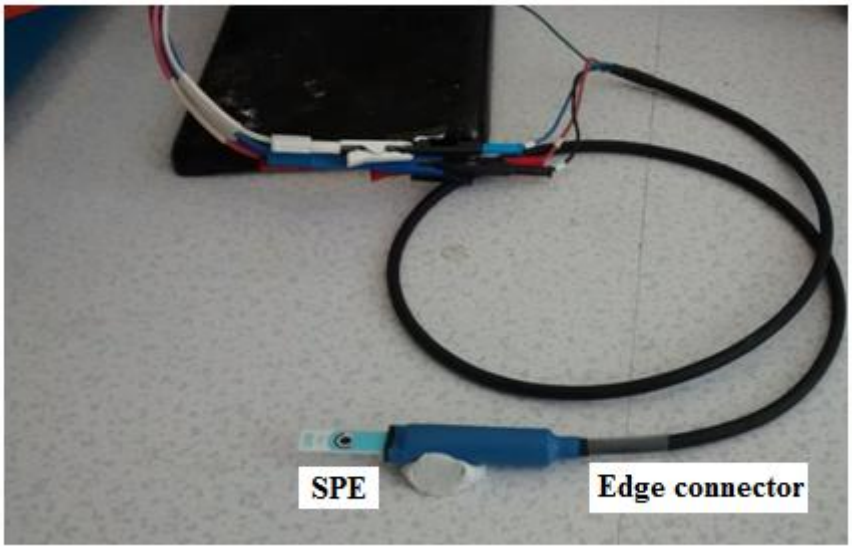

Figure 2.3 Offline electrochemical synthesis. SPE was concected via an edge connector interface with the potentiostat, permiting in this way the electrochemical synthesis of the metabolites.

2.1.5 Microfluidic device

A microfluidic device with a SPE (Figure 2.4) was developed and used for the formation of phase II GSH adducts. The chip was made of three polycarbonate layers, bonded together with a double adhesive tape and silicon rubber. The fluidic connections, the 32 µL chamber and a 24 µL serpentine channel were drilled in the middle layer using a CNC machine (Datron, Germany). An O-ring with a 1.2 cm diameter was placed around the SPE chamber to prevent leakage. The general dimensions of the micro-device were 1.8 cm × 3.3 cm (length x width). The actual electrochemical synthesis of the metabolites occurred within the SPE chamber, which served as a miniaturized electrochemical cell and the GSH conjugation within the serprtine chamber.

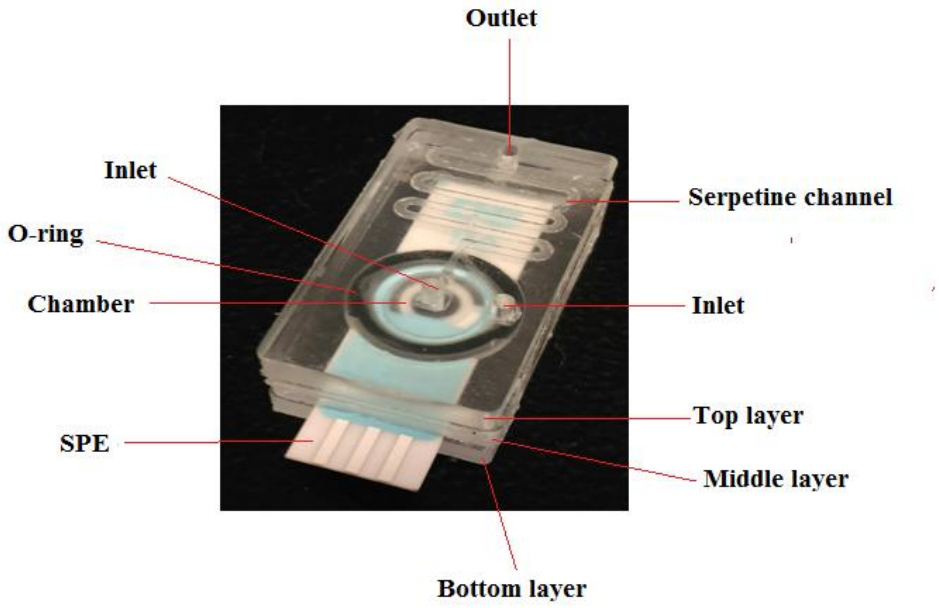

Figure 2.4 Polycarbonate microfluidic device.

2.1.6 Microfluidic device coupled online to MS

The microfluidic device was connected directly to the ESI/MS (Figure 2.5) via transfer capillaries.In the particular instrumental set up, the electrochemical synthesis and detection were optimized together. Solutions of $2.5x10^{-5}$ M APAP, DOPA, and RLX in 0.1 M ammonium acetate (pH 7 or pH 7.4) were infused constantly by an infusion pump into the chip, at the optimized flow rate of 5 $\mu L min^{-1}$ .GSH solution ($5x10^{-5}$ M). In the same buffer was also infused into the chip and directed to serpentine channel for GSH conjugation. Potentials were applied through a palm sense potentiostat (Palmsense, Netherlands) via an edge connector interface (DROPESENSE, Spain).

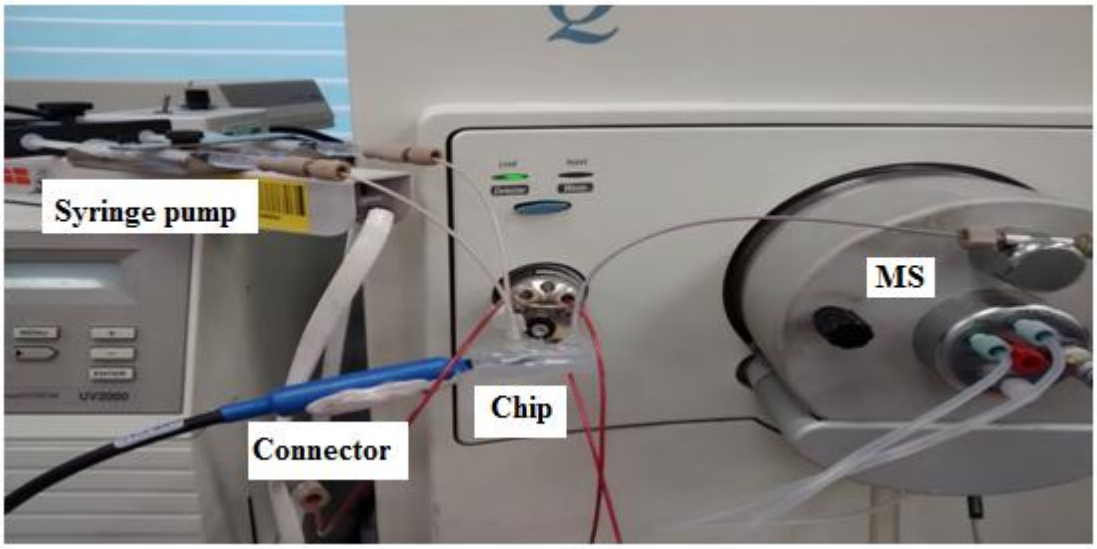

Figure 2.5 Online coupling of chip with MS. Electrochemical synthesis and detection were optimized together since the microfluidic device was connected directly with the mass spectrometer.

Each time (n=3) a new microfluidic device was used to avoid memory effects.The generated GSH-adduct travelled to ESI/MS via transfer capillaries for detection**.** The mass spectrometric conditions are outlined below:

m/z range:145-1000, 150-1000
Spray voltage [KV]: 4:05
Spray current [µA]: 0.39
Sheath gas flow rate: 50
Auxiliary gas flow rate: 0
Capillary voltage: 47.72
Capillary temperature [^{O}C]: 200.30
Tube lends [U, SP]: 35.00
Flow rate: 5 µL min^{-1}

2.2 Reagents

All the chemicals were utilised without further purification. The solutions were prepared using water that was deionised in the laboratory using the Elgastat prima 3 reverse osmosis unit (Elga Ltd., High Wycombe, UK).

2.2.1 Solutions of exogenous and endogenous solutions

RLX (>98%) was purchased from Sigma Company (UK). Considering the poor solubility of the compound in water, a stock solution of RLX ($2.5x10^{-3}$ M) in methanol was prepared and then diluted in aqueous buffers for molar concentrations of $2.5x10^{-4}$ M and $2.5x10^{-5}$ M. Eugenol (99%) was received from Alfa Aesar (UK) and prepared in the same fashion as RLX, with stock solutions in ethanol; On the other hand, water soluble compounds such as GSH, DOPA and DOXO were purchased from Sigma (UK) and LC (USA) respectively and dissolved directly in aqueous buffers. Phosphate buffers in pH 1, 2, 3, 4, 5, 6, 7, 8 were prepared by potassium phosphate monobasic 99% (Sigma, UK) and sodium phosphate dibasic 99% (Sigma, UK), adjusted accordingly with phosphoric acid (Fisher, UK) and NAOH (Alpha, UK). Ammonium acetate and acetic acid were received from Fisher (UK), the former was adjusted to 7.4 with ammonium bicarbonate (Fisher, UK).

2.3 Reuse of SPEs

According to literature[115], SPEs are used as single shot sensors with reliable data. However for the development of a reusable microfluidic device, the multiple use of the same sensor is essential. Thus, identification of the memory effects in SPEs and the effective removal of the adsorpted materials via the appropriated treatmetment method can provide a reusable solution for the microfluidic device.

2.3.1 Memory effects of SPEs

Identifying the nature of memory effects provides a tool for comparison of the treatment methods. The memory effects were identified by CV (n =10) on the same SPE, without any treatment in between the cycles. In this case, 1 mM of APAP was chosen as a model compound in 0.1 M phosphate buffer, pH 6.9. The result of this investigation with the measured potentials and currents is presented in (Table 2.1). According to the obtained potentials and currents, the multiple use of SPE without any treatment, generated non-reproducible data for the majority of the tested parameters. The general trend regarding the cathode potential, involved a significant shift to more negative values, reaching -0.280 V on the 10^{th} cycle. Highly reproducible cathode currents were obtained for all the test cycles with only a slight increase of 0.001 mA during the last four cycles.

Table 2.1 Untreated SPE.

Cycles	Anode potential (V) (n = 3)	Anode current (mA) (n = 3)	Cathode potential (V) (n = 3)	Cathode current (mA) (n = 3)
1st (Single use)	0.313	0.050	-0.060	-0.025
2nd	0.342	0.048	-0.070	-0.025
3rd	0.356	0.047	-0.080	-0.025
4th	0.370	0.046	-0.110	-0.025
5th	0.343	0.045	-0.144	-0.025
6th	0.280	0.043	-0.203	-0.025
7th	0.270	0.041	-0.231	-0.026
8th	0.262	0.040	-0.250	-0.026
9th	0.251	0.037	-0.260	-0.026
10th	0.265	0.037	-0.280	-0.026
-	RSD: 14.6%	RSD: 10.5%	RSD: 50.6%	RSD: 2.0 %

The anode potential showed variation, as seen during the first four cycles – the potential increased by 0.057 V. However, after the 4th cycle, the potentials were reduced with a decrease of 0.105 V until the 10th cycle. The anode current showed a decrease, with the first five cycles generating relatively reproducible data within the range of 0.050–0.045 V; however, in the first and last cycles, the currents produced non-reproducible results. The greatest variation during the course of 10 cycles was seen in the cathode potential (RSD: 50.6%) and in anode potential (RSD: 14.6%). In contrast, anode current (RSD: 10.5%) and cathode current (RSD: 2.0%) presented a lower variation and thus more stability.

The memory effects were reflected in the shape of the voltammograms obtained. Repeating the experiment on the same electrode caused a peak broadening, in both anode and cathode potentials (Figure 2.6). As the numbers of cycles increased, the peak broadening became more prominent owing to the continued adsorption of material on the electrode surface.

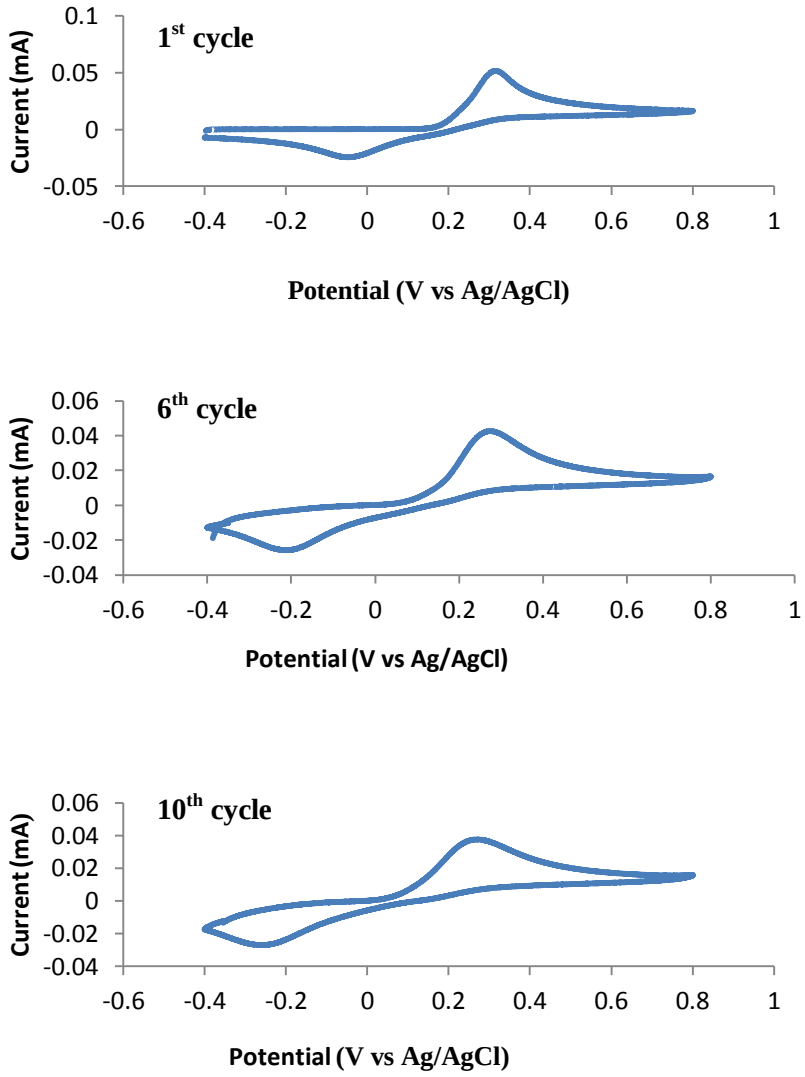

Figure 2.6 Peak broadening effect in untreated SPE. As the cycles were increased the anode potential shifted to more positive values and the cathode potential to more negative values due to the continuous adsorption.

In order to compare the reproducibility and memory effects between SPEs and conventional electrodes, the same experiment was conducted on a glassy carbon electrode since both types of electrodes are made from carbon and thus are more closely related .The data are shown in (Table 2.2).

Table 2.2 Glassy carbon electrode.

Cycles	Anode potential (V) (n = 3)	Anode current (mA) (n = 3)	Cathode potential (V) (n = 3)	Cathode current (mA) (n = 3)
1st (Single use)	0.516	0.033	0.040	-0.015
2nd	0.520	0.032	0.040	-0.014
3rd	0.530	0.033	0.040	-0.014
4th	0.533	0.032	0.030	-0.014
5th	0.540	0.031	0.040	-0.014
6th	0.540	0.031	0.030	-0.014
7th	0.550	0.030	0.020	-0.014
8th	0.550	0.030	0.020	-0.014
9th	0.560	0.030	0.020	-0.014
10th	0.560	0.030	0.020	-0.014
-	RSD: 2.84 %	RSD: 3.94 %	RSD: 31.4 %	RSD: 2.2 %

The memory effects were more prominent on the SPE than on the solid electrode, implying a higher surface fouling tendency. As seen in (Table 2.2), the calculated RSDs in glassy carbon presented less variation in the majority of the tested parameters as compared to the SPE (Table 2.1). Anode potentials showed a minor shifting towards more positive values with a potential difference of 0.044 V between the initial and final cycles.

Furthermore, cathode potentials were more reproducible although this parameter in the SPEs experienced a significant shift towards to more negative potentials. Stable and reproducible anode currents were also obtained, with minor fluctuation between the cycles. The RSD for anode current was slightly higher in the glassy carbon electrode than in the untreated SPE.

Fabricating materials was the main reason behind the observed memory effects in SPEs. In particular, the organic ink binders covered the active sites of graphite particles, blocking the access of the analyte, thereby preventing the electrochemical reactions from occurring. As a consequence, a limited number of graphite particles participated in the electron transfers, which were eventually blocked by the electrodeposited material. The particle coverage by organic binders was reported previously in carbon SPEs by Wei *et al.*[239] In contrast, the glassy carbon electrode is pure,[240] resulting in full exposure of the active sites to the sample solution. Moreover, the ink layers are very thin and do not provide the electrochemical and chemical stability of a glassy carbon electrode. As a result, the reproducibility cannot be maintained and the SPEs become restricted to a single use. Thus, electrode past history, adsorption, and fabricating materials alter the surface properties of the SPEs making them less suitable for multiple use, without any reactivation treatment.

2.3.2 Treatment methods

The removal of the adsorbed material was investigated via organic treatment, polishing and electrochemical activation

2.3.2.1 Organic Solvent

Cyclic voltammetry was conducted in the presence of 1 mM APAP in 0.1 M phosphate buffer (pH 6.9). The scan rate was set to 0.1 Vs^{-1} with a potential window range of -0.4 V

to 0.8 V. After completion, the sample solution was removed and 50 µL of a highly pure organic solvent such as methanol, ethanol, acetone, or acetonitrile were loaded on the three-electrode configuration for 1 min. The wash solvent was then removed and the SPE was allowed to dry. Finally, a new sample solution was loaded and a new voltammogram was recorded. The procedure was repeated 10 times using the same SPE. This was carried out with three different SPEs. A wide range of solvents were used to investigate their destructive behaviour oin disposable SPE. So

lvent treatments were adapted from previous investigations in a solid glassy carbon electrode [93] with slight modifications.

2.3.2.2 Mechanical polishing

Various materials have been used for the cleaning and regeneration of SPEs. A list with a brief description is shown in (Table 2.3). After the polishing procedure, graphite debris was removed by rinsing thoroughly with distilled water. Subsequently cyclic voltammograms were recorded in 1 mM APAP solution, over the same conditions, as described above.

Table 2.3 Mechanical polishing methods.

Material	Description
Polishing pad	SPEs were polished for 20 s with 0.3 μm of alumina on a soft polishing pad.
Office paper	Common A4 printing paper, cut into smaller pieces (1cm); polished for 20 s.
Sponge	A soft sponge; polished for 20 s.
Tissue	A soft lab tissue; polished for 20 s.
Soft brush	A soft brush; polished for 20 s.
Rough brush	An rough brush that was used for only 8 s.
Bandage	A soft bandage; polished for 20 s.
Abrasive material	Commonly used for the cleaning of MS parts; as the surface of this material was rough, the polishing was done for 10 s.

2.3.2.3 Electrochemical treatment

Potential cycling prior to or after the voltammetric analysis was tested at specified times, pH values, and scan rates (Table 2.4). The same sample solution was used as described in the previous section. The electrochemical pre activations were adapted from Noel *et al*.,[241] as applied in a solid glassy carbon electrode.

Table 2.4 Electrochemical methods.

Electrolyte	Ph	Potential window (V)	Scan rate (Vs^{-1})	Time (min)	Number of cycles	Prior or after CV
0.1 M KCL	7	-0.1-0.8	0.02	15	5	Prior
0.1 M NAOH	12	-0.1-0.8	0.02	15	5	Prior
0.1 M H_2SO_4	1	-0.5-1.3	0.02	15	5	Prior
0.1 M KH_2PO_4 / Na_2HPO_4	7	-0.4-0.8	0.02	15	7	After

2.3.2.4 Effect of treatment methods on SPEs

The investigated treatment methods failed to generate reproducible voltammograms, according to the obtained RSD**,** as shown in (Table 2.5). The treatments were repeated 10 times using the same SPE and this was carried out with three different SPEs. However, alternations in the functionality of the SPE restricted the polishing with bandage and sponge to four trials, while abrasive material and rbrush were used for five and six trials, respectively. In addition, potential cycling in phosphate buffer (KH_2PO_4/Na_2HPO_4) was limited in seven cycles. The most reproducible data for each treatment based on the calculated RSDs were obtained with ethanol (Anode potential: 5.3%, anode current: 3.3%, cathode potential: 15.0%, cathode current: 4.0%), sbrush (Anode potential: 5.1%, anode current: 4.1%, cathode potential:16.8%, cathode current: 3.7%, and potential cycling in phosphate buffer (Anode potential: 7.3%, anode current: 4.2%, cathode potential: 23.6%, cathode current: 5.5%): however the varations were still high to allow a multiple use. Comparing the obtained RSDs of the best treatments with the untreated sensor in (Table 2.1), some parameters were improved significantly. For example, in all treaments (ethanol,

sbrush, phosphate buffer) the anode potential, anode current and cathode potential presented lower variations. However the cathode current was the only parameter that generated the highest variation.

Table 2.5 Treatment methods.

	RSD (%)			
Treatment	**Anode potential (V) (n = 3)**	**Anode current (mA) (n = 3)**	**Cathode potential (V) (n = 3)**	**Cathode current (mA) (n = 3)**
Methanol	16.8	22.0	66.6	92.9
Acetonitrile	8.6	18.7	71.4	23.0
Acetone	11.7	16.7	80.6	30.0
Ethanol	5.3	3.3	15.0	4.0
Office paper	8.5	29.5	59.4	26.8
Sbrush	5.1	4.1	16.8	3.7
Rbrush	15.0	48.4	80.0	42.4
Polishing pad	8.7	1.5	19.7	5.0
Tissue	14.5	6.3	76.5	10.5
Sponge	18.3	17.3	20.0	42.4
Bandage	11.7	6.5	33.8	1.5
Abrasive material	8.5	29.4	59.4	26.8
0.1 M KCL	16.0	5.2	52.3	13.3
0.1 M NAOH	21.7	28.0	86.6	1.67
0.1 M H_2SO_4	1.5	8.4	17.2	14.3
0.1 M KH_2PO_4/ Na_2HPO_4	7.3	4.2	23.6	5.5

2.4 Surface damage to the SPEs

Besides the non-reproducible voltammograms, surface damages altered the functionality of the SPE, resulting in a restriction of their usage.

2.4.1 Solvent treatment

Ethanol had the less destructive effects on the surface of SPEs, since the working, counter, and reference electrodes remained relatively intact. However, white layers were clearly seen in the entire area of carbon ink (Figure 2.7), implying the formation of cracks in areas filled only with organic binders. The same cracks were obtained with the other solvents. Moreover, treatment with acetone, methanol, and acetonitrile destroyed the silver reference electrode completely. In terms of ethanol, a slight colour change was observed, as compared to the other solvents; however, the damage was enough to alter the physical properties of the electrode and as a consequence the functionality of the entire SPE. The colour changes were possibly due to trace sulphur impurities in organic solvents,[242] which progressively deactivated the sensor through the formation of Ag_2S. In methanol, ethanol, and acetonitrile, the carbon working ink was not affected, while in acetone treatment, the ink was removed progressively in each cycle, leading to its complete removal from the ceramic substrate. As a consequence, the working area was reduced progressively and in long-term experiments, such as a CPE, this would cause a significant reduction in the conversion efficiencies.

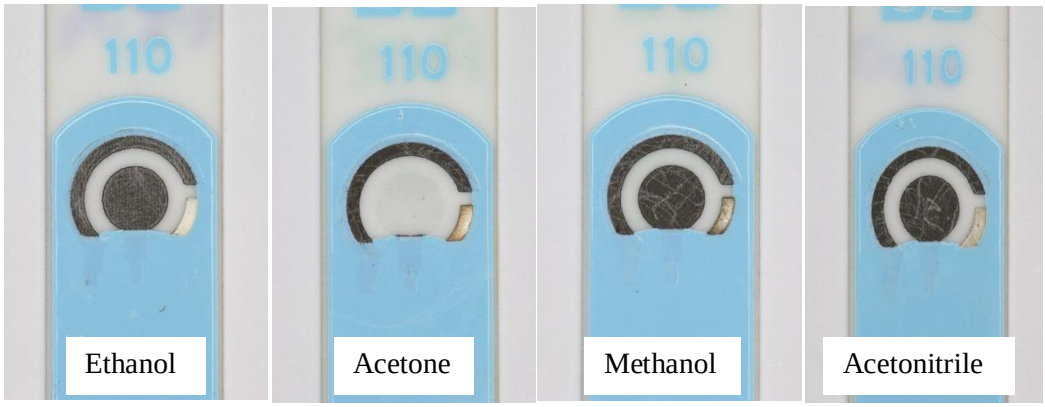

Figure 2.7 Damages on the SPE surface caused by organic solvent treatments. Ethanol caused the less destruction effects, however restrictions on functionality were seen.

2.4.2 Polishing treatments

Severe damages were observed in mechanical polishing with office paper, rbrush, and sponge, (Figure 2.8). The layers from the working electrode were removed progressively, after each polishing trial, thereby reducing the working active area and creating potential limitations for CPE experiments. On the other hand, abrasive material caused minor removal of the carbon working ink, whereas it remained relatively intact with the sbrush bandage, polishing pad and tissue. Restricted functionality with the rbrush, bandage, abrasive material, and sponge was probably caused by the breakage of carbon-carbon bonds in the graphite microstructure[243, 244] or the removal of carbon layers, resulting in the removal of the available active sites. All the other materials led to a loss in functionality after the completion of 10 cycles, probably for similar reasons. White cracks were formed in all the polishing treatments, as seen in the organic solvents.

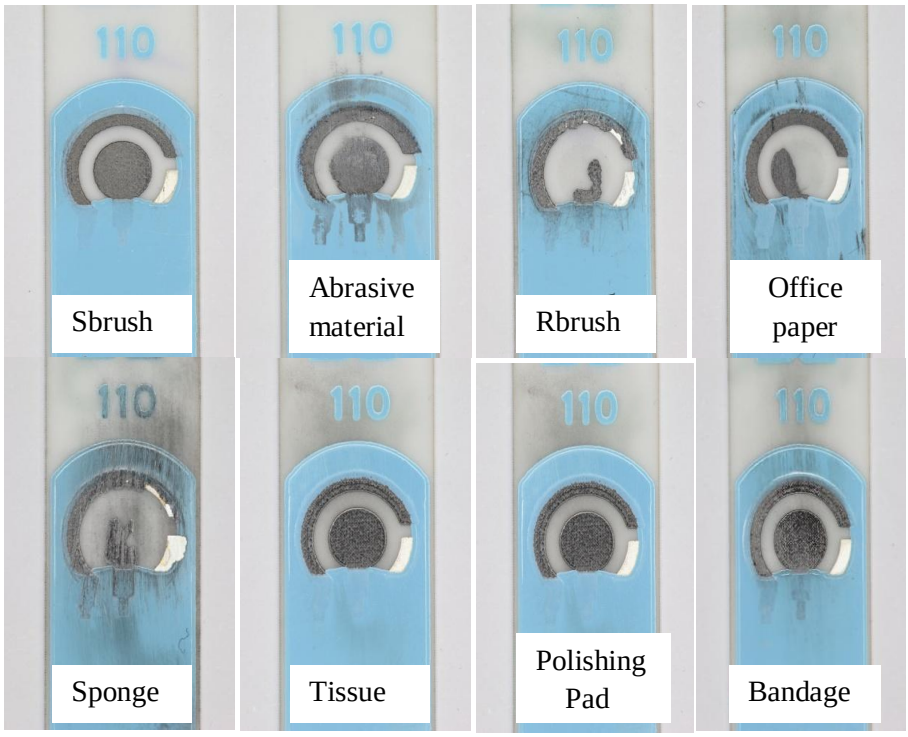

Figure 2.8 Polishing-related damages on the SPE surface. Severe damages were seen in rbrush, office paper and sponge.

2.4.3 Electrochemical activation methods

Electrochemical treatment with NAOH and HCL caused damage to the reference electrode, as seen by the colour change in (Figure 2.9). Similar damages on the reference electrode were seen in the case of organic solvent treatment, owing to the gradual deposition of sulphur impurities, from the investigated buffers and led to the formation of Ag_2S,[242]. On the other hand, cleaning with the phosphate electrolyte and activation in H_2SO_4, kept the surface intact; however, again the SPE had limited use, probably because of molecular and coulometric adsorption, which led to the attraction of counter ions on the charged electrode.[245, 246], causing alternations on the physical properties of the working electrode.The phenomenon was more intense in phosphate buffer, considering that the SPEs recorded successfully only seven voltammetric cycles.. White cracks were formed at all the electrochemical treatments, as in the previous treatments.

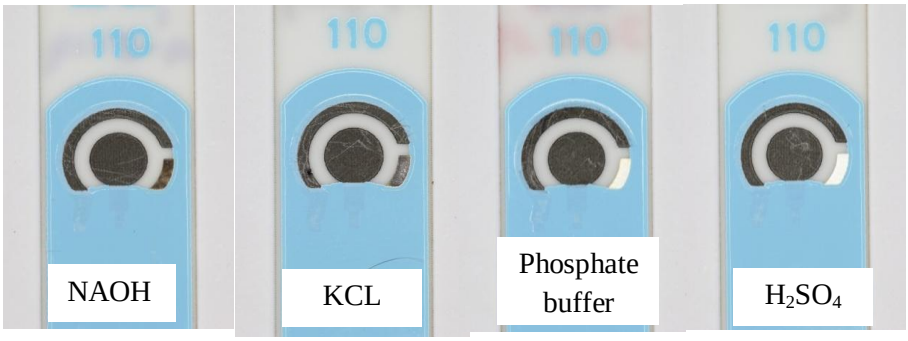

Figure 2.9 Electrochemical damages in the surface of SPE. Phosphate buffer caused the less destruction among the tested electrochemical methods.

2.5 Variation on different batches of SPE

The reproducibility of SPEs in different batches was investigated using acetonitrile treatment. The process was repeated 10 times using the same SPE and this was carried out with three different SPEs from three different batches. The obtained RSD were compared with the treatment on SPEs from the same batch and as concluded the variation was greater

among the different batches, implying poor quality control during the fabrication process and poor reproducibility. As seen, in (Table 2.6), the variation in anode and cathode potentials was found to be 9.5 % and 98.4 %, respectively. Whereas, the anode current and cathode current were 23.6 % and 34.9 %, respectively.

Table 2.6. Variation in different batches of SPEs.

	RSD (%)			
Acetonitrile Treatment	**Anode potential (V) (n = 3)**	**Anode current (mA) (n = 3)**	**Cathode potential (V) (n = 3)**	**Cathode current (mA) (n = 3)**
Same batch	8.6	18.7	71.4	23.0
Different batch	9.5	23.6	98.4	34.9

2.6 Conclusion

Memory effects were more prominent on SPEs than on conventional electrodes, owing to the fabrication process .Reusability of SPE was not archived via the treatment methods and thus the development of a reusable microfluidic device for quantitations purposes was not feasible. The kinetics were strongly affected leading to false conclusions regarding the optimum potential and as a consequence a decrease in conventional efficiencies. In addition the treatment methods altered the functionality of the sensor, restricting their usage in long term experiments such as CPE. In contrast acccording to literature, the particular cleaning methodologies were successfully applied in conventional electrodes[247-254], owing to fabrication materials. Considering the application of the chip on tracking the metabolism rather than quantitation it was feasible to use untreated SPEs. What is more, for maximum metabolite yields, pure kinetics and avoidance of strong adsorption, SPEs were used as single shot devices in the following experiments. In addition, variations were also seen in potentials via the single use of SPEs from different batches.

Chapter 3: Phase I and phase II metabolism of DOPA and RLX on a SPE

3.0 Introduction

Phase I metabolic reactions involving the transfer of two electrons and two protons, usually known as dehydrogenations, are frequently observed in metabolic research. DOPA[255] and RLX[256] are characteristic examples that can lead to toxicity via the particular metabolic reaction.

DOPA is an endogenous neurotransmitter found in dopaminergic neurons, which is metabolised to reactive dopaminoquinone via dehydrogenation ,through the catalytic action of CYP 450.[255, 257] There is evidence that the the reactive electrophile dopaminoquinone is the causal agent of Parkinson's disease. In the presence of GSH, dopaminoquinone is detoxified through the formation of DOPA-GSH adducts via Michael addition[258] (Scheme 3.1). However, in the absence of GSH, the reactive intermediate acts as a precursor for neuromelanin generation. In particular, dopaminoquinone is converted to leucodopaminochrome via intramolecular cyclization. Then, leucodopaminochrome is oxidised to aminochrome and subsequently polymerised to neuromelanin.[259] Aminochrome quinone is also probably one of the causal agents of Parkinson disease.[258]

In addition, a second reactive pathway is observed, involving the formation of depurinated adducts between dopaminoquinone with N3 adenine (Ade) and N7 guanine (Gua). A competition is observed between these two processes (polymerisation and GSH conjugation), affected strongly by the pH. In particular, in extremely acidic conditions, the amino group of dopaminoquinone is partially protonated, permitting, in this way, the dominance of depurinated adduct formation over neuromelanin, while in neutral conditions, only the formation of neuromelanin is favoured.[259]

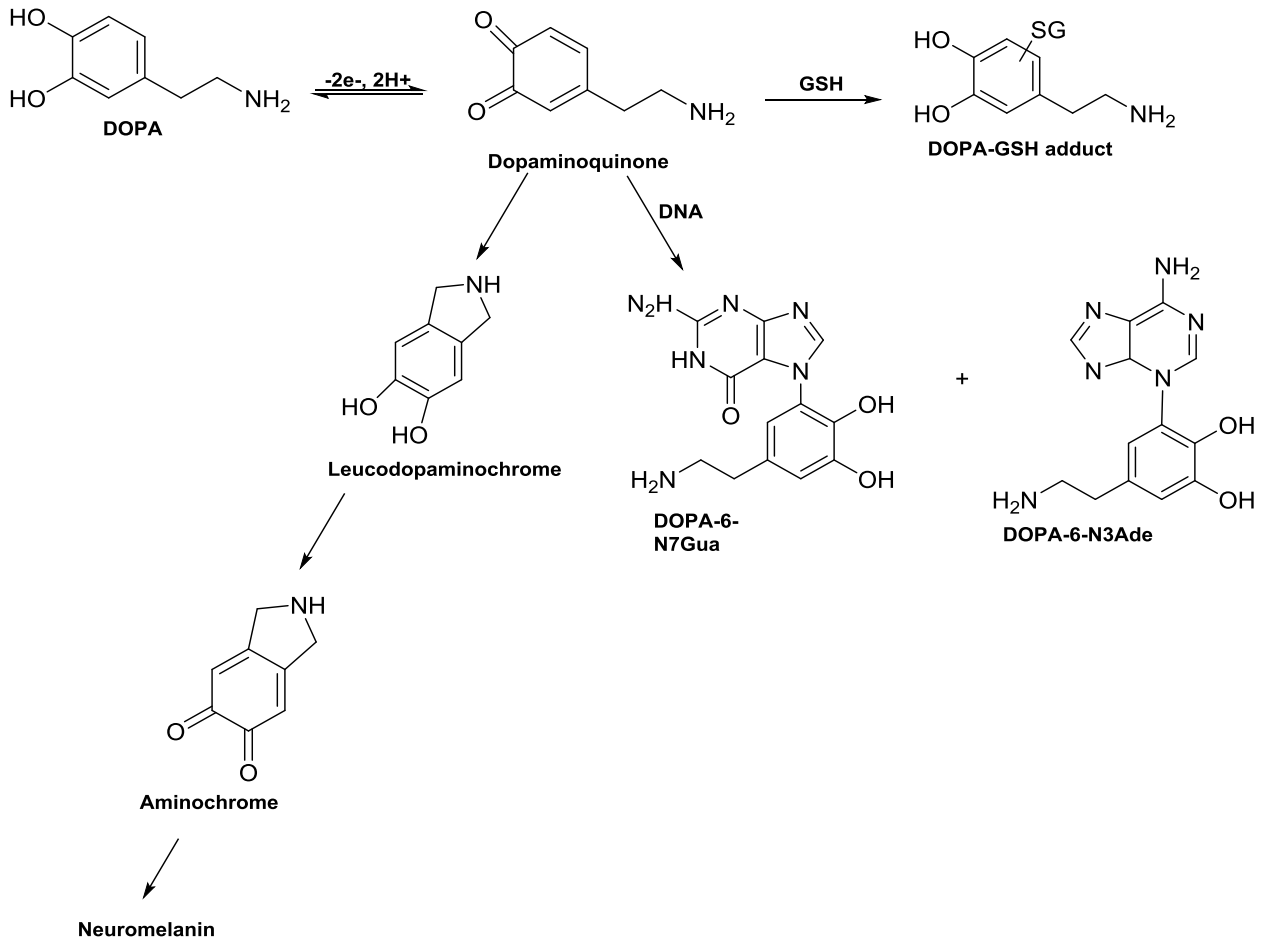

Scheme 3.1 ***In vitro*** **metabolic pathway of DOPA.[258, 259] The reactive dopaminoquinone was generated via the transfer of two electrons and two protons. Subsequently, the metabolite was covalently bonded with GSH or generated depurinated adducts. In addition, in the absence of GSH a polymerisation process had occured leading to neuromelanin formation.**

RLX is a second-generation selective estrogen receptor modulator (SERM). The drug is widely used for the treatment of osteoporosis and, currently, showed inhibitory actions in mammary tumours during clinical trials. *In vitro* studies revealed the toxicity of the drug via the formation of RLX di-quinone methide and RLX 6,7,-o-quinone intermediates by CYP 450 during phase I reactions. The metabolic activation of RLX is shown in (Scheme 3.2).[256] As can be seen, two bioactivation pathways are involved, and the first pathway shows the dehydrogenation of RLX via the loss of two electrons and two protons, leading to the formation of RLX di-quinone methide.

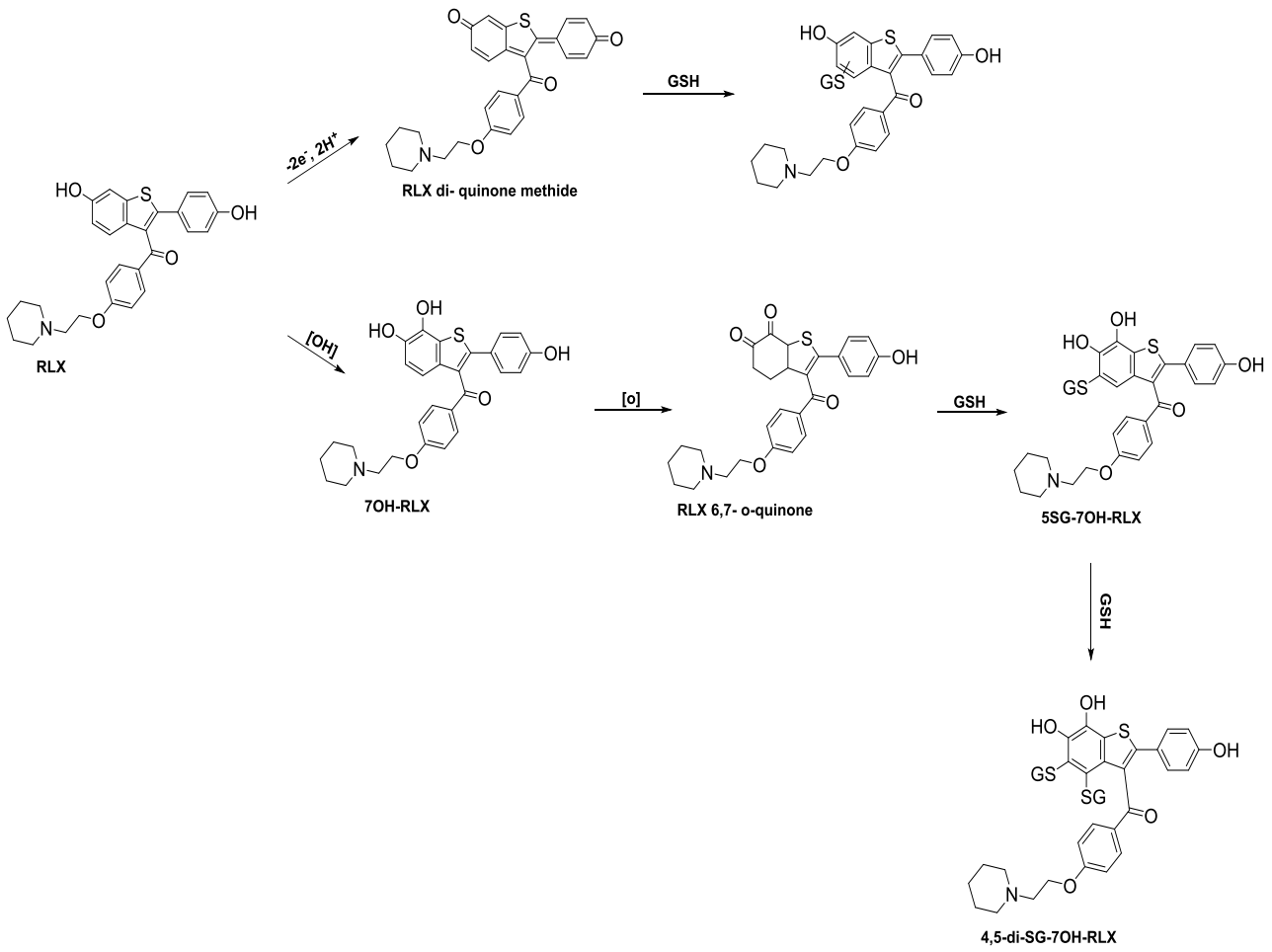

Scheme 3.2 *In vitro* metabolic pathway of RLX.[259] RLX di-quinone methide was generated via a two electron and a two proton transfer. In addition, a second metabolite was formed by aromatic hydroxylation. Both metabolites reacted covalently with GSH molecules.

Subsequently, the generated intermediate reacts rapidly with GSH and on detoxification, forms a RLX-GSH adduct. In the second pathway, RLX is hydroxylated in position C7 and then dehydrogenated via the loss of two electrons and two protons into RLX 6,7-o-quinone methide, which reacts further with GSH, forming mono- and di-GSH-adducts.

Kauffmann *et al.*[115] successfully simulated the metabolism of APAP in a bare SPE and generated electrochemically the corresponding quinone imine (NAPQI) via dehydrogenation. Herein, the possibility of generating electrochemically reactive quinones and quinone methides via the transfer of two electrons and two protons was investigated in disposable SPEs. DOPA and RLX were selected as probe compounds considering that both compounds are capable to generate the particular metabolites through the transfer of two electrons and two protons.

The objectives of the chapter were:

1) Investigate the reaction mechanisms of DOPA and RLX on SPEs.
2) Simulate the phase I reactions of DOPA and RLX .Particularly, the electrochemical generation of the reactive dopaminoquinone and RLX di-quinone methide by CPE.
3) Simulate the phase II GSH reactions via the covalent conjugation of dopaminoquinone and RLX di-quinone methide with GSH and subsequent detection by ESI/MS.
4) In addition, the mimicry of aromatic hydroxylation (two electron-two proton transfer) using RLX as probe compound, for the formation of the reactive ortho quinone and subsequent covalent reaction with GSH.

3.2 Results and discussion – DOPA

The ability of SPEs to mimick inexpensively the phase I and phase II metabolism of DOPA was investigated in detail, aiming the potential of integrating a SPE into a miniaturized device and provide an online coupling with MS.

3.2.1 Electrochemical behaviour of DOPA

DOPA solution ($2.5x10^{-5}$ M) in 0.1 M phosphate buffer (pH 5) was investigated by CV at 0.155 Vs^{-1} (Figure 3.1). The neurotransmitter was oxidized at 0.128 V during the forward scan and reduced back to its initial form at -0.08 V, during the reverse scan. The calculated separation peak potential was found to be 0.208 V and the obtained peak currents were 0.0012 mA and -0.0011 mA for anode and cathode potentials, respectively.

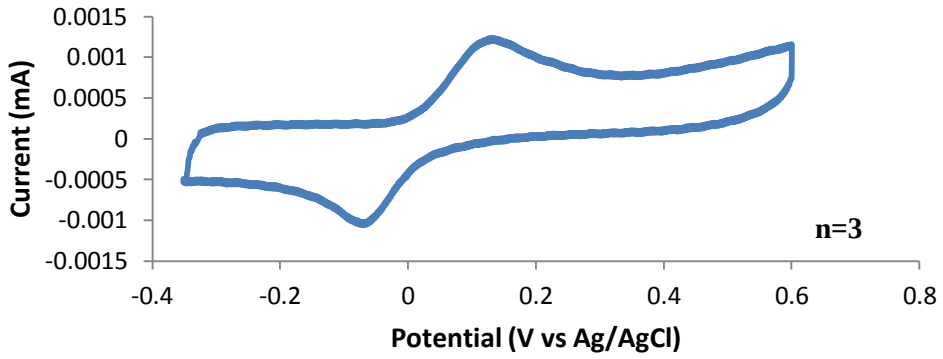

Figure 3.1 Electrochemical behavior of DOPA on a SPE. A well defined redox pair appeared at 0.128 V (anode potential) and at -0.08 V (cathode potential).

3.2.2 Effect of pH

3.2.2.1 Participation of protons

DOPA ($2.5x10^{-5}$ M) in 0.1 M of phosphate buffer solutions (pH 1, 2, 3, 4, 5, 6, 7, 8) was investigated during CV at 0.1 Vs^{-1} within the potential range of -0.3 V to 0.6 V (Figure 3.2), to investigate the participation of protons during the electron transfer process. For each pH value a new SPE was used and the process was repeated for a total of three trials (n=3). A linear relationship was obtained between the anode potential and pH, confirming the participation of protons in the system, [261] since at higher pH values the availiability of protons is reduced and as a consequence the proton competition is also reduced, leading to lower potentials. The obtained slope from the equation of the graph was 0.051 VpH^{-1}, which was very close to the Nernstian slope of 0.057 VpH^{-1}, suggesting the participation of the same number of protons and electrons.[262]

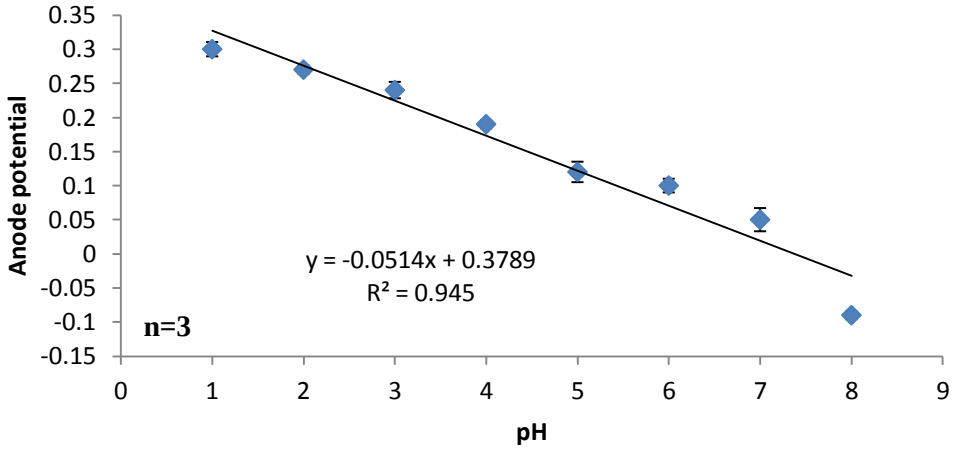

Figure 3.2 Participation of protons in DOPA oxidation. A gradual decrease on anode potential implied the participation of protons. Also, the obtained slope was close to Nernestian slope suggesting the same number of electron and proton transfer.

3.2.2.2 Stability of the generated product

The effect of pH in peak current ratios can determine the stability of the generated product. In particular, peak current ratios of a unity suggest high stability at the given pH,[90] since the obtained anode current does not interact further with molecules in solution and as a consequence the cathode current on the reverse scan has the same magnitude as the anode, leading to unity. A relatively steady state was observed in acidic conditions that was slightly reduced in pH 5 and pH 6 (Figure 3.3). In more alkaline conditions, the peak current ratios started to increase, leading to a more unstable product. Moreover, the most stable product was observed at pH 5 with a peak current ratio of 1.08 and the greatest instability was seen at pH 8, where the peak current ratio was close to 3.2. For each pH value a new SPE was used and the process was repeated for a total of three trial (n=3).

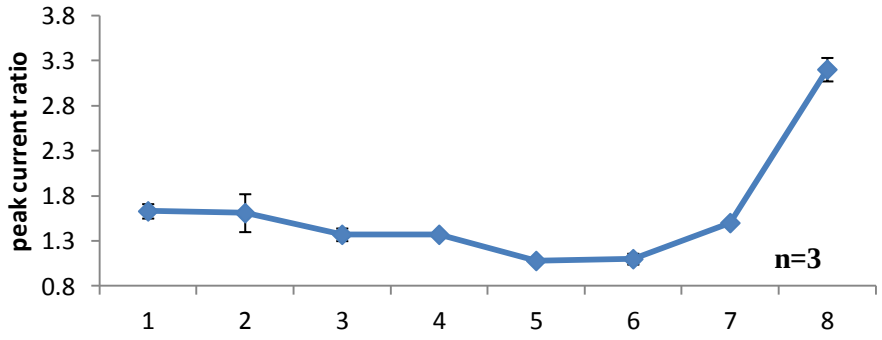

Figure 3.3 Stability of DOPA intermediate. In pH 5 the most stable product was obtained since the peak current ratio was close to unity.

3.2.2.3 Effect of pH on current

Variations in current as a function of pH, imply changes in the concentration of the investigated compound[263] due to te formaton of the electrochemical product. Anode and cathode currents presented the same behaviour until pH 4, with maximum signals found at pH 1 and 4 (Figure 3.4). In pH 2 and 3, the currents were decreased considering the non reproducible nature of SPEs, due to poor quality control, as proved in chapter 2. A current decrease was obtained at pH 5 for both, which was maintained at a relatively steady state up to pH 8 for the anode current, whereas a significant decrease was seen in cathode current. Thus, the highest product generation was found in pH values of 1 and 4.

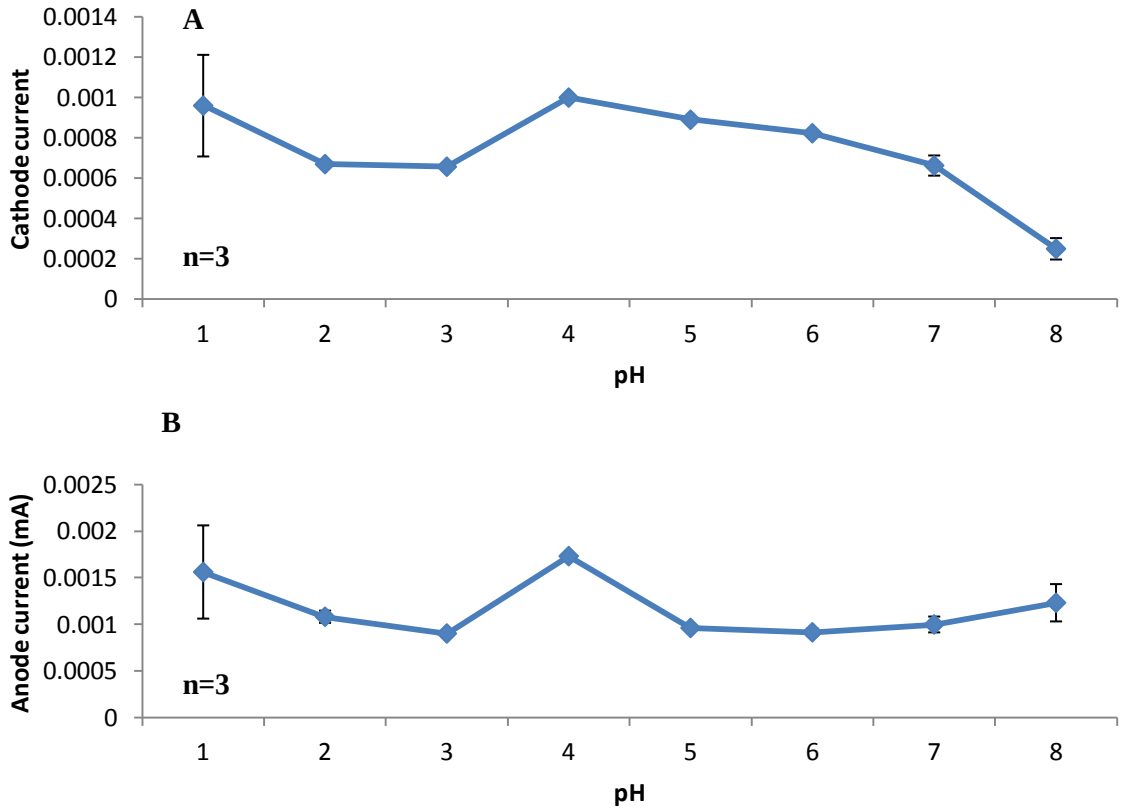

Figure 3.4 Relationship of DOPA currents with pH. A) Cathode current; B) Anode current. The highest current signals were found in pH 1 and pH 4. In alkaline conditions the lowest product formation was found. Considering the non-reproducible nature of SPE, the pHs from 1 to 4 presented instability.

3.2.3 Effect of scan rate in electron kinetics

The electron kinetics are determined by a series of investigations thought the the effect of scan rate. Herein, the effect of scan rate on DOPA was studied in the range of 0.02 Vs^{-1} to 0.155 Vs^{-1} (Figure 3.5) to characterise the elecron trasfer kinetics of the endogenous compound on the surface of the SPE. A new SPE was used and the process was repeated for a total of three trial (n=3).

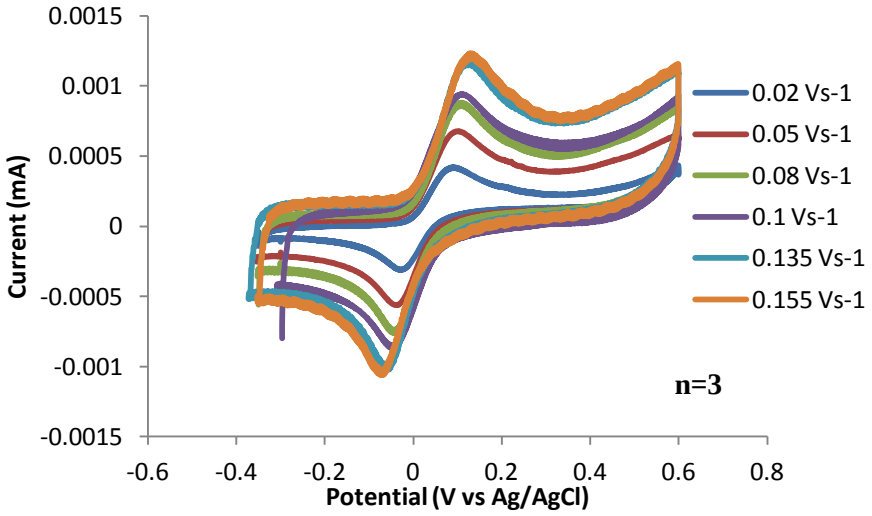

Figure 3.5 Effect of scan rate in DOPA. A series of scan rates from 0.02 Vs^{-1} to 0.155 Vs^{-1} were applied for the determination of electron transfer kinetics.

A linear dependence of anode and cathode currents with the SQRT of scan rate was observed (Figure 3.6). The separation peak potentials were higher than those expected for a diffusion control system and shifted to more positive values with increasing scan rates, suggesting a quasi reversibility[131, 132] (Figure 3.7). Additionally, the anode potentials

shifted to more positive values and the cathode potentials, to more negative values, as the scan rate kept increasing. The same electron transfer behaviour was previously seen in conventional modified glassy carbon electrodes,[263, 264] which indicated the participation of two electrons and two protons, leading to the formation of dopaminoquinone.

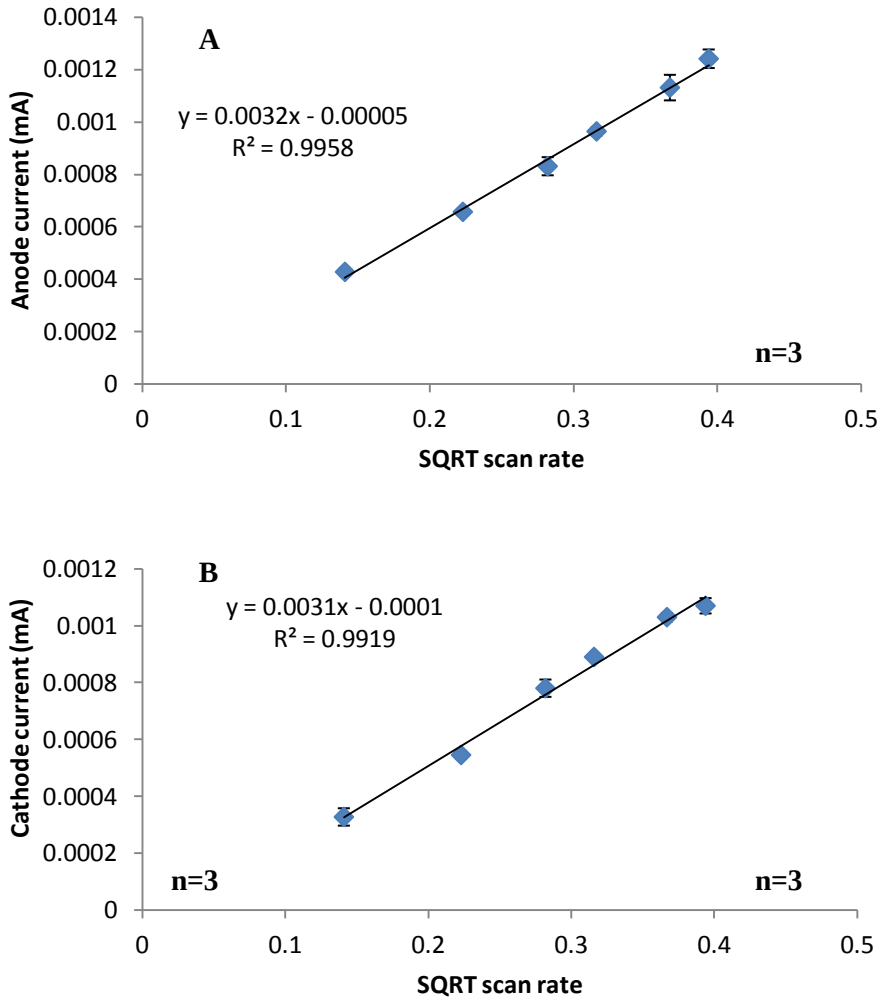

Figure 3.6 Linear dependence of DOPA currents with the SQRT of scan rate. A) Anode current; B) Cathode current. The correlation coefficient for anode current was 0.9958 and for cathode current was found to be 0.9919.

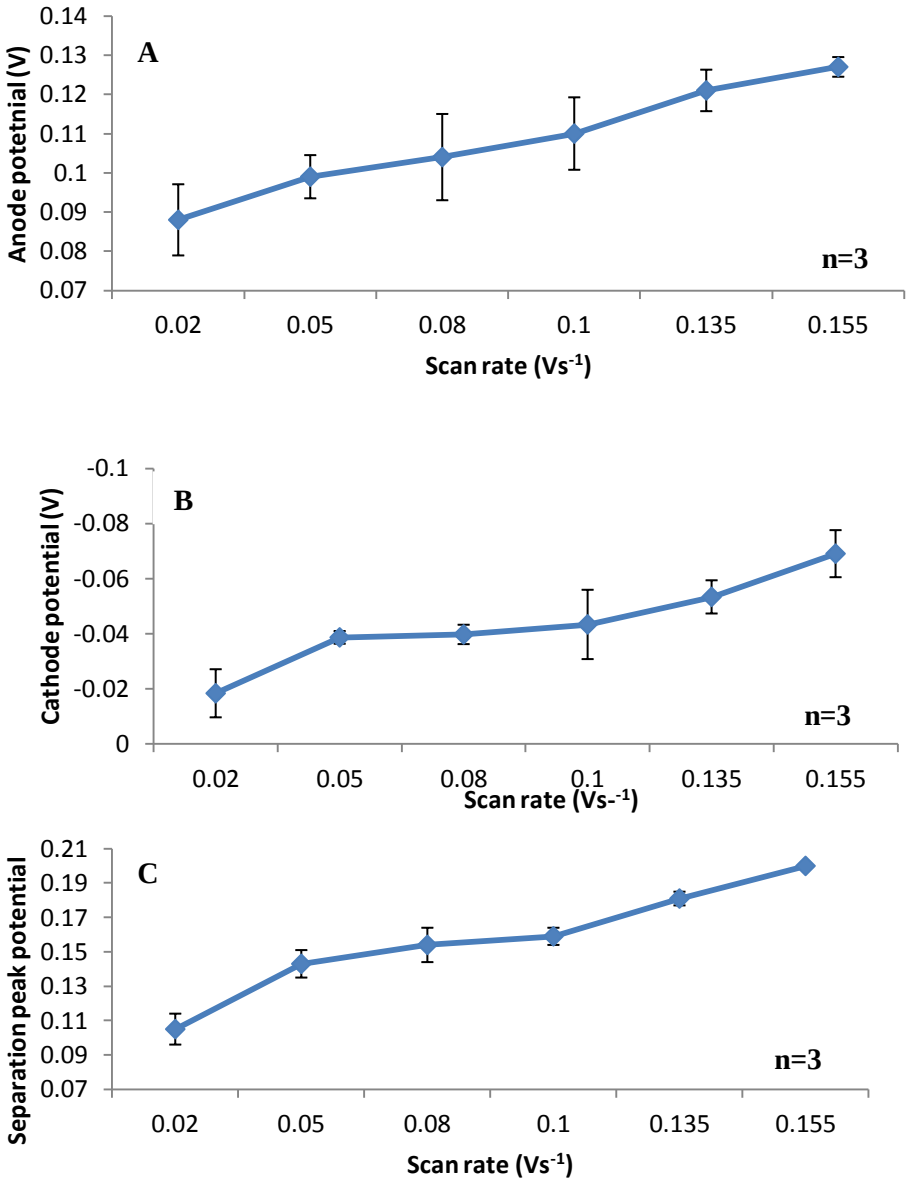

Figure 3.7 Dependence of DOPA potentials on scan rate. A) Anode potential; B) Cathode potential; C) Separation peak potential. All investigated parameters were shifted as a function of scan rate implying the slow electron kinetics of DOPA on the SPE surface.

3.2.4 Mass transport mode

The transport mode of the analyte to the electrode is determined by the slope of the log (current) vs. log (scan rate). As seen in (Figure 3.8), the obtained slopes of 0.52 for anode potential and 0.60 for cathode potential, suggested a mass transport controlled by both diffusion and adsorption.

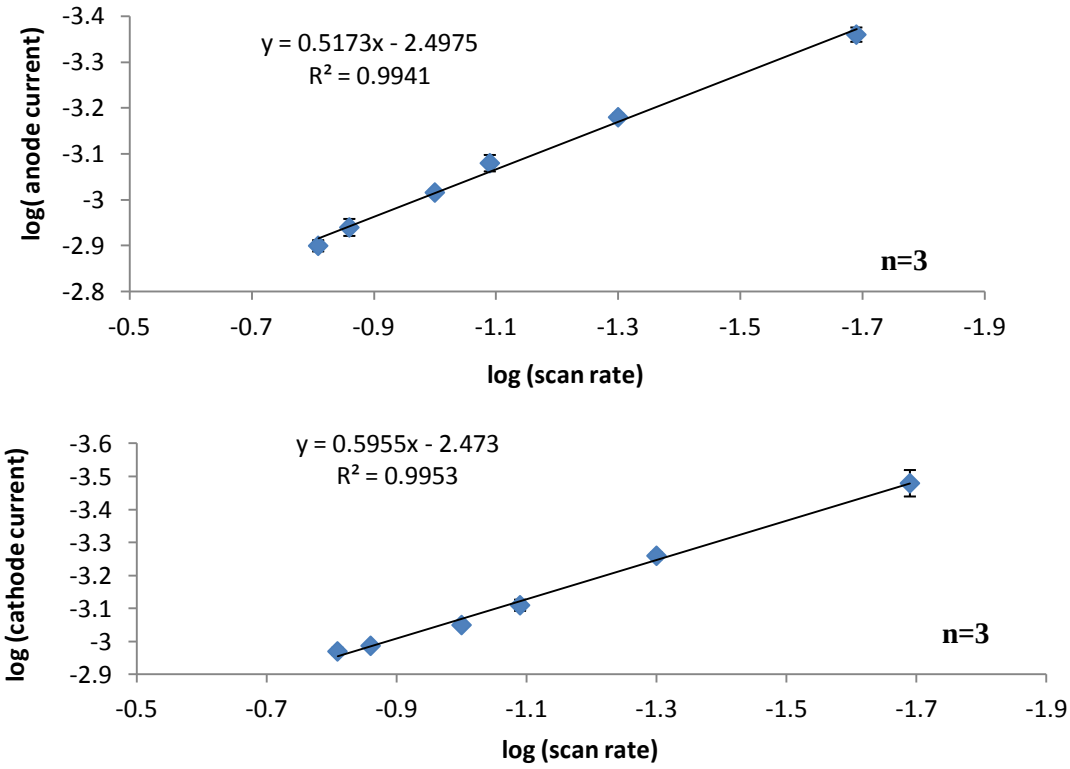

Figure 3.8 Mass transport mode of DOPA. A) Anode current; B) Cathode current. The obtained slopes indicated a mixture of both diffusion and adsorption. However, the values were closer to 0.5 and suggested the dominance of diffusion over adsorption.

In particular, slopes near 1 indicate an adsorption control process, whereas those below 0.5, a diffusion control system; values between 0.5 and 1.0 indicate a mixture of both diffusion and adsorption,[265] as in the present case. A mixture of mass transport was also seen in a modified carbon paste electrode by Manjunatha *et al.*[266] However, in the literature, cases involving either a total diffusion or a total adsorption[267, 268] have been reported with the use of solid electrodes, probably as an effect of the differences in the modified processes that have been followed.

3.2.5 Effect of concentration

Various DOPA concentrations, ranging from $2.5x10^{-5}$ M to $2.5x10^{-3}$ M, in 0.1 M of ammonium acetate (pH 7.4) were investigated by CV (Figure 3.9). For each concetration a new SPE was used and the process was repeted for a total of three trials (n=3). In higher concentrations from $5x10^{-5}$ M to $5x10^{-3}$ M, a second reductive peak was generated, which was not formed in lower concentrations of $2.5x10^{-5}$ M. Repetitive voltammetry (n = 2) generated a second redox pair, suggesting the formation of an electroactive intermediate from dopaminoquinone. The finding suggested the dependence of concentration on the formation of a second metabolite. At $2.5x10^{-5}$ M, the concentrations were very low to permit the further reaction of dopaminoquinone, while at higher concentrations; a sufficient quantity of intermediates drove the formation of multiple metabolites. The same concentration dependence was observed previously by Gonzalez-Diequez *et al.*,[269] suggesting the formation of a melanin like polymer. The redox pair was the result of the oxidation of leucodopaminochrome into dopaminochrome, which subsequently led to polymer formation. However, details of the formation and structure of the polymer were not provided.

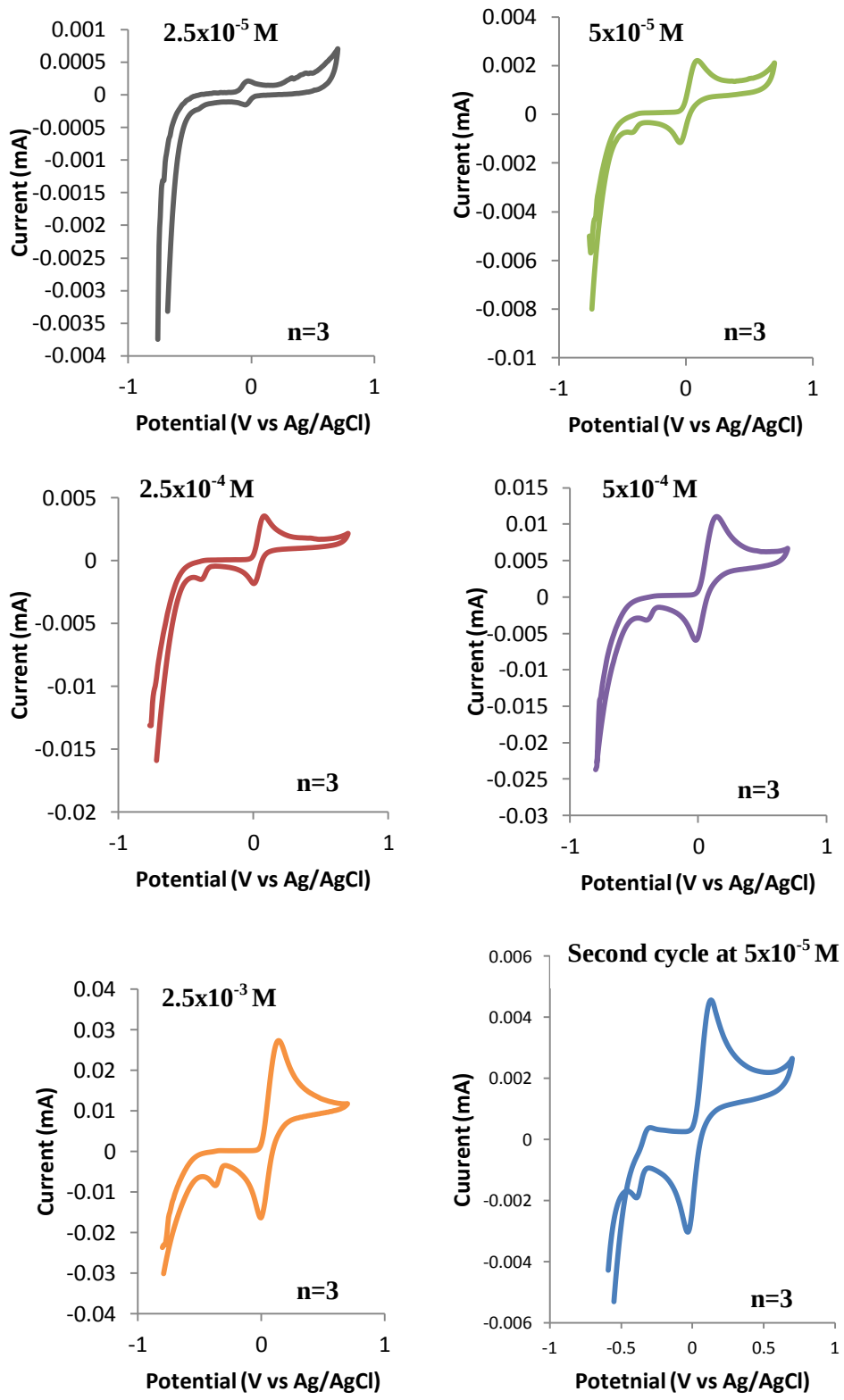

Figure 3.9 Voltammetry in various DOPA concentrations. In higher concentrations of $5x10^{-5}$ M - $2.5x10^{-3}$ M a second reductive peak appeared that was not seen during the $2.5x10^{-5}$ M of DOPA. A second cycle at $5x10^{-5}$ M generated the coresponding anode peak and suggested the oxidation of leucodopaminochrome to aminochrome.

On the other hand, a detail mechanistic investigation of DOPA in glassy carbon by Ke *et al.*[270] showed that DOPA followed an ECE reaction mechanism, leading to the formation of melanin-like polymers. As shown in (Scheme 3.3), DOPA is dehydrogenated electrochemically (E) to dopaminoquinone, followed by a chemical (C) step, which involved the intramolecular cyclization to the corresponding leucodopaminochrome. Finally, a second electrochemical (E) step dehydrogenated leucodopaminochrome to aminochrome. Subsequently, DOPA molecules reacted with aminochrome leading to polymer formation.

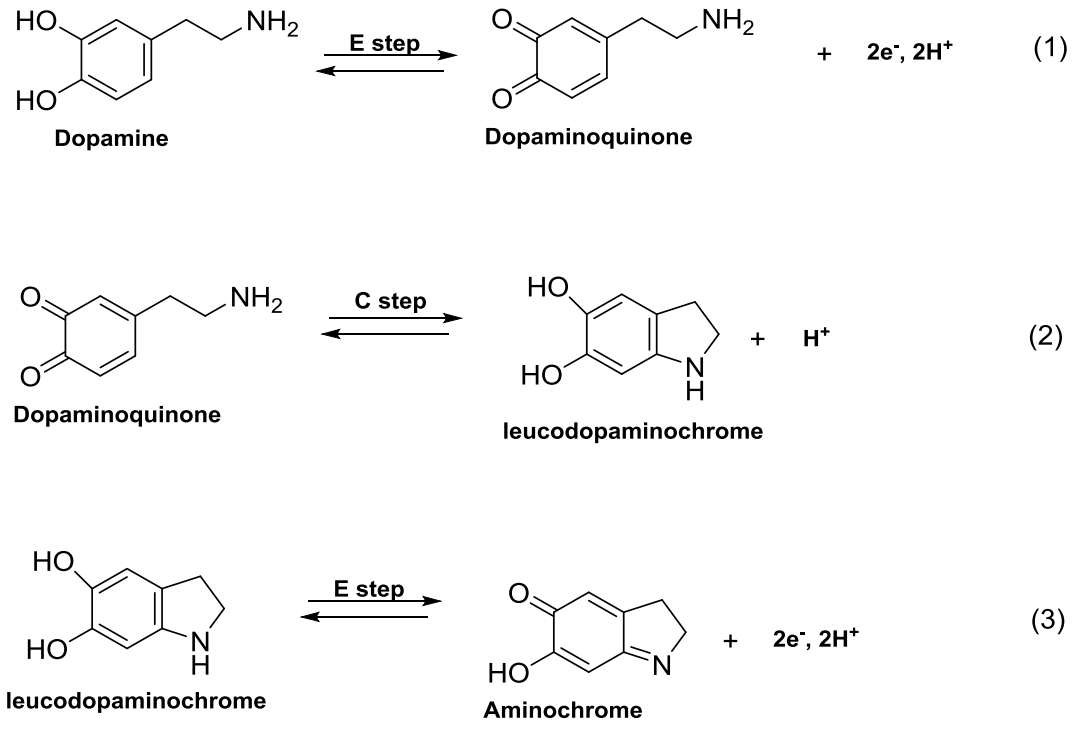

Scheme 3.3 ECE reaction mechanism in glassy carbon electrode.[269] 1) Electrochemical formation of dopaminoquinone. 2) Intramolecular cyclization of Dopaminoquinone to leucodopaminochrome. 3) Electrochemical formation of aminochrome via a two electron and a two proton transfer.

3.2.6 CV in the presence of GSH

The reactivity of the generated product in various GSH concentrations from 0 M to $2.5x10^{-4}$ M was investigated, in the presence of $2.5x10^{-5}$ M of DOPA, in 0.1 M of ammonium acetate (pH 7.4). The addition of GSH caused changes on the voltammograms (Figure 3.10): the anode current increased with increasing GSH concentration, up to $1.24x10^{-4}$ M and then decreased, owing to GSH depletion at $2.5x10^{-4}$ M In particular, the current was increased since two products were generated, the reactive phase I quinone and the phase II DOPA-GSH adduct. However, the signal was decreased at $2.5x10^{-4}$ since all of the reactive quinones reacted with GSH. Furthermore, the anode potential shifted to more positive values, indicating the formation of the GSH adduct that was also electroactive. In addition, the cathode potential reduced gradually and disappeared at $2.5x10^{-4}$ M of GSH, implying the depletion of dopaminoquinone through its covalent conjugation with GSH. Based on the obtained changes in potentials and currents, it can be concluded that a reaction occurred between the generated intermediate and GSH, which implied the possible reactivity of the generated intermediate.

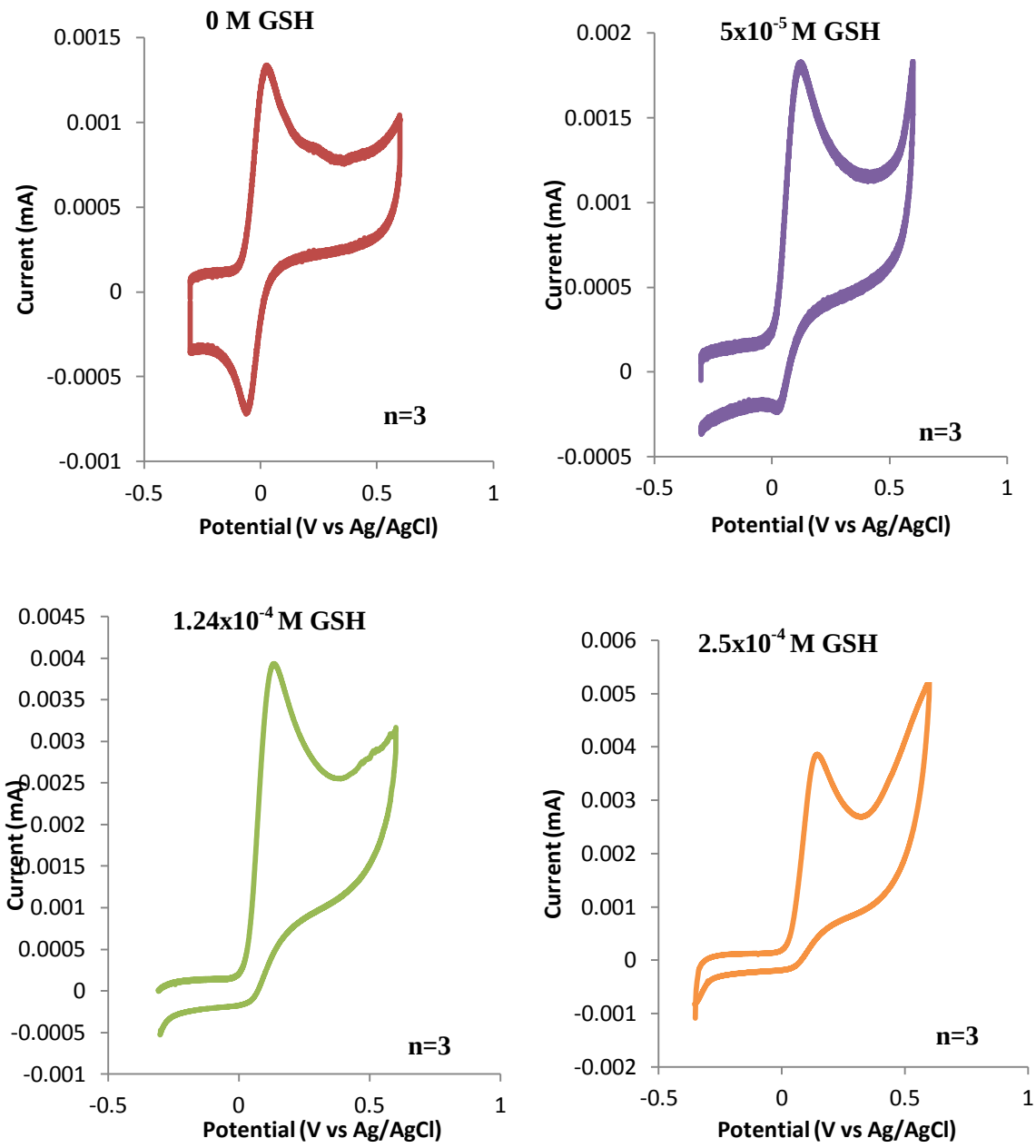

Figure 3.10 Effect of various GSH concentrations in $2.5x10^{-5}$ M of DOPA. The cathode potential disappeared at $2.5x10^{-4}$ M since the reactive dopaminoquinone was depleted via GSH conjucation. The anode current increased until the $1.24x10^{-4}$ M GSH due to the formation of the GSH adduct that was also electrochemically active. However, at $2.5x10^{-4}$ M the signal was depleted since all the dopaminoquinone molecules had reacted with GSH.

3.2.7 Potential optimization

CPE of $2.5x10^{-5}$ M DOPA in the presence of $5x10^{-5}$ M GSH, in 0.1 M of ammonium acetate (pH 7.4) was investigated for 0.5 min, in a potential range from 0.17 V to 0.52 V, with increasing steps of 0.05 V. The range was selected according to previous voltammetry studies (Figure 3.10) and recorded over a mass transport rate limit, [127] to ensure maximum metabolite formation. After the completion of CPE, the electrolysed solution was subsequently analysed offline by ESI/MS in positive ion mode. The aim was to determine the optimum potential for generating the highetst possible yields of DOPA-GSH adduct. The obtained metabolites are outlined in (Figure 3.11). The DOPA-GSH adduct was generated in all potentials leading to a DOPA depletion. However, the highest generation of DOPA-GSH adducts was observed at 0.27 V and the lowest, at 0.42 V. Thus, 0.27 V was chosen as the optimum potential for further investigations.

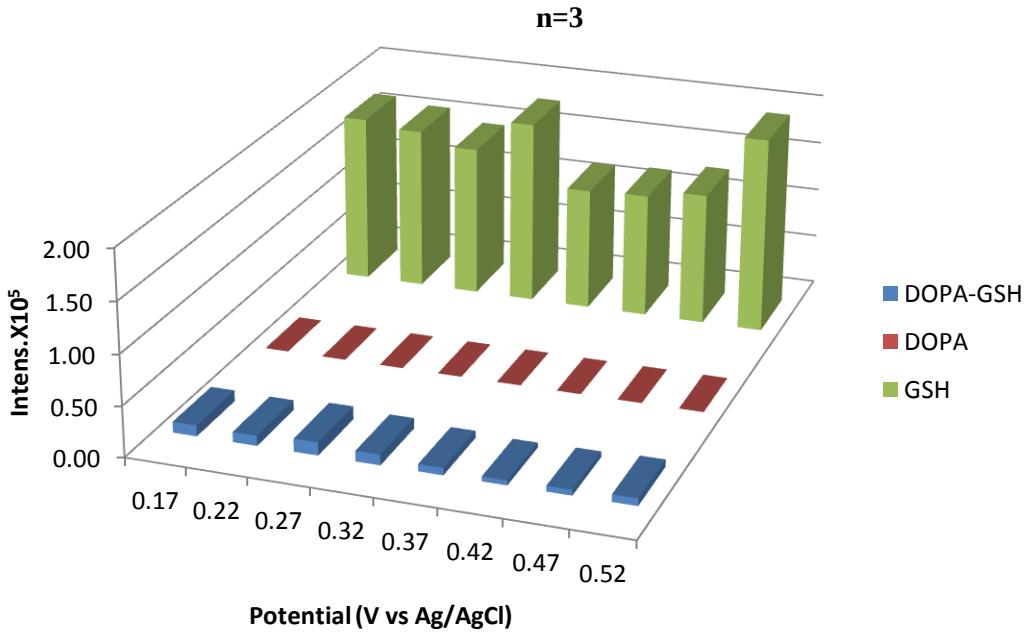

Figure 3.11 Potential optimization of DOPA. The highest intensity for the DOPA-GSH adduct was obtained at 0.27 V and the lowest intensity at 0.42 V.

3.2.8 Exhaustive electrolysis and offline MS

Exhaustive electrolysis at the optimized potential of 0.27 V, over the same conditions was recorded for 30 min, to obtain maximum adduct generation or formation of additional metabolites, as a function of time. A brownish colour change was observed in the electrolysed solution after the completion of CPE (Figure 3.12), which was not observed during potential optimization.

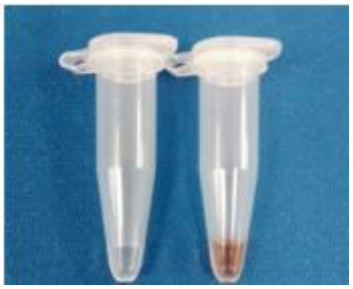

Figure 3.12 Colour change after CPE.

The obtained mass spectrum is shown in (Figure 3.13). It was found that DOPA and GSH were depleted completely and the expected metabolite of DOPA-GSH adduct (*m/z* 459) was clearly seen; however, it was not the most abundant ion. A new metabolite was formed with a *m/z* of 301, which belonged to DOPA polymer and it was the most abundant ion. Gonzalez-Diequez *et al.*[269] observed a similar dark colour change and linked the finding with the formation of a polymer, but the metabolite was not identified. GSSG (*m/z* 612.80) was also observed during prolonged electrolysis, which was not seen during the potential optimization.The mass spectrum of the DOPA blank solution did not present the DOPA-GSH adduct, suggesting the effect of pure electrolysis on the surface of the SPE, (Figure 3.14).

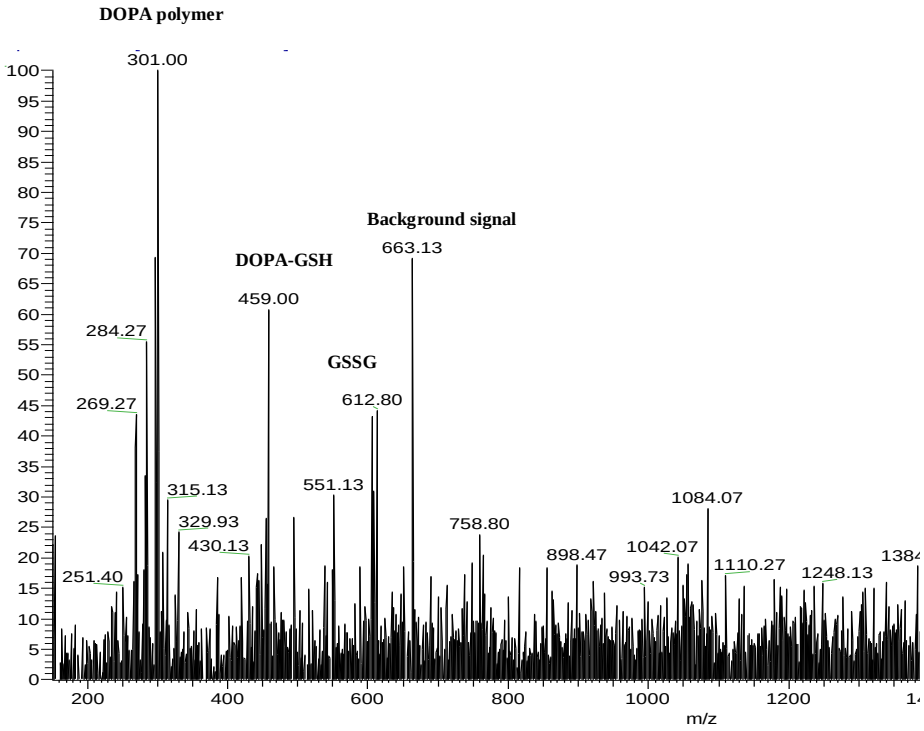

Figure 3.13 Partial mass spectrum of DOPA metabolism at 0.27 V. The most abundant peak was found at 301 *m/z*, which implied the existence of a parallel metabolic pathway. In addition, a DOPA-GSH adduct was obtained as expected through GSH conjugation.

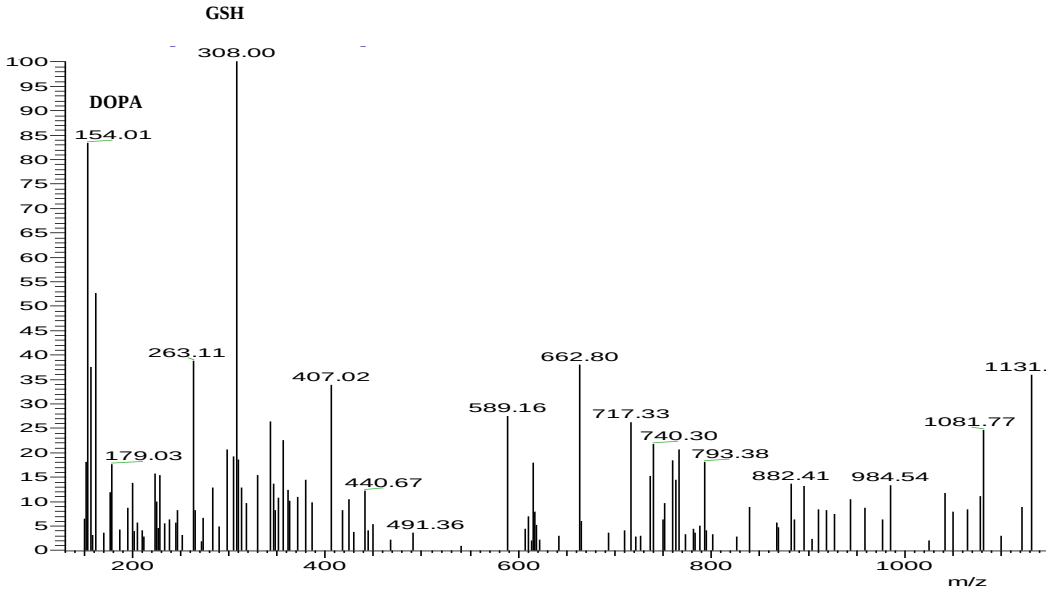

Figure 3.14 Partial mass spectrum of DOPA blank solution. The DOPA-GSH adduct (*m/z 459*) was not obtained, neither the polymeric peak (*m/z 301*) comfirming the result of pure electrolysis.

3.2.9 Proposed reaction mechanism of DOPA

The proposed reaction mechanism (Scheme 3.4) involved the electrochemical dehydrogenation of DOPA into dopaminoquinone, followed by three parallel metabolic pathways.

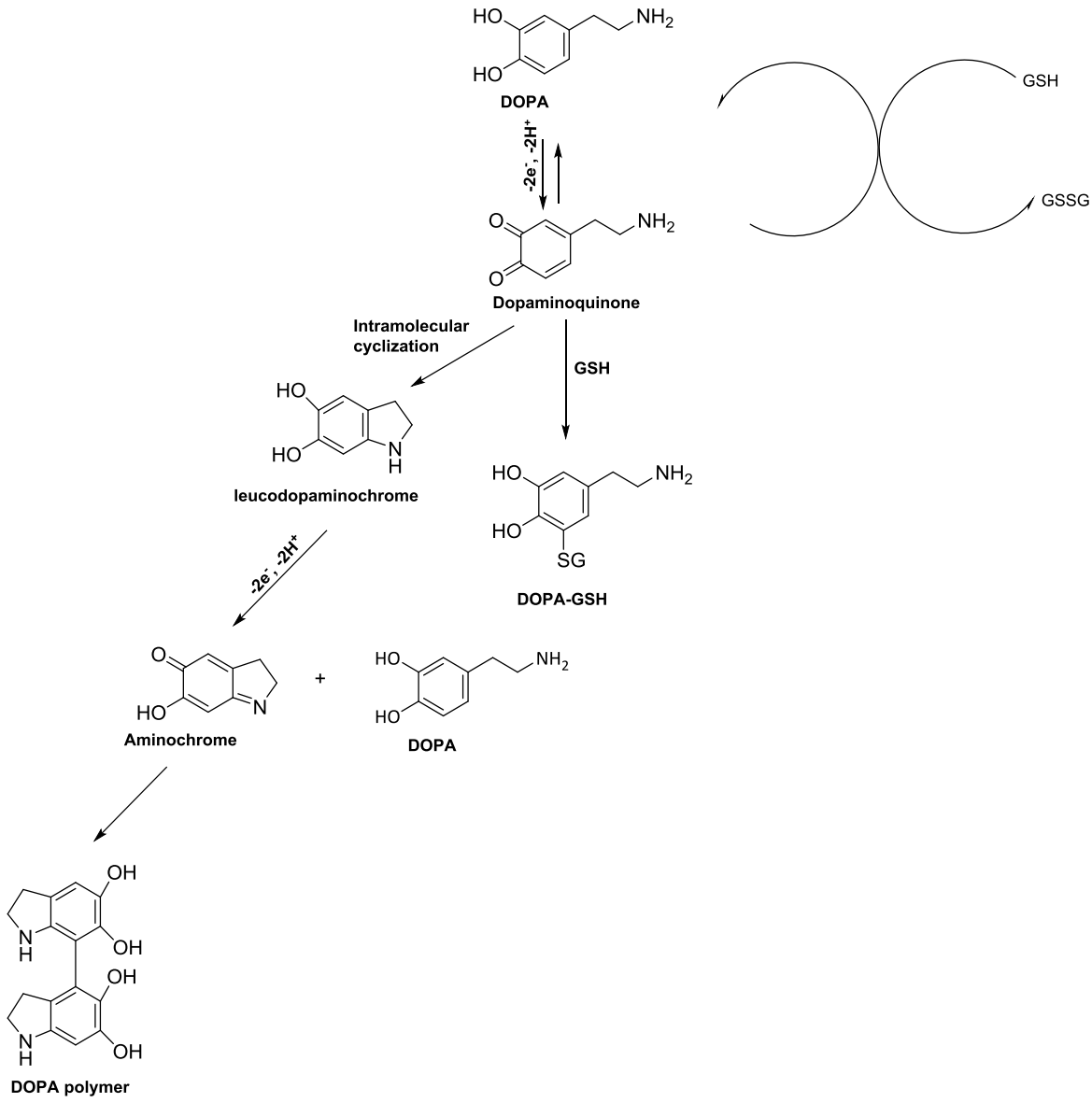

Scheme 3.4 Proposed reaction mechanism of DOPA based on mass spectra. Three parallel metabolic pathways were identified leading to DOPA polymer via a series of electrochemical and chemical steps, a DOPA-GSH adduct via covalent conjugation and GSSG via catalysis.

The first pathway involved a Michael addition between the electrophilic ortho quinone and GSH, which resulted to the formation of DOPA-GSH adduct. In the second pathway, a catalytic mechanism had occurred leading to the formation of GSSG and DOPA regeneration. Finaly, the third pathway led to the formation of a DOPA polymer with a brownish colour. The relative instability of dopaminoquinone in pH 7.4, as indicated during the electrochemical studies in section 3.2.2.2 and the prolonged duration of electrolysis (30 min), permitted the intramolecular cyclization of dopaminoquinone and the subsequent generation of leucodopaminochrome, which was dehydrogenated electrochemically into aminochrome at the optimized potential of 0.27 V. As a consequence, the resultant dopaminochrome reacted with DOPA molecules that were either regenerated through the catalytic process or remained unchanged during electrolysis, leading to the formation of a DOPA polymer.

The generated metabolites were in agreement with findings from *in vitro* studies[258] , suggesting the successful simulation of DOPA metabolism with SPEs. The expected phase II GSH adduct was obtained, enabling the indirect detection of the unstable dopaminoquinone. Even though the formation of GSSG was not reported [258] in the *in vitro* studies, GSSG is also part of the detoxification mechanism of GSH [271]. GSSG is frequently obtained in electrochemical studies involving the mimicry of human metabolism and is considered as a possible detoxification metabolite.[91,115]

The effect of molar concentration, time of electrolysis, and pH determined the generation of the DOPA polymer. As shown by voltammetry studies in section 3.2.5, at higher DOPA concentrations from of $5x10^{-5}$ M to $2.5x10^{-5}$ M, the generation of dopaminoquinone increased, permitting the formation of leucodopaminochrome and aminochrome, the

building blocks of DOPA polymers. At a concentration of $2.5x10^{-5}$ M DOPA, only dopaminoquinone was obtained since quinone was generated at lower yields, preventing the formation of further metabolites.

With longer durations of CPE (30 min), the generation of dopaminoquinone was increased through the continuous oxidation of DOPA. This led to the formation of the DOPA-GSH adduct, GSSG and DOPA polymer, with the latter found in a greater abundance, suggesting its dominance over the other two metabolic pathways. In contrast, with shorter durations of CPE (0.5 min), only the DOPA-GSH adduct was seen because the dopaminoquinone levels were low and favoured the formation of GSH adducts only.

Also, the pH in combination with the time of electrolysis and concentration affected the generation of the DOPA polymer. For example, at pH 7.4, the generation of dopaminoquinone was expected to be low, as suggested by the effect of pH on the generated current (3.2.2.3). Therefore, higher concentrations were required to drive the polymerisation process. In addition, as shown in section 3.2.2.2, the stability of dopaminoquinone was decreased in alkaline conditions. As a result, at pH 7.4, the reactive dopaminoquinone was unstable, favouring the polymerisation process, as seen in the mass spectrum obtained after a 30-min CPE. The longer durations of electrolysis generated more quinones and thus their preference over polymerisation, owing to instability, was more obvious.

However, in acidic conditions and in particular at pH 5 and pH 6, the highest stability of dopaminoquinone was obtained with peak current ratios of 1.08 and 1.1, respectively. Thus, the greater availability of protons permitted the protonation of dopaminoquinone, in its amine moiety, leading, subsequently, to a more stable product. The same relationship

was also found in the *in vitro* methodology,[258] suggesting that SPEs were capable of mimicking the metabolism of DOPA and providing an alternative approach to *in vitro* studies.

Moreover, the applied potential of 0.27 V permitted two electrochemical reactions (dehydrogenations) to occur during CPE. In addition, the limited surface area of the sensor as compared with the conventional flow cells[168] allowed the generation of various metabolites, which was a great advantage, since multiple metabolites can be formed in a more economical fashion. Also, the same metabolic pathway was obtained in a glassy carbon electrode, in the absence of GSH,[270] indicating that SPEs can be used as an alternative approach, in a more economical and disposable manner, to the traditional glassy carbon electrodes.

3.3 Conclusion

Primary voltammetry studies suggested the formation of dopaminoquinone via an ECE mechanism and confirmed its electrophilic character towards GSH. The obtained reaction mechanisms were in agreement with previous studies in the conventional glassy carbon electrode. The metabolism of DOPA was successfully simulated in slightly alkaline conditions (pH 7.4) by CPE and offline MS at the optimized potential of 0.27 V. Three parallel metabolic pathways were obtained leading to the formation of the DOPA-GSH adduct, DOPA polymer, and GSSG. The reactive dopaminoquinone was synthesised electrochemically at 0.27 V, by dehydrogenation and reacted covalently and catalytically with GSH, leading to the formation of DOPA-GSH adduct and GSSG, respectively. On the other hand, the DOPA polymer was synthesised via a series of electrochemical and chemical steps such as intramolecular cyclization of dopaminoquinone, electrochemical dehydrogenation of leucodopaminochrome to aminochrome, and chemical reaction of aminochrome with the parent DOPA molecules. The formation of DOPA polymer was favoured in higher DOPA concentrations ($5x10^{-5}$ M to $2.5x10^{-3}$ M), in slightly alkaline conditions and at extended durations of electrolysis (30 min). In contrast, the DOPA-GSH was favoured in lower DOPA concentration ($2.5x10^{-5}$ M) and at shorter durations of electrolysis (0.5 min). The proposed methodology generated metabolites that were in agreement with previous *in vitro* studies.

3.4 Results and discussion – RLX

The capability of generating the phase I RLX di-quinone methide and the corresponding phase II RLX-GSH adduct, via a two electron and a two proton transfer was investigated on bare SPEs. In addition, the formation of RLX 6,7,-0-quinone via aromatic hydroxylation was also examined.

3.4.1 Electrochemical behaviour of RLX

A redox couple was obtained after the addition of $2.5x10^{-5}$ M of RLX in 0.1 M phosphate buffer (pH 6), at 0.155 Vs^{-1} (Figure 3.15). The anode potential was generated at 0.26 V and the cathode potential, at 0.16 V; the calculated separation peak potential was 0.1 V. Additionally, the obtained anode current was 0.004 mA and the cathode current was found to be -0.008 mA. The process was repeated in three different SPEs (n=3).

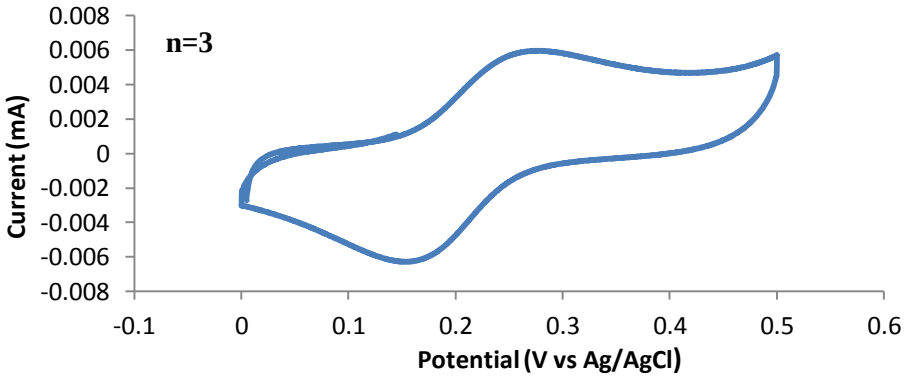

Figure 3.15 Electrochemical behavior of RLX on a SPE. A redox pair appeared comfirming the electroactivity of RLX, the obtained anode potential was seen at 0.26 V and the cathode potential at 0.16 V.

3.4.2 Effect of PH

3.4.2.1 Participation of protons

The influence of pH on anode potential was investigated in a wide range of pH values. Specifically, $2.5x10^{-5}$ M of RLX in 0.1 M phosphate buffer (pH: 1, 2, 3, 4, 5, 6), 0.1 M ammonium acetate (pH: 7.4) and 0.1 M ammonium bicarbonate (pH: 8.8) was studied by voltammetry at 0.1 Vs^{-1}. The dependence of pH on anode potential was clearly seen in (Figure 3.16); the potential was shifted to less positive values as the pH was increased to more alkaline values, indicating the participation of protons. The slope was found to be 0.04 VpH^{-1}, from the best line fit (inset in Figure 3.16), which was close to the Nernstian slope of 0.057 VpH^{-1}, implying the involvement of an equal number of electrons and protons. For each pH value a new SPE was used and the process was repeted for a total of three trial (n=3).

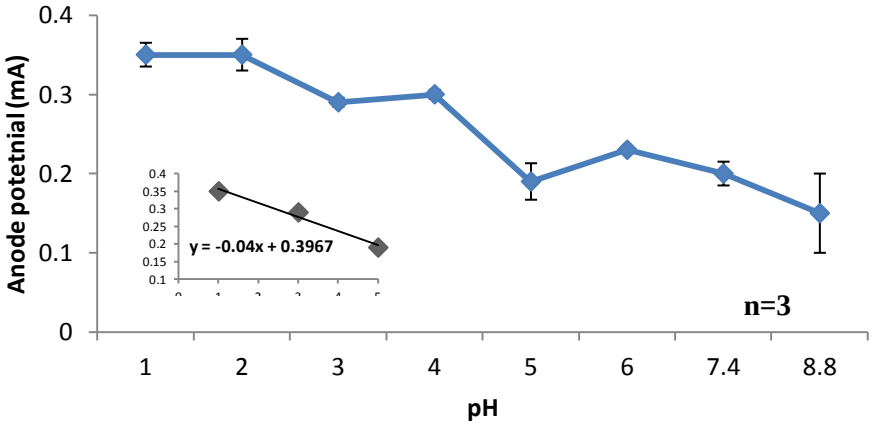

Figure 3.16 Involvement of protons in RLX oxidation. The anode potential shifted to less positive values implying the involvement of protons during the electron transfer.

3.4.2.2 Stability of the generated product

RLX presented the highest instability in highly acidic conditions and in particular at pH 1 and pH 2, with peak current ratios of 1.8 (Figure 3.17). However, as the pH increased in less acidic conditions, the intermediate gradually became more stable and in particular at pH 6 showed the highest stability with a peak current ratio of 1.06. The stability was decreased in alkaline conditions of pH 7.4 and 8.8, since the obtained peak current ratios were 1.44 and 1.54, respectively. For each pH value a new SPE was used and the process was repeated for a total of three trials (n=3).

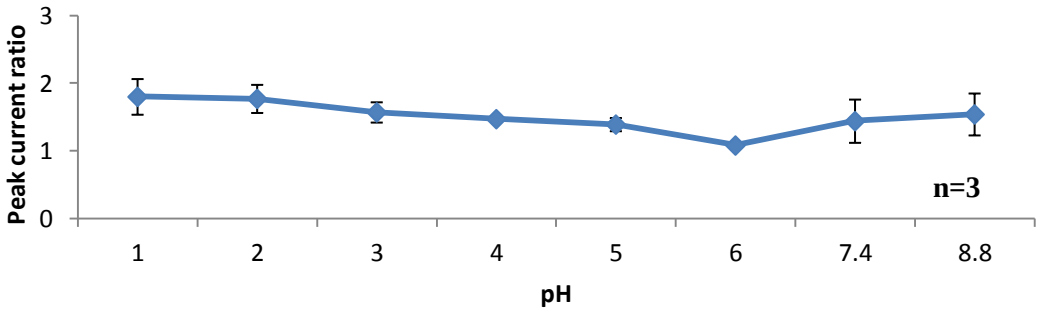

Figure 3.17 Stability of RLX intermediate. The most stable product was in pH 6 with a peak current ratio of 1.08.

3.4.2.3 Effect of pH on voltammetric currents

The pH-current plots for anode and cathode potentials presented a relatively steady state at low pH values (Figure 3.18). The highest current signal was seen at pH 6, with a decrease in more alkaline conditions. The highest product generation was found at pH 6.

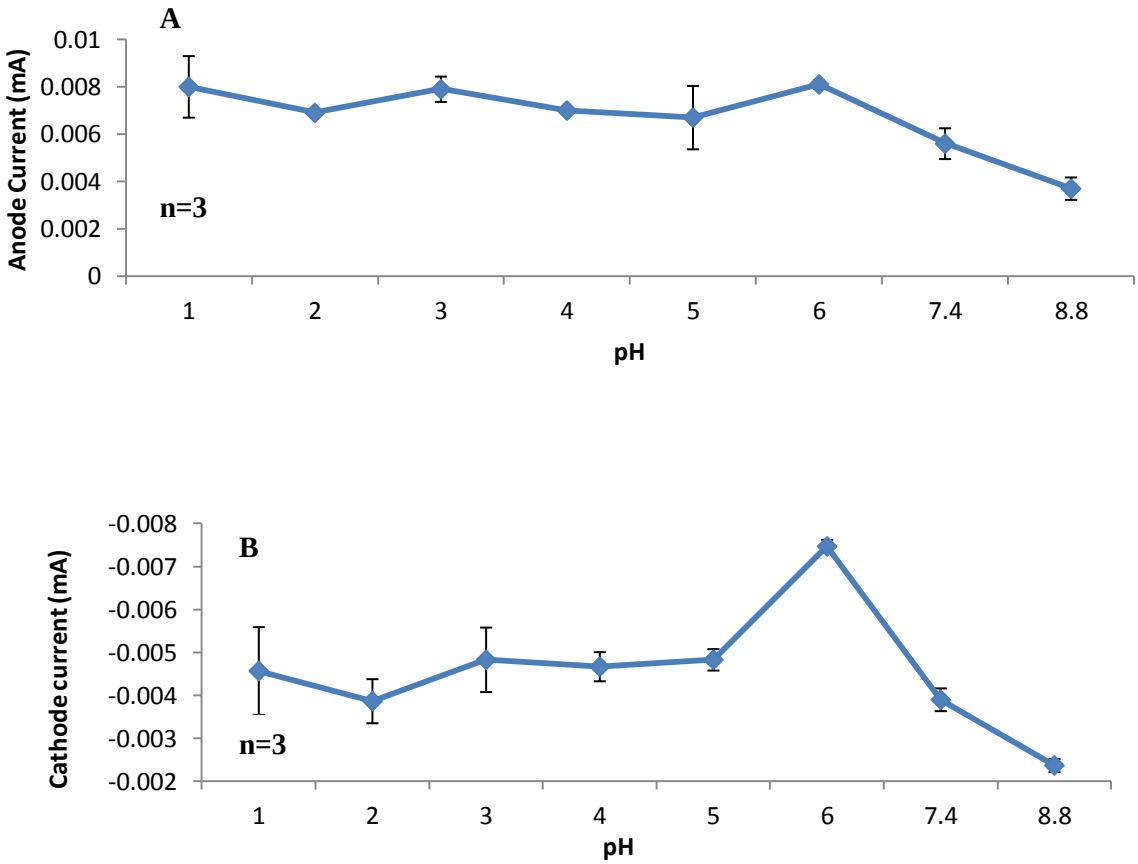

Figure 3.18 Effect of pH on RLX currents. A) Anode current; B) Cathode current. The highest currents and as a consequence the highest metabolite yields were found for both in pH 6.

3.4.3 Effect of scan rate and electron transfer kinetics

CV of $2.5x10^{-5}$ M RLX in 0.1 M phosphate buffer (pH 6) at different scan rates from 0.01 Vs^{-1} - 0.155 Vs^{-1} (Figure 3.19) indicated a quasi-reversible process. The process was repeated three times (n=3) on different SPEs.The anode and cathode currents increased with the increase in the SQRT of scan rate (Figure 3.20). The separation peak potentials were increased at varying scan rates, confirming clearly the slow electron transfer rates. The obtained reversibility on the separation peak potentials at 0.01 V and 0.05 V is a characteristic behaviour of quasi-reversibility in relatively slow scan rates,[129] since at higher scan rates, the slow electron transfer does not permit the establishment of Nernestian equilibrium.

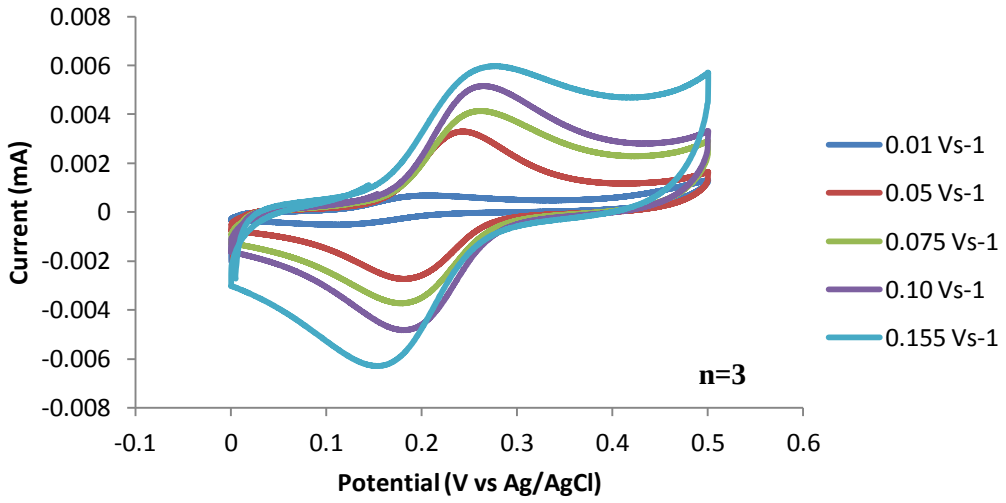

Figure 3.19 Effect of scan rate on RLX. Various scan rate from 0.01 Vs^{-1} to 0.155 Vs^{-1} were applied to determine the electron kinetics.

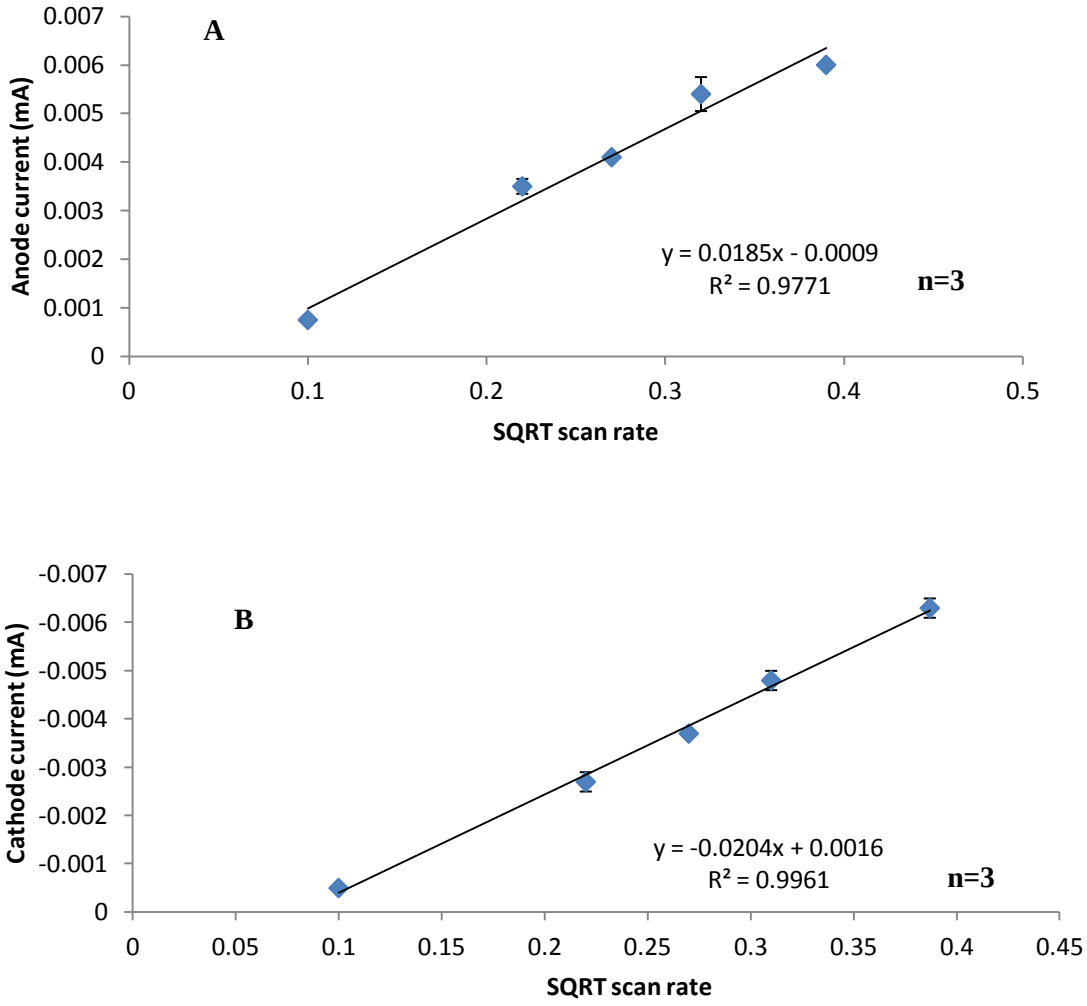

Figure 3.20 Linear relationship of RLX currents with the SQRT of scan rate. A) Anode current; B) Cathode current. The correlation coefficient for the anode current was found to be 0.997 and for cathode current was 0.996.

In addition, the potentials were varied as a function of scan rate, confirming further the quasi-reversibility of the system (Figure 3.21). The quasi-reversible kinetics were in agreement with the findings of previous studies on RLX with a bare and modified glassy carbon electrode,[260, 271] implying the formation of RLX di-quinone methide via dehydrogenation in the hydroxyl moieties.

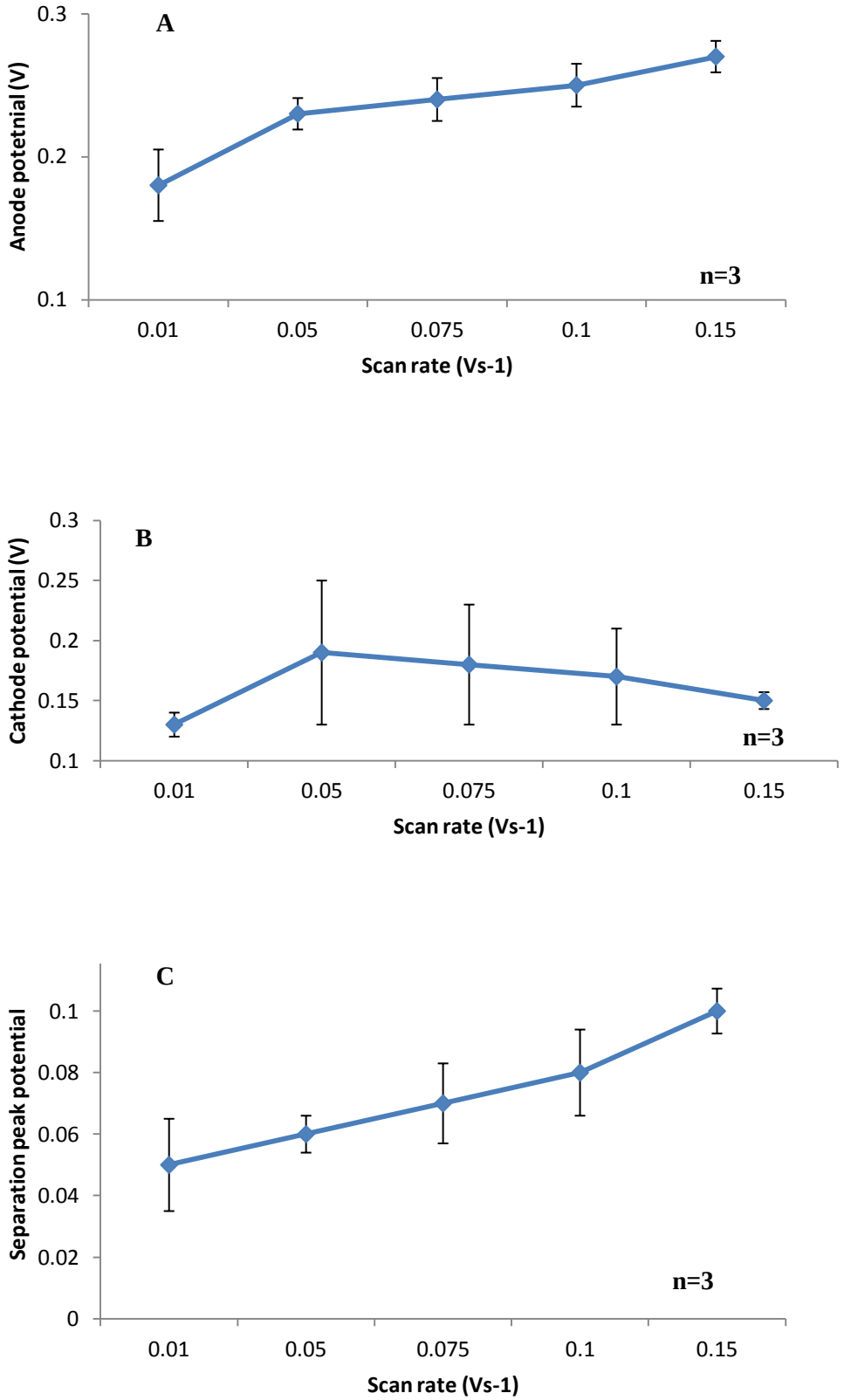

Figure 3.21 Dependence of RLX potentials with scan rate. A) Anode potential; B) Cathode potential; C) Separation peak potential.

3.4.4 Mass transport

The plot of log (current) vs. log of (scan rate) implied a mixture of a diffusion and adsorption, as a transport mode (Figure 3.22), since the obtained slopes were 0.76 and 0.74 for anode and cathode currents, respectively, indicating the strong adsorption properties of the drug in the SPE surface. Earlier investigations with bare glassy carbon and graphite elecrodes[260, 272] presented the same transport mode, whereas total adsorption was observed with a mercury electrode.[273]

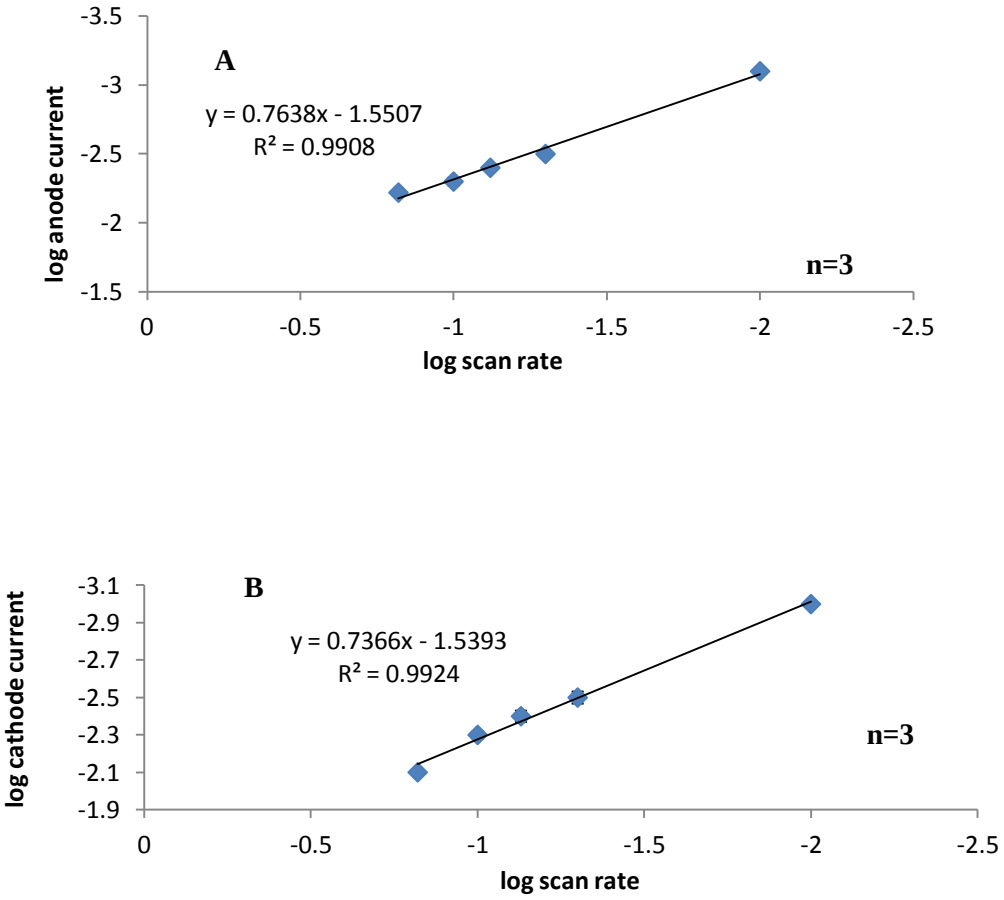

Figure 3.22 Mass transport mode of RLX. A) Anode current; B) Cathode current. A mixture of both adsorption and discussion was found for both anode and cathode currents.

3.4.5 CV in the presence of GSH

CV in the presence of $2.5x10^{-5}$ M RLX and various GSH concentrations from 0 M to $2.54x10^{-4}$ M, in 0.1 M ammonium acetate (pH 7.4) was conducted at a scan rate of 0.1 Vs^{-1} (Figure 3.23). Changes were observed in the obtained voltammograms, confirming the generation of a new product as an effect of increased GSH addition. In particular, the anode and cathode potentials were shifted to more positive values with the increase in GSH concentrations, suggesting hte formation of GSH adduct that was electroactive and oxidized at a new potential. The anode current was also increased as a function of concentration and the cathode current presented an increased trend until the $1.24x10^{-4}$ M, whereas at $2.5x10^{-4}$ M, it deceased significantly, suggesting that only a part of the generated products reacted with GSH. A possible explanation for this peculiar behaviour is the existence of a parallel catalytic pathway leading to the formation of GSSG, causing GSH depletion. In the highest GSH concentration, the cathode current eventually decreased since the availability of the trapping agent was increased.

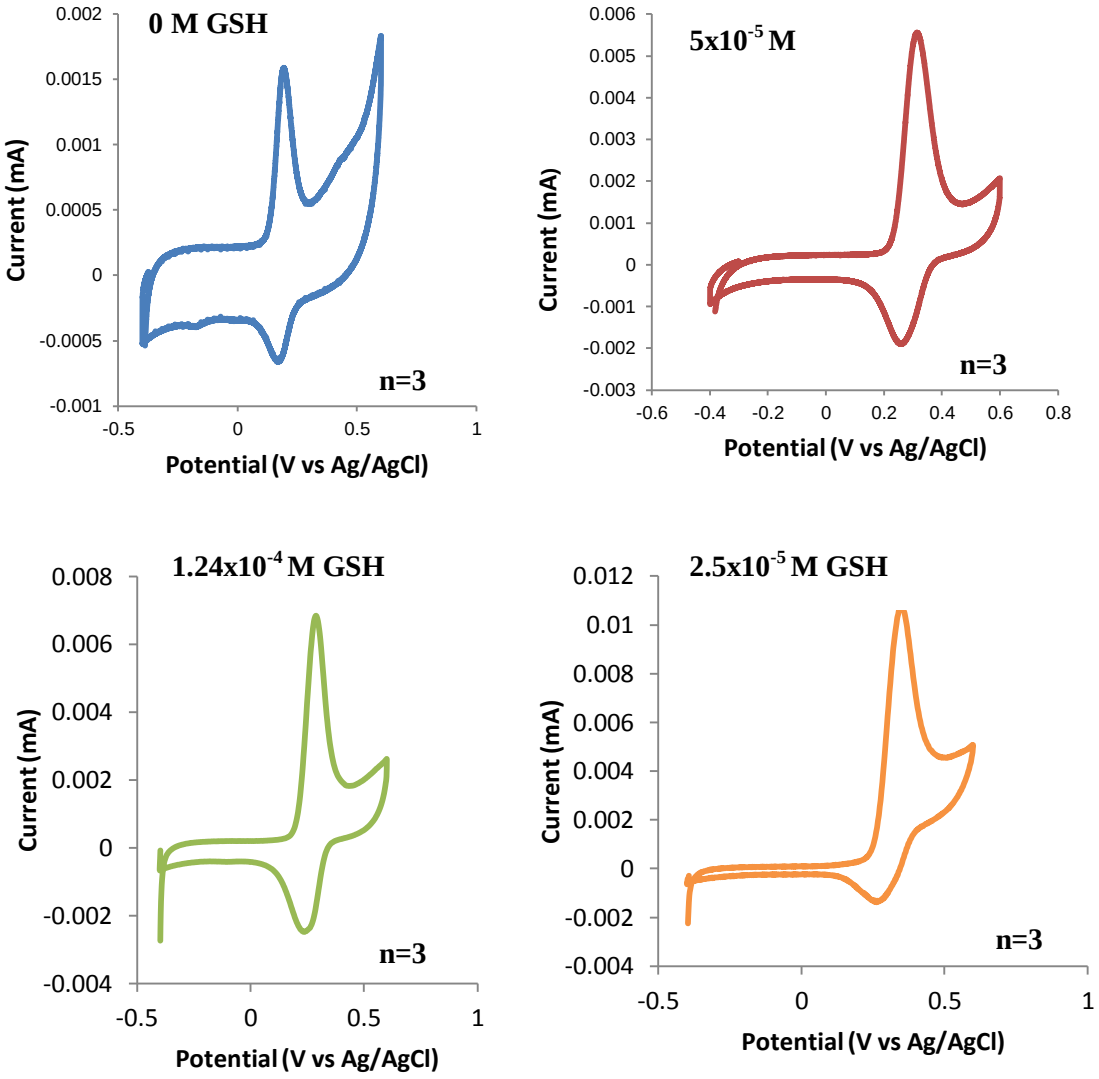

Figure 3.23 RLX in the presence of various GSH concentrations. Shifiting in anode and cathode potentials confirm the formation of a new metabolite, probably a GSH adduct that was electroactive and oxidized at a new potential. Increase in anode current spported further the formation of the new metabolite due to the parallel generation of RLX quinone methide and GSH adduct. However, at $1.24x10^{-4}$ M a peculiar behaviour was seen since the cathode current was increased suggesting the existing of a parallel catalytic mechanism and in particular the formation of GSSG, leading to parent drug regeneration and subsequent reduction.

3.4.6 Potential optimization

CPE of $2.5x10^{-5}$ M RLX in the presence of $5x10^{-5}$M of GSH was conducted for 0.5 min from 0.35 V to 0.70 V, with increasing steps of 0.05 V. The process was repeated three times (n=3) on different SPEs, for each potemtial. The potentials were chosen by CV, as specified in section 3.4.5, operated over a mass transport limit. The electrogenerated metabolites were detected by positive ESI/MS. A three-dimensional plot was constructed to reflect the oxidation behaviour of RLX in the tested potentials (Figure 3.24).

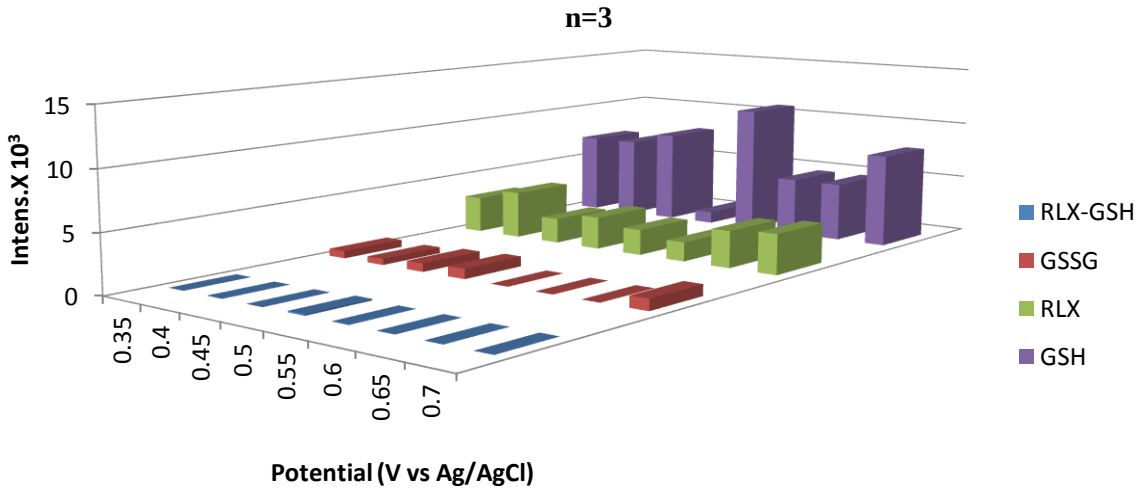

Figure 3.24 Potential optimization of RLX. The RLX-adduct was obtained at trace levels only at 0.55 V. The catalytic peak of GSSG was also obtained confirming the existence of a parallel metabolic pathway.

The RLX-GSH adduct was obtained only at 0.55 V; however, the signal was very poor and did not provide clear indications. Additionally, the formation of GSSG confirmed the possibility of a parallel catalytic pathway. As concluded, the electrochemical generation of RLX di-quinone methide and subsequent conjugation was achieved at extremely low yields, which were detectable slightly at 0.55 V. Earlier findings in section 3.4.2.3 supported the idea, since at pH 7.4, the corresponding oxidative current was one of the lowest recorded, in the tested pH range, suggesting low metabolite generation.

Additionally, the adsorption properties of RLX di-quinone methide might cause a significant impact on the decreased signals. The effect of strong adsorption was identified in section 3.4.4. Also, the stability of quinone di-methide at pH 7.4 in section 3.4.2.2 was found to be 1.44, higher than the expected unity, confirming its possible involvement in the obtained low yields.

3.4.7 Exhaustive electrolysis and offline MS

Exhaustive electrolyses (30 min) at various potentials were conducted, considering the limited information gained in section, 3.4.6. The chosen potentials were 0.55 V, which gave a more clear indication for the formation of the RLX-GSH adduct, and all the potentials that presented in their mass spectra the GSSG. A mass spectra at 0.55 V is shown in (Figure 3.25) the signal of the RLX–GSH adduct (*m/z 778.85*) was still very poor, without any clear conclusions regarding the formation of the phase II metabolite. The mass spectra of the other potentials also presented the same information as in section 3.4.6.

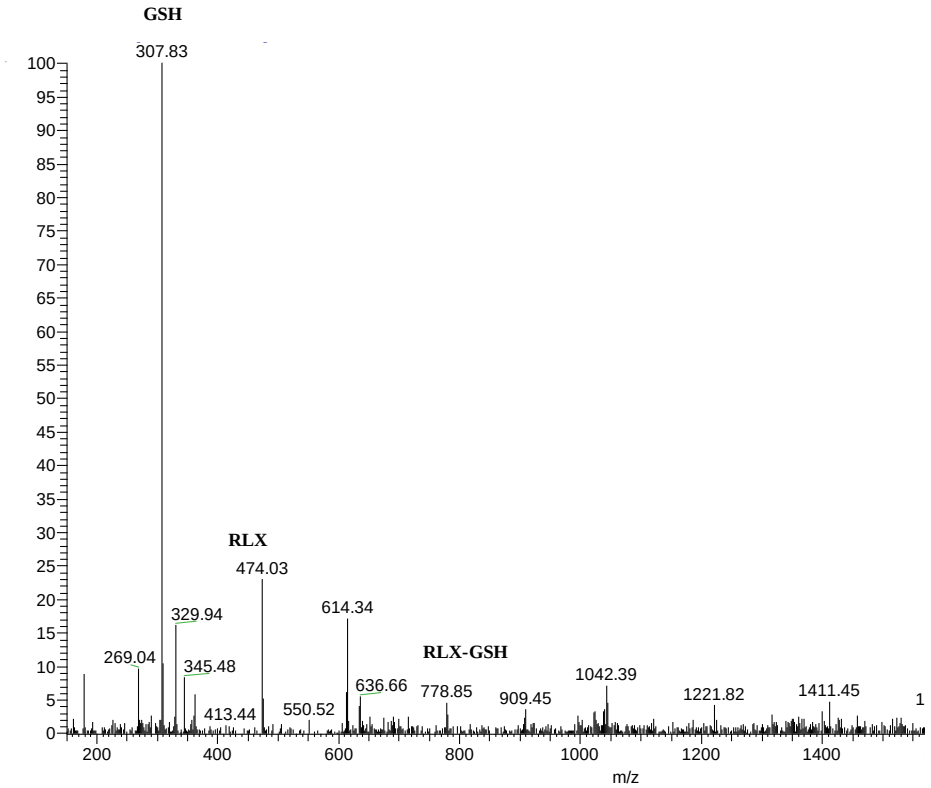

Figure 3.25 Partial mass spectrum of 2.5 x10^{-5} M RLX metabolism at 0.55 V. The signal of RLX-GSH adduct (*m/z* 779) was very poor without any clear indications.

3.4.8 Exhaustive electrolysis-influence of concentration

Exhaustive electrolysis of $2.5x10^{-4}$ M of RLX in the presence of $5x10^{-4}$ M of GSH was investigated for 30 min at 0.55 V. The obtained *m/z* are seen in (Figure 3.26); at higher concentrations and long-term exposure of RLX in the applied potential, the RLX-GSH adduct (*m/z* 779.09) was formed. The fact that GSH was depleted, GSSG (*m/z* 612.96) was formed and RLX was the most dominant ion, confirmed the existence of a parallel catalytic pathway. By increasing the concentration, higher yields of the corresponding GSH adducts were synthesised, overcoming the limitations of low production in $2.5x10^{-5}$ M at pH 7.4 and the effect adsorption effects. In addition, a di-GSH adduct (*m/z 1084*) was obtained as a result of increased concentration, which was not seen in lower concentrations of $2.5x10^{-5}$ M.

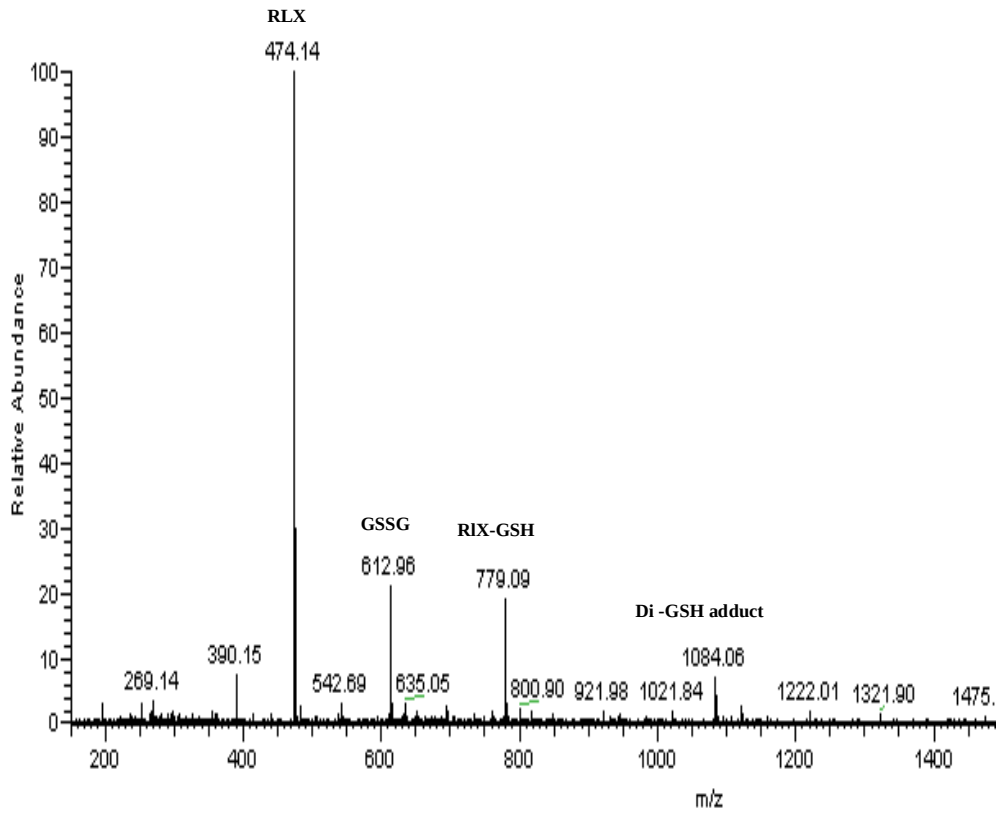

Figure 3.26 Partial mass spectrum of 2.5 $X10^{-4}$ M RLX metabolism at 0.55 V. The sensitivity of RLX-GSH adduct was improved at higher concentrations.

3.4.9 Formation of RLX 6, 7-o-quinone

In previous studies by Jurva *et al*., aromatic hydroxylation was successfully simulated in acidic media (pH = 3)[179] by the online coupling of EC and MS. However, the generated catechol was unstable and oxidised further into quinone. The methodology involved the use of commercially available flow cells with large surface areas and the working electrode was made of graphite. The metabolic reactions were simulated at 0.2 V, relying in the potential limits of the carbon SPE.

3.4.9.1 Voltammetry in acidic media

CV of 2.5.x10^{-5} M RLX was conducted in 1 mM of acetic acid (pH 3) at a scan rate range of 0.002–0.124 Vs^{-1}. Voltammograms with two oxidative and two reductive peaks were expected. The first peak would represent the aromatic hydroxylation and the second, the dehydrogenation process, considering the fact that hydroxyl moieties in aromatic rings, exhibit strong electroactive properties.[115, 260, 272, 273] However, according to the obtained voltammograms in (Figure 3.27), a well-defined redox pair appeared at all scan rates, as in the case of pH 7.4. A low-magnitude reduction peak appeared owing to adsorption rather than the result of kinetics since repetitive voltammetry did not generate a second redox pair. As concluded, in the present conditions, the formation of the second metabolite was not feasible.The process was repeated three times (n=3).

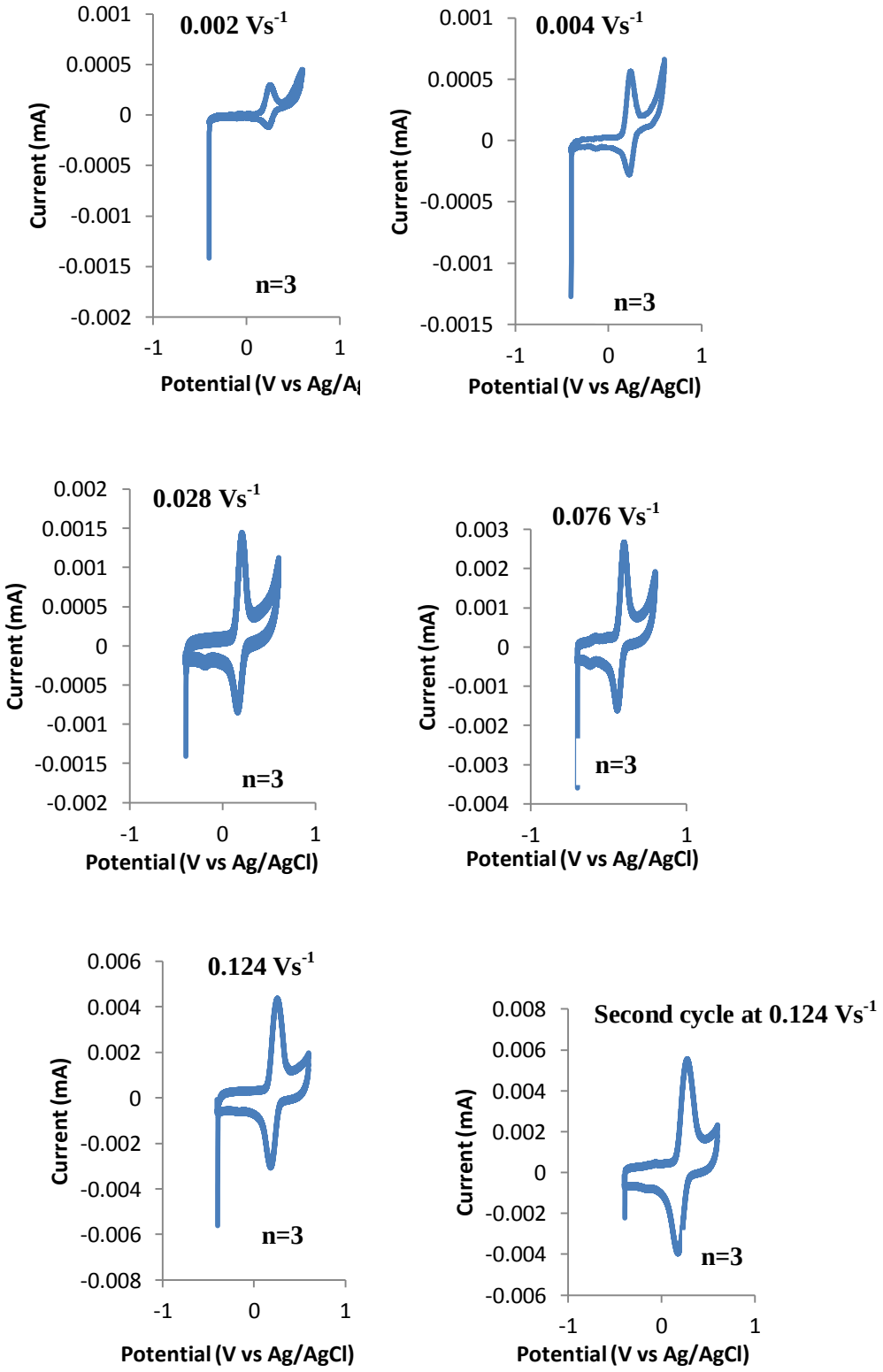

Figure 3.27 Effect of scan rate of RLX in acidic media. At all scan rate a second redox pair was not seen that might suggest the formation of the second reactive metabolite.

3.4.9.2 Effect of concentration

Various concentrations of RLX from $2.5x10^{-5}$ M to $2.5x10^{-3}$ M, in 1 mM acetic acid (pH 3) were subjected to voltammetry at 0.1 Vs^{-1}. The expected redox pair was obtained with a significant increase in the current magnitudes, owing to the increased concentrations (Figure 4.33). A low-magnitude cathode peak appeared at 0.12 V, but a second cycle did not generate the expected anode potential in the reverse scan in all of the selected concentrations, suggesting the effect of an impurity or strong adsorption. A representative voltammogram of a second cycle at $2.5x10^{-3}$ M is shown in (Figure 3.28). The process was repeated three times (n=3). Thus, as concluded, higher concentrations of RLX failed to mimic aromatic hydroxylation.

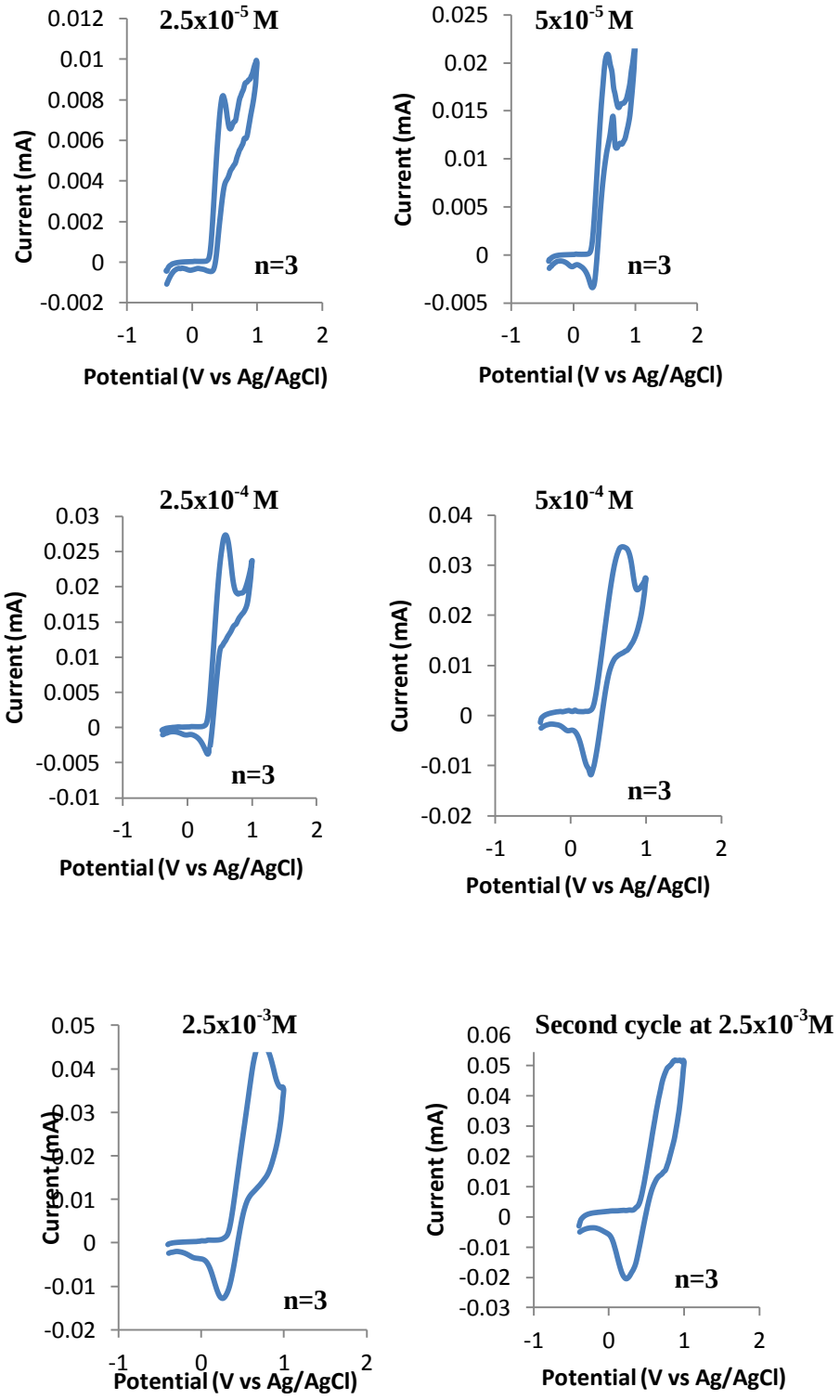

Figure 3.28 Voltammetry in various RLX concentrations. The formation of RLX 6,7, -o-quinone as a function of concentration was investigated, however the metabolite was not obtained even at the highest concentration of 2.5X10^{-3} M.

3.4.9.3 Effect of surface area

Jurva *et al.*[174] simulated the particular reactions in a coulometric cell in acidic conditions (1 mM acetic acid, pH 3). In an attempt to investigate the effect of surface area on the formation of RLX 6,7,-o-quinone metabolite; $2.5x10^{-5}$ M of the drug, in 1 mM acetic acid was electrolysed for 2 min, in a μ-prep cell (Antec, Netherlands) with a surface area of 1.9 cm^2,[179] equipped with a glassy carbon working electrode. The RLX 6,7-o-quinone (*m/z* 488.17) was formed at all potentials in the range of 0.2 V to 0.8 V, with increasing steps of 0.2 V. A representative mass spectrum at 0.6 V is shown in (Figure 3.29). The process was repeated three times (n=3).

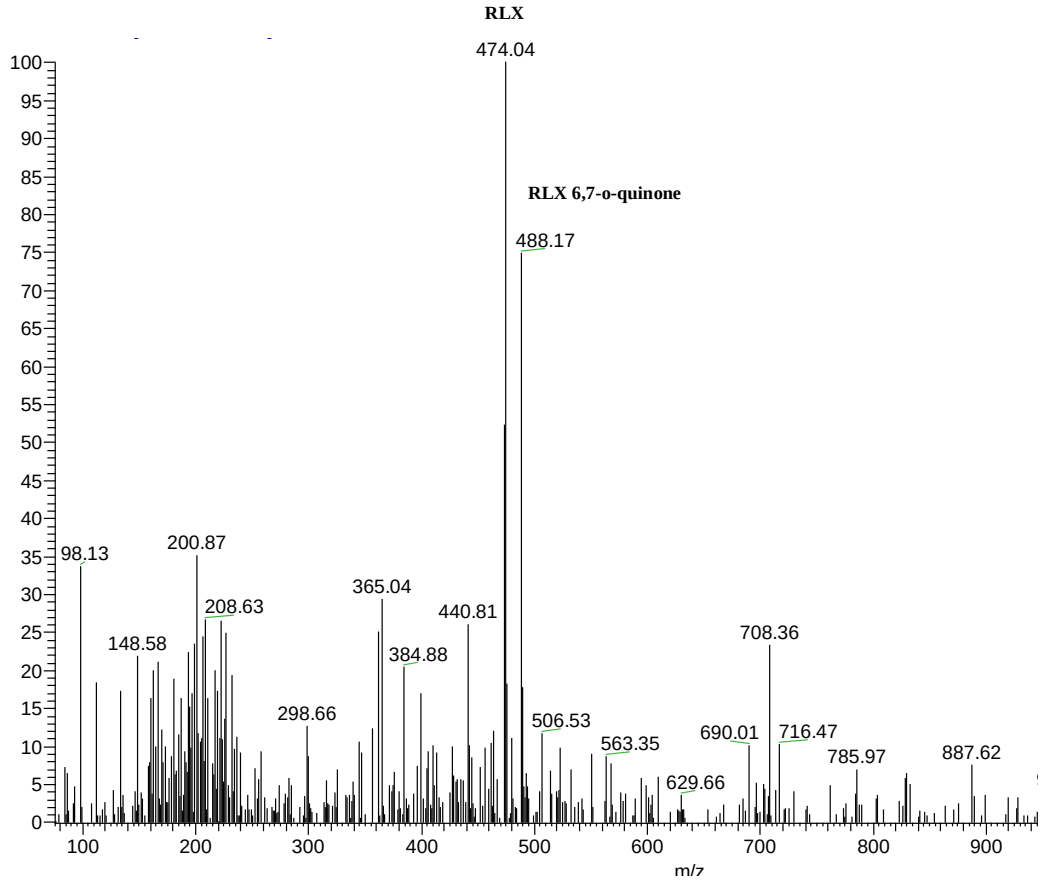

Figure 3.29 Partial mass spectrum for the generation of RLX 6,7-o-quionone at 0.60 V in a μ-prep cell. The orho quinone (*488 m/z*) was clearly seen in the obtained spectrum.

surface area of 0.126 cm^2. However, herein, higher concentrations of $2.5x10^{-4}$ M and duration of 30 min of electrolysis were applied, considering the findings in section 4.4.7. However, RLX 6,7-o-quinone was not formed on the surface of the SPE. Thus, as concluded, aromatic hydroxylation requires a higher surface area and in particular, a greater number of active sites in the working electrode. A representative mass spectrum is shown in (Figure 3.30).

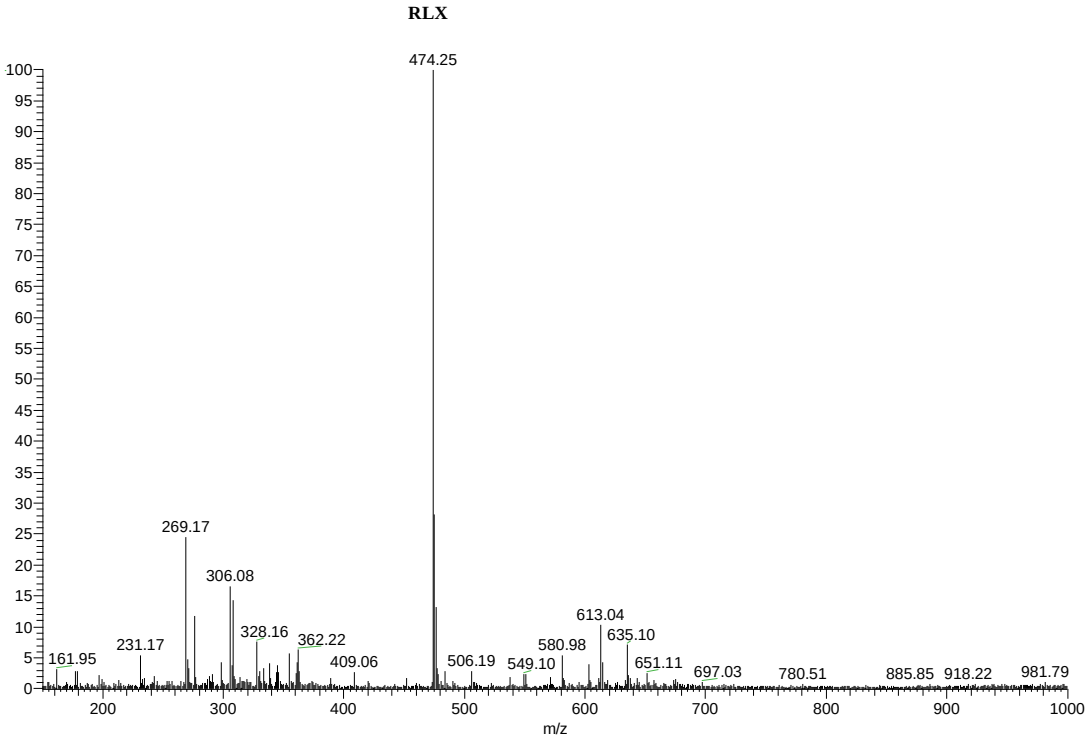

Figure 3.30 Partial mass spectrum for the generation of RLX 6,7-o-quionone at 0.62 V on SPE. The reactive metabolite was not formed suggesting limitations with the restricted surface area.

3.5 Reaction mechanism of RLX

Considering the individual electrochemical studies and offline mass spectra analysis, the electrochemical oxidation of RLX in the presence of GSH is described in (Sheme 3.5). The proposed reaction mechanism involved the initial dehydrogenation of RLX via a twoelectron and two proton transfer, into the RLX di-quinone methide, which followed two main pathways: 1) conjugation and 2) catalysis. In conjugation, the reactive intermediate covalently bonded with the thiol group of GSH forming mono- and di-GSH adducts. In catalysis, the GSSG metabolites were formed and the parent drug was regenerated.

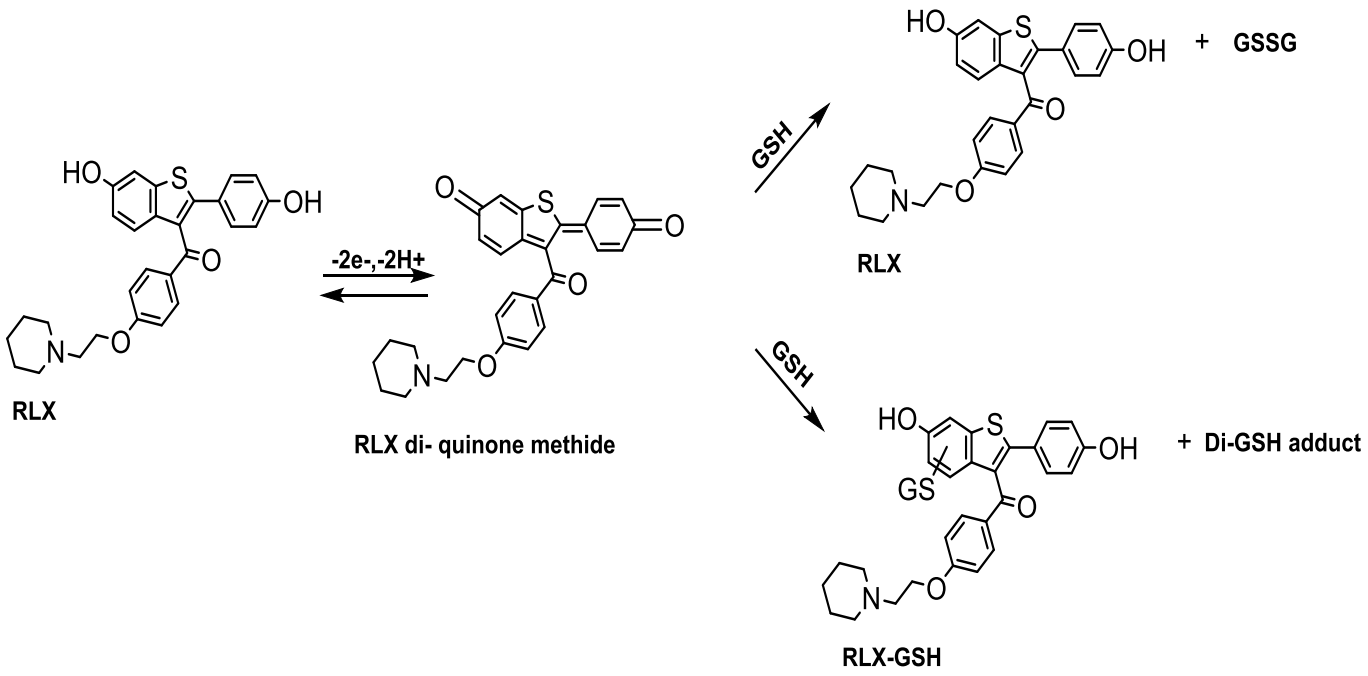

Scheme 3.5 Proposed reaction mechanism of RLX according to the obtained mass spectra. RLX di- quinone in the presence of GSH followed two main pathways conjugation and catalysis.

SPEs mimicked successfully the dehydrogenation of RLX into the short-lived RLX di-quinone methide[274] at pH 7.4. The obtained data were in good agreement with previously published *in vitro* data.[259, 274- 276] The formation of di-GSH adducts in RLX metabolism is frequently observed in *in vitro m*etabolism studies. The present mass spectrometry data supported the formation of a di-GSH adduct; however, the particular di-GSH adduct was not reported in existing literature. Similar di-GSH adducts were obtained in the electrochemical bioactivation of APAP by Kauffmann *et al*.,[115] suggesting the existence of a unique electrochemical mechanism. However, the generation of a second reactive metabolite, RLX 6,7,-o-quionone was not achieved owing to the limited surface area of the sensor. As proven, the large surface area of the conventional flow cells permit the simulation of aromatic hydroxylation and subsequent dehydrogenation, since they provide multiple active sites, as compared to SPEs. In addition, as proven in Chapter 3, owing to the fabrication process, some of the active sites of the particular sensors might be covered with binders, thus limiting their availability. As a consequence, probably, the metabolite was formed at very low yields below the detection limits of a mass spectrometer. The reaction mechanism and kinetics were in agreement with those in previous studies on RLX with glassy carbon electrodes, involving the transfer of two electrons and two protons from the hydroxyl moieties, confirming the rebalance of carbon SPEs with glassy carbon electrodes. The possibility of generating a phenoxyl radical via single electron and a single proton transfer, as proposed by Li *et al*.,[277] in carbon tubes was rejected, since the expected dimmers were not detected in MS.

During potential optimization, the dominance of the catalytic pathway was reflected on the obtained mass spectra. The GSSG metabolites were in greater abundance than the GSH adducts. Thus, as concluded a competition for RLX di-quinone methide was established between the two metabolic pathways. The dominance of the catalytic pathway was also reflected in CV studies, in the presence of various GSH concentrations. According to the obtained results, the formation of GSSG had cause a GSH depletion, leading to increased cathode currents.The generation of GSSG metabolite as a part of RLX bioactivation was reported by Liu *et al* .[278]

3.6 Conclusion

The RLX-GSH was generated successfully on the surface of the SPE at the optimized potential, confirming the ability of the sensor to mimick inexpensively both the phase I and phase II metabolism of RLX. The proposed mechanism was in agreement with already published *in vitro* data, involving the formation of highly unstable and short-lived RLX di-quinone methide that was trapped with GSH. In lower concentrations of $2.5x10^{-5}$ M, the RLX-GSH adduct was not obtained owing to adsorption effects, relative metabolite instability, and low metabolite yields at pH 7.4. On increasing the time of electrolysis to 30 min and the concentration to $2.5x10^{-4}$ M, the RLX-GSH adduct was detected. In addition, a di-GSH adduct was obtained, as part of the detoxification mechanism, which was detected only at the RLX concentration of $2.5x10^{-4}$ M. A parallel catalytic mechanism was identified in the early stages of electrochemical investigation. Voltammetry in the presence of increased GSH concetrations showed an increase in cathode current, suggesting GSH depletion due to GSSG formation. The second metabolite RLX 6,7-o-quinone was not generated on the surface of the SPE, probably due to the small area of the working

electrode and the limited availability in active sites. The required metabolic reactions of aromatic hydroxylation and dehydrogenation were mimicked successfully by Jurva *et al*. through the use of conventional flow cells with large surface areas. Herein, the same conditions were set in a μ-prep cell, confirming the relationship between a large surface area and aromatic hydroxylation. The observed kinetics and reaction mechanisms were in agreement with those recorded in glassy carbon electrode. In conclusion, a novel electrochemical methodology was developed using disposable and inexpensive SPEs for tracking the metabolism of DOPA and RLX, through the transfer of two electrons and two protons.

Chapter 4: Phase I and phase II metabolism of eugenol and DOXO on a SPE

4.0 Introduction

Phase I metabolic reactions involving the transfer of one electron and one proton, can lead to toxicity via interactions with macromolecules such as DNA and proteins. Eugenol[279] and DOXO[280] are two examples, as proved by the *in vitro* methodologies that lead to toxicity via the particular metabolic reaction.

Eugenol is an essential oil with a wide range of applications in dental practice, food industry, and cosmetics.[279] However, toxic effects such skin sensitisation,[281] have been reported that are associated with the metabolic process of eugenol. Over the years, *in vitro* and *in vivo* methodologies[282, 283] proposed different metabolic pathways of eugenol, catalyzed either by CYP 450 or peroxidase. However, a significant part of published data points out that both enzymes may lead to the formation of a toxic quinone methide via a single electron and a single proton transfer.[284] According to Thomson *et al.*,[282] the reaction mechanism, as shown in (Scheme 4.1), involved a single electron and a single proton transfer from the phenol moiety, leading to the formation of a phenoxyl radical. In the presence of GSH, the phenoxyl radical generated a GSSG metabolite via a catalytic mechanism and caused the regeneration of eugenol. In addition, the phenoxyl radical was also polymerised or stabilised to the corresponding eugenol quinone methide, that either formed a GSH adduct or underwent polymerisation.

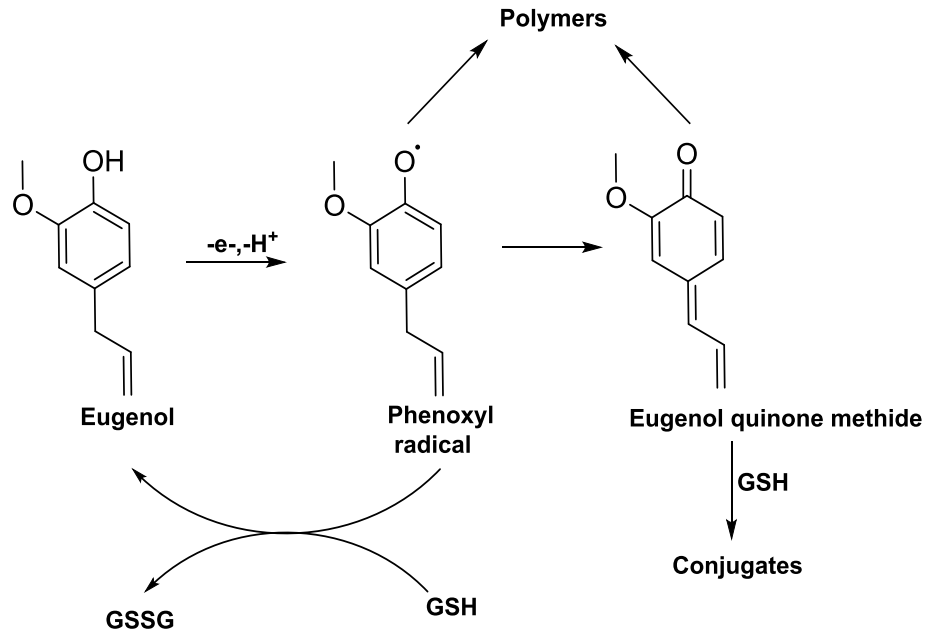

Scheme 4.1 ***In vitro*** **metabolic pathway of eugenol.[281] The eugenol phenoxyl radical was formed via the transfer of one electron and one proton. In the presence of GSH, the reactive metabolite follows a catalytic pathway and conjugation.**

DOXO is an anthracycline chemotherapeutic agent used for the treatment of solid tumours. However, the particular drug has limited use, since at high cumulative doses, there is a risk of cardiomyopathy.[284] The cardiotoxicity is believed to be induced though the reductive bioactivation of DOXO into the corresponding metabolites DOXO C7 free radical and DOXO quinone methide, catalysed mainly by CYP 450 reductases.[285] *In vitro* and *in vivo* studies suggested that the above intermediates are capable of inducing toxicity via DNA and protein alkylation.[285, 286, 287] As shown in (Scheme 4.2), the proposed reaction mechanism involves a single electron reduction in the quinone moiety, leading to the generation of DOXO semiquinone, which can be rearranged into the corresponding DOXO C7 free radical via a hydrolytic cleavage or oxidised back to the parent drug and generate oxygen radicals or follow a second electron reduction by DT-diaphorase enzymes, leading

to DOXO quinone methide. In addition, a direct two-electron reduction and a hydrolytic cleavage on the quinone moiety can also lead to the formation of the corresponding DOXO quinone methide.

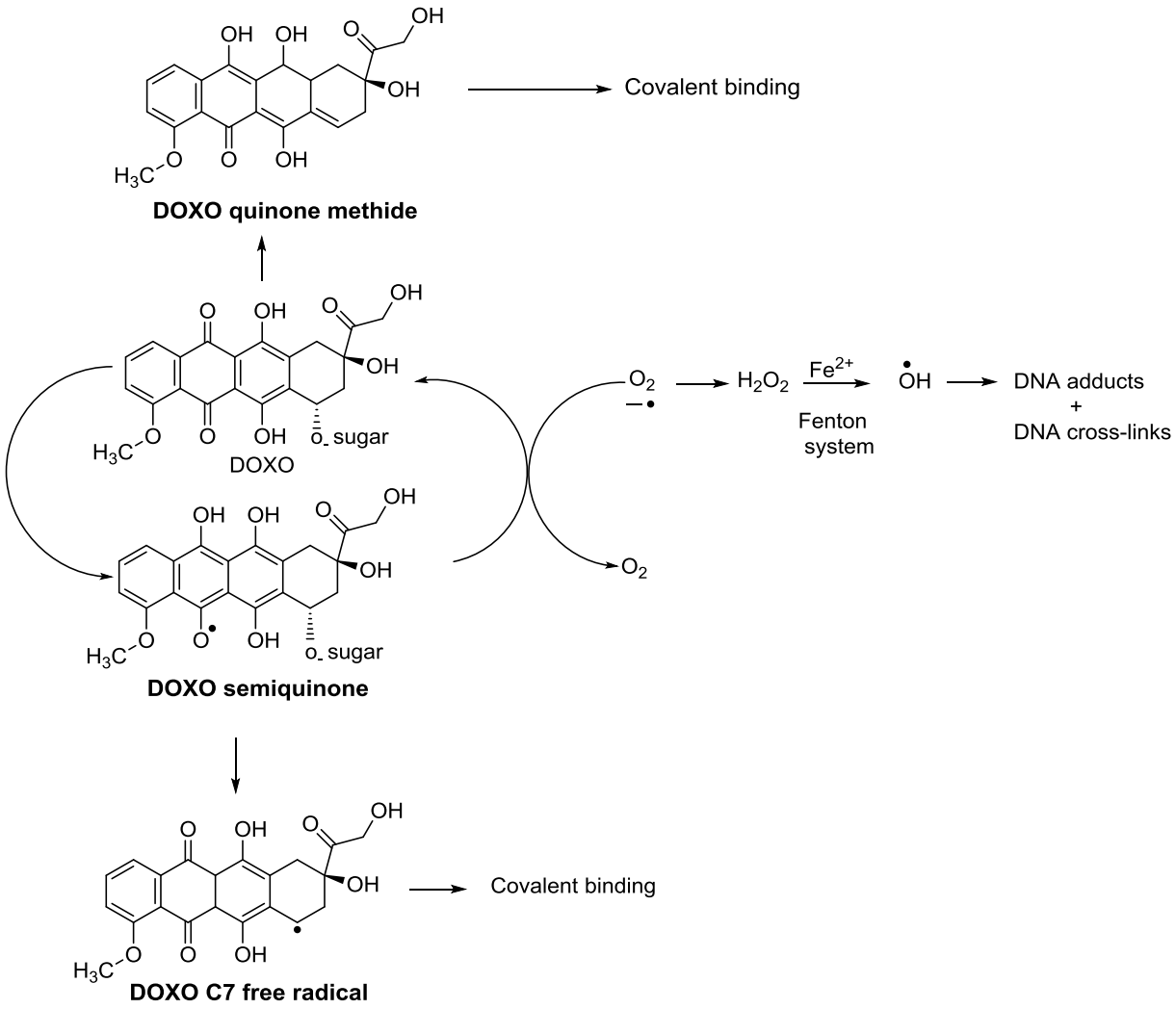

Scheme 4.2 *In vitro* metabolic pathway of DOXO.[285] DOXO semiquinone was generated via a single electron and a single proton transfer. Subsequently, the DOXO C7 free radical was formed via rearegement and hydrolytic cleavage. In addition, an additional electron-proton transfer leaded to DOXO quinone methide.

In Chapter 3, the metabolism of DOPA and RLX was simulated successfully by SPEs. The metabolic reactions involved the transfer of two electrons and two protons via dehydrogenation. This indicated the possible mimicry of single electron-proton transfers, as in the case of eugenol quinone methide and DOXO semiquinone.

The objectives of the experiment detailed in this chapter were:

1) Investigate the reaction mechanisms of DOXO and eugenol on SPEs.
2) Simulate the phase I reactions of DOXO and eugenol. Particularly, the electrochemical generation of the reactive DOXO semiquinone, DOXO C7 free radical, DOXO quinone methide and eugenol quinone methide by CPE.
3) Simulate the phase II GSH reactions via the covalent conjugation of DOXO semiquinone, DOXO free radical and eugenol quinone methide with GSH and subsequent detection by ESI/MS.

4.2 Results and discussion – eugenol

The electrochemical generation of eugenol quinone methide and GSH adduct via a single electron -proton treansfer and conjugations respectively was examined on the surface of the inexpensive sensor.

4.2.1 Electrochemical behaviour of eugenol

Eugenol ($2.5x10^{-5}$M) in ammonium acetate (pH 7.4) at 0.1 Vs^{-1}, generated a well-defined anode potential at 0.210 V (A1) with a peak current of 0.002 mA (Figure 3.1). Also, two low-magnitude cathode potentials appeared at 0.120 V (B1) and at -0.120 V (C1). The application of a second cycle generated the corresponding anode potentials at -0.150 V (B2) and -0.050 V (C2). The process was repeated three times (n=3).

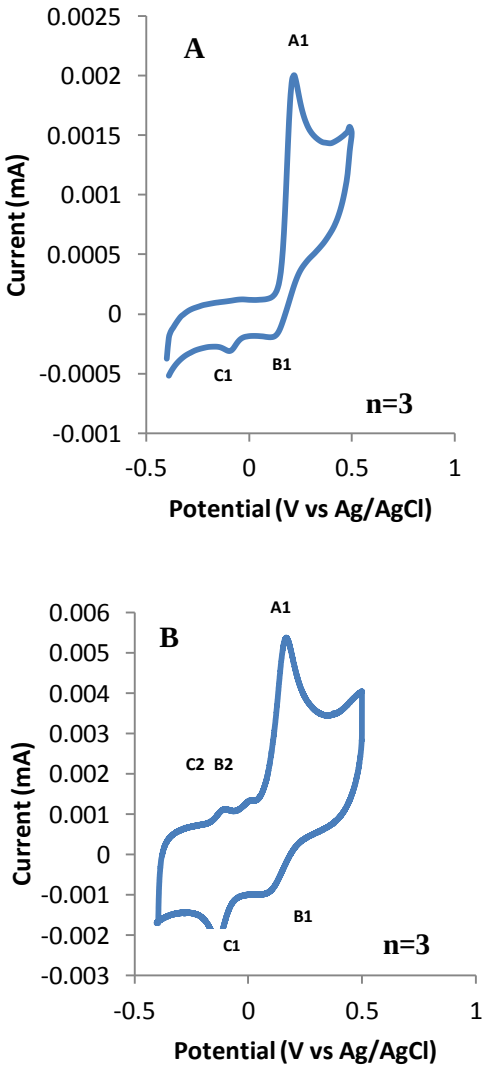

Figure 4.1 Electrochemical behavior of eugenol. A) First cycle; B) Second cycle. A second reversible pair was generated during the conducting of a second cycle.

Mono-phenols behave irreversibly in solid electrodes, but very often cathode potentials can be obtained during the reverse scan, as a result of product electrodeposition.[289] Thus, eugenol as a mono-phenol compound generated the electrodeposited cathode potentials at the surface of the SPE. As a consequence, according to the general rule of phenol oxidation on solid electrodes, it was concluded that A1 was a totally irreversible peak and involved the oxidation of phenol moiety into the corresponding phenoxyl radical. The redox pairs B1/B2 and C1/C2 implied the occurrence of a reversible process of the electrodepositede catechol and hydorquinone, respectively (Scheme 4.3). However, further studies were conducted to confirm the irreversibility of A1 and phenoxyl radical formation. Thus, the following experiments focused on A1 and were mainly recorded by DPV, unless otherwise stated.

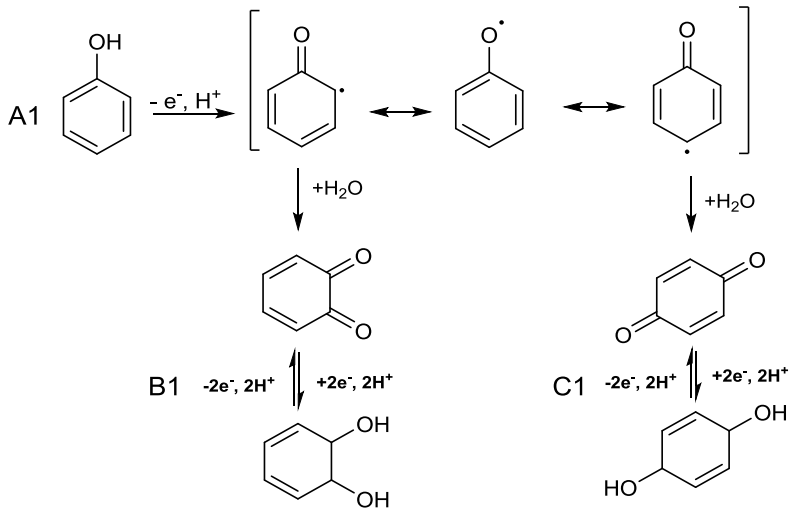

Scheme 4.3 Reaction mechanism of mono phenol moiety,[288] The reasonance form of the phenoxyl radical reacts further with water leading to catechol and hydroquinone.

4.2.2 Effect of pH

4.2.2.1 Participation of protons

The influence of pH on $2.5x10^{-5}$ M of eugenol was investigated by CV over a wide range of pH values (2, 4, 6, 7.4, 9, 10.5, 12). The buffer solutions were prepared in 0.1 M ammonium acetate and 0.1 M sodium hydroxide. The potential range was -0.4 V to 0.5 V and the scan rate was set at 0.1 Vs^{-1}. The process was repeated three times (n=3), in different. A linear relationship was obtained as shown in (Figure 4..2), implying the participation of protons during the oxidation process. Additionally, the slope was found to be 0.41 VpH^{-1}, which was close to the Nernstian slope, suggesting the participation of an equal number of protons and electrons.

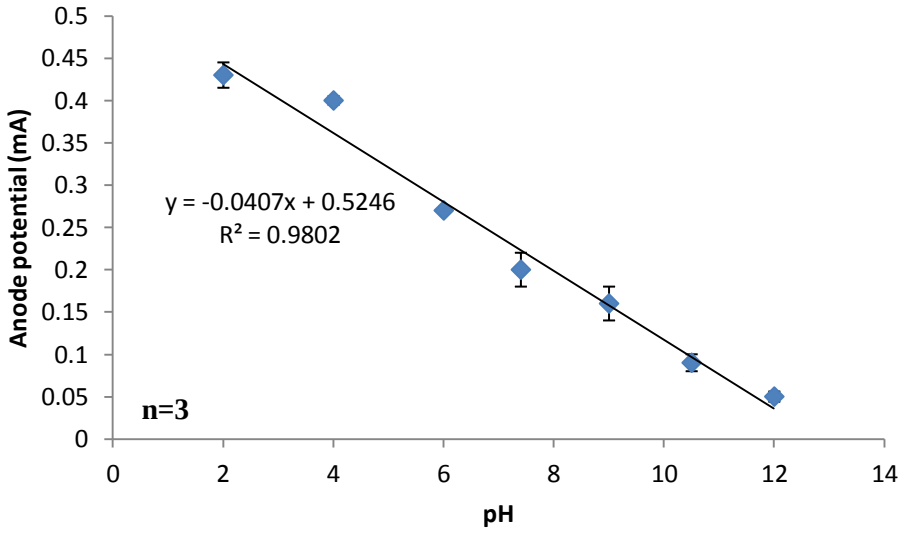

Figure 4.2 Participation of protons in eugenol oxidation. The anode potential shifted gradually to more negatives values due to proton participation.

4.2.2.2 Effect of pH on current

The effect of pH on anode current was investigated over the same conditions, as in section 4.2.2.1. Highly alkaline conditions generated lower currents than highly acidic pH, (Figure 4.3). The highest current was obtained at pH 6, which indicated the maximum generation of the product. The lowest current and minimum metabolite formation was observed at pH 10.5.

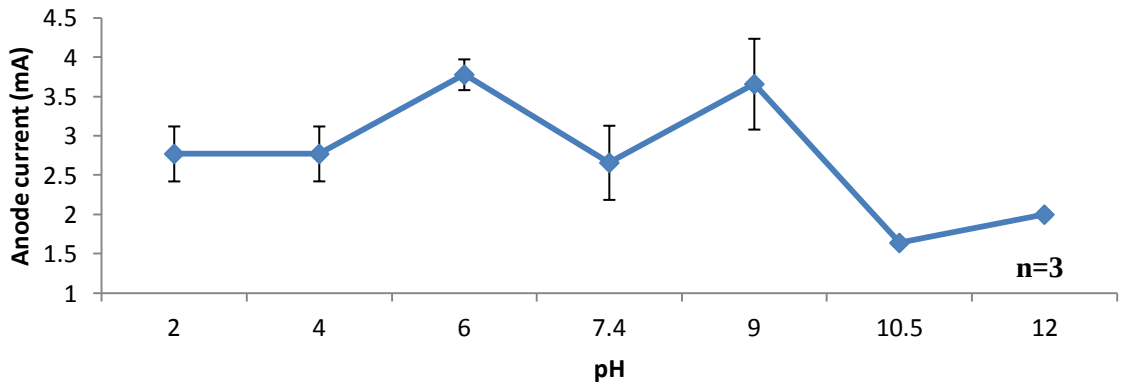

Figure 4.3 Relationship of eugenol anode current with pH. The highest current was obtained at pH s 1 and 4 suggesting the highest metabolite yields.

4.2.3 Effect of scan rate in electron transfer kinetics

Eugenol ($2.5x10^{-5}$M) was investigated by DPV, at a wide range of scan rates from 0.015 Vs^{-1} to 0.155 Vs^{-1} (Figure 5.7). The aim was to confirm the irreversibility of the system. Considering that the highest anode potential was obtained at pH 6, all solutions were prepared in the particular pH value. The irreversibility of eugenol was confirmed by the linear dependence of anode peak current with the SQRT of scan rate and the variation of anode potential with the scan rate[131,132] (Figure 4.5). The obtained kinetics were in agreement with those observed in previous studies on glassy carbon electrodes.[290]

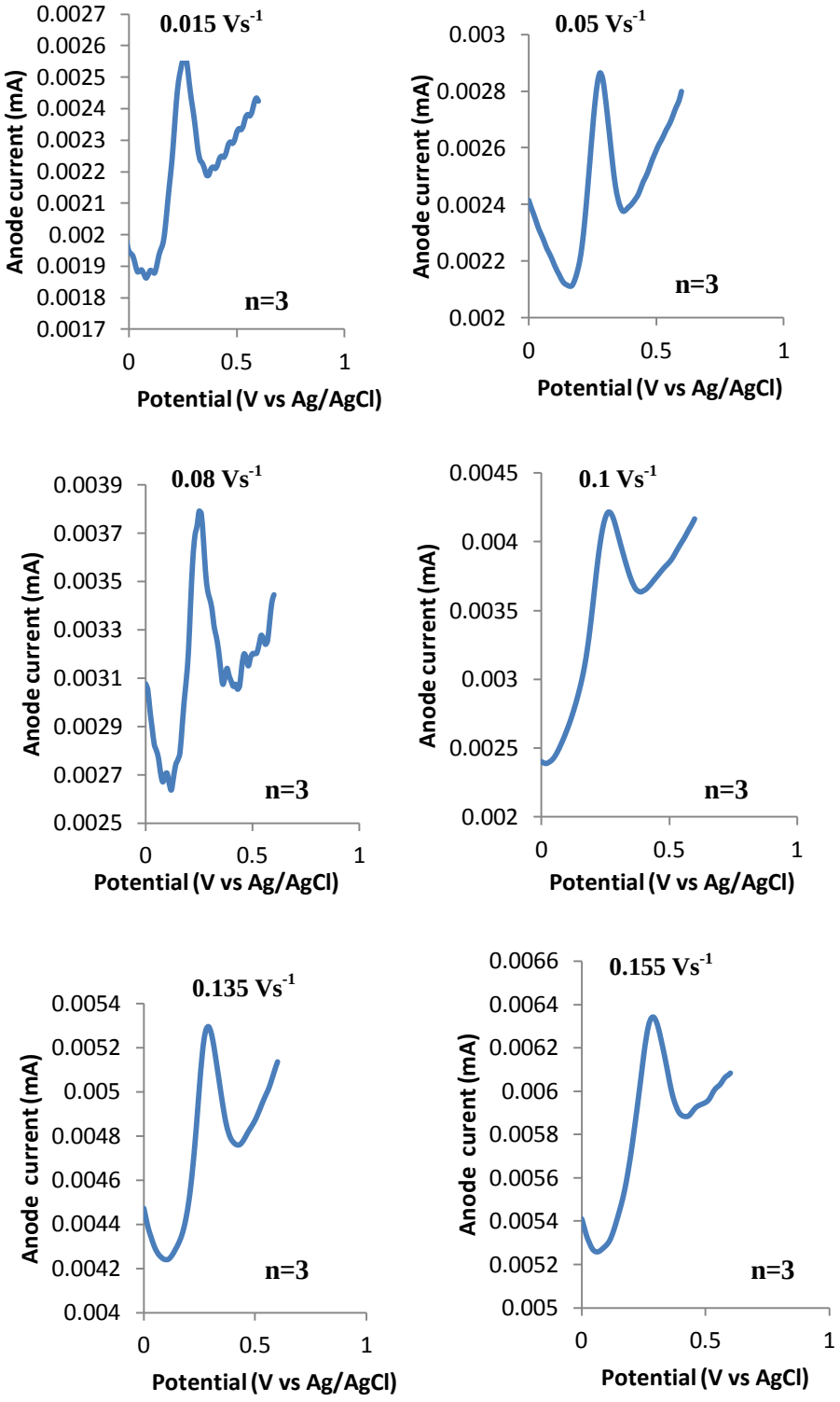

Figure 4.4 DPV of eugenol in various scan rates. A wide range of scan rates was applied from 0.015 Vs^{-1} to 0.155 Vs^{-1} to dermine the electron transfer kinetics.

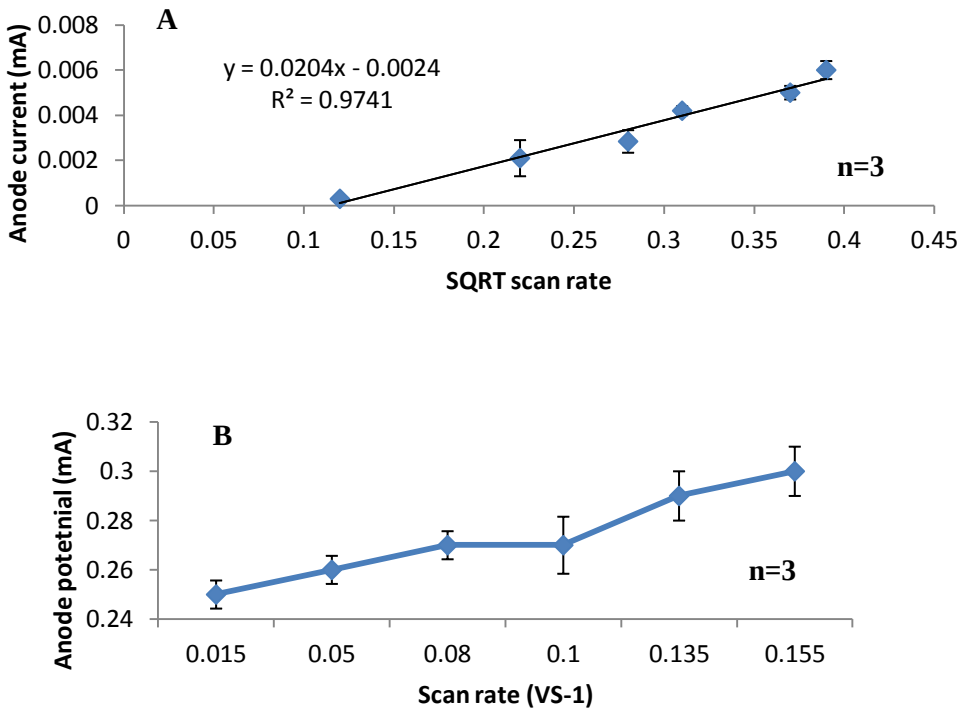

Figure 4.5 Irreversibility of eugenol. A) Anode current dependence with SQRT of scan rate; B) Variation of anode potential with scan rate.

4.2.4 Effect of transport mode

The obtained slope for the log (anode current) vs. log (scan rate) was 1.17, suggesting strong adsorption (Figure 4.6). Investigation in a glassy carbon electrode[291] suggested a mixture of both diffusion and adsorption; but adsorption was the dominant mode.

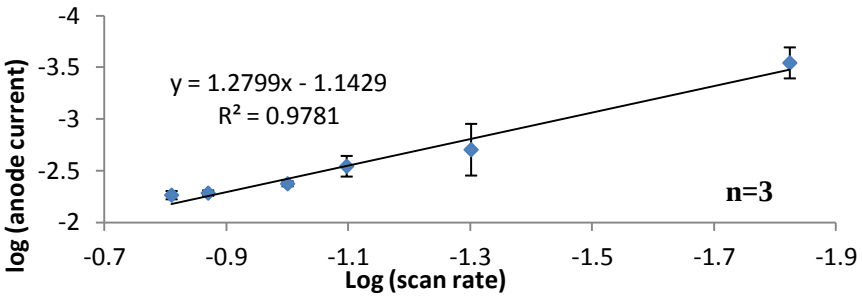

Figure 4.6 The transport mode of eugenol was controlled by strong adsorption. The calculated slope was found to be 1.27, implying an ideal adsorption.

4.2.5 Effect of concentration

As shown in (Figure 4.7), voltammograms of various eugenol concentrations from $2.5x10^{-5}$ M to $2.5x10^{-3}$ M at 0.1 Vs^{-1} suggested the independence of concentration with the formation of new metabolites. However, the electrodeposition of catechol and hydroquinone reduced progressively at $2.5x10^{-4}$ M and stopped completely from $5x10^{-4}$ M to $2.5x10^{-3}$ M, probably due to saturation.

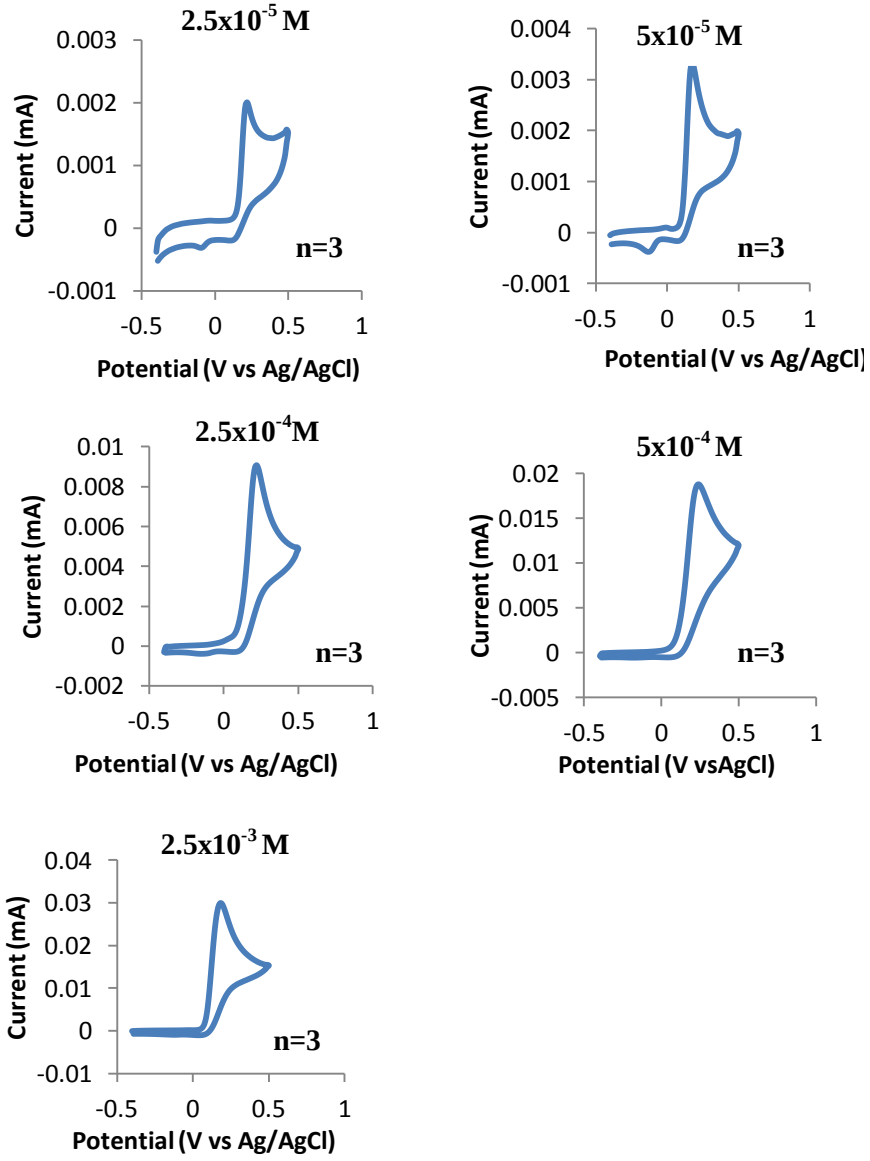

Figure 4.7 Voltammetry at various eugenol concentrations. Additional metabolites were not observed with the increase of eugenol concentration. Saturation effects were seen in higest concetration of $5x10^{-4}$ M and $2.5x10^{-3}$ M.

4.2.6 DPV in the presence of GSH

DPV was recorded in $2.5x10^{-5}$ M eugenol, in ammonium acetate (pH 7.4). The scan rate was 0.1 Vs^{-1}, the potential range was set from -0.1 V to 0.5 V, the pulse amplitude was 0.010 V, and the voltage step was 0.010 V. Each time, increasing GSH concentrations from 0 M to $2.5x10^{-4}$ M were added to examine changes in currents and potentials (Figure 4.8). As proven, the generated anode current depended strongly on GSH concentration, since it increased with an increase in GSH, suggesting the formation of a new metabolite and its subsequent reaction with GSH, probably leading to the formation of a GSH adducts. Changes were also observed in anode potential causing a significant shift to more positive values indicating the oxidiation of the generated metabolite at a new potential. Thus, the generated intermediate was reactive towards the thiol moiety of GSH.

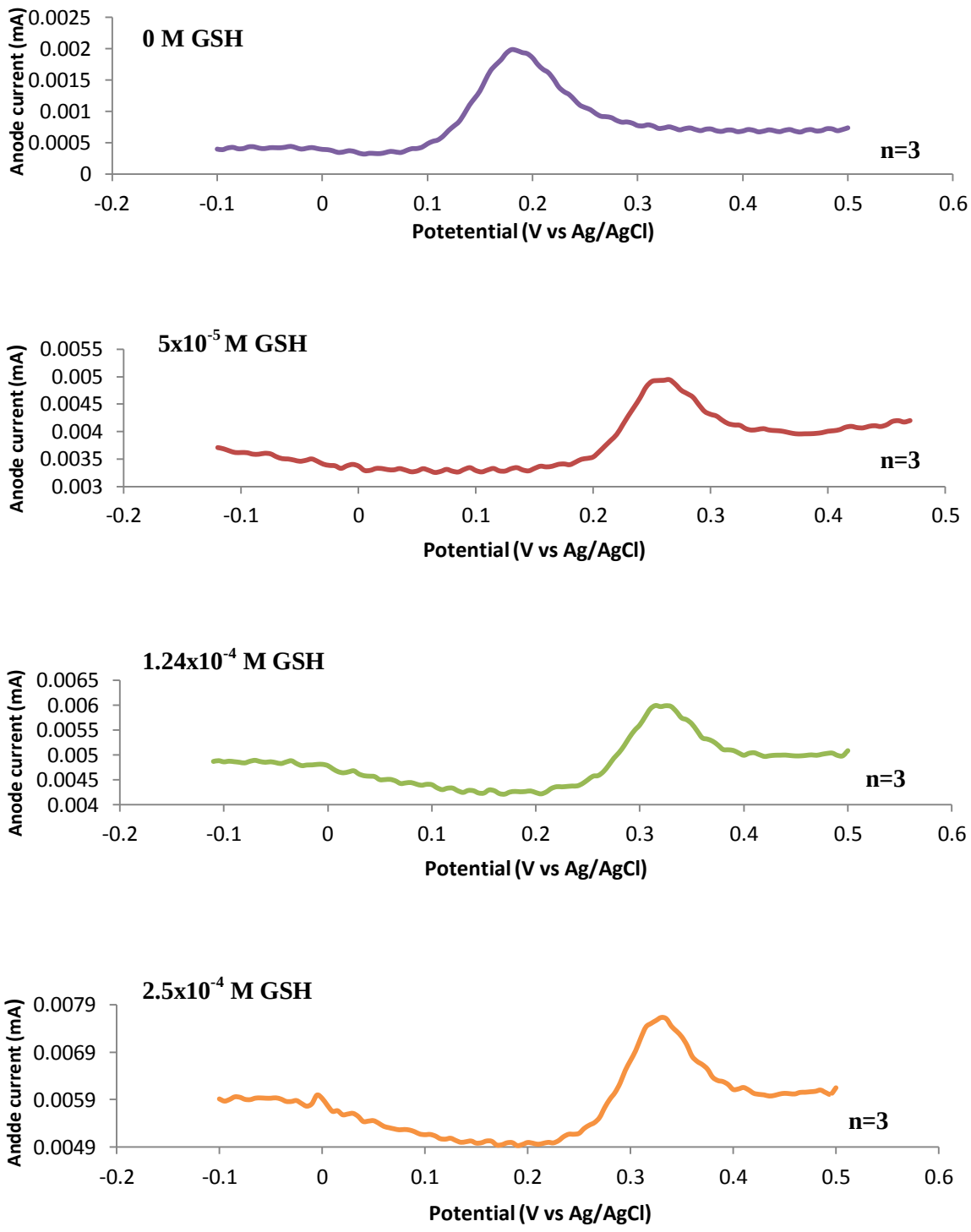

Figure 4.8 Eugenol in the presence of various GSH concentrations. The addition of various GSH caused shiftings in potentials and increase in current suggesting the formation of a new metabolite. Probably a GSH adduct was formed that was oxidized at a new potential. In addition the currents were increased since two metabolites were formed, as compared with the voltammogram in the absence of GSH.

4.2.7 Potential optimization

Eugenol ($2.5x10^{-5}$M) in 0.1 M ammonium acetate (pH 7.4) was electrolysed over a wide a range of potentials from 0.30 V to 0.65 V, in the presence of $5x10^{-5}$ M GSH. The potential range was determined by the oxidative peak in DPV, in section 4.2.5 and operated in a mass transport rate limit, with increasing steps of 0.050 V. The metabolites were detected by negative ESI/MS. The expected eugenol-GSH adduct was not formed in any of the applied potentials, whereas the catalytic GSSG was obtained at all potentials (Figure 4.9). At 0.45 V, GSH was depleted and a new metabolite (*m/z 325*) had emerged, which probably corresponded to the formation of a eugenol dimer, known as bis-eugenol.[292] The regeneration of the parent compound was seen only at 0.45 V, probably owing to the strong adsorption, preventing its detection at the other potentials. According to previously published *in vitro* data,[281] the presence of polymers in eugenol metabolism was a strong indication of the formation of either a eugenol phenoxyl radical or a eugenol quinone methide. Thus, 0.45 V was chosen as the optimum potential for the exhaustive electrolysis.

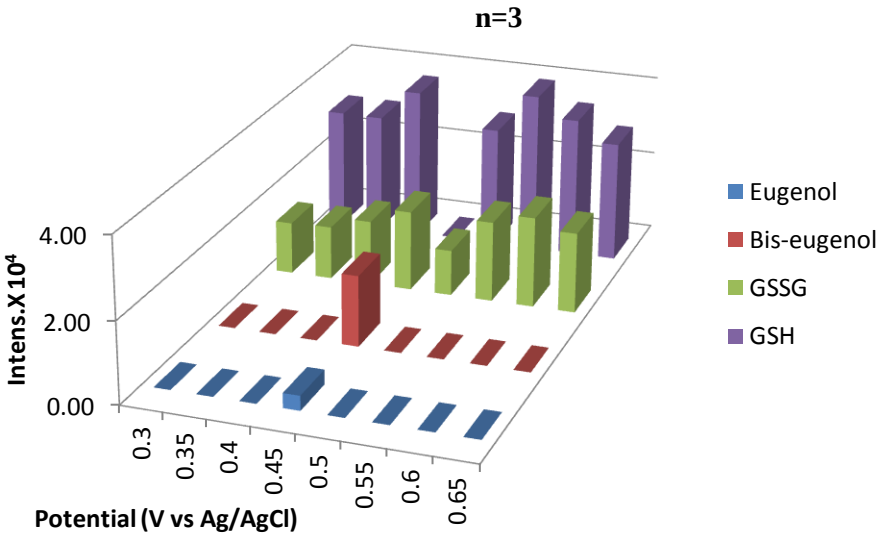

Figure 4.9 Potential optimization of eugenol. The catalytic GSSG was obtained at all potentials. Instead of a eugenol-GSH adduct, a eugenol dimer (bis-eugenol) was found at 0.45 V.

4.2.8 Exhaustive electrolysis and MS

Eugenol was electrolysed for 30 min at the optimized potential of 0.45 V, over the same conditions as specified in section 4.2.6. As seen in (Figure 4.10), the eugenol-GSH adduct was not formed and only the GSSG (*m/z* 610.80) and bis-eugenol (*m/z* 325.20) which was the most abundant ion, were obtained in the mass spectrum. Electrolyses (30 min) were carried out in acidic (pH 4) and in alkaline conditions (pH 9) to examine the possibility of generating either a more stable intermediate or higher intermediate yields, based on earlier observations in section 4.2.2.2. However, again, the phase II GSH adducts were not formed. As concluded, the dimer was probably the result of the polymeric reaction of the eugenol phenoxyl radical and not of eugenol quinone methide, since a route like this would have resulted to the formation of the corresponding eugenol-GSH adduct, according to Thomson *et al.*[281]

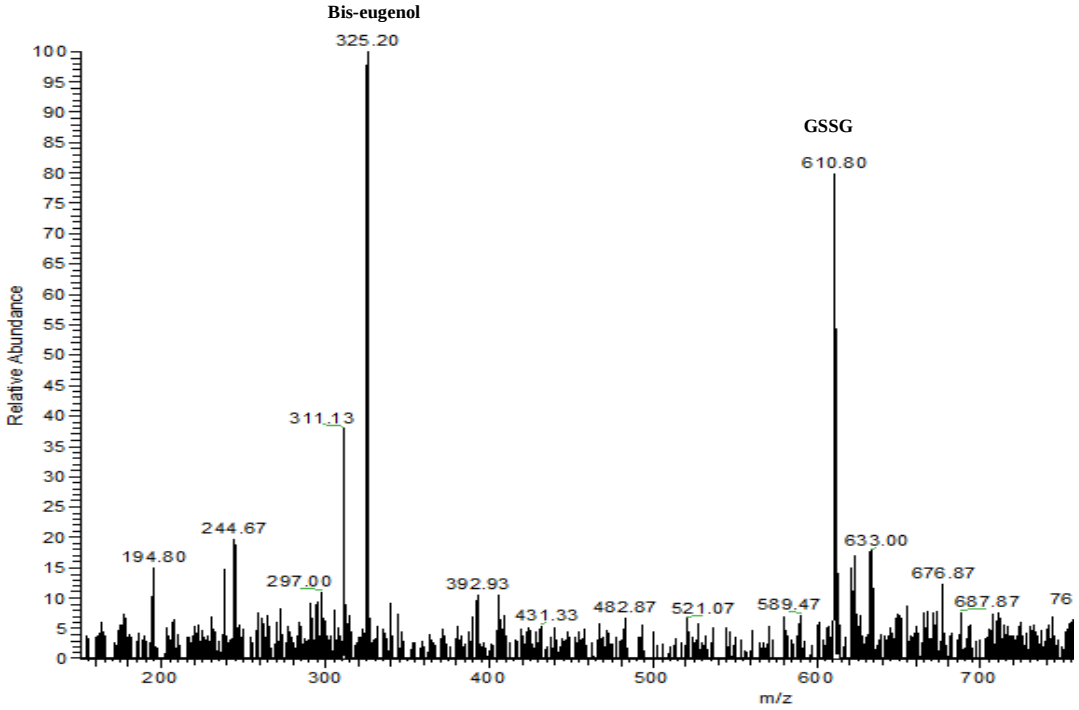

Figure 4.10 Partial mass spectrum of eugenol metabolism at 0.45 V. The bis-eugenol dimer (*m/z* 325.25) and GSSG (*m/z* 610.80) were obtained after 30 min of electrolysis.

4.2.9 Proposed reaction mechanism of eugenol

The proposed reaction mechanism as shown in (Figure 4.4), involved the formation of a eugenol phenoxyl radical via the loss of one electron and one proton. Then, the eugenol phenoxyl radical was detoxified through a catalytic reaction with GSH, leading to the formation of GSSG and parent compound regeneration. Also, a second pathway was observed which corresponded to the polymerisation of the phenoxyl radical and subsequent generation to bis-eugenol.

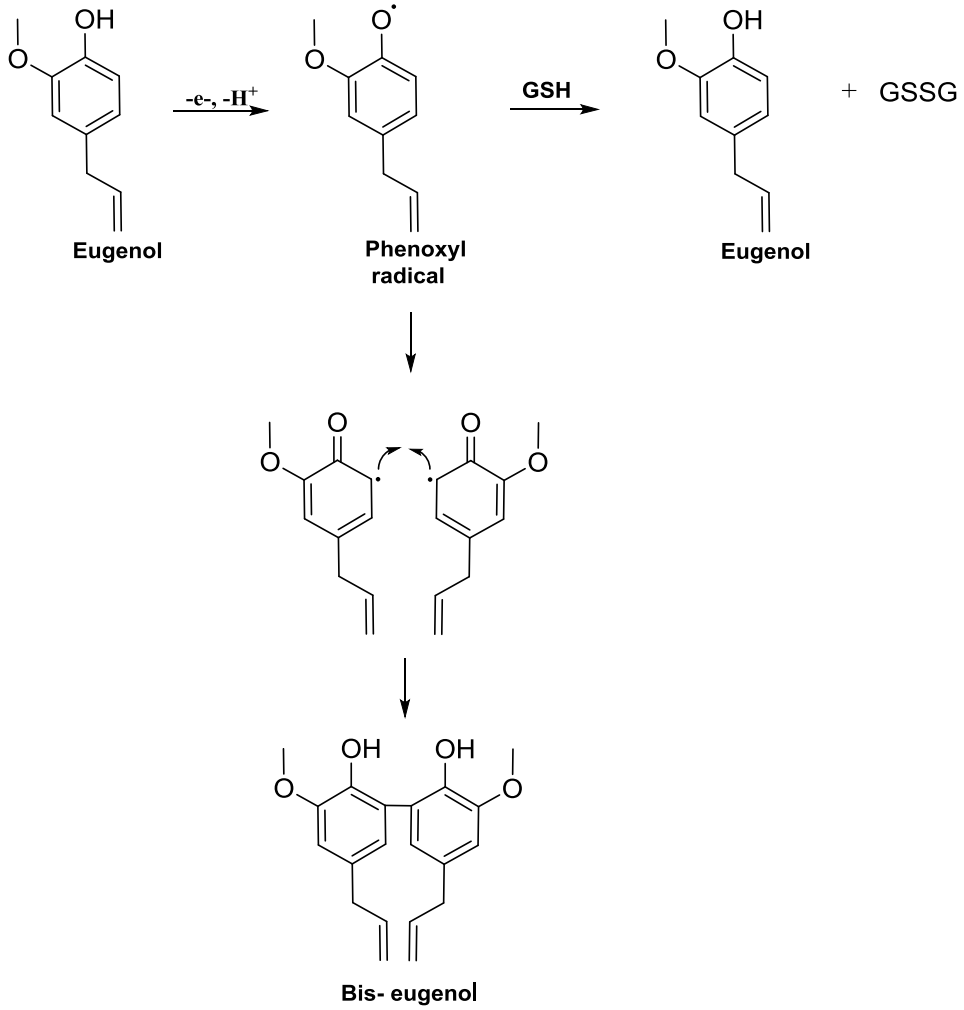

Scheme 4.4 Proposed reaction mechanism of eugenol based on mass spectra. The phenoxyl radical was generated electrochemically and followed a polymerisation process and a catalysis pathway.

The parent compound was not obtained in the mass spectrum (Figure 4.10) owing to its depletion, since it was participating in two parallel pathways simultaneously. In addition, the strong adsorption properties of eugenol, as shown in section 4.2.4, might have had an impact on eugenol detection.

The proposed reaction mechanism was in good agreement with the findings of Thomson *et al*.[281] (Sheme 4.1), suggesting the mimicry of peroxidase rather than CYP 450. A strong indication was the dimer formation, which was seen exclusively in peroxidase metabolism. Also, in the same study, it was proposed that GSH had an inhibitory effect on the formation of eugenol quinone methide, and lower yields of eugenol–GSH adducts were obtained. In particular, a proportion of the eugenol phenoxyl radicals was depleted through the catalytic process and never stabilised to the corresponding quinone methide. Herein, the possibility of generating the eugenol quinone methide was rejected since this would have led to the formation of both polymers and eugenol-GSH adducts. Thus as concluded the electro-generated eugenol phenoxyl radicals were depleted completely through the catalytic pathway. SPEs successfully mimicked a significant part of eugenol metabolism involving both phase I and phase II reactions. The main reactive metabolite (eugenol phenoxyl radical) was formed and detected indirectly via the formation of GSSG and the phase I polymer bis-eugenol.

The electrochemical metabolism of eugenol was investigated previously by the Karst research group[293] using a conventional amperometric flow cell coupled online with LC/MS. The cell was equipped with a boron-diamond working electrode, a Pd/H_2 reference electrode, and a Teflon block as the counter electrode. In the conventional method, different metabolic reactions and intermediates were obtained than with the use of SPEs,

owing to differences in electrode properties and the available working area. In particular, the diamond electrode permitted the application of a wide potential window (0 V - 2.5 V) and, as a consequence, the mimicry of various metabolic reactions such O-demethylation, dehydrogenation and oxygen addition that eventually led to the formation of quinones and quinone methides, at the optimised potential of 2 V (Scheme 4.5). On the other hand, carbon ink provided a limited potential range (less than 1 V) and such diversity in metabolic reactions was not obtained by the SPEs.

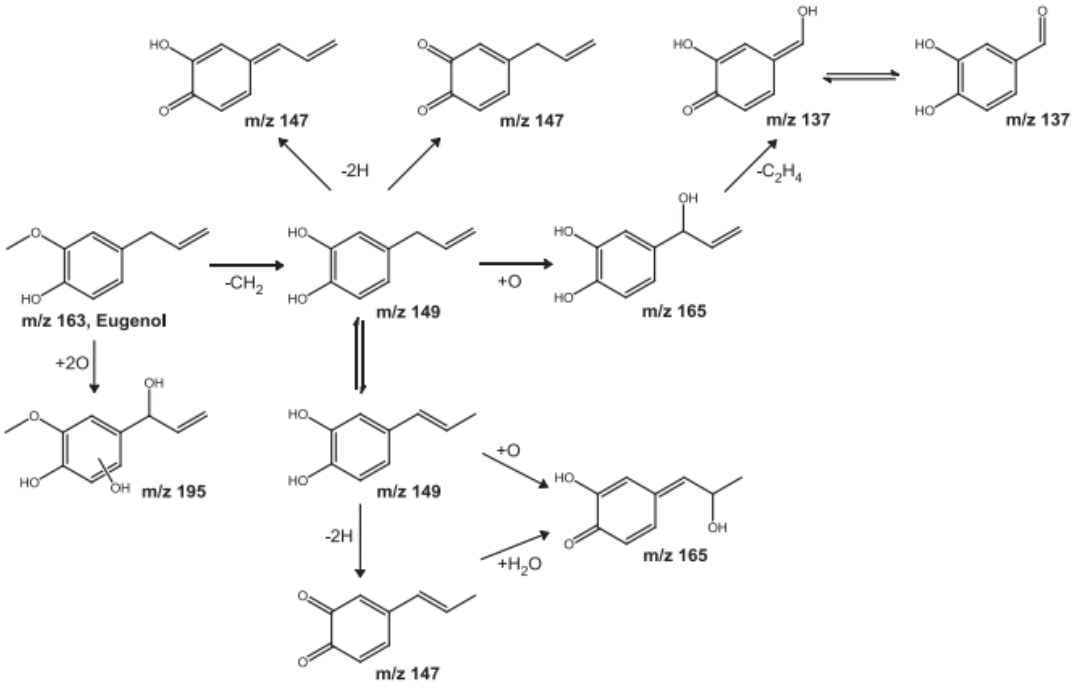

Scheme 4.5 Eugenol metabolism in a diamond, reprinted with permission from Melles *et al.*[293] Conventional electrode leaded to generation of different metabolites compared to SPEs due to the applications of high potentials and larger working diameter.

O-demethylation was the main reaction that occurred even at low potentials, so it was expected to occur in SPEs. However, the smaller surface area of the SPE (12.5 mm^2) than that of the diamond electrode (50.24 mm^2)[294] probably generated the particular metabolite

at insufficient yields for detection or the particular reaction was not favoured in SPEs. The single electron and single proton transfer that was seen in SPEs was not mimicked in the diamond electrode. Probably, the formation of the particular intermediate was not favoured in the applied conditions.

The proposed metabolic pathway for the flow cell was in agreement with animal studies and mimicked the catalytic action of CYP 450, while SPE provided similar results with *in vitro* peroxidase experiments. As concluded, different electrode materials and geometries were capable of mimicking certain types of enzymes such as CYP 450 and peroxidases with a potential to replace the expensive use of the particular enzymes at some extent in pharmaceutical research.

4.3 Conclusion

The possibility of mimicking the reactive pathway of eugenol into eugenol quinone methide was investigated with disposable SPEs. Primary electrochemical investigations on SPEs presented a similar behaviour with the glassy carbon electrode. In both solid electrodes and SPEs, eugenol was oxidised irreversibly via a single electron and a single proton transfer. At the optimized potential of 0.45 V, the corresponding eugenol-GSH adduct was not formed, but the GSSG metabolite and bis eugenol dimer were formed. The proposed reaction mechanism suggested the oxidation of eugenol into the corresponding eugenol phenoxyl radical, which led to radical polymerisation and catalytic process. The formation of eugenol-GSH adduct was prevented by the catalytic process since the electro-generated eugenol phenoxyl radical was depleted and never stabilised to the corresponding quinone methide. The electrochemical method was in good agreement with the catalytic activity of peroxidase. Previous electrochemical studies in flow cells simulated the

metabolic process of eugenol by CYP 450 and generated completely different metabolites, compared to SPEs, owing to differences in electrode material and geometry. Thus, the limited available area of the SPE was proven to be beneficial, since it permitted the mimicry of a particular reaction (single electron and single proton transfer) which was not seen in flow cells. Thus, different electrodes with different configurations could mimic the catalytic action of various phase I enzymes.

4.4 Results and discussion – DOXO

The simulation of phase I reductions on the SPE was studied using DOXO as a model comopound. Both the reactive DOXO quinone methide and DOXO C7 radical formation were aimed for generation through an initial single electron and single proton reduction and their subsequent trapping with GSH.

4.4.1 Electrochemical behaviour

Investigations regarding the reduction of 2.5×10^{-5} M DOXO in 1 mM acetic acid (pH 3) at 0.155 Vs^{-1} generated a well-defined redox pair (Figure 4.11). The cathode potential was obtained at -0.680V with a current of -0.069 mA, whereas the anode potential appeared at -0.63 V with a 0.036 mA current. The separation peak potential was 0.05 V, which suggested a reversible system, but the peak current ratio was found to be 1.9, larger than the expected value of unity.

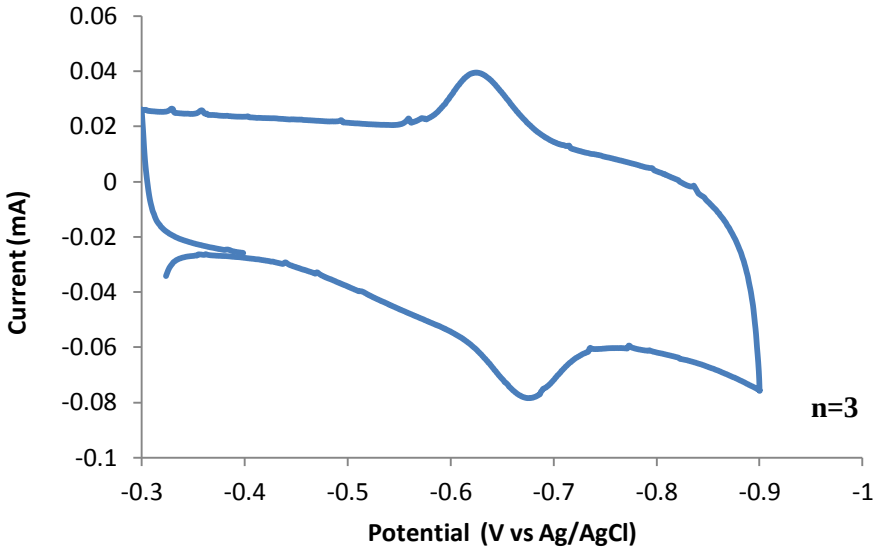

Figure 4.11 Electrochemical behavior of DOXO. A pair of a reversible redox peaks were obtained at -0.680V and at -0.63 V.

4.4.2 Effect of PH

Herein, $2.5x10^{-5}$ M DOXO was studied at a wide range of pH values, in 0.1 M ammonium acetate (pH 2, 3, 4, 6, 7.4, 9, 10.5) and in 1 mM acetic acid (pH 3), at 0.155 Vs^{-1}. A reversible pair was only seen at pH 3, as shown in (Figure 4.11), whereas the electrochemical signal disappeared at the other pH values, (Figure 4.12). Investigations of DOXO in a carbon paste electrode[295] showed strong adsorption phenomena at pH 4.5 and desorption effects at higher pH values, leading to decreased electrochemical signals. Herein, a similar desorption process had probably caused the disappearance of the electrochemical signals. Also, the participation of protons through the effect of pH was not feasible, so no indications regarding the formation of the required metabolites were observed. The process was repeated three times (n=3), in different SPE.

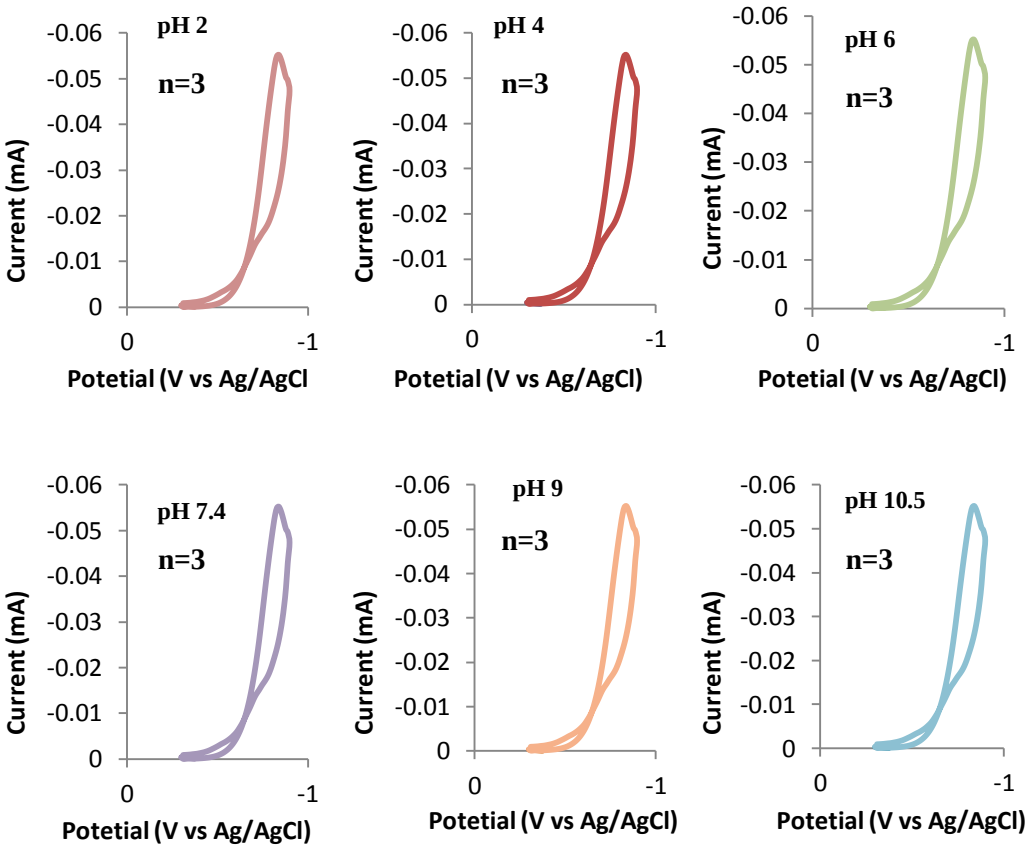

Figure 4.12 Voltammograms of DOXO at various pH values. Strong desorption effects had probably caused the disappearance of the electrochemical signal.

4.4.3 Effect of scan rate

DOXO ($2.5x10^{-5}$ M) in acidic conditions (pH 3) was investigated at the scan rate range of 0.015 Vs^{-1} – 0.20 Vs^{-1} (Figure 4.13). The process was repeated three times (n=3). The aim was to determine the kinetics of DOXO in SPE. A linear dependence of the anode and cathode currents with the SQRT of scan rate was observed (Figure 4.14).

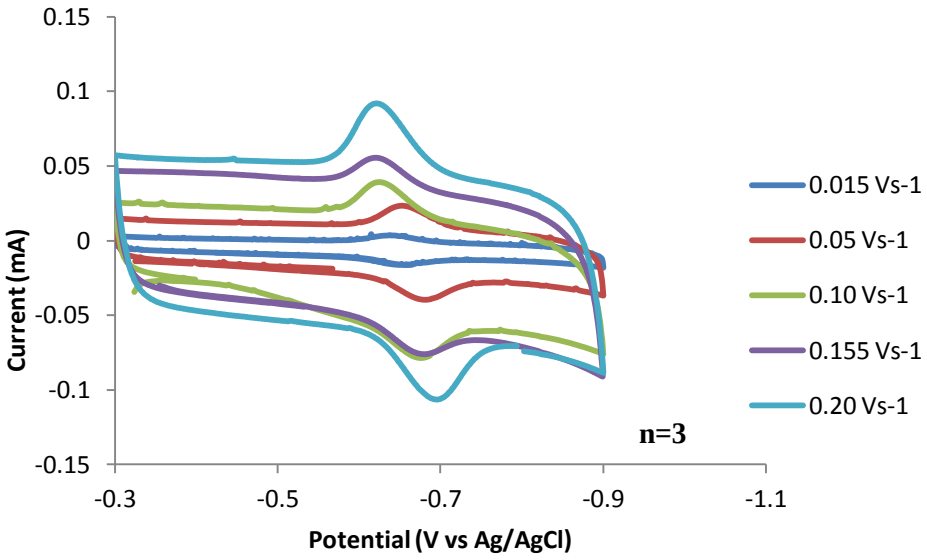

Figure 4.13 Voltammograms of DOXO in various scan rates. The scan rate range was applied from 0.015 Vs^{-1} to 0.20 Vs^{-1}.

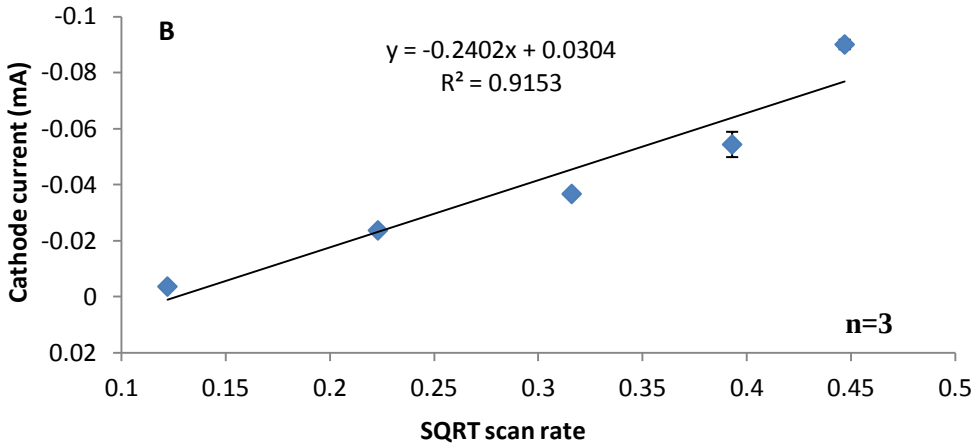

Figure 4.14 Linear relationship of DOXO currents with SQRT of scan rate. A) Anode current; B) Cathode current.

Additionally, the anode and cathode potentials were independent of the increasing scan rate. The separation peak potentials showed an increasing trend with the increasing scan rate. However, the values were in the acceptable range of reversible kinetics[130] (Figure 4.15). Thus, as concluded, the reduction of DOXO on SPE was reversible.

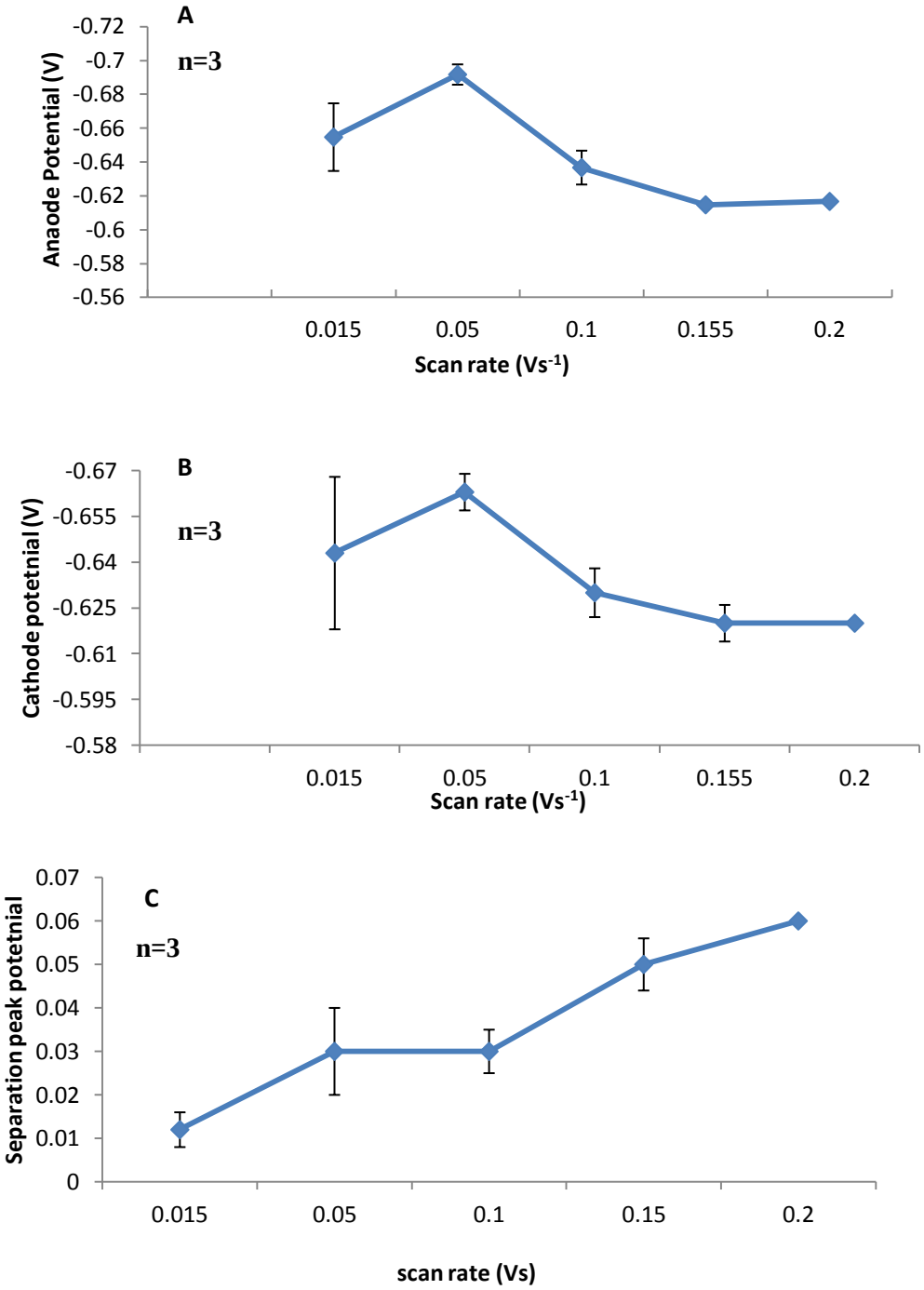

Figure 4.15 Dependence of DOXO potentials with scan rate. A) Anode potential; B) Cathode potential; C) Separation peak potential.

Thus, the kinetics were reversible and in good agreement with voltammograms obtained with glassy carbon electrodes.[296, 297] In their study, the reversible pair represented the reduction of DOXO to DOXO dianion via a two-electron transfer and without the participation of protons (Scheme 4.6).

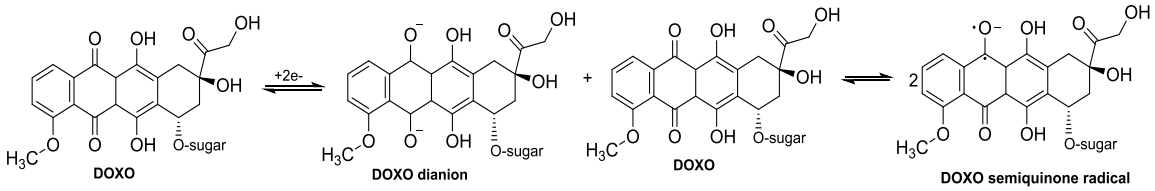

Scheme 4.6 Dianion formation. DOXO was reduced via the transfer of two electrons into the corresponding DOXO dianion, which subsequently reacted with DOXO, leading to DOXO semiquinone radical.

In both cases, the electrochemical reduction was followed by a chemical step, leading to the formation of a DOXO semiquinone radical. Subsequently, the generated DOXO dianion reacted chemically with the parent DOXO and formed the reactive semiquinone radical that was subsequently trapped with DNA.

Moreover, reversible pairs of DOXO were also obtained with mercury[298, 299] and graphite electrodes.[300] However, in these cases, a hydroxyl DOXO product was formed via a two-electron reduction. Thus, the possibility of generating either the dianion or the hydroxyl DOXO or the required metabolites such as DOXO C7 free radical and DOXO quinone methide were all considered, since the participation of protons was not confirmed, owing to the dependence of DOXO on pH at pH 3.

.

4.4.4 Mass transport mode

The transport mode was controlled by strong absorption. The calculated slopes (Figure 4.16) were found to be 1.20 and 1.18 for anode and cathode potentials, respectively. A strong adsorption was reported in previous electrochemical investigations with solid electrodes.[295, 298- 300] The findings supported the earlier pH dependence of the drug at pH 3 and were in good agreement with electrochemical investigations with carbon paste electrodes,[295] which supported the fact that in acidic conditions, the strong adsorption generated high currents, whereas in alkaline media, the drug was gradually desorbed leading to decreased and lower-magnitude currents. Herein, the DOXO was completely desorbed at the pH values of 2, 4, 6, 7.4, 9, 10.5 and as a consequence, the lack of the transport mode on the SPE surface prevented the formation of the electrochemical signal.

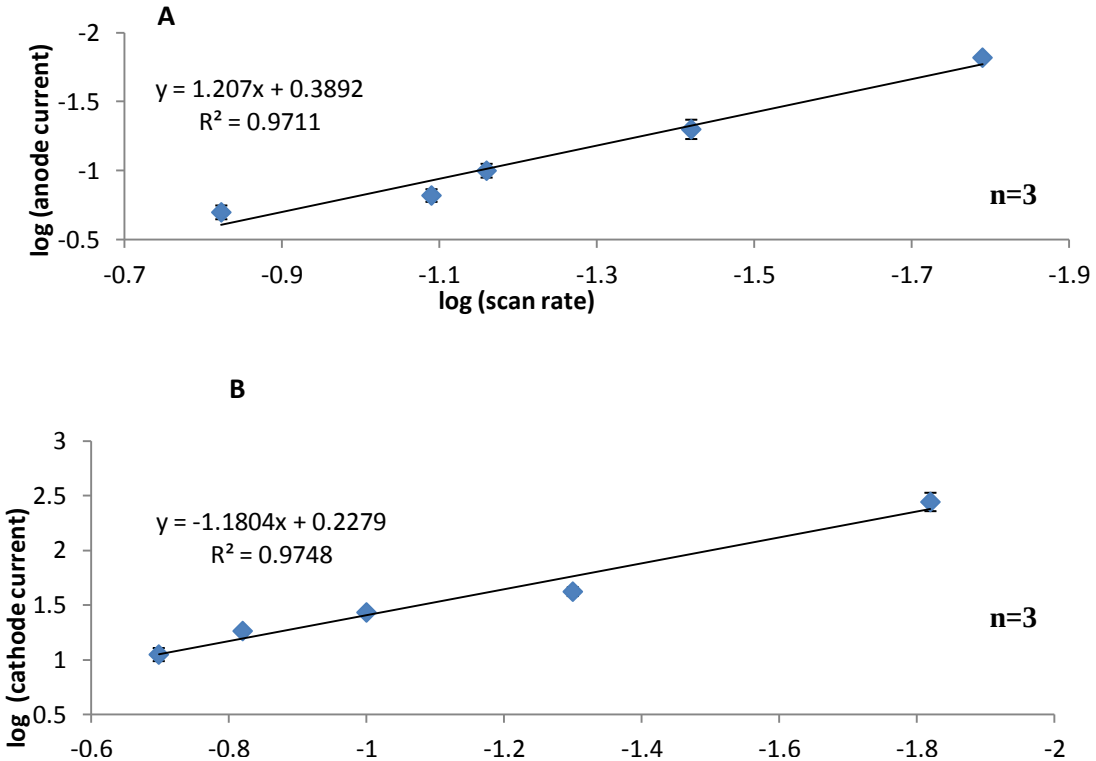

Figure 4.16 Mass transport mode of DOXO. A) Anode current; B) Cathode current. Strong adsorption properties of DOXO on the surface of the SPE, the obtained slopes were higher than unity.

4.4.5 Effect of concentration

Various concentrations of DOXO in the range of $2.5x10^{-5}$ M to $2.5x10^{-3}$ M, in 1 mM acetic acid (pH 3) were investigated in terms of CV (Figure 4.17). In the obtained voltammograms, additional peaks or changes corresponding to the formation of additional metabolites were not seen. For example, the appearance of a second reduction peak would have corresponded to the formation of DOXO quinone methide via the reduction of DOXO semiquinone.

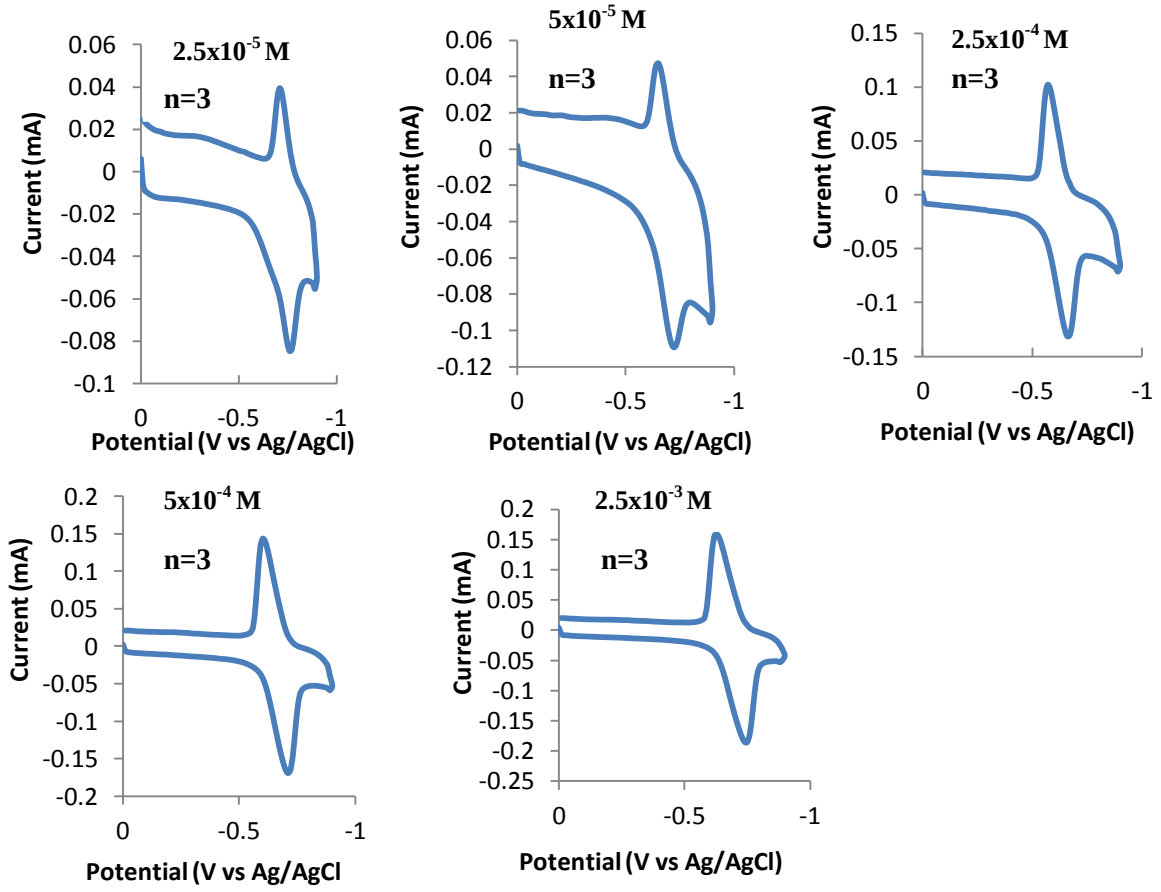

Figure 4.17 Voltammetry at various DOXO concentrations. In the range of $2.5x10^{-5}$ M to $2.5x10^{-3}$ M the same reversible peak was seen without any indications regarding the formation ofnew metabolites as a function of concentration.

4.4.6 CV in the presence of GSH

The reactivity of the generated product was investigating voltammetrically in the presence of increasing GSH concentrations, at the range of 0 M to $2.5x10^{-4}$ M. Changes have been observed on the cathode and anode potentials and, in particular, a shift to more positive values was observed, suggesting the formation of a new product, (Figure 4.18). However, the obtained currents were maintained at the same values, as obtained in the voltammetry without the addition of GSH, even at the highest GSH concentration of $2.5x10^{-4}$ M. Thus, inconclusive results were obtained since the potential shifting might provide an indication of the formation of a reactive metabolite such as the DOXO semiquinone, DOXO C7 free radical, or DOXO quinone methide. However, the maintenance of the generated currents indicated the probable formation of non-reactive products such as DOXO dianion or hydroxyl DOXO.

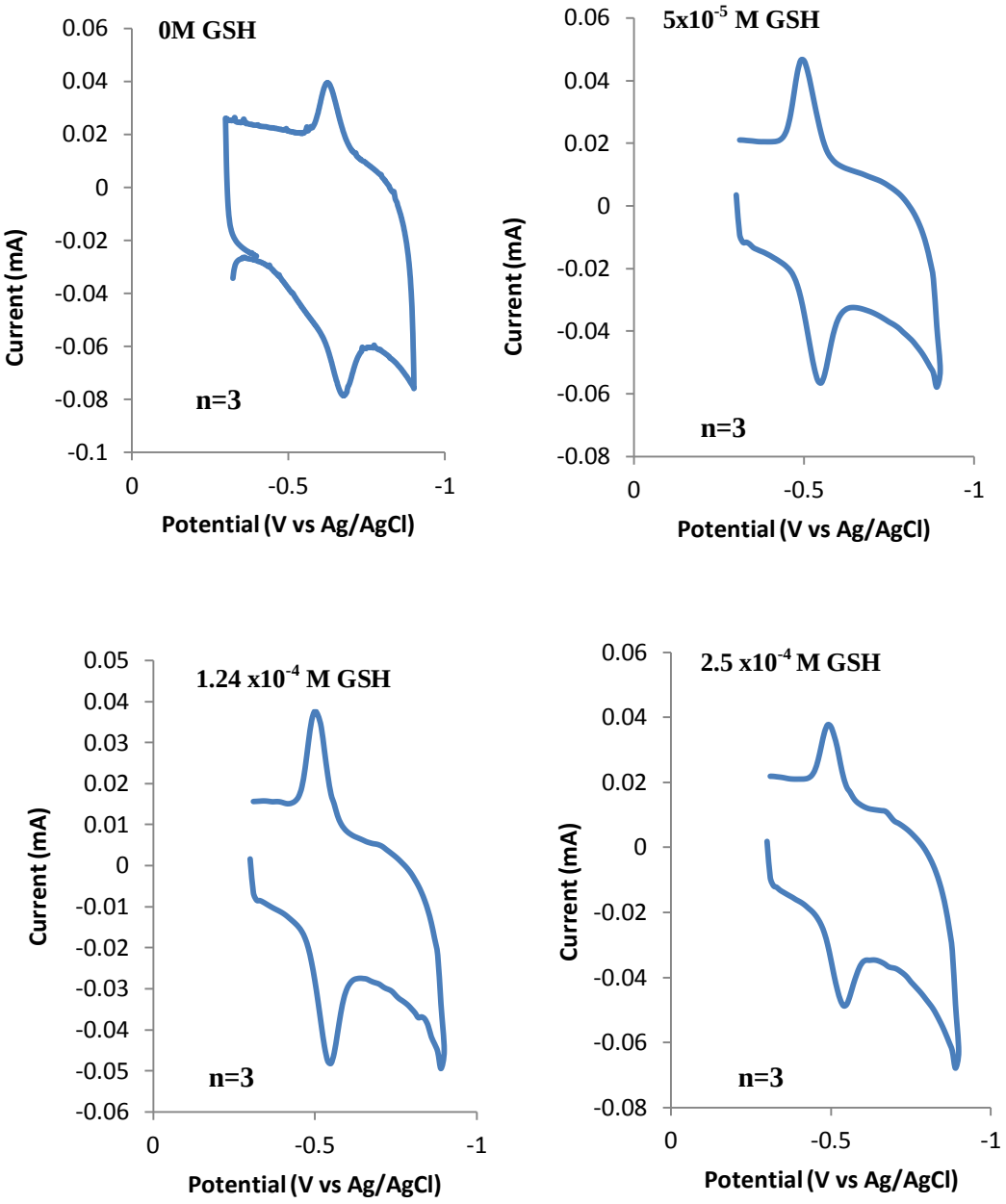

Figure 4.18 DOXO in the presence of various GSH concentrations. Incoclusive results regarding the formation of a DOXO- GSH adduct were obtained since the current were maintained at the same levels, at all the investigated GSH concentrations. The anode potential shifted to new potentials after the addition of increased GSH concentration, suggesting the possible formation of an electroactive.

4.4.7 Potential optimization

Herein, $2.5x10^{-5}$ M of DOXO in the presence of $5x10^{-5}$ M GSH was electrolysed for 0.5 min, over a wide range of potentials from -0.058 V to -0.93 V with increasing steps of 0.05 V, in the optimized buffer of pH 3. In (Figure 4.19), the GSH adduct or the catalytic metabolite of GSSG was not formed at any of the applied potentials. This indicates the possibility of generating the non-reactive products of hydroxyl DOXO or DOXO dianion that were unstable and oxidised immediately back to DOXO. However, considering the *in vitro and in vivo* studies, the DOXO semiquinone, as a reactive and short-lived intermediate, could have probably oxidised immediately back to the parent drug or formed at insufficient yields, preventing its subsequent formation to DOXO C7 free radical or DOXO quinone methide. In addition, the direct formation of DOXO quinone methide as an electropositive intermediate was expected to give some indications in the obtained mass spectrum, as seen in the previous cases in Chapter 3.

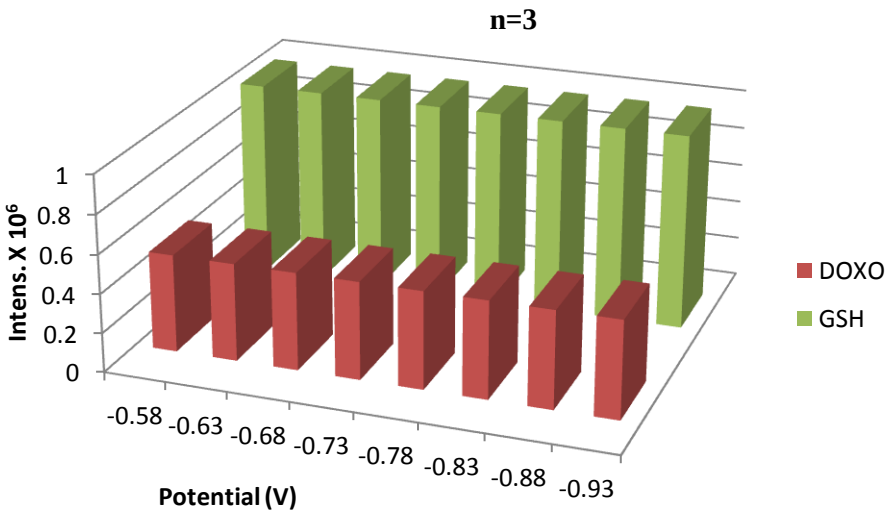

Figure 4.19 Potential optimization of DOXO. Only the parent drug and GSH were obtained leading to inconclusive results.

4.4.8 Exhaustive electrolysis and offline MS

Exhaustive electrolysis (30 min) was conducted at all potentials, as seen in section 4.4.7. However, a longer duration of electrolysis failed to generate the DOXO-GSH adducts or GSSG. A representative mass spectrum at -0.73 V is shown in (Figure 4.20): only DOXO (*m/z* 544.2) and GSH (*m/z* 308) were obtained. In addition, mass spectrometric detection in the negative ion mode was conducted for investigating the possibility of detecting the negatively charged dianion; however, the product was not obtained. The experiment was conducted at higher concentrations of $2.5x10^{-4}$ M DOXO in the presence of $5x10^{-4}$ M GSH but again only the parent drug and GSH were obtained

.

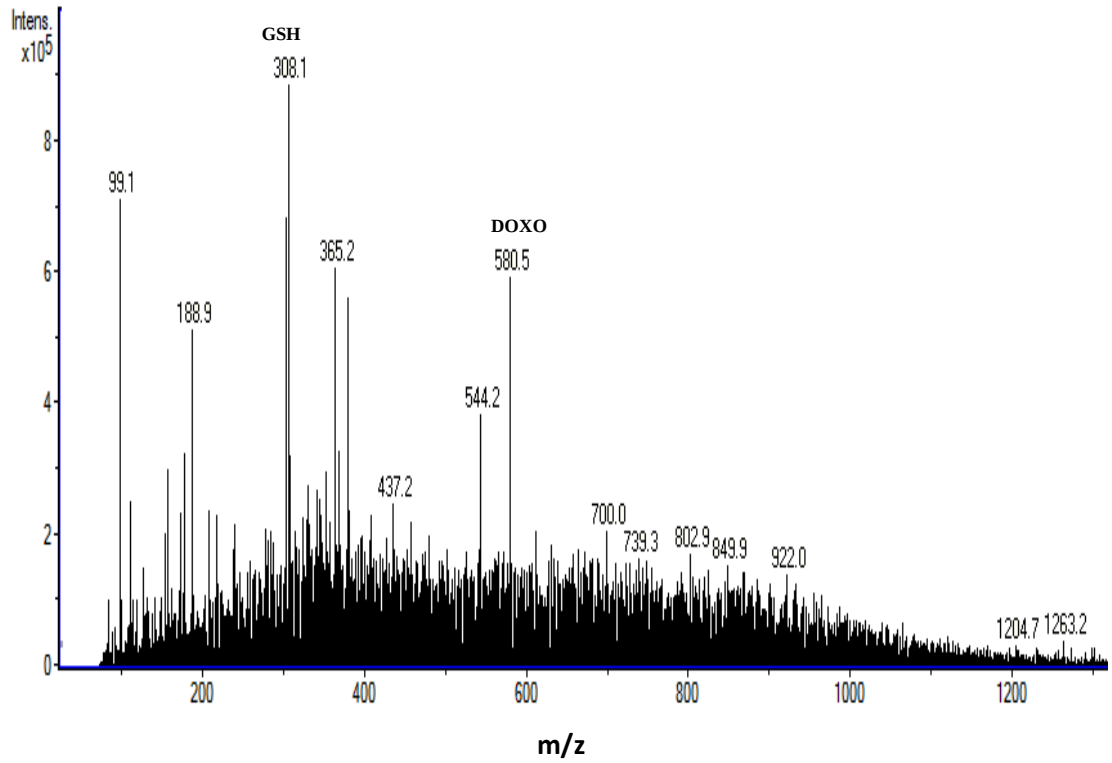

Figure 4.20 Partial mass spectrum of DOXO metabolism at -0.73 V. GSH adducts were not detected even at exhaustive electrolysis.

4.4.9 Proposed reaction mechanism of DOXO

The lack of product signals in the obtained mass spectra and the unclear indications regarding the reactivity of the generated product with GSH, in section 4.4.6, indicated three possible reaction mechanisms. According to the first pathway (Scheme 4.7), DOXO semiquinone was generated successfully at low concentrations, and in combination with the strong adsorption, it led to the insufficient yields of DOXO C7 free radical or DOXO quinone methide. As a consequence, the generation of GSH adducts was below the detection limit of the mass spectrometer. In addition, considering the calculated peak current ratio of 1.9, in section 4.4.1, the possibility of generating an unstable semiquinone that was oxidised quickly to DOXO was also likely, preventing its further reaction to DOXO C7 free radical or DOXO quinone methide. The possibility of a parallel route between oxidation and GSH conjugation can be also considered. The particular pathway is in agreement with the metabolic pathway proposed in *in vitro* and *in vivo* studies.[285]

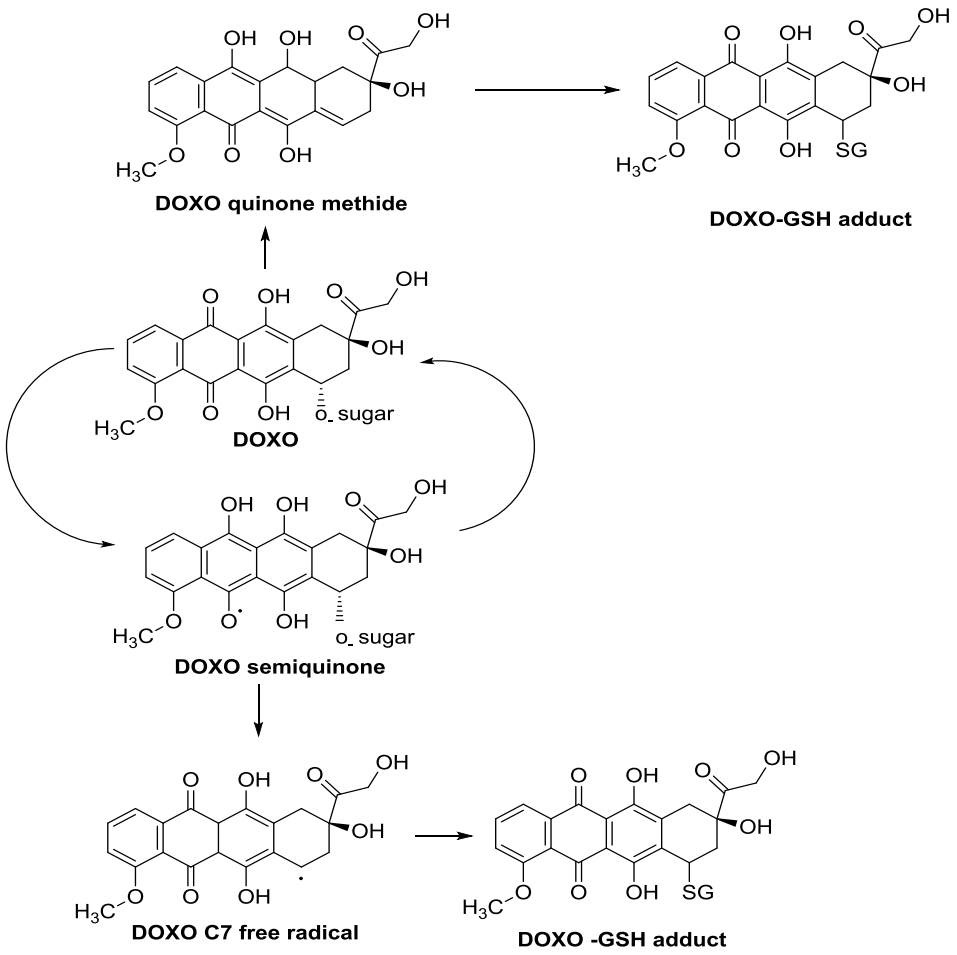

Scheme 4.7 First proposed pathway of DOXO. The expected GSH addcuts were formed as a consequence of GSH conjugation with DOXO C7 free radical and DOXO quinone methide.

However, the stability in currents that were observed in section 4.4.6, in combination with the same kinetics observed in conventional solid electrodes, suggested the possible formation of the negatively charged DOXO dianion via a two-electron reduction (Figure 4.8). The possibility of a chemical reaction between the dianion and DOXO was rejected considering the instability of the electrogenerated product at pH 3, as obtained by the calculated peak current ratio of 1.9.

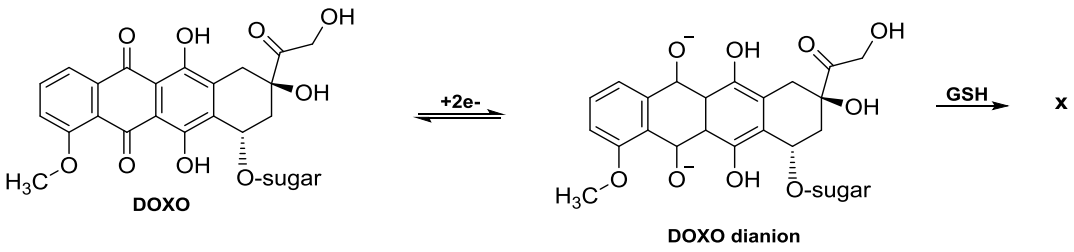

Scheme 4.8 Second proposed pathway of DOXO. According to this pathway the transfer of two electrons leaded to the formation of the negatively charged DOXO dianion, which is not capable to form GSH adducts due to its charge.

The third pathway refers to the formation of a hydroxyl DOXO via the reduction of two electrons and two protons (Scheme 4.9). Both DOXO dianion and hydroxyl DOXO are not reactive with GSH and characterised by instability, permitting their immediate oxidation back to DOXO.

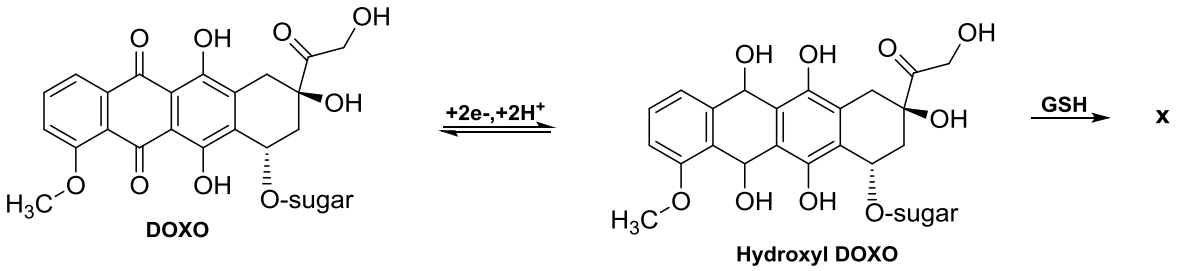

Scheme 4.9 Third proposed pathway of DOXO. In this case the investigated compound was reduced to hydroxyl DOXO, which is not capable to form GSH adducts.

4.5 Conclusion

The behaviour of DOXO presented similarities in kinetics and mass transport with previous investigations in solid electrodes. DOXO was reduced reversibly with strong adsorption at pH 3. However, a lack of signal was observed, in the other pH values, owing to desorption phenomenon. A similar behaviour was seen in a carbon paste electrode, but here, the effect was more intense leading to a complete disappearance of currents. The obtained mass spectra presented only the parent drug and GSH, leading to the proposal of three pathways.

The first pathway suggested the formation of the DOXO semiquinone in low molar concentrations, leading to the generation of DOXO-GSH adducts that were below the detection limits of the mass spectrometer. Also, it was also likely that the DOXO semiquinone was unstable and oxidised very quickly back to DOXO, as seen in the *in vitro* and *in vivo studies*, preventing further reactions resulting in reactive DOXO C7 free radical and DOXO quinone methide.

However, the possibility of generating non-reactive products towards GSH was also considered since primary electrochemical investigations in various GSH concentrations generated inconclusive data, regarding the reactivity of the generated products towards GSH. Thus, the second pathway suggested the generation of a negatively charged DOXO dianion via a two-electron reduction and the third pathway, the formation of a hydroxyl DOXO via the reduction of two electrons and two protons in the quinone moiety. The possibility of generating the DOXO quinone methide via a direct two-electron reduction was rejected since electropositive compounds like this are easily detected in concentrations up to 2.5 $x10^{-4}$ M and in extensive electrolysis. Inability to investigate DOXO in various pH values was a major limitation since more stable products might be generated permitting their detection.

In conclusion, investigations on bare SPEs proved the novelty of the particular sensors in tracking the metabolism over a wide range of phase I reactive metabolites (quinones, quionone methides and radicals) through the transfer of a single electron- proton transfer or the transfer of two electrons-protons. As a consequence, it provided valuable application for later experiments in chips.

Chapter 5: Design and development of a microfluidic device containing a SPE

5.0 Introduction

SPEs have a potential for integration into a microfluidic device owing to their miniature size and portability.[108, 109] However, in the field of electrochemical metabolism only two microfluidic devices have been developed by the Rusling research group,[301, 302] for the early screening of genotoxic metabolites. The first chip[301] involved an array of eight carbon SPEs coated with rat liver microsomes, ruthenium–polyvinylpyridine, and DNA, incorporated into a 63 μL PDMS channel with a long silver/silver chloride reference electrode and a platinum wire as the counter electrode (Figure 5.1). Then, 50 μL min^{-1} of the oxygenated sample solution was infused into the chip; the enzymatic reactions were initiated first by CPE, which involved the donation of electrons to CYP 450, causing enzyme activation and subsequent reaction with the exogenous pollutants.

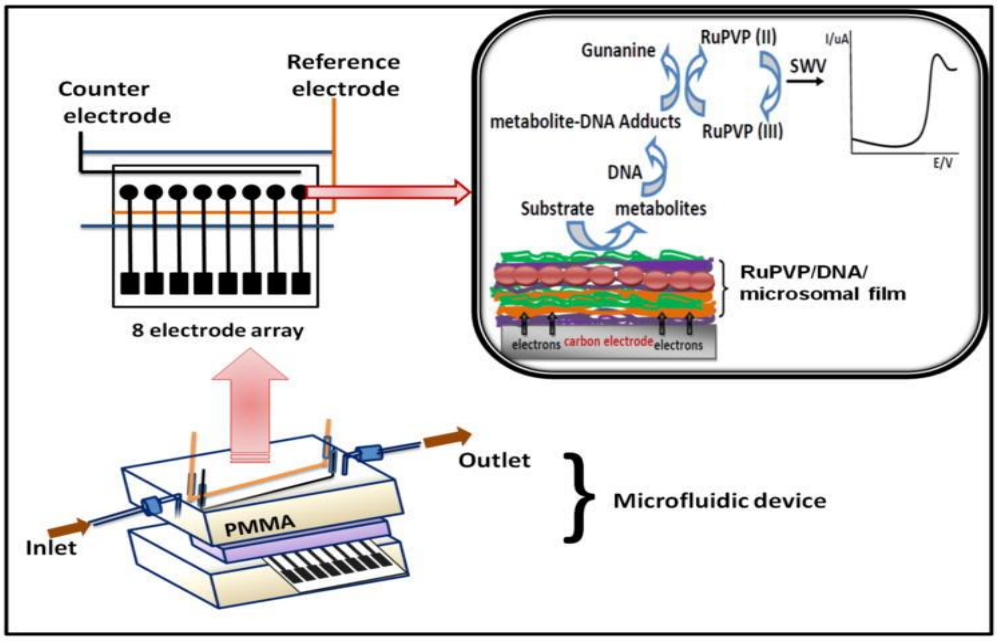

Figure 5.1 SPEs into a microfluidic device.[301] An array of eight SPEs was developed for the generation of reactive phase I epoxides that were covalently bonded with DNA. SPEs supplied CYP 450 with the required electrons to drive the metabolic reaction and replaced the expensive use of NADPH.

The reactive metabolites reacted covalently with DNA and a catalytic square wave voltammogram was recorded, in the presence of ruthenium–polyvinylpyridine polymer for detection purposes. The reactive pathways of well-known pollutants such as styrene, *N*-nitrosopyrrolidine (NPYR), 46*N*-(9*H*-fluoren-2-yl)acetamide(2-AAF), and benzo[a]pyrene (B[a]P) that are metabolised by aromatic hydroxylation and epoxidation were mimicked successfully by replacing the expensive use of NADPH with electrode.

The same research group modified the above design by connecting four microfluidic channels in parallel,[302] for the simulation of multi-enzyme pathways found in arylamine and benzo[a]pyrene. Each channel contained an eight-electrode SPE array coated with the ruthenium–polyvinylpyridine catalyst, DNA, and multiple enzyme sources involving human liver microsomes, CYP 450, 1B1 supersomes, human S9 liver fractions, *N*-acetyltransferase, and microsomal epoxide hydrolase; each time, the solution was driven to the desired channel via a switching valve (Figure 5.2). The obtained voltammograms confirmed damages on the DNA structure through the formation of aryl nitrenium ion and benzo[a]pyrene epoxides.

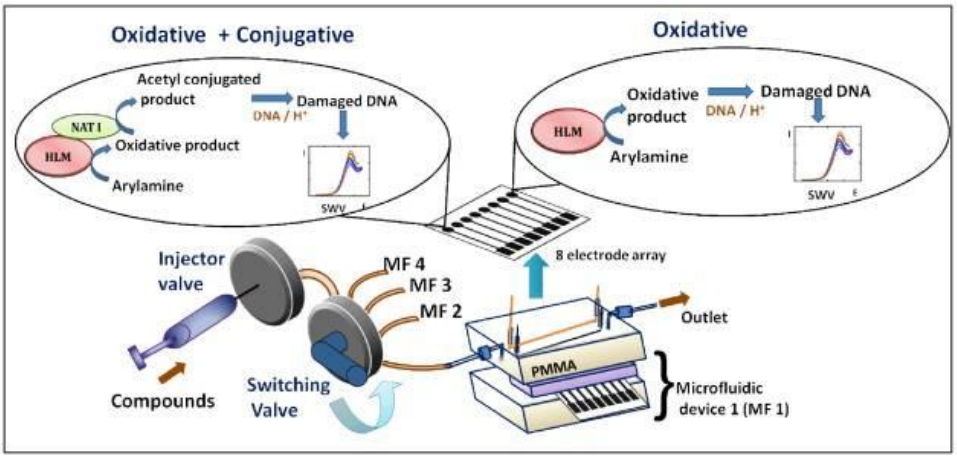

Figure 5.2 Multiplex SPE microfluidic device.[302] Multiple sources were coated into the SPEs permitting in parallel the conduction of multiple metabolic pathways.

The development of a microfluidic device involving the integration of a bare SPE without the involvement of expensive enzymes would provide a more economical approach and a faster screening methodology, over the current *in vivo* and *in vivo* methodologies for monitoring reactive metabolites. In earlier chapters, SPEs mimicked successfully the metabolites of various compounds both endogenous and exogenous in 30 min, while *in vitro* and *in vivo* methodologies require months of extensive work.Thus the possibility of integrating a SPE into a microfluidic device would permit the electrochemical synthesis of the metabolties over flow conditions and thus reduce furher the time scale. Also, the disposable nature of the SPE does not require any tedious cleaning procuderes saving time and providing simplicity of use and minium reagent consumption.

The objectives of the chapter were:

1) Design and development of an inexpensive microfluidic device involving the integration of a bare SPE with a serpentine channel for tracking phase II metabolism.
2) The online coupling of the integrated microfluidic device with ESI/MS for an automated approach and simplicity of use.
3) Mimicking the phase II GSH metabolism of RLX, DOPA and APAP within the microfluidic device.Determination of the optimum potential by CV and actual electrochemical synthesis by CPE.

5.1Working principle of the proposed microfluidic device

The proposed chip aimed to follow the same working principle as commercially available flow cells. However, herein, the SPE would be integrated with a serpentine channel in the same microfluidic device. The particular type of reactor was selected to keep the chip compact and small. The metabolites would be generated on the surface of the SPE and subsequently driven to the serpentine channel for continuous mixing with GSH. The GSH adducts would then travel via the outlet into the ESI source for detection in MS (Figure 5.3).

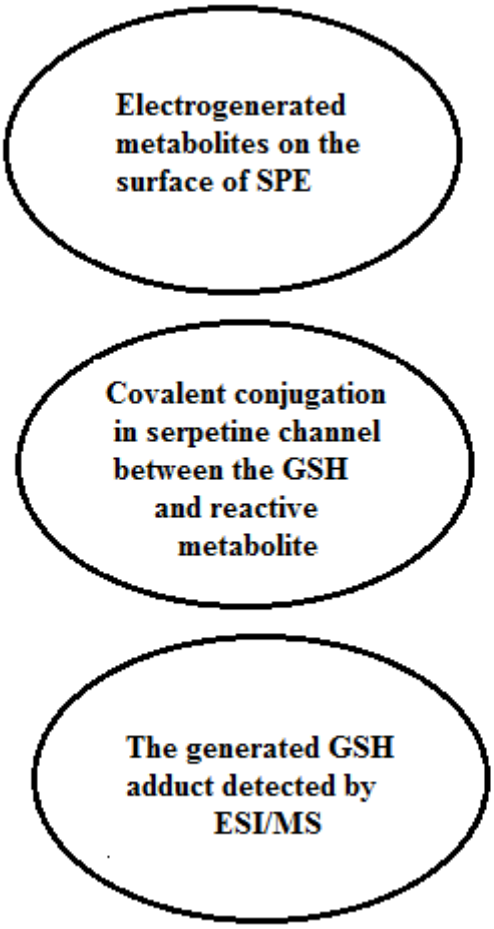

Figure 5.3 Working principle of the microfluidic device.

In particular, the three-electrode configuration of the SPE would form the electrochemical cell. In order for the electrochemical synthesis to occur, it is essential that all electrodes are covered with a sufficient sample solution. Offline experiments have shown that partial coverage of only 20 μL generated noisy voltammograms or, as expected, the currents were not produced at all. Thus, all geometrical dimensions involved in the development of an SPE cell-on-chip must be carefully considered for full electrode coverage. Offline experiments provided reliable data and full coverage when 50 μL of the solution was loaded onto the three-electrode configuration. A chamber or a well around the three-electrode configuration would form the electrochemical cell. However, in constant flow conditions and in a well-defined miniaturised electrochemical cell, lower volumes can be used for full electrode coverage. Thus, the application of even lower volumes than the ones used traditionally can further reduce the cost. Considering the fact that the auxiliary electrode has a smaller surface area than the working electrode, it was not isolated from the rest of the electrodes.

.

5.2 Selection of fabrication material

The development of a cost effective microfluidic device requires affordable materials for mass production. The disposable and inexpensive SPEs[109, 110] are a favourable option for the development of an economical chip. Therefore, polycarbonate was chosen for the fabrication of the microfluidic devices. The compatibility of polycarbonate with the tested exogenous and endogenous compounds was investigated by loading 50 μL of the investigated solutions onto a polycarbonate strip. In particular, $2x10^{-5}$ M of APAP, DOPA, and RLX in 0.1 M ammonium acetate buffer (pH 7.4) were loaded onto the strip and left overnight for 24 h. The polymer strip did not present any changes, indicating its compatibility with the investigated compounds (Figure 5.4).

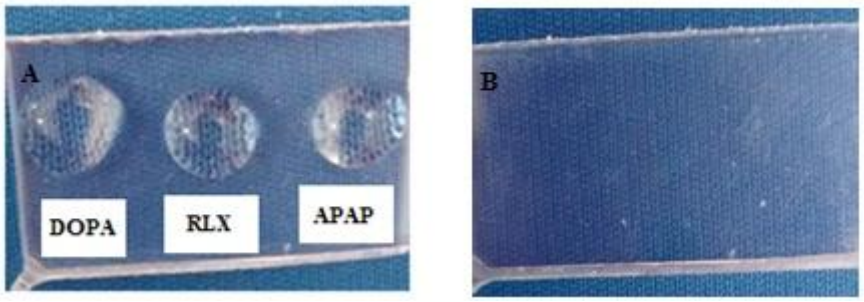

Figure 5.4 Resistance of tested compounds loaded onto polycarbonate. A) Sample loading; B) After 24 h. Alternations on the polycarbonate wafer were not seen after the removal of the tested solution implying the compatability of the material with the reagents used.

5.3 Reusable polycarbonate chip (1ST generation chip)

The concept was the development of a microfluidic device with an exchangeable SPE that would permit the multiple use of the chip and SPEs would maintain their disposable nature. As a consequence the replacement of the SPE would prevent unwanted memory or fouling effects.

5.3.1 Factors affecting the design of reusable chip

Several factors affected the design of chip such the flow rate, duration of electrolysis, dimensions of serpentine chnanel and time of diffusion between the electrogenerated metabolites and GSH Herein, the above factors and analysed and presented in detail.

5.3.1.1 Duration of controlled potential electyrolysis in SPE cell

The duration of electrolysis was determined by the residential time of the compound within the 50 μL electrochemical cell, which in turn is affected by the applied flow rate. The selection of the flow rate depended on two main factors: 1) compatibility with MS and 2) compatibility with the chip. Mass spectrometers like Thermo Scientific are developed to operate at relatively high flow rates (up to 1000 μL min^{-1}) while the lowest flow rate that can be applied is 2.5 μL min^{-1}. Lower flow rates can cause poor ionisation and the products may not be detectable. Regarding the chip, low flow rates were required, considering its delicate microstructure and need for maximum metabolite synthesis. As a consequence, the highest flow rate that could be applied was 50 μL min^{-1}. As concluded, the acceptable flow rates for both the chip and MS were in the range of 2.5 μL min^{-1} to 50 μL min^{-1}. As seen in (Equation 5.1) the time of electrolysis as a function of the applied flow rate was determined by dividing the volume of the channel with the applied flow rate. The residential times and

as a consequence the relative duration for electrolysis, depending on the applied flow rate, are shown in (Table 5.1).

$$\boldsymbol{Time\ of\ electrolysis} = \frac{\boldsymbol{Volume\ of\ channel}\ (\boldsymbol{\mu L})}{\boldsymbol{Flow\ rate}\ (\boldsymbol{\mu L\ min-1}\ )} \qquad \textbf{(Equation 5.1)}$$

Table 5.1 Duration of electrolysis for reusable chip.

Flow rate (µL min^{-1})	**Electrolysis (min)**
2.5	20
5	10
10	5
20	2.5
30	1.66
50	1

5.3.1.2 Dimensions of serpetine channel

The fluid flow within the microfluidic devices is described by the number of reynold number, Re (Equation 5.2).Where: ρ is the density of solution, d is the diameter of channel; v is the average velocity of moving liquid and η viscosity of liquid. An Re value < 2000 represents a laminar flow, whereas an Re value of > 2300 a turbulence flow[303].

$$Re = \frac{\rho d v}{\eta}$$ **(Equation 5.2)[303]**

Thus, considering the laminar flow the two investigated compound solutions (GSH and endogenous/exogenous compounds) need to diffuse in each other faster than the reaction time. Widths that lead to higher diffusion times were rejected. Thus, a longer diffusion time would not permit the covalent interactions to occur because the compounds would not be completely mixed. The combined flow rates for the metabolite and GSH were considered for the estimation of the metabolite-GSH reaction time in a 40 µL serpentine channel by dividing the volume of channel with the flow rate (Equation 5.3), whereas the length was 100 mm. As expected, the reaction time decreased significantly with the increase in flow rate (Table 5.3).

$$\boldsymbol{Time\ of\ covalent\ reaction} = \frac{\boldsymbol{Volume\ of\ channel\ (\mu L)}}{\boldsymbol{Combined\ flow\ rate(\mu L\ min-1)}}$$ **(Equation 5.3)**

According to the calculated reaction times in (Table 5.2) and calculated diffusion time in (Equation 5.4), the width of the serpentine channel (X) was found to be 0.01 cm, with a known diffusion constant of $2x10^{-6}$.[304] Thus, the reactive metabolites would diffuse with GSH in 0.28 min, permitting the application of the required flow rate range.

$$\boldsymbol{Diffusion\ time} = \frac{(\boldsymbol{X})^{\boldsymbol{2}}}{\boldsymbol{2x(Diffusion\ constant)}} \qquad \textbf{(Equation 5.4)}$$

Table 5.2 Time of covalent reaction in reusable chip.

Combined flow rate (µL min^{-1})	Covalent reaction (min)
5	8
10	4
20	2
40	1
60	0.7
100	0.4

5.3.2 Design and fabrication of reusable chip

The microfluidic device was composed of two polycarbonate wafers with dimensions of 5 cm x 5cm (length and width), as shown in (Figure 5.5). The design was drawn by solidwork software considering the calculated dimensions in section 5.3.1. In the top waffer, the microfluidic channels, 40 µL-serpentine channel, inlets, outlet, fluid connections and 50 µL- SPE cell were drilled by CNC machine based on the electronic design from solidwork. Whereas, the bottom waffer served as a base for the chip without any drawn features. The two polycarbonate wafers (top and bottom) were bonded together with an adhesive double side tape and subsequently placed in press machine for a complete sealing. In total ten microfluidic devices were developed with the particular methodology.

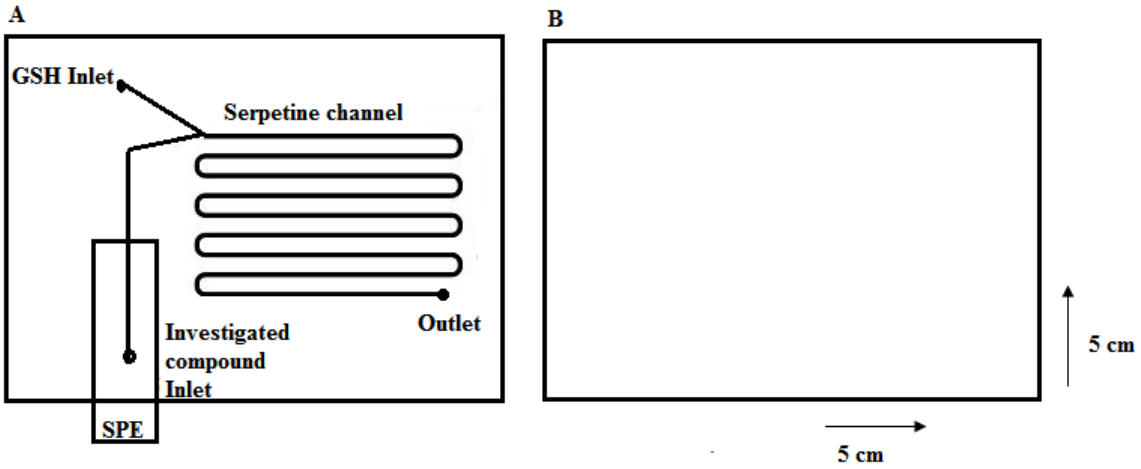

Figure 5.5 Schematic diagram of the top and bottom wafers. A) Top polycarbonate wafer with the drilled 40 µL serpentine channel and 50 µL SPE electrochemical cell. B) A bottom wafer that served as a base for the microfluidic device.

The full chip design of the two bonded waffers is shown in (Figure 5.6). The silver connections of the sensor relied outside the microfluidic device for the coupling of the SPE with the potentiostat via an edge connector interface.

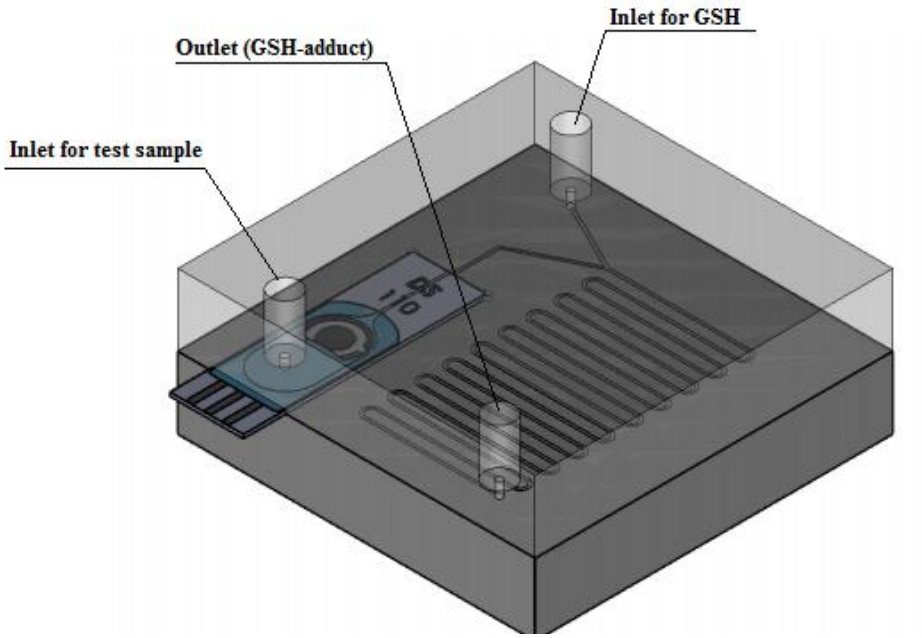

Figure 5.6 Reusable chip with dimensions of 5 cm x 5 cm (lenght x width).

5.3.3 Challenges and limitations of reusable chip

The functionality of the chip was tested by infusing food dyes at a constant flow rate of 5 μL min^{-1}. The main objectives were to test the fluid directions from the inlets\outlets and mixing behaviour in the serpentine channel. The blue dye represented the fluid direction of the test sample and the red dye, the direction of GSH. Two limitations were encountered that altered the proper function of the chip and did not allow its further use. A leaking problem was encountered at the insertion point of the electrochemical cell, suggesting problems with the sealing method. In particular, the difference in height between the sensor and insertion point created the leakage problem. Additionally, back pressure problems had arisen from the GSH inlet, leading to changes in its direction, i.e. directed towards the miniaturised electrochemical cell. As a consequence, the particular behaviour aggravated the leakage problem at the insertion point. Thus, a new design was required to prevent the said problems when using the reusable microfluidic device.

Table 5.3 Limitations and challenges in reusable chip.

Limitations/challenges	Description
Leakage and sealing	The SPE cell encountered leakage problems due sealing limitations.
Backpressure	The flow of GSH inlet was directed towards the SPE chamber instead of serptetine channel.

5.4 Disposable polycarbonate chip (2nd generation chip)

Herein, the concept was the permanent bonding of the sensor into the microfluidic device for preventing the leakage problems that were encountered with the reusable microfluidic device. However, considering the disposable nature of the SPE, the permanent bonding would permit only the disposable use of the microfluidic device.

5.4.1 Factors affecting the design

The same factors as in section 5.3.1 were considered for the designing a disposable microfluidic device towards the mimicry of phase II metabolism.

5.4.1.1 Duration of controlled potential electyrolysis in SPE cell

The calculated durations of electrolysis depending on the applied flow rate in the 32-µL chamber are shown in (Table 5.4).

Table 5.4 Duration of electrolysis for disposable chip.

Flow rate (µL min^{-1})	Electrolysis (min)
2.5	12.8
5	6.4
10	3.2
20	1.6
30	1.1
50	0.6

5.4.1.2 Serpetine dimensions

The time for the covalent interaction of the reactive metabolite with GSH in a 24-μL serpentine channel is shown in (Table 5.5).

Table 5.5 Time for covalent reaction in disposable chip.

Combined flow rate (μL min^{-1})	Covalent reaction (min)
5	4.8
10	2.4
20	1.2
40	0.6
60	0.4
100	0.2

Depending on the obtained reaction times, the width of the serpentine channel was found to be 0.01 cm, using the formula of diffusion time (Equation 5.4). The particular width allows the diffusion of the metabolite with GSH at a faster rate, at 0.28 min, prior the covalent conjugation, which was found to be very close even at the highest flow rate of 5 μL min^{-1}.

5.4.1.3 Design and fabrication of a disposable chip

In the particular design (Figure 5.7), the working principle was maintained, but the chamber containing the SPE had a circular shape and was fitted exactly with the circular area of the SPE. This resulted in the isolation of the electrodes and formation of a proper electrochemical cell, allowing the direct contact of the tested solution with the electrodes only and not with the entire sensor as in the reusable design. In particular, three polycarbonate wafers were bonded together with silicone and double adhesive tape. First, the bottom waffer was bonded with the middle waffer containing the SPE and allowed to dry for an overnight. Subsequently; the top waffer was bonded and dried again for an onvernigh. In the middle wafer, the microfluidic channels, serpentine channel, inlet, outlet, and SPE chamber were drilled by CNC machine. Whereas the bottom wafer served as a base for the microfluidic device. In total 30 microfluidic devices have been developed with the particular methodology.

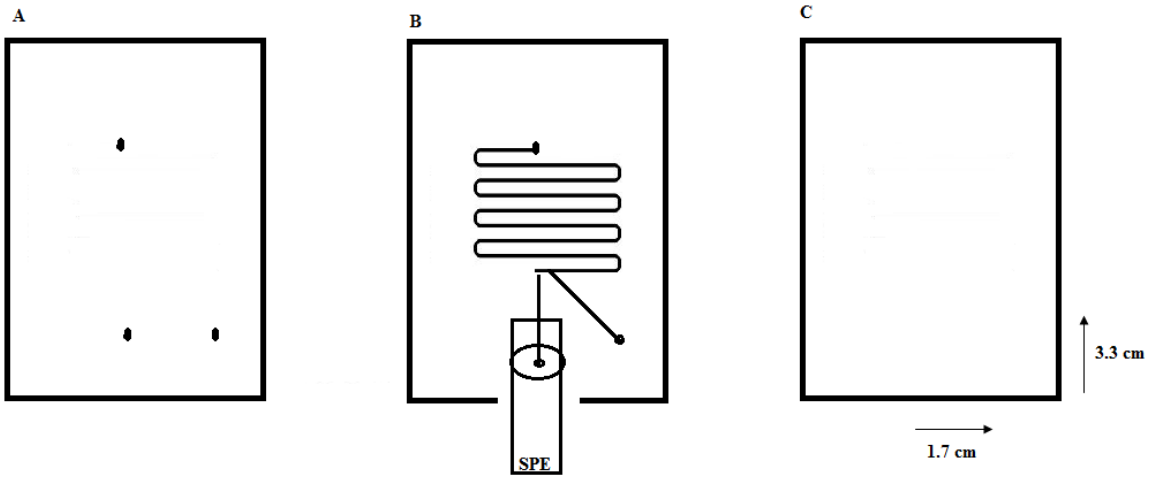

Figure 5.7 Schematic diagram of the three polycarbonate wafers. A) The top wafer containing the outles of the wafer. B) The middle wafer with the 32 µL SPE cell and 20 µL serpentine channel. C) The base wafer that completes the microfluidic device.

In addition, an O-ring was place around the chamber to prevent leakages. The dimensions of the new design were reduced significantly, aiming for the lowest possible reagent consumption. The volume of the chamber containing the SPE was reduced to 32 μL and the general dimensions for the disposable microfluidic device were reduced to 3.3 cm ×1.7 cm (length x width).The full design of the chip is shown in (Figure 5.8).

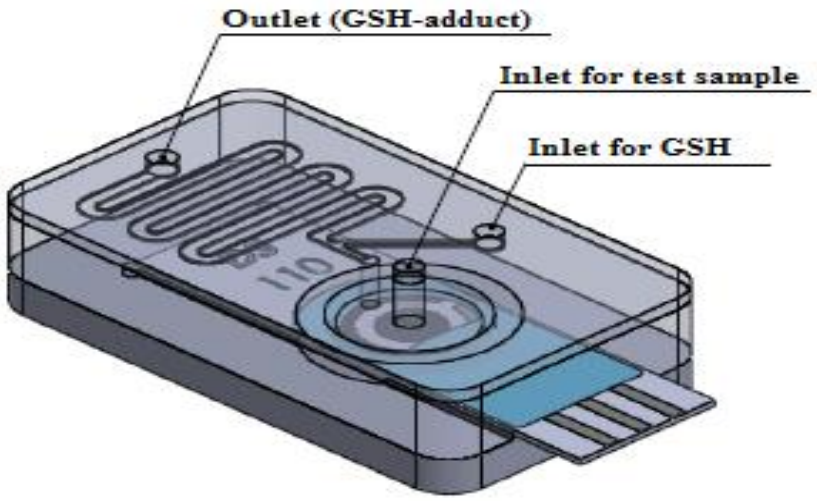

Figure 5.8 Full design of the disposable microfluidic device with dimensions of 3.3 m x 1.7 cm (length x width).

5.4.1.4 Leakage test

The functionality was tested with blue food dyes at a constant flow rate of 5 μL min^{-1} and as proved the microfluidic device was leakage free. Thus, it was selected for further studies with exogenous and endogenous compounds.

5.4.1.5 Chip modifications for reusability

The base wafer was replaced by silicone, which is easily removed, allowing the replacement of SPE for a multiple use (Figure 5.9).

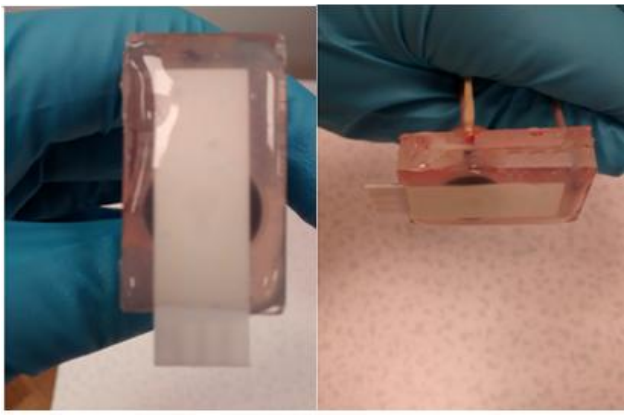

Figure 5.9 Modifications for multiple use. The middle wafer covered with silicone glue only, permitting its easy removal for re-use.

After 2 min of good functionality the continuous flow damaged the silicone layer due backpressure problems from both inlets, causing the leaking of food dye from the O-ring. Therefore, only the disposable microfluidic device was selected for further studies, considering the leaking problems encountered with the reusable designs.

5.5 Results and discussion

The metabolism of APAP, DOPA, and RLX was investigated, and their selection was based on offline experiments that were conducted in previous sections. DOPA and RLX generated successfully the desired GSH adducts and APAP was already investigated on a bare SPE, by Kauffmann *et al.*[115]

5.5.1 CV in the microfluidic device

Performing voltammetry studies in the microfluidic device is an essential parameter for identifying the required potential range and subsequent synthesis of reactive metabolites, providing both an automated methodology and a complete functional cell, like the conventional ones. As a consequence, CV, in the presence of 1 mM APAP in 0.1 M ammonium acetate (pH 7.4), was conducted in both stop flow conditions (CPE over steady conditions) and continuous flow conditions from 2.5 μL min^{-1} to 50 μL min^{-1}. Additionally, voltammetry on bare SPE was conducted for comparison reasons; all voltammograms are shown in (Figure 5.10). Each time (n=3) a new polycarbonate chip was used to avoid memory effects. CV within the chip generated a well-defined redox pair, like the investigation on a bare SPE. In terms of kinetics as seen in (Table 5.6), the currents were maintained at relatively similar values without any significant changes. However, the anode and cathode potentials were shifted to more positive and more negative values, respectively. This happened because the applied constant flow permitted the continued adsorption of material on the SPE surface. The low magnitude peak that appeared at -0.8, over flow condition was also the result of adsorption. A peak was also seen at 0 μL min^{-1} since the microfluidic device was initially filled with solution at 50 μL min^{-1}, prior voltammetry, to ensure full electrode coverage. As concluded, a potential range can be determined by voltammetry since the shift was in an acceptable level

.

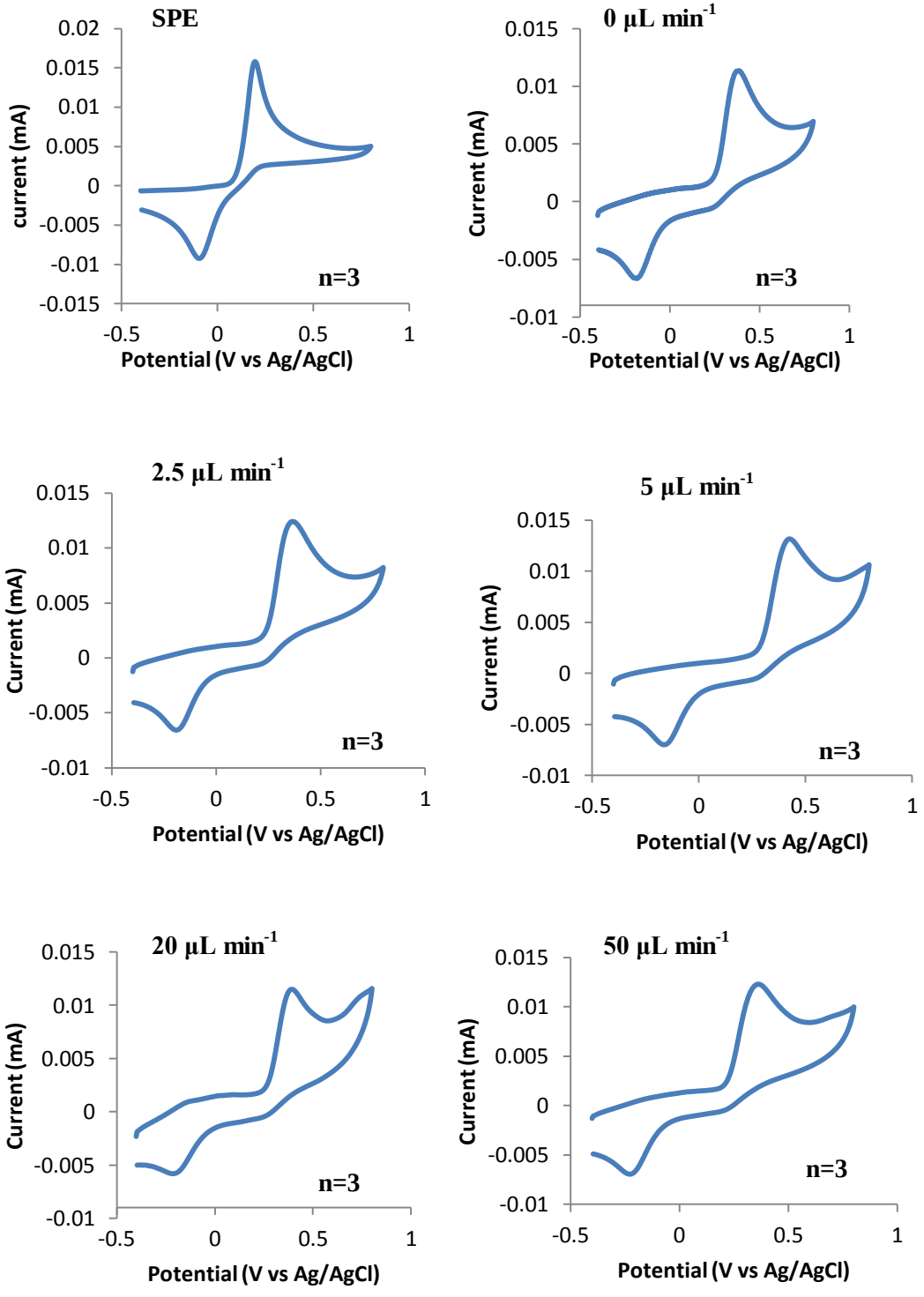

Figure 5.10 CV in the microfluidic device. The applied constant flow (2.5 µl min^{-1}- 50µL min^{-1}) permitted the continuous adsorption of material on the SPE surface causing shifts in the obtained potentials. However, a potential range can be determined by voltammetry since the shift was in an acceptable level.

However, the potential shift needs to be carefully considered for accurate results. This can be achieved by subtracting the calculated potential difference, which it was observed between the SPE and voltammetry within the microfluidic device. The difference for the anode potential was found to be in the range of 0.13 V to 0.21 V and that for the cathode potential, in the range of -0.13 V to 0.17 V. Thus, it was advisable to subtract 0.2 V from the obtained redox peaks for the determination of the investigated potential range.

Table 5.6 Obtained potentials and currents.

Flow rate (μL min^{-1})	**Anode potential (V) (n=3)**	**Anode current (mA) (n=3)**	**Cathode potential (V) (n=3)**	**Cathode current (mA) (n=3)**
0-SPE	0.190	0.015	-0.080	-0.008
0	0.350	0.011	-0.240	-0.007
2.5	0.320	0.011	-0.250	-0.006
5	0.390	0.012	-0.210	-0.006
20	0.400	0.012	-0.240	0.006
50	0.370	0.012	-0.250	0.005

5.5.2 Microfluidic device coupled offline with MS

The functionality of the chip on mimicking metabolism was investigated by infusing $2.5x10^{-5}$ M APAP and $5x10^{-5}$ M GSH into the chip, at a constant flow rate of 5 μL min^{-1} (without optimization). Each time (n=3) a new polycarbonate chip was used to avoid memory effects. The effluent was collected via the outlet and injected subsequently with a syringe into ESI/MS. The obtained mass spectrum, as shown in (Figure 5.11), confirmed the formation of the APAP-GSH adduct (*m/z* 456.84), indicating the successful synthesis of NAPQI and its subsequent reaction with GSH in the serpentine channel. The catalytic peak GSSG (*m/z* 612.84) was also formed, as seen in offline experiments[115]. The parent drug was depleted, suggesting an exhaustive electrolysis at the applied potential of 0.5 V. The potential was not optimized at the current stage but it was dominated by mass transport since the obtained oxidative potential from CV was set 0.15 V higher.

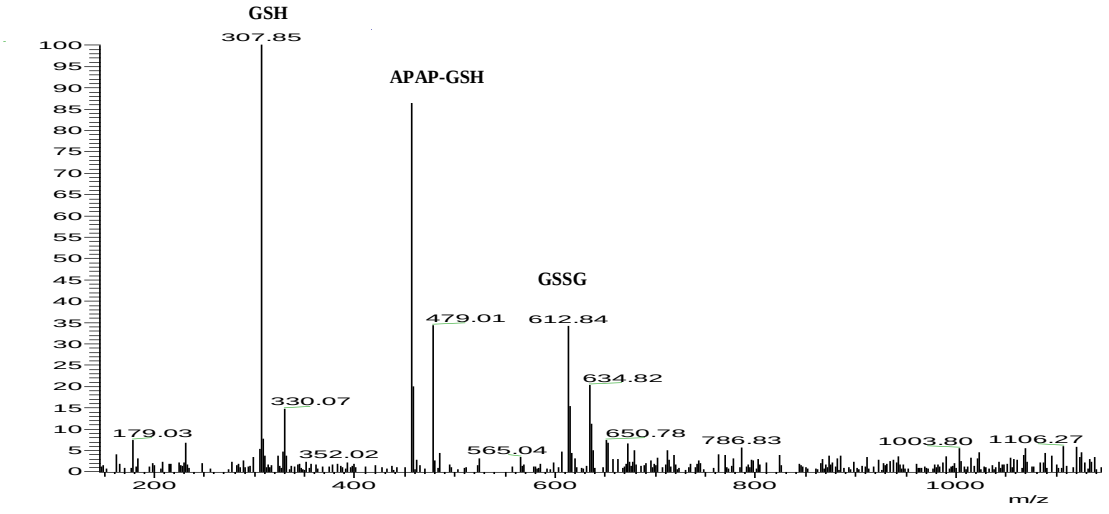

Figure 5.11 Partial mass spectrum of the Offline detection of APAP-GSH adducts. The chip synthesized electrochemically the NAPQI within the SPE cell, over a constant flow rate (5 μL min^{-1}) and permitted the subsequent reaction of the metabolites with GSH in the 20 μl serpentine channel.

5.5.3 Optimization of flow rate

Early calculations in section 5.3.1.2 suggested that the microfluidic device would be capable of synthesising phase II adducts at a flow rate range of 2.5 μL min^{-1} to 50 μL min^{-1}. Each time (n=3) a new polycarbonate chip was used to avoid memory effects. n order to determine the optimum flow rate, $2.5x10^{-5}$ M APAP and $5x10^{-5}$ M GSH in 0.1 M ammonium acetate (pH 7.4) were investigated by on-chip CPE at 0.5 V, in the above flow conditions. At flow rates of 2.5 μL min^{-1} and 5 μL min^{-1}, the APAP-GSH adduct (*m/z* 456.93) showed the highest peak in the mass spectra, as shown in (Figure 5.12). However, at higher flow rates such as 10, 20, 30 and 50 μL min^{-1}, the APAP-GSH adduct was found at the baseline region, suggesting lower conversion rates. The effect of flow rate is strongly related with the available surface area. Amperometric flow cells[168] and microfluidic cells[236] with small planar working areas can achieve high conversion rates, only at low flow rates. Herein, the SPEs also had small planar area and as proven by the present data, the conversion rates were affected by the applied flow rate over the electrode.

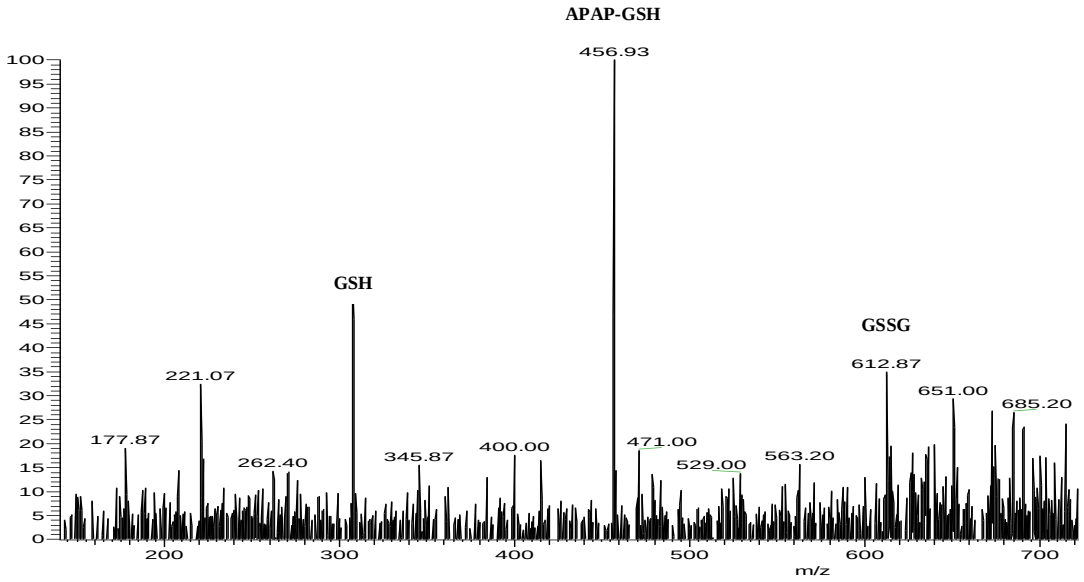

Figure 5.12 Partial mass spectrum of APAP-GSH at the optimized flow rate of 5 μL min^{-1}. The particular flow rate enabled the online coupling of the chip with ESI-MS and the generation of the GSH adduct with the highest possible intensity.

5.5.4 Potential optimization

Optimum potentials generate higher yields of products, so potential optimization is a key parameter for electrochemical metabolism.[192, 193] Offline experiments with SPEs, successfully optimized the applied potentials. However, under flow conditions, the potentials needed to be re-optimized to produce the best quality signals. Herein, the potentials for APAP, DOPA, and RLX were optimized on the disposable polymer chip. The potentials were controlled by a mass transport limit and were applied for 6.4 min to ensure that the cell was filled and provided a constant residence time for the analytes. Owing to the disposable nature of SPEs and the issues created around SPE re-use, always a new microfluidic device was used for each potetnial optimization.

5.5.4.1 Acetaminophen

Solutions of $2.5x10^{-5}$ M APAP and $5x10^{-5}$ M GSH in the presence of 0.1 M ammonium acetate (pH 7.4) were loaded onto the chip at a constant flow rate of 5 μL min^{-1}. Each time (n=3) a new polycabornate microflidic device was used to avoid memory effects. A series of potentials from 0.4 V to 0.75 V were applied in 0.05 V steps (Figure 5.13) to determine the optimum potential for maximum production of electrolysis products under CPE conditions. The oxidative anode potential was determined to be 0.35 V by CV. As expected, the APAP-GSH adduct (*m/z* 456.96) was generated at all the applied potentials since the process was controlled by mass transport. At the optimized potential of 0.5 V, increased intensities were obtained, and the metabolite was found to be the most dominant ion in the mass spectrum (Figure 5.12). The ion intensities were maintained at high levels up to 0.6 V, whereas at higher potentials from 0.65 V to 0.75 V, the metabolite generation was reduced significantly. The catalytic metabolite GSSG was also obtained,

as observed in the offline experiments by Kauffmann *et al*.[115] This confirmed the successful mimicking of the parallel metabolic pathway within the microfluidic device. The formation of GSSG was seen from 0.45 V to 0.60 V and then decreased significantly up to 0.7 V. The highest intensity of GSSG was obtained at 0.75 V, suggesting a dominance of the catalytic pathway over conjugation at the highest applied potential.

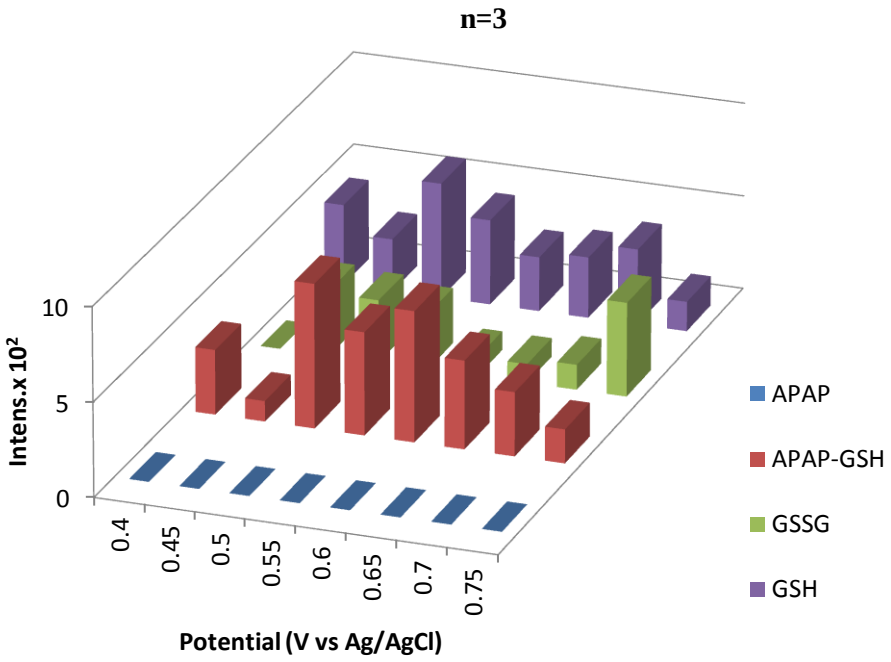

Figure 5.13 Potential optimization of APAP.The APAP-GSH adduct was obtained at all potentials with the highest intensity at 0.5 V. In addition the catalytic metabolite GSSG was generated from 0.45 V to 0.75 V.

The parent drug was depleted at all potentials, proving the occurrence of exhaustive electrolysis in the specified time. When the cell was off, only the parent drug and GSH were obtained (Figure 5.14), confirming that the APAP-GSH adducts were generated electrochemically on the surface of SPE.

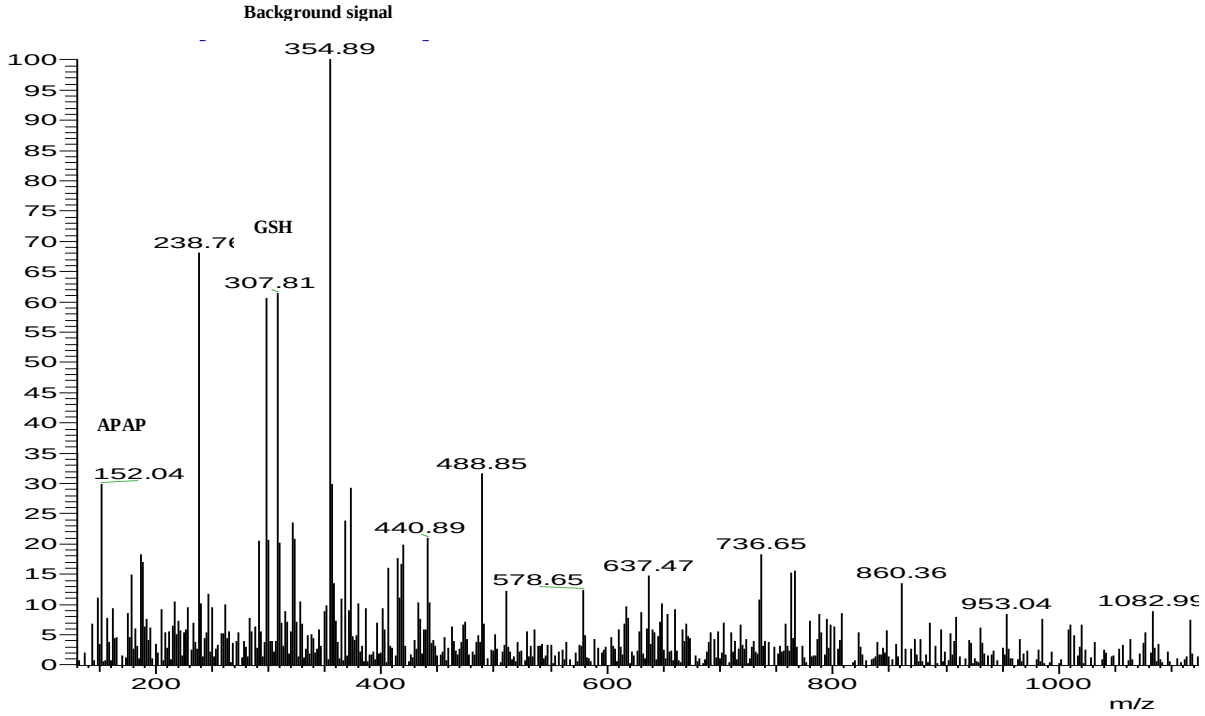

Figure 5.14 Partial mass spectrum for APAP metabolism at off cell. Only the parent drug and GSH were obtained confirming that the process of GSH formation was purely electrochemically driven.

5.5.4.2 Dopamine

The oxidative potential for solutions of $2.5x10^{-5}$ M DOPA in the presence of 0.1 M ammonium acetate (pH 7) and $5x10^{-5}$ M GSH in the same buffer was optimized in the range of 0.17 V-0.52 V. Each time (n=3) a new polycarbonate chip was used to avoid mempry effect. Considering the instability of dopaminoquinone in alkaline conditions, which resulted in the formation of phase I DOPA polymer in off-chip investigations, the pH value was adjusted to seven to increase the formation of the GSH adduct and reduce the generation of the phase I polymer. As shown in the graph (Figure 5.15), the DOPA-GSH adduct (*m/z* 458.87) and GSSG (*m/z* 612.81) were obtained at all tested potentials with depletion of the parent drug, but as expected, the phase I polumer was not formed owing to the neutral pH buffer conditions and shorter time of electrolysis (6.4 min). The highest intensities of DOPA-GSH adduct were obtained at 0.37 V (Figure 5.16).Both GSSG and DOPA-GSH adduct decreased at higher potentials, from 0.42 V -0.52 V. When the cell was off, only DOPA (*m/z* 153.89) and GSH *(m/z* 307.92) were obtained (Figure 5.17).

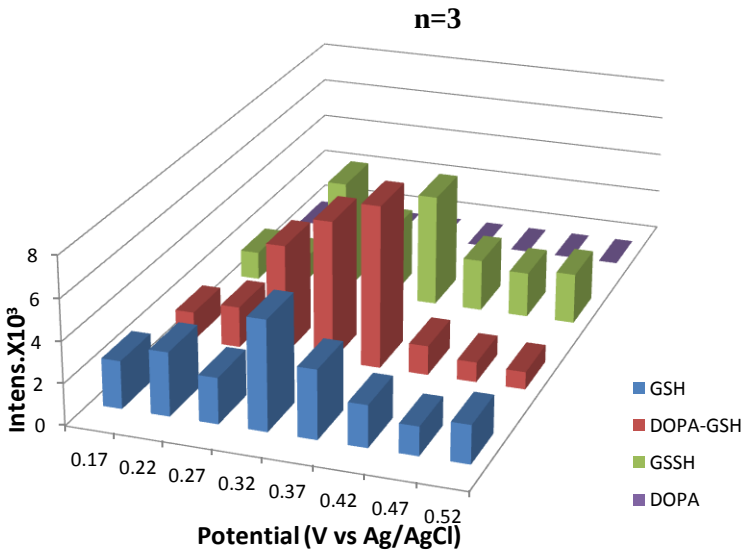

Figure 5.15 Potential optimization of DOPA. The expected DOPA-GSH adduct and GSSG were obtained at all potentials, suggesting the succesfull simulation of GSH conjugation and catalysis within the chip.

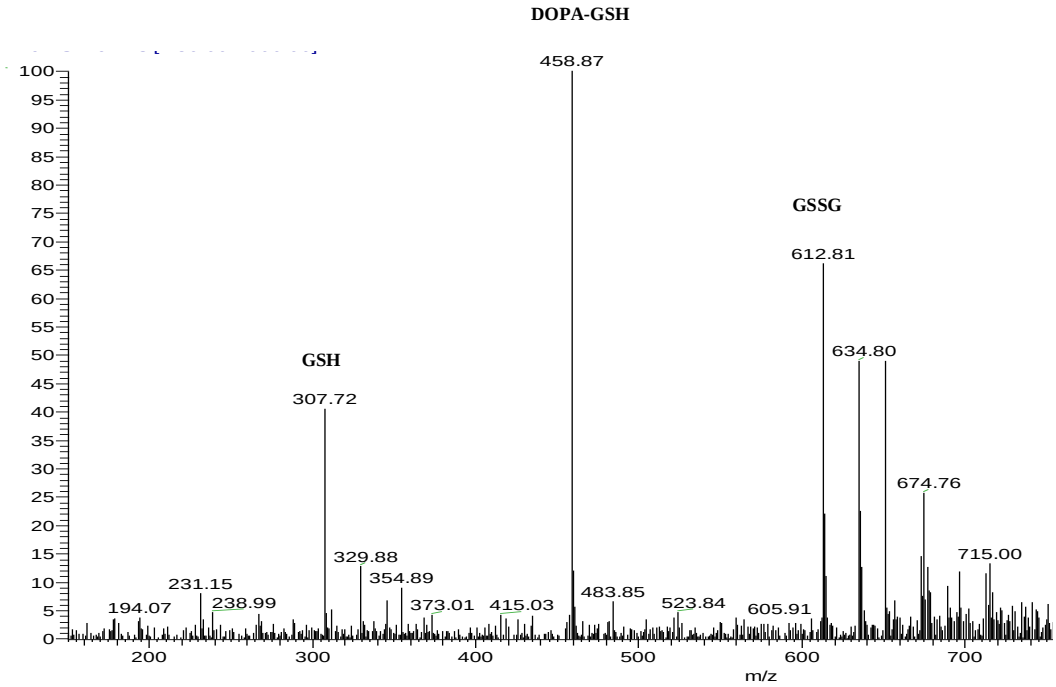

Figure 5.16 Partial mass spectrum for the on-chip DOPA metabolism at 0.37 V. The DOPA-GSH adduct was the most abundant peak in the whole spectrum. In addition the catalytic metabolite (GSSG) was also seen, whereas the parent drug was depleted.

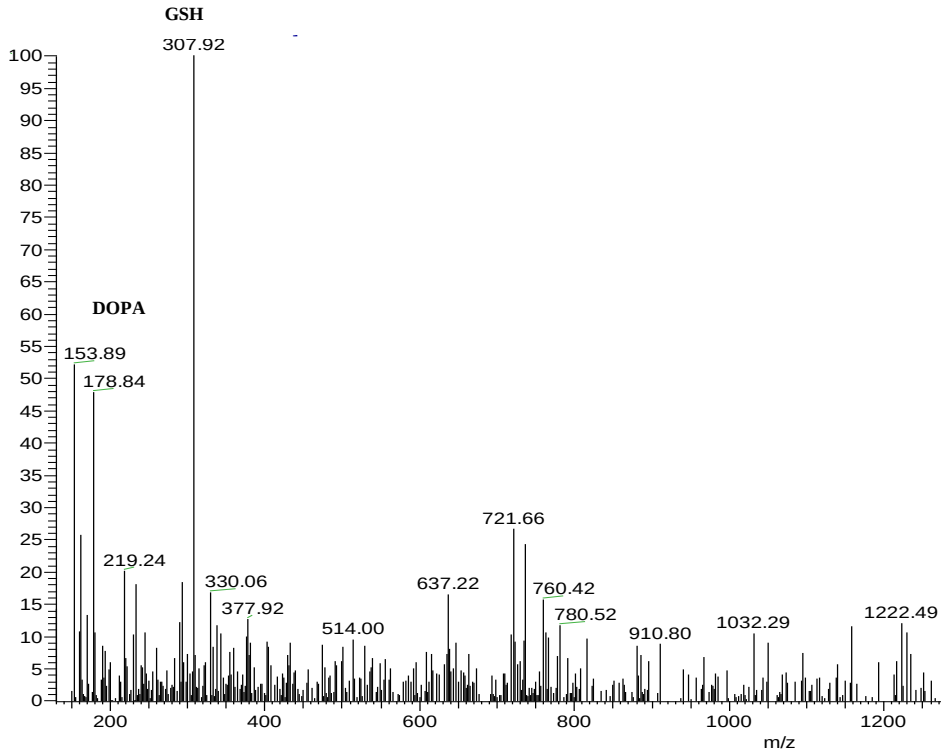

Figure 5.17 Partial mass spectrum for the on-chip DOPA metabolism at off cell. The DOPA-GSH and GSSG metabolties were absent confirming the electrochemical capabilities of the system.

5.5.4.3 Raloxifene

Previous investigations of the metabolism of RLX showed that higher molar concentrations and longer duration of electrolysis (30min) were required for generating the RLX-GSH adduct. However, herein, lower concentrations were used, for example $2.5x10^{-5}$ M RLX and $5x10^{-5}$ M GSH, to examine the possibility of generating the RLX-GSH adduct through the continuous mixing of RLX di-quinone methide and GSH in the serpentine channel. The process was repeated three times on different chips to avoide adsorption effects. As seen in (Figure 5.18), the expected GSH adduct was not formed, but at higher potentials from 0.55

V to 0.70 V, the intensities for both RLX and GSH were reduced significantly, indicating the possibility of generating the RLX-GSH adduct at non-detectable yields.

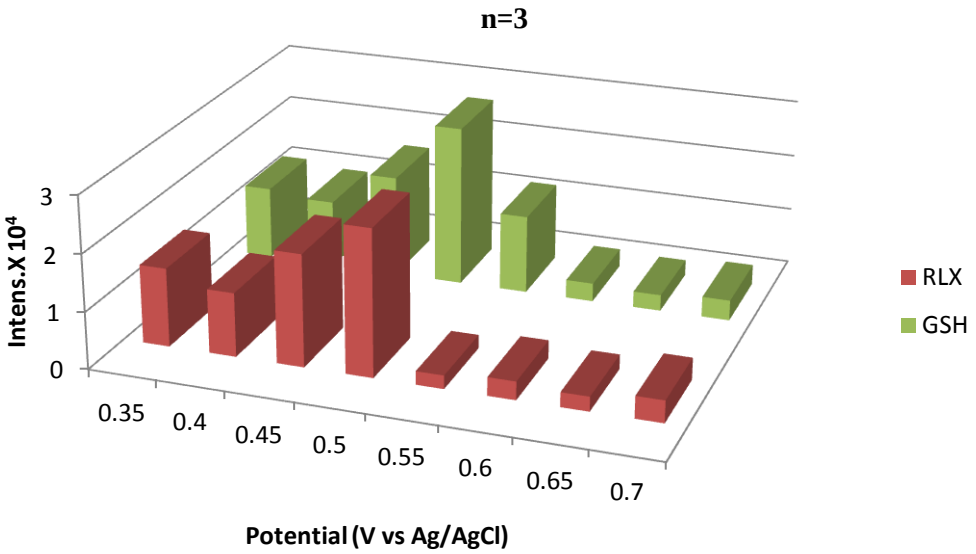

Figure 5.18 Potential optimization of $2.5x10^{-5}$ M RLX. Only the parent drug and GSH were seen in the obtained mass spectra. The expected metabolites such as the GSH adduct and GSSG were not seen in any of the applied potentials.

Probably the continuous mixing in the serpentine channel from the two laminar flows of RLX di-quinone methide and GSH, had caused the dilution of the GSH adducts. The dilution effect was possibly enhanced by the strong adsorption of RLX on the SPE and the lower molar concentration that was used, so the quantity of the generated RLX-GSH was below the detection limits of the mass spectrometer. Thus, the mixing in the serpentine channel at the given molar concentration was not beneficial but probably led to even lower yields. However, other reasons can be considered such as the possible hydrophobic interaction of RLX with the polycarbonate chip or the extreme short half-life of RLX di-quinone methide that was reported in *in vitro* studies[259], was probably seen also in the

electro-generated intermediate. A representative mass spectrum at 0.50 V is shown in (Figure 5.19). When the cell was off, only RLX and GSH were obtained (Figure 5.20).

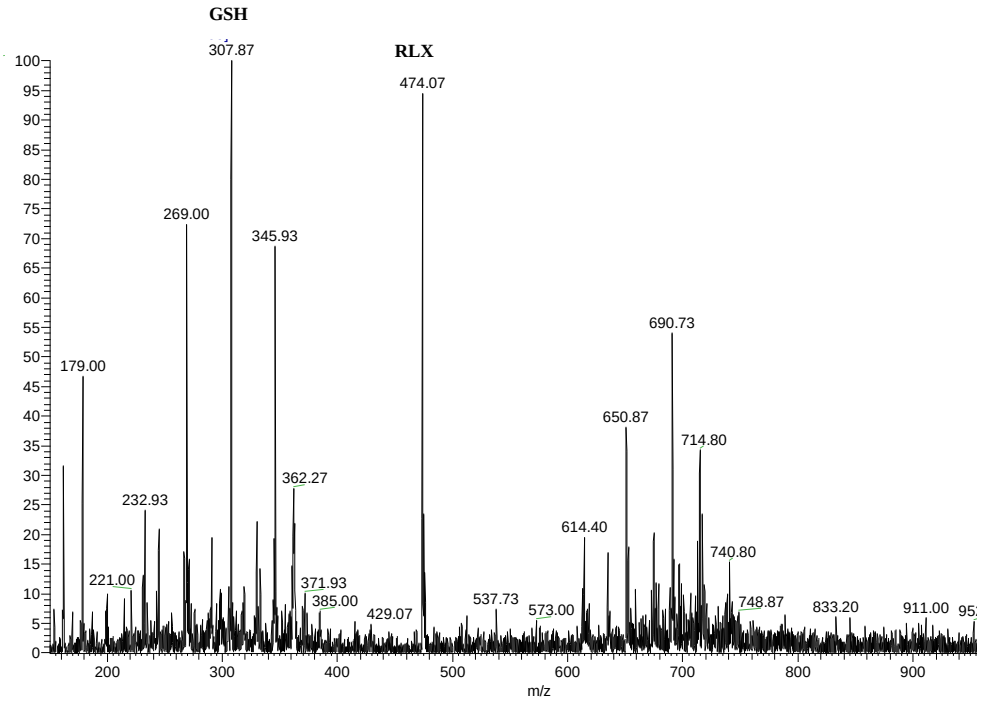

Figure 5.19 Partial mass spectrum of RLX metabolism in 2.5E^{-5} M at 0.50 V. The expected RLX-GSH adduct was not obtained, whereas GSH and RLX were present in the spectrum with high intensities.

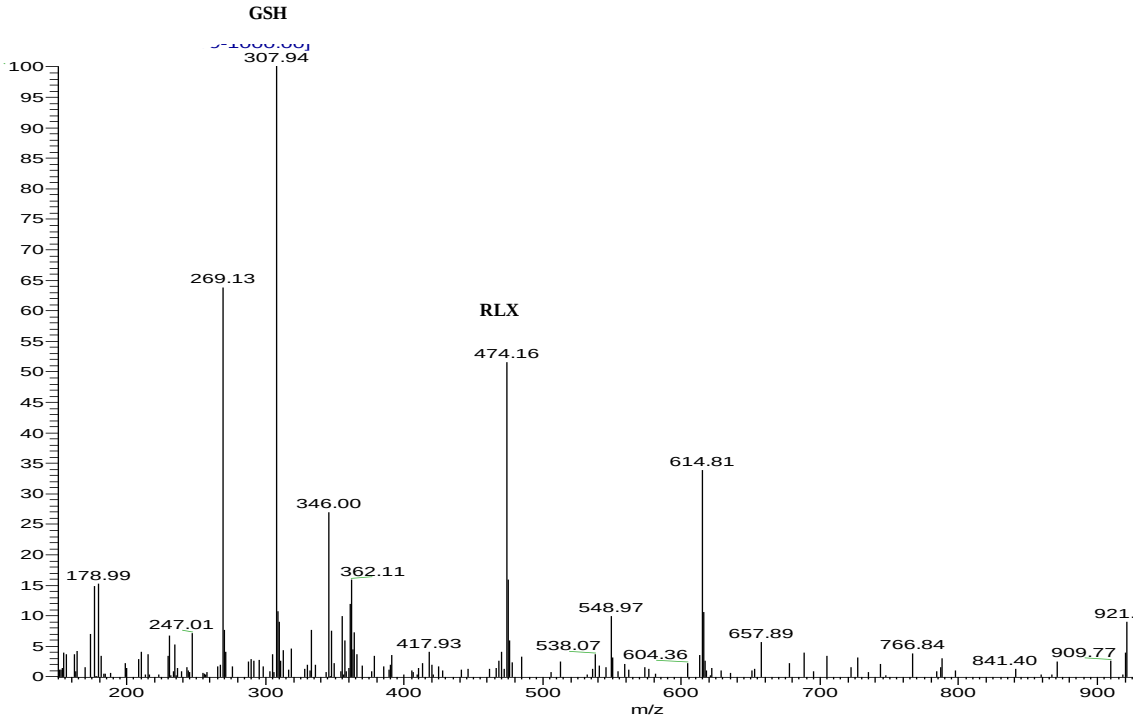

Figure 5.20 Partial mass spectrum of RLX metabolism at off cell. Only RLX and GSH were obtained as expected since potential was not applied.

5.5.5 Further investigation of RLX

5.5.5.1 Hydrophobic interactions

In section 5.5.4.3, several issues had been addressed regarding the non-detection of the RLX-GSH adduct. One possibility was the hydrophobic interaction of RLX with polycarbonate, leading to RLX or RLX-GSH adduct trappingwithin the microfluidic device. Thus, 50 µL of $2.5x10^{-4}$ M drug in 0.1 M ammonium acetate (pH 7.4) was loaded onto the polymeric surface (n=3) and left for 10 min since it is the expected time that the solution spends on the chip. On comparing the obtained intensities in the MS of the blank solution (RLX solution not applied to the polymeric surface) with that of the RLX solution loaded onto the polycarbonate surface (Figure 5.21), it was concluded that hydrophobic reactions between RLX and polycarbonate material did not occur since the obtained intensities were similar. Thus, the possibility of RLX adsorption on the polycarbonate was unlikely.

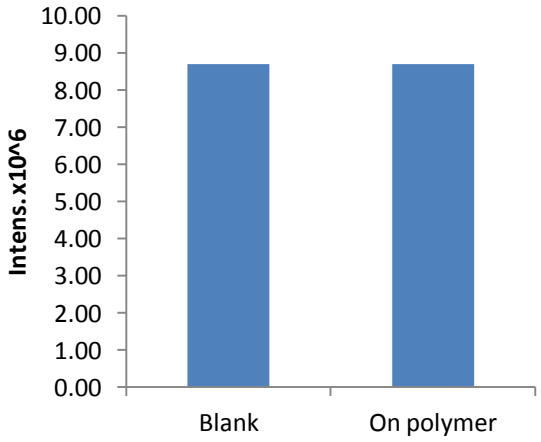

Figure 5.21 RLX on polycarbonate.

5.5.5.2 Short half-life of quinone methide and dilution effect

The extreme short half-life (t = 1s) of RlX di-quinone methide that was reported in the *in vitro*[259] investigations and the possibility of the continuous dilution of the RLX-GSH adduct in the serpentine channel, as proposed in section 5.5.4.3, might be the reasons behind the unsuccessful generation and detection of the RLX-GSH adduct. RLX di-quinone methide was possibly formed on the chamber but owing to its short half-life, it never reached the serpentine channel for covalent interaction, since the certain distance that it had to travel was 0.8 min. As a consequence, slight changes were made to the chip for permitting the direct contact of RLX with GSH, as in chapter three. As seen in (Figure 5.22), RLX and GSH were infused together from the same syringe into the SPE cell, and the second inlet was blocked with a connector. In addition, higher molar concentrations of RLX ($2.5x10^{-4}$ M) and GSH ($5x10^{-4}$ M) were used to increase the yields of the electrogenerated metabolite. The process was repeated for a total of three trials

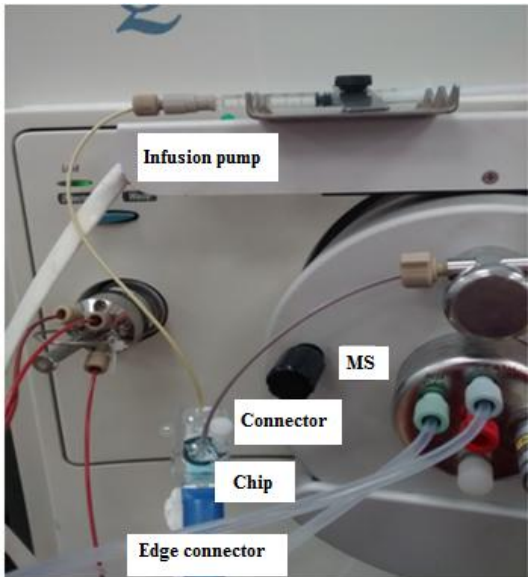

Figure 5.22 Instrumental set-up of RLX and GSH on the same chamber. Both RLX and GSH solutions were infused together from the same syringe into the SPE chamber, at a constant flow rate of 5 μL min^{-1}. The electrochemical synthesis was conducted in the direct presence of GSH as previously in chapter 3.

The particular instrumental set-up allowed the direct interaction of the short-living metabolite RLX di-quinone methide with GSH on the same chamber and prevented possible metabolite dilution, which resulted from the two laminar flows of the metabolite and GSH in the serpentine channel. The potential range was applied from 0.42V to 0.82, as determined by CV at the increased molar concentrations of RLX and GSH. However, the RLX-GSH adduct was not obtained. On the other hand, the GSSG was generated successfully (Figure 5.23) at all potentials, with the highest ion intensity obtained at 0.42 V.

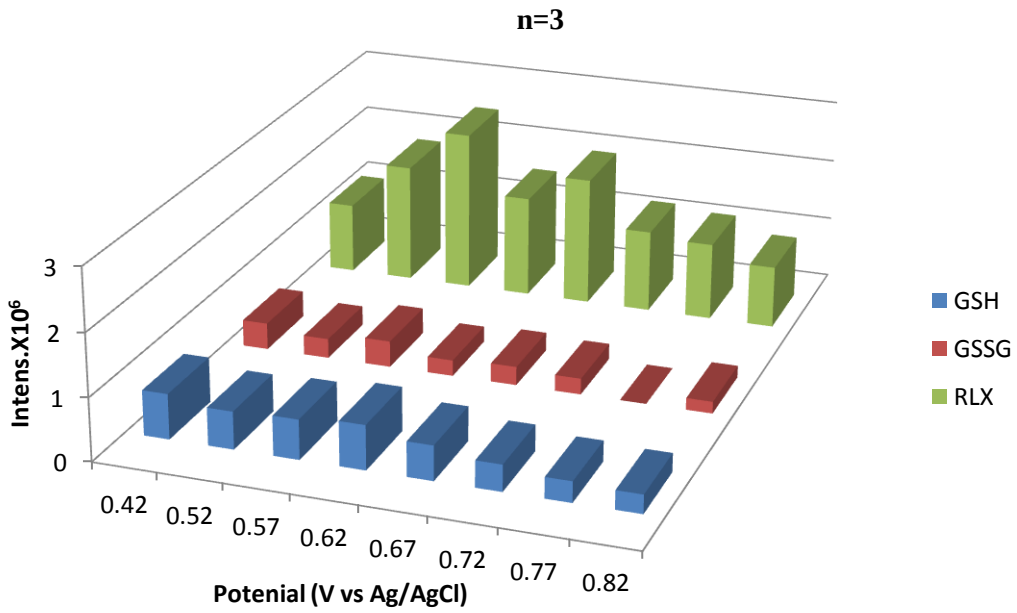

Figure 5.23 Potential optimization for RLX in the direct presence of GSH. Only the GSSG was generated with the highest intensity obtained at 0.42 V. The RLX-GSH adduct was not formed over the particular experimental conditions.

5.5.5.3 Polymer chip/T-piece/ESI/MS

The possibility of dilution towards the GSH adduct formation probably did not have a significant effect since the proposed chip modification in section 5.2.5.2 prevented any dilution effects. As concluded, during flow conditions, the corresponding RLX-GSH adduct was not formed since the duration of electrolysis was reduced significantly to 6.4 min. In off-chip experiments, the GSH adduct was obtained after 30 min of electrolysis over steady-state conditions. However, longer residential duration and, consequently, longer duration for on-chip electrolysis, require low flow rates of 1 μL min^{-1}, that were not compatible with MS. For this reason, a T-piece was added in between the chip and mass spectrometer, as shown in (Figure 5.24), to enable the microfluidic device to operate at 1 μL min^{-1}. A combined flow from the T-piece and chip would allow a total flow rate of 5 μL min^{-1} for the mass spectrometric detection. However, backpressure problems did not permit the successful application of the particular instrumental set-up, so the investigation of RLX metabolism within the chip was not feasible.

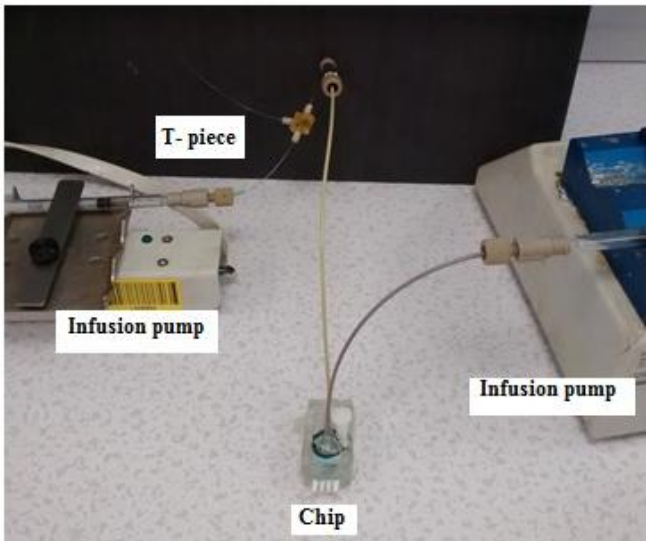

Figure 5.24 Addition of a T-piece for longer duration of electrolysis. The microfluidic device operated at the flow rate of 1μL min^{-1} and the combined flow from T –piece and chip at 5 μL min^{-1}.

5.6 General considerations for the offline and online approaches

The offline approach played a supporting role and provided an optimized parameter for the successful generation of GSH adducts during the microfluidic investigations. Valuable information was obtained regarding the behaviour of tested compounds with their corresponding metabolites and this improved the conditions for generating purely phase II adducts, as seen in the case of DOPA. However, some parameters in the offline approach were significantly better than the online approach.

In particular, offline experiments presented improved sensitivities of the obtained ion intensities. A combination of factors had probably resulted in lower ion intensities for the experiments in the microfluidic device. For example, over steady-state conditions, solutions were not mixed and thus not diluted, whereas experiments in the microfluidic and in particular within the serpentine channel, compounds were continuously diluted through the mixing of the two laminar flows of the sample solution and GSH. In addition, the continuous flow over the SPE surface possibly created strong adsorption effects, leading to lower sensitivities. Also, the poor quality control and the consequent lack of reproducibility during the manufacture of the SPEs probably caused the intensity and optimum potential difference among the offline and online methods. The same reasons could have led to intensity differences between the APAP and DOPA during on-chip electrolysis. On the other hand, the formation of RLX-GSH was favoured by the offline approach since a longer duration of electrolysis was required. In constrast, the backpressure problems arise via the T-piece addition prevented the mimicry of RLX metabolism.

5.7 Advantages of the polycarbonate microfluidic device

The developed chip has potential for future application in pharmaceutical industry and medical research, as a primary screening method, which can be used during the early stages of drug development and minimise the expensive use of current *in vitro* and *in vivo* studies. The integrated chip targeted specific categories of soft reactive electrophiles such as quinones, quinone imines and quinone methides, which are frequently observed in toxicology and can lead to the formation of further toxic metabolites, such as DOPA.[257] In addition, the online coupling with ESI/MS provided a semi-automated methodology in which phase II metabolites were formed and detected in a few minutes.

The disposable nature of the integrated chip offers simplicity of use, mass production, and cost-effectiveness. Also, contamination or memory effects were minimised and tedious polishing or activation methods were avoided, making the device approchable even to the non highly expert operators. In contrast, current reusable chips[236-238] contain metal rods as electrodes that require frequent activation for reproducible and reliable data. However, the permanent bonding of electrodes into glass wafers makes the polishing method impossible and surface regeneration can be achieved only by solvent cleaning and electrochemical activation. However, as proven, in solid electrodes, solvent cleaning did not completely prevent the adsorption effects[248] and the same disadvantage is seen with the microfluidic devices. As a consequence, the lack of polishing eventually would lead to electrode deactivation or to non-reliable data and the chip would need to be replaced. This means glass chips with metal rods do not provide long-term reusability and the cost of mass manufacturing a glass chip is higher than that for a polymeric chip.

On the other hand, microfluidic devices proposed by Rusling *et al*.[301, 302] did not generate pure electrochemical data, since a wide range of expensive enzyme sources were still added. The great benefit from the above studies was the replacement of NADPH by carbon SPE, but the generation of epoxides was still enzymatically driven and not the result of direct electrochemistry. As a consequence, devices like this cannot be used as totally inexpensive primary screening tools. In the present microfluidic device, SPEs were used without any enzyme modification on their surface, thereby reducing the cost and providing an alternative *in vitro* approach.

In addition, more efficient results were obtained compared to existing microfluidic devices[236-238,301, 302] since voltammetry within the microfluidic device, provided a reference point for determining the appropriate potential range. The potentials were applied over a mass transport limit, ensuring the generation of products seen during CV and the depletion of the parent compound, as proven in most cases. Thus, the use of several potentials that either does not lead to metabolite generation or facilitates limited metabolite formation and irrelevant data were avoided. Furthermore, the selection of the mass-controlled potential range allowed the use of fewer chips, since the desired metabolites were obtained in the particular range, further reducing the costs. In contrast, traditional flow cells[188-190] and microfluidic devices[236- 238] usually cover a wider range of potentials without voltammetry studies as a guidance.

5.8 Disadvantages of the polycarbonate microfluidic device

In conventional flow cells, adsorption can be prevented by preparing the solutions in relatively high percentages of organic solvent.[85, 168, 173] However, in the present polycarbonate chip, the adsorption phenomenona cannot be prevented, since organic solvents caused severe damages and altered the functionalities of the SPEs. As a result, the obtained intensities of generated metabolites in the mass spectra were affected by metabolite or parent compound adsorption.

The application of higher potentials (>1 V) was not feasible since non-reliable results were obtained and carbon ink removal was seen, probably owing to the electrochemical instability of the SPE and delicate surface. Thus, the electrochemical generation of multiple metabolites that are frequently seen at higher potentials, in conventional methods[188-190] was not achievable with the SPEs. Therefore, the usability of the microfluidic device is meant exclusively for the generation soft electrophiles like quinone, quinone methide, and quinone imine that rely on potentials below the 1 V.

The small surface area of the sensor did not favour the formation of the second RLX metabolite (RLX 6,-7-o-quinone), which involved a direct aromatic hydroxylation. Conventional methods in conventional flow cells generated the desired metabolite with a great success since the available working area was larger (1.2 cm^2)[179]. Thus, electrochemical reactions that require larger surface areas and more active sites for generating detectable metabolite yields in MS cannot be simulated with the particular microfluidic device.

5.9 Conclusion

A novel polycarbonate microfluidic device containing a SPE was developed successfully for monitoring phase II GSH adducts. The integrated microfluidic device provided simplicity of use, avoidance of cleaning methods, reliability, and disposability. .It was found to be a cheaper alternative to conventional flow cells and current *in vitro* and *in vivo* methodologies, since the cost of each microfluidic device was only 5 GBP. The simple design and inexpensive fabrication materials such as the polycarbonate waffers and SPEs contributed to the low cost.The proposed chip has the potential to be used as a primary screening tool for the generation of soft phase I electrophiles.

In particular, a 32-μL chamber with a SPE, served as miniaturised electrochemical cell in which the investigated compound was electrolysed, on the selected potential range. The electrogenerated metabolites reacted subsequently with GSH in the serpentine channel and the corresponding GSH adducts were detected online by ESI/MS.

In addition, the developed microfluidic device, offered the possibility of recording voltammograms for the determination of the potential range. However, for accurate determination, a subtraction of 0.2 V in the obtained potentials was essential, since the continuous flow favoured material deposition and led to shifts in potentials. The proposed chip successfully generated the GSH adducts for APAP and DOPA. In the case of DOPA, the generation of the phase I DOPA polymer that was seen during the experiments in chapter three was prevented by slight changes in the working solution. For example, the pH was reduced to pH 7, leading to a more stable dopaminoquinone, and the shorter duration of electrolysis (6.4 min) generated only the DOPA-GSH.

Moreover, the obtained intensities for the GSH adducts were lower than those obtained with the offline methodology. This happened because of adsorption effects, which were created via the continuous flow. Also, as a consequence of the continued dilution in the serpentine channel, the generated GSH adducts were also diluted, resulting in lower intensities.

In the case of RLX, lower flow rates of 1 μL min^{-1} were required that were not compatible with ESI/MS. A T-piece was added to the instrumental set-up, to enable the chip to operate at 1 μL min^{-1}; then, a coupled flow of 5 μL min^{-1} from the chip and T-piece drove the electrolysed solution into ESI/MS. However, backpressure limitations prevented the proper functioning of the particular instrumental set-up. Thus, mimicry of RLX metabolism within the chip was not feasible.

.

Chapter 6: Conclusion and future work

6.0 Conclusion

The overall aim of the thesis was the development of a simple, inexpensive and a fast screening system for monitoring the metabolism in pharmaceutical and medical research.The hyphenation of EC with MS can reduce the expensive and time consuming use of the current *in vitro* and *in vivo* methodologies. SPEs were selected as synthesing tools considering their low cost, minuaturized format and possibility of integration into microfluidic devices. The disposable nature of SPEs was confirmed in chapter 2, since the applied treatment methods (solvent, polishing and electrochemical activation), did not provide any significant improvements towards their reusability. Chapters 3 and 4 proved the suitability of SPEs on tracking the metabolism over a wide a wide range of compounds such DOPA, RLX, eugenol and DOXO via two electron-two proton transfers and single electron –proton transfers. In chapter 5, the aim was fulfilled, a bare SPE and a serpentine channel were integrated into a disposable polycarbonate microfluidic device and a platform was developed for monitoring phase II metabolism. The novel chip generated successfully the corresponding phase II GSH adducts of the investigated compounds with minimum reagent consumption. The simple chip design and inxexpensive materials that were used during the fabrication leaded to the development of an inexpensive screening method of only 5 GBP. In addition, the generated metabolites were detected in 9.6 min, whereas the current *in vitro* and *in vivo* methodologies require months of extensive research.The chip was coupled directly to MS providing an automated methodology and simplicity of use, easily conducted even by non-expert individuals.

6.1 Future work

Future studies can lead to the development of SPEs with various configurations, since the simulation of further metabolic reactions such as aromatic hydroxylation, was proven to be affected by the surface area. Isolation of counter electrode from the working electrode is essential in configurations with larger surface areas since currents from the counter might interfere with the generated metabolites on the working electrode. In addition, further studies could look at other sub-categories of soft electrophiles such as a, b unsaturated carbonyls, isocyanate, isothiocyanates, aziridinium, and episulfonium. The possibility of investigating hard electrophiles can also be considered with the proposed screening method.Finally, the formation of protein or DNA adducts would result in a true mimicry of the reactive metabolic pathways.

References

1. A. Li, *Drug-drug interactions: scientific and regulatory perspectives,* Academic press, USA, 1st edn., 1997, p. 104.
2. R. Greger, *Comprehensive human physiology from cellular mechanisms to integration,* ed. R. Greger and U. Windohorst, Springer, Germany, 1st edn., 1996, p. 151.
3. L.S. Edwards and I. Coyne, *A survival guide to children's nursing 1: a survival guide to children's nursing*, Elsevier, UK, 1st edn., 2013, p 371.
4. C. J. Xu, C. Y. T. Li and A. N. T. Kong, *Archives of Pharmacal Research,* 2005, **28** (3), 249-268.
5. K. P. Akarwal, *Everything about pharmacology*. Mitosis International, India, 1st edn., 2013, p. 7.
6. I. Simpkins, *Principles and techniques of practical biochemistry,* Cambridge University Press: UK, 5th edn., 2000, p. 43.
7. W. C. Ritchie, *Oxford textbook of old age psychiatry,* ed. T. Dening and A. Thomas, Oxford University Press, UK, 2nd edn., 2013, p. 194.
8. L. B. Yoost and R. L. Crawford, *Fundamentals of nursing: Active learning for collaborating practice*. Elsevier, USA, 1st edn., 2016, p. 85.
9. B. Pavan, A. Dalpiaz, N. Ciliberti, C. Biondi, S. Manfredini and S. Vertuani, *Molecules,* 2008, **13** (5), 1035-1065.
10. T. Iyanagi, *International Review of Cytology - a Survey of Cell Biology,* 2007, **260,** 35-112.
11. T. Lynch and A. Price, *American Family Physician,* 2007, **76** (3), 391-396.
12. W. Lohmann and U. Karst, *Analytical and Bioanalytical Chemistry*, 2008, **391** (1), 79-96.
13. F. P. Guengerich and T. L. Macdonald, *Accounts of Chemical Research,* 1984, **17** (1), 9-16.
14. F. P. Guengerich. and T. L. Macdonald, *Faseb Journal,* 1990, **4** (8), 2453-2459.
15. M. Shebley, U. M. Kent, D. P. Ballou and P. F. Hollenberg, *Drug Metabolism and Disposition,* 2009, **37** (4), 745-752.
16. J. Chadwick and C. I. Shaw, *Principles of environmental toxicology*, Taylor and Francis, USA, 1st edn., 2002, p. 130.
17. I. Amunom, S. Srivastava and R. A. Prough, *Current protocols in toxicology / editorial board, Mahin D. Maines,* 2011, *Chapter 4*, Unit 4.37-Unit 4.37.
18. S. Tafazoli and P. J. O'Brien, *Drug Discovery Today,* 2005, **10** (9), 617-625.
19. F. P. Guengerich, *Chemical Research in Toxicology,* 2001, **14** (6), 611-650.
20. J. C. Van Leeuwan, *Risk assessment of chemicals: An introduction*, Springer, Netherlands, 2007, 1st edn., pp. 136-139.
21. H. Raza, *Febs Journal* 2011, **278** (22), 4243-4251.
22. G. Lindwall and T. D. Boyer, *Journal of Biological Chemistry*, 1987, **262** (11), 5151-5158.
23. P. Jancova, P. Anzenbacker and E. Anzenbacherova, *Biomedical Papers,* 2010, **154** (2), 103-116.
24. J. D. Hayes, J. U. Flanagan and I. R. Jowsey, *Annual review of pharmacology and Toxicology,* 2005, **45** (10), 51-88.
25. C. G. Alfafara, A. Kanda, T. Shioi, H. Shimizu, S. Shioya and K. Suga, *Applied*

Microbiology and Biotechnology, 1992, **36** (4), 538-540.
26. F. M. Rubino, *Toxics*, 2015, **3**, 20-62.
27. W. Wang and N. Ballatori, *Pharmacological Reviews*, 1998, **50** (3), 335-355.
28. M. Finel, X. Li, D. Gardner-Stephen, S. Bratton, P. I. Mackenzie and A. Radominska-Pandya, *Journal of Pharmacology and Experimental Therapeutics*, 2015, **315** (3), 1143-1149.
29. L. McLaughlin, B. Burchell, M. Pritchard, C. R. Wolf and T. Friedberg, *Journal of Cell Science*, 1999, **112** (4), 515-523.
30. P. J. Vetrencht and W. Trager, *Drug metabolism: chemical and enzymatic aspects*, CRC press, USA, 1st edn., 2007, pp. 130-131.
31. A. L. Sikora, B. A. Frankel and J. S. Blanchard, *Biochemistry*, 2008, **47** (40), 10781-10789.
32. H. Q. Wang, L. Liu, P. E. Hanna, C. R. Wagner, *Biochemistry*, 2005, **44** (33), 11295-11306.
33. F. Dyda, D. C. Klein and A. B. Hickman, *Annual Review of Biophysics and Biomolecular Structure*, 2009, **29**, 81-103.
34. M. So, *Electrochemical and electrochemiluminescent genotoxicity screening using DNA*, UMI, USA, 1st edn., 2008, pp. 68-69.
35. M. Rajasekaran, S. Abirami and C. Chen, Effects of Single Nucleotide Polymorphisms on Human N-Acetyltransferase 2 Structure and Dynamics by Molecular Dynamics Simulation. *Plos One*, 2011, **6** (9).
36. A. Srivastava, J. L. Maggs, D. J. Antoine, D. P. Williams, D. A. Smith and B. K. Park, *Handbook of experimental pharmacology*, 2010, **196**, 165-94.
37. K. C. Fussell, R. G. Udasin, P. J. S. Smith, M. A. Gallo and J. D. Laskin, *Carcinogenesis*, 2011, **32** (8), 1285-1293.
38. R. Kleinman, *Walkers pediatric gastrointestinal disease.* BC Decker, India, 1st edn., 2008, p. 894.
39. Z. Zhang and J. Gan. *Drug development in drug designs and development*. Wiley, Canada, 1st edn., 2008, p. 471.
40. R. Cope, *Veterinary toxicology and clinical principles*, Elsevier: USA, 2nd edn., 2012, p. 801.
41. S. M. Attia, *Oxidative Medicine and Cellular Longevity*, 2010, **3** (4), 238-253.
42. F. Li, J. Lu and X. Ma, *Chemical Research in Toxicology*, 2011, **24** (5), 744-751.
43. W. Dekant, *Molecular, clinical and environmental toxicology*, ed. A. Luch, Birkhowser, Germany, 2009, 1st edn., pp. 81-83.
44. I. Rietjens, H. M. Awad, M. G. Boersma, M. van Iersel, J. Vervoort and P. J. Van Bladeren, *Biological Reactive Intermediates Vi: Chemical and Biological Mechanisms in Susceptibility to and Prevention of Environmental Diseases*, 2001, **500**, 11-21.
45. A. S. Kalgutkar, K. R. Henne, M. E. Lame, A. D. N. Vaz, C. Collin, J. R. Soglia, S. X. Zhao and C. Hop, *Chemico-Biological Interactions*, 2005, **155** (1-2), 10-20.
46. F. Li, F. Gonzalez and X. Ma, *Drug metabolism and transport*, 2012, **2** (2), 118-125.
47. V. Lobo, A. Patil, A. Phatak and N. Chandra, *Pharmacognosy reviews* 2010, **4** (8), 118-26.
48. K. Rahman, *Clinical journal of intervention aging* 2007, **2** (2), 219-236.
49. S. Ma and R. Subramanian, *Journal of mass spectrometry*, 2006, **4** (9), 481-493.
50. S. L. Regan, J. L. Maggs, T. G. Hammond, C. Lambert, D. P. Williams and B. K. Park,

Biopharmaceutics & Drug Disposition, 2010, **31** (7), 367-395.
51. D. A. Smith, C. Allerton, H., Kalgutlar, D. K. Walker, *Pharmacokinetics and metabolism in drug analysis*, Wiley, Germany, 3rd edn., 2012, pp. 166-167.
52. L. Fieser, *Journal of cancer research*, 1938, **34**, 37-124.
53. M. Younes, *Toxicology*, ed. H. Marquard, S. G. Schafer and R. O. McClellan, Academic press, USA, 1st edn., 199, pp. 117-118.
54. W. Wieczorek and J. Naish, *Medical sciences*, ed. D. S. Court and J. Naish, Elsevier, China, 2nd edn., 2015, p. 112.
55. D. R. A. Mans, M. V. M. Lafleur, E. J. Westmijze, I. R. Horn, D. Bets, G. J. Schuurhuis, J. Lankelma and J. Retel, *Biochemical Pharmacology*, 1992, **43** (8), 1761-1768.
56. S. A. Wrighton, B. J. Ring and M. Vandenbranden, *Toxicologic pathology*, 1995, **23** (2), 199-208.
57. R. S. Obach, J. G. Baxter, T. E. Liston, B. M. Silber, B. C. Jones, F. MacIntyre, D. J. Rance and P. Wastall, *Journal of Pharmacology and Experimental Therapeutics*, 1997, **283** (1), 46-58.
58. Y. Naritomi, S. Terashita, S. Kimura, A. Suzuki, A. Kagayama and Y. Sugiyama, *Drug Metabolism and Disposition* **2001,** *29* (10), 1316-1324.
59. P. F. Guenqerich, *Journal of drug metabolism and pharmacokinetics*, 2011, **26** (1), 3-14.
60. F. Zoccarato, P. Toscano, A. Alexandre, *Journal of Biological Chemistry*, 2005, **280** (16), 15587-15594.
61. M. I. Ekstrand and D. Galter, *Parkinsonism & related disorders*, 2009, **15** *Suppl 3*, S185-8.
62. L. Jia and X. Liu, *Current Drug Metabolism*, 2007, **8** (8), 822-829.
63. D. Zhang, G. Luo, X. Ding and C. Lu, *Acta pharmaceutica sinica B*, 2012, **2** (6), 549-561.
64. E. F. A. Brandon, C. D. Raap, I. Meijerman, J. H. Beijnen and J. H. M. Schellens, *Toxicology and Applied Pharmacology*, 2003, **189** (3), 233-246.
65. R. A. Stringer, C. Strain-Damerell, P. Nicklin, J. B. Houston, *Drug Metabolism and Disposition* 2009, **37** (5), 1025-1034.
66. S. Rendic, E. Nolteernsting and W. Schanzer, *Journal of Chromatography B*, 1999, **735** (1), 73-83.
67. C. Li and N. Klayanaraman, *ADME-enabling technologies in drug design and development*, ed. D. Zhang, Surapaneni, Wiley, Canada, 1sr edn., 2012, p. 197.
68. S. Schulz, R. J. Wong, H. J. Vreman and D. K. Stevenson, *Frontiers in Pharmacology*, 2012, *4-16*.
69. C. M. B. Neves, M. M. Q. Simoes, F. M. J. Domingues, M. G. P. M. S. Neves, J. A. S. Cavaleiro, *Quimica Nova*, 2012, **35** (7), 1477-U265.
70. J. T. Groves and Y. Z. Han, *Cytochrome P450, Structure, Mechanism, and Biochemistry*, ed. De Montellano, Plenum Press, USA, 1995, pp. 3-48.
71. J. N. Sousa-Junior, B. A. Rocha, M. D. Assis, A. P. F. Peti, L. A. B. Moraes, Y. Iamamoto, P. J. Gates, A. R. M. de Oliveira, N. P. Lopes, *Revista Brasileira De Farmacognosia-Brazilian Journal of Pharmacognosy*, 2013, **23** (4), 621-629.
72. T. Johansson, L. Weidolf and U. Jurva, *Rapid Communications in Mass Spectrometry*, 2007, **21** (14), 2323-2331.

73. R. E. Long, *Pharmacokinetics in drug development: Regulatory and development paradigms*, ed. P. L. Bonate and D. R. Howard, American association of pharmaceutical scientists, USA, 1st edn., 2004, p. 94.
74. L. Dalgaard, *Journal of pharmacological and toxicological methods.* (Forthcoming 2015).
75. F. J. Gonzalez and C. Cheung, *Journal of pharmacological experimental therapy* **2008**, 327(2), 288-299,
76. M. B. Bracken, *Journal of the Royal Society of Medicine*, 2009, **102** (3), 120-122.
77. F. Botre, *Clinical chemistry*, 2009, **55** (10), 1763-1764.
78. W. Xie, J. L. Barwick, M. Downes, B. Blumberg, C. M. Simon, M. C. Nelson, B. A. Neuschwander-Tetri, E. M. Brunt, P. S. Guzelian and R. M. Evans, *Nature*, 2000, **406**, 435-439.
79. X. Ma, Y. Shah, C. Cheung, G. L. Guo, L. Feigenbaum, K. W. Krausz, J. R. Idle and F. J. Gonzalez, *Drug Metabolism and Disposition*, 2007, **35**, 94-200.
80. C. Cheung, T. E. Akiyama, J. M. Ward, C. J. Nicol, L. Feigenbaum, C. Vinson and F. J. Gonzalez, *Cancer Research*, 2004, **64**, 849-3854.
81. C. P. Granvil, A. M. Yu, G. Elizondo, T. E. Akiyama, C. Cheung, L. Feigenbaum, K. W. Krausz and J. Gonzalez, *Drug Metabolism and Disposition*, 2003, **31**, 548-558.
82. I. Hendrix, P. Anderson, B. May and H. Morris, *Journal of Steroid Biochemical Molecular Biology*, **2004**, 89-90, 139-142.
83. T. Vandebroak, *Biochemical characterization and validation of the yeast saccharomyces cerevisiae as a model system for the function of human protein tau.* Leuven University press, Belgium, 1st edn., 2006, p. 101.
84. M.-C. Menet, J. Marchal, A. Dal-Pan, M. Taghi, V. Nivet-Antoine, D. Dargere, O. Laprevote, J.-L. Beaudeux, F. Aujard, J. Epelbaum and C.-H. Cottart, *Plos One*, 2014, **9** (3).
85. W. Lohmann, A. Baumann and U. Karst, *Lc Gc Europe*, 2010, **23** (1), 1-7.
86. R. Stalder and G. P. Roth, *Acs Medicinal Chemistry Letters*, 2013, **4** (11), 1119-1123.
87. Y. Jurva and L. Weifolf, *Trends in analytical chemistry*. (Forthcoming 2015).
88. L. Jia and X. Liu, *Current Drug Metabolism*, 2007, **8** (8), 815-821.
89. R. V. Cadag and N. Shetty, *Engineering chemistry*, International publishing house, India, 1st edn., 2006, p. 41.
90. D. Nematollahi, H. Shayani-Jam, M. Alimoradi and S. Niroomand, *Electrochimica Acta*, 2009, **54** (28), 7407-7415.
91. H. Shayani-Jam and D. Nematollahi, *Chemical Communications*, 2010, **46** (3), 409-411.
92. A. P. Bruins, *Trends in analytical chemistry* (In press 2015).
93. C. C. Zoski, *Handbook of electrochemistry*, Elsevier, UK, 1st edn., 2007, pp. 34-146.
94. Basi reference electrode. https://www.basinc.com/products/ec/ref.php (accessed Jun 10, 2015).
95. J. Newman and K. E. Thomas-Alyea, *Electrochemical systems*, Wiley, place, 3rd edn., 2004, p. 3.
96. O. A. Farghaly, R. S. A. Hameed and A.-A. H. Abu-Nawwas, *International Journal of Electrochemical Science*, 2014**, 9** (6), 3287-3318.

97. I. N. Acworth and M. Bowers, *Coulometric electrode array detectors for HPLC*, ed. I. N. Acworth, M. Naoi, H. Parvez and S. Parvez, VSP, Netherlands, 1st edn., 1997, pp. 12-13.
98. O. Niwa and D. Kato, *Nanobiosensors and nanobioanalysis*, ed. M. C. Vestergard, E. Kagan, I-M. Hsing, E. Tamiya, Springer, Japan, 1st edn., 2015, p. 121.
99. S. Papavisam, *Techniques for corrosion monitoring*, ed. L. Yang, CNC, USA, 1st edn., 2008, p. 75.
100. G. M. Schalkhammer, *Analytical biotechnology*, Springer, Netherlands, 1st edn., 2002, p. 171.
101. M. C. Elvington and K. J. Brewer, *Applications of physical methods to inorganic and bioinorganic chemistry*, ed. A. R. Scott, Wiley, UK, 1st edn., 2007, pp. 17-38.
102. A. Hayat and J. L. Marty, *Sensors*, 2014, **14** (6), 10432-10453.
103. S. Sanllorente-Mendez, O. Dominguez-Renedo and M. Julia Arcos-Martinez, *Sensors* [online], 2010, **10** (3), 2119-2128. http://www.mdpi.com/1424-8220/10/3/2119
104. R. O. Kadara, N. Jenkinson, C. E. Banks, Characterisation of commercially available electrochemical sensing platforms. *Sensors and Actuators B-Chemical*, 2009, **138** (2), 556-562.
105. E. P. Randviir, D. A. C. Brownson, J. P. Metters, R. O. Kadara and C. E. Banks, *Physical Chemistry Chemical Physics*, 2014, **16** (10), 4598-4611.
106. Z.-H. Li, H. Guedri, B. Viguier, S.-G. Sun and J.-L. Marty, *Sensors*, 2013, **13** (4), 5028-5039.
107. A. Simonian, G. Vertelov and W. Gale, *Chemical sensors 7-and-MEMS/NEMS 7*, ed. P. Hesketh, S. Akbar, O. Brand, M. Carter, E. Enikov, C. Kranz, R. Maboudian, C. Roper, A. Simonian, G. Hunter, S. Bhansali, C. Brucner-Lea, J. L. Davidison, R. Hilman, J. Li, R. Mukundan, S. Shojl and M. Tabib-Azar, Electrochemical society, USA, 1st edn., 2006, p. 27.
108. M. Li, Y.-T. Li, D.-W. Li and Y.-T. Long, *Analytica Chimica Acta*, 2012, **734**, 31-44.
109. A. E. Radi, A. Khafagy, A. El-shobagy, H. El-mezeyen, *Journal of pharmaceutical analysis*, 2012, **3** (2), 132-136.
110. S. V. Pereira, F. A. Bertolino, M. A. Fernandez-Baldo, G. A.; Messina, E. Salinas, M> I. Sanz and J. Raba, *Analyst*, 2011, **136** (22), 4745-4751.
111. K. K. Mistry, K. Layek, A. Mahapatra, C. Roy Chaudhuri and H. Saha, *Analyst*, 2014, **139** (10), 2289-2311.
112. C. Martinez-paredes, B. M. Gonzalez-Garcia and A. Costa-Garcia, *Electrochemical DNA biosensors*, ed. M. S. Ozsoz, Stanford Publishing, USA, 1st edn., 2012, pp. 292-293.
113. O. Laczka, O.; Skillman, L.; Ditcham, W. G.; Hamdorf, B.; Wong, D. K. Y.; Bergquist, P.; Sunna, A., *Journal of Microbiological Methods*, 2013, **95** (2), 182-185.
114. K. A. Fahnrich, M. Pravda and G. G. Guilbault, *Biosensors & Bioelectronics*, 2003, **18** (1), 73-82.
115. J.-M. Kauffmann, P. Van Antwerpen, A. Sarakbi, B. Feier, S. Tarik and Z. Aydogmus *Electroanalysis*, 2011, **23** (11), 2643-2650.
116. J. P. Smith, J. P. Metters, D. K. Kampouris, C. Lledo-Fernandez, O. B. Sutcliffe and C. E. Banks, *Analyst*, 2013, **138** (20), 6185-6191.
117. G. F. Thomsa and G. Henze, *Introduction to voltammetric analysis: Theory and practise*, CSIRO, Australia, 1st edn., 2001, pp. 13- 37.
118. N. Kularatna. *Energy storage devices for electronic systems: Rechargeable batteries*

and supercapacitors. Elsevier, USA, 1st edn., 2015, p. 169.
119. R. H. Buitrago and S. B. Concari, *New research semiconductors*, ed. T. B. Elliot, NOVA, USA, 1st edn., 2006, p. 175.
120. P. S. Monk., *Fundamentals of electroanalytical chemistry*. Wiley, UK, 1st edn., 2001, p. 18.
Author, *Development of electronic DNA hybridization detection using nanotube*, UMI, USA, 1st edn., 2007, pp. 14-54.
121. Z. Cazes, *Analytical instrumentation handbook*, CRC, USA, 3rd edn., 2004, pp. 234-532.
122. A. C. Fisher, *Electrode Dynamic.* Oxford University Press, UK, 1st edn., 1996, pp. 13-40.
123. D. Pletcher, R. Greff, R. Peat and J. Robinson, *Instrumental methods in electrochemistry*, Woodhead, USA, 1st edn., 2001, p. 26.
124. P. T. Kissinger, C. R. Predy, R. E. Shoup and W. R. Heineman, *Laboratory techniques in electroanalytical chemistry,* Marcel Deker, USA, 2nd edn., 1996, p. 12.
125. A. D. Bott, *Current separations,* 1996, **14**, 104-109.
126. J. Fuchs, M. Podda and J. Packer, *Redox–Genome interactions in health and disease,* CNC, USA, 1st edn., 2004, p. 21.
127. D. R. Gompton and E. C. Banks, *Understanding Voltammetry*. Imperial College press: UK, 2nd edn., 2011, pp. 114-121.
128. A. Bott, *Current separation*, 1997, **16** (1), 23-26.
129. M. A. Bond, *Broadening electrochemical horizons: Principles and illustration of voltammetric and related techniques,* Oxford University press, USA, 1st edn., 2002, pp. 61-64.
130. X. Yuan, C. Song, H. Wang and J. Zhang. Electrochemical impendence: Fundamentals and applications, Springer, USA, 1st edn., 2010, p. 25.
131. M. P. Pujado, Carbon nanotubes as platforms for biosensors and electrochemical and electronic transduction. Springer, UK, 1st edn., 2012, p. 53.
132. P. Zuman, *Electrolysis in biomedical and pharmaceutical sciences,* ed. S. A. Ozksan, J. M. Kauffmann and P. Zuman, Springer, USA, 1st edn., p. 52.
133. E. J. Ukpong, E. Effiung, U. M. Etesin and J. Projad, *International journal of pure and applied science and technology*, 2012, **8** (1), 26-37.
134. S. P. Kounaves, *Handbook of instrumental techniques in analytical chemistry,* Prentice Hall, USA, p. 720.
135. A. J. Fry, *Synthetic organic electrochemistry,* Wiley, USA, 2nd edn., 1989, p. 71.
136. B. Izutsu and K. Izutsu, *Electrochemistry in non-aqueous solutions*, Wiley-VCH, Berlin, 1st edn., 2009, p. 147.
137. G. L. V. Zachetti, M. A. Granero, B. N. S. Robledo, A. M. Zon, A. C. DaRocha Rosac and H. Héctor Fernández, *Journal of Brazilian Chemical Society*, 2012, **23** (6), 1131-1139.
138. D. Pletcher, *A first course in electrode process*, Royal Society of Chemistry, Place, 1st edn., 2009, pp. 36-151.
139. J. J. Zuckeman, *Inorganic reactions and methods, Electron-transfer and electrochemical reactions. Photochemical and other energized reactions*, VCH, **USA**, year, p. 142.
140. S. Kowalska, A. Lukomska, P. Los, T.Chmielewski and B.Wozniak, *International journal of electrochemical science*, 2015, **10** (2), 1186-1198.

141. J. B. Fenn, M. Mann, C. K. Meng, S. F. Wong and C. M. Whitehouse, *Science,* 1989, **246** (4926), 64-71.
142. D. L. Wong, J. G. Pavlovich and N. O. Reich, *Nucleic Acids Research,* 1998, **26** (2), 645-649.
143. S. Paolella, M. Bencivenni, F. Lambertini, B. Prandi, A. Faccini, C. Tonetti, C. Vineis and S. Sforza, *Journal of Mass Spectrometry,* 2013, **48** (8), 919-926.
144. M. Li, E. Butka and X. Wang, *Scientific Reports,* 2014, **4**.
145. R. Nirogi, G. Bhyrapuneni, V. Kandikere, K. Mudigonda, P. Komarneni, R. Aleti and K. Mukkanti, *Biomedical Chromatography,* 2009, **23** (4), 371-381.
146. V. S. Ponnunu, B. R. Challa and R. Nadendla, *Journal of pharmaceutical analysis,* 2012, **2** (4), 249-257.
147. C. S. Ho, C. W. K. Lam, M. H. M. Chan, R. C. K. Cheung, L. K. Law, L. C. W. Lit, K. F. Ng, M. W. M. Suen and H. L. Tai, *The Clinical biochemist. Reviews/Australian Association of Clinical Biochemists*, 2003, **24** (1), 3-12.
148. S. Banerjee and S. Mazumdar, *International Journal of Analytical Chemistry,* 2012. DOI.
149. P. S. Patel, M. Roy, and G. K. Dutt, *Veterinary world,* 2012, **5** (3), 185-192.
150. J. J. Pitt, *The Clinical biochemist. Reviews/Australian Association of Clinical Biochemists,* 2009, **30** (1), 19-34.
151. S. Banerjee and S. Mazumdar, *International Journal of Analytical Chemistry,* 2012. DOI.
152. K. R. Jonscher and J. R. Yates, *Analytical Biochemistry,* 1997, **244** (1), 1-15.
153. G. L. Glish and R. W. Vachet, *Nature review* **2003,** 2,140-146.
154. R. J. Mishur and S. L. Rea, *Mass Spectrometry Reviews,* 2012, **31** (1), 70-95.
155. Yinon, J., Counterterrorist detection techniques of explosives. Elsevier: USA, 1st edn., 2007, p. 45.
156. Y. Pico, Chemical analysis of food: Techniques and applications, Elsevier, USA, 1st edn., 2012, p. 256.
157. P. Liu, I. T. Lanekoff, J. Laskin, H. D. Dewalnd and H. Chen, *American chemistry society,* 2012, **8** (13), 5737-5743.
158. H. Faber, M. Vogel and U. Karst, *Analytica Chimica Acta,* 2014, **834**, 9-21.
159. I. Lyons, *Lecture notes: Biomedical sciences*. Wiley, UK, 1st edn., 2001, p. 91.
160. X. Chen, Y. Lai and Z. Cai, *Journal of Analytical Toxicology,* 2012, **36** (3), 171-176.
161. Author names, *Analytical and Bioanalytical Chemistry,* 2012, **403** (2), 355-365.
162. Remington, *The science and practice of pharmacy*, Lippincott Williams and Wilkins, USA, 21st edn., 2006, p. 1163.
163. J. Bergquist and J. Silberring, Identification of catecholamines in the immune system by electrospray ionization mass spectrometry. *Rapid Communications in Mass Spectrometry,* 1998, **12** (11), 683-688.
164. F. M. Zhou and G. J. Vanberkel, *Analytical Chemistry,* 1995, **67** (20), 3643-3649.
165. G. J. Vanberkel and F. M. Zhou, *Analytical Chemistry,* 1995, **67** (17), 2916-2923.
166. H. Oberacher, F. Pitterl, R. Erb and S. Plattner, *Mass Spectrometry Reviews,* 2015, **34** (1), 64-92.
167. T. A. Getek, T. A. Korfmacher McRae, J. A. Hinson, *Journal of analytical chromatography,* 1989, **474** (1), 245-256.
168. A. Baumann and U. Karst, *Expert Opinion on Drug Metabolism & Toxicology,* 2010,

6 (6), 715-731.
169. C. Brauckmann, H. Faber, C. Lanvers-Kaminsky, M. Sperling, U. Karst, *Journal of Chromatography A*, 2013, **1279**, 49-57.
170. P. H. Gamache, D. F. Meyer, M. C. Granger, I. N. Acworth, *Journal of the American Society for Mass Spectrometry*, 2004, **15** (12), 1717-1726.
171. A. Baumann, W. Lohmann, S. Jahn, U. Karst, *Electroanalysis*, 2010, **22** (3), 286-292.
172. V. Kertesz, G. J. Van Berkel and M. C. Granger, *Analytical Chemistry*, 2005, **77** (14), 4366-4373.
173. U. Jurva, H. V. Wikstrom and A. P. Bruins, *Rapid Communications in Mass Spectrometry*, 2002, **16** (20), 1934-1940.
174. ANTEC Technical report. µ-PrepCell™ High Conversion and Flow Rate. 2014_productflyer µ-PrepCell.
175. A. T. Blades, M. G. Ikonomou and P. Kebarle, *Analytical Chemistry*, 1991, **63** (19), 2109-2114.
176. N. A. Mautjana, J. Estes, J. R. Eyler and A. Brajter-Toth, *Electroanalysis*, 2008, **20** (23), 2501-2508.
177. N. A. Mautjana, D. W. Looi, J. R. Eyler and A. Brajter-Toth, *Electrochimica Acta*, 2009, **55** (1), 52-58.
178. N. A. Mautjana, J. Estes, J. R. Eyler and A. Brajter-Toth, *Electroanalysis*, 2008, **20** (18), 1959-1967.
179. U. Jurva, H. V. Wikstrom and A. P. Bruins, *Rapid Communications in Mass Spectrometry*, 2000, **14** (6), 529-533.
180. U. Jurva, H. V. Wikstrom, L. Weidolf, A. P. Bruins, *Rapid Communications in Mass Spectrometry*, 2003, **17** (8), 800-810.
181. B. Blankert, H. Hayen, S. M. van Leeuwen, U. Karst, E. Bodoki, S. Lotrean, R. Sandulescu, N. M. Diez, O. Dominguez, J. Arcos and J. M. Kauffmann, *Electroanalysis*, 2005, **17** (17), 1501-1510.
182. S. M. Van Leeuwen, B. Blankert, J. M. Kauffmann and U. Karst, *Analytical and Bioanalytical Chemistry*, 2005, **382** (3), 742-750.
183. W. Lohmann and U. Karst, *Analytical Chemistry*, 2007, **79** (17), 6831-6839.
184. A. J. Pedersen, L. Ambach, S. Koenig and W. Weinmann, W., *Bioanalysis*, 2014, **6** (19), 2607-2621.
185. W. Lohmann and U. Karst, *Analytical and Bioanalytical Chemistry*, 2009, **394** (5), 1341-1348.
186. K. Tahara, T. Nishikawa, Y. Hattori, S. Iijima, Y. Kouno and Y. Abe, *Journal of Pharmaceutical and Biomedical Analysis, 2009,* **50** (5), 1030-1036.
187. W. Lohmann and U. Karst, *Analytical and Bioanalytical Chemistry*, 2006, **386** (6), 1701-1708.
188. A. Baumann, W. Lohmann, B. Schubert, H. Oberacher and U. Karst, *Journal of Chromatography A*, 2009, **1216** (15), 3192-3198.
189. S. Jahn, A. Baumann, J. Roscher, K. Hense, R. Zazzeroni and U, Karst, *Journal of Chromatography A*, 2011, **1218** (51), 9210-9220.
190. U. Bussy, M. Delaforge, C. El-Bekkali, V. Ferchaud-Roucher, M. Krempf, I. Tea, N. Galland, D. Jacquemin and M. Boujtita, *Analytical and Bioanalytical Chemistry*, 2013, **405** (18), 6077-6085.
191. S. Plattner, R. Erb, F. Pitterl, H.-J Brouwer and H. Oberacher, H., *Journal of*

Chromatography B-Analytical Technologies in the Biomedical and Life Sciences, 2012, 883, 198-204.
192. U. Bussy, Y.-W. Chung-Davidson, K. Li and W. Li, *Analytical and Bioanalytical Chemistry* **2014,** *406* (28), 7253-7260.
193. W. Lohmann, R Doetzer, G. Guetter, S. M. Van Leeuwen and U. Karst, *Journal of the American Society for Mass Spectrometry*, 2009, **20** (1), 138-145.
194. A. Baumann, W. Lohmann, T. Rose, K. C. Ahn, B. D. Hammock, U. Karst and N. H. Schebb, *Drug Metabolism and Disposition*, 2010, **38** (12), 2130-2138.
195. H. Faber, D. Melles, C. Brauckmann, C. A. Wehe, K. Wentker and U. Karst, *Analytical and Bioanalytical Chemistry*, 2012, **403** (2), 345-354.
196. W. Lohmann, H. Hayen and U. Karst, *Analytical Chemistry*, 2008, **80** (24), 9714-9719.
197. R. G. De Lima, P. S. Bonato and R. S. da Silva, *Journal of Pharmaceutical and Biomedical Analysis*, 2003, **32** (2), 337-343.
198. S. Tasoglu, U. A. Gurkan, S. Wang and U. Demirci, *Chemical Society Reviews*, 2013, **42** (13), 5788-5808.
199. Y. Zhu, L.-N. Zhu, R. Guo, H.-J. Cui, S. Ye and Q. Fang, *Scientific Reports*, 2014, **4**, 1-9.
200. T. Hatakeyama, D. L. Chen and R. F. Ismagilov, *Journal of the American Chemical Society*, 2006, **128** (8), 2518-2519.
201. J. Melin, G. Gimenez, N. Roxhed, W. van der Wijngaart and G. Stemme, *Lab on a Chip*, 2004, **4** (3), 214-219.
202. 203) Y. Z. Liu, B. J. Kim and H. J. Sung, *International Journal of Heat and Fluid Flow*, 2004, **25** (6), 986-995.
203. I. Doh and Y. H. Cho, *Sensors and Actuators a-Physical, 2005*, **121** (1), 59-65.
204. P. Bhardwaj, P. Bagdi, A. K. Sen, *Lab on a Chip*, 2011, **11** (23), 4012-4021.
205. X. Chen, D. F. Cui, C. C. Liu and H. Li, *Sensors and Actuators B-Chemical*, 2008, **130** (1), 216-221.
206. W. Dungchai, O. Chailapakul and C. S. Henry, *Analytical Chemistry*, 2009, **81** (14), 5821-5826.
207. W. Lee, D. Kwon, W. Choi, G. Y. Jung and S. Jeon, *Scientific Reports*, 2015, **5**, 1-6.
208. C. K. Fredrickson and Z. H. Fan, *Lab on a Chip*, 2004, **4** (6), 526-533.
209. M. L. Y. Sin, J. Gao, J. C. Liao and P. K. Wong, *Journal of Biological Engineering*, 2011, **5** (1), 2-21.
210. D. Craig, M. Mazilu and K. Dholakia, *Plos One*, 2015, **10** (5), 1-10.
211. K. J. Shaw, R. Vasiliadou, J. Parton, N. Pamme and S. Haswell,*16th International Conference on Miniaturized Systems for Chemistry and Life Sciences*, Okinawa, Japan, October 28–November 1, 2012.
212. A. M. Thompson, A. L. Paguirigan, J. E. Kreutz, J. P. Radich and D. T. Chiu, *Lab on a Chip*, 2014, **14** (17), 3135-3142
213. A. D. Beaton, C. L. Cardwell, R. S. Thomas, V. J. Sieben, F.-E. Legiret, E. M. Waugh, P. J. Statham, M. C. Mowlem and H. Morgan, *Environmental Science & Technology*, 2012, **46** (17), 95148-9556.
214. C. C. Lin, J. Wang, Hm, H. W. Wu and G. B. Lee, *Journal of laboratory automation*, 2010, **15** (3), 253-274.
215. X. Yang, J. Liu, Y. L. Xie, Y. Wang, H. Ying, Q Wu, W. Huang and G. Jenkins,

Analyst, 2014, **139** (11), 2683-2686
216. K. C. Cheung, M. Di Berardino, G. Schade-Kampmann, M. Hebeisen, A. Pierzchalski, J. Bocsi, A. Mittag and A. Tarnok, *Cytometry Part A*, 2010, **77A** (7), 648-666.
217. J. Godin, C.-H. Chen, S. H. Cho, W. Qiao, F. Tsai and Y.-H. Lo, *Journal of Biophotonics*, 2008, **1** (5), 355-376.
218. P. Yager, T. Edwards, E. Fu, K. Helton, K. Nelson, M. R. Tam and B. H. Weigl, *Nature*, 2006, **442** (7101), 412-418.
219. S. C. Terry, J. H. Jerman and J. B. Angell, *Ieee Transactions on Electron Devices*, 1979, **26** (12), 1880-1886
220. D. J. Harrison, A. Manz, Z. H. Fan, H. Ludi and H. M. Widmer, *Analytical Chemistry*, 1992, **64** (17), 1926-1932.
221. J. Wang, C. J. Bettinger, R. S. Langer and J. T. Borenstein, *Organogenesis*, 2010, **6** (4), 212-216.
222. R. Yang, D. L. Feeback and W. L., Wang, *Sensors and Actuators a-Physical*, 2005, **118** (2), 259-267.
223. J. S. Mecomber, A. M. Stalcup, D. Hurd, H. B. Halsall, W. R. Heineman, C. J. Seliskar, K. R. Wehmeyer and P. A. Limbach, *Analytical Chemistry*, 2006, **78** (3), 936-941.
224. K.-Y. Hwang, J.-H. Kim, K.-Y. Suh, J. S. Ko and N. Huh, *Sensors and Actuators B-Chemical*, 2011, **155** (1), 422-429.
225. A. W. Martinez, S. T. Phillips and G. M. Whitesides, *Proceedings of the National Academy of Sciences of the United States of America*, 2008, **105** (50), 19606-19611
226. A. K. Yetisen, M. S. Akram and C. R. Lowe, *Lab on a Chip*, 2013, **13** (12), 2210-2251.
227. X. Li, J. Tian and W. Shen, *Acs Applied Materials & Interfaces*, 2010, **2** (1), 1-6.
228. C. Iliescu, H. Taylor, M. Avram, J. Miao and S. Franssila, *Biomicrofluidics*, 2012, **6** (1), 016505–0165016.
229. L. Wang and Y. Zhang, *Advances in transport phenomena 2010*, ed. L. Wang, Springer, Germany, 1st edn., 2011, p. 185.
230. S. Badilescu and M. Pasckirisamy, CRC, USA, 1st edn., 2011, p. 10.
231. P. N. Nge, C. I. Rogers and A. T. Woolley, *Chemical Reviews*, 2013, **113** (4), 2550-2583.
232. E. Sollier, C. Murray, P. Maoddi and D. Di Carlo, *Lab on a Chip*, 2011, **11** (22), 3752-3765.
233. F. Labeeb, H. O. Fatoyinbo, S. M. Reddy and D. Arrigan, Royal society of chemistry, UK, 1st edn., 2014, p. 11.
234. A. W. Martinez, S. T. Phillips, B. J. Wiley, M. Gupta, G. M. Whitesides, *Lab on a Chip*, 2008, **8** (12), 2146-2150.
235. Microfluidic device, http://store.micronit.com/fluidic-chips/polymer-microreactors/pack-of-3-pc-microreactor-chips-76.html, (accessed June 2015).
236. M. Odijk, A. Baumann, W. Lohmann, F. T. G. van den Brink, W. Olthuis, U. Karst and A. van den Berg, *Lab on a Chip*, 2009, **9** (12), 1687-1693.
237. M. Odijk, W. Olthuis, A. van den Berg, L. Qiao and H. Girault, *Analytical Chemistry*, 2012, **84** (21), 9176-9183.
238. F. T. G. Van den Brink, L. Bueter, M. Odijk, W. Olthuis, U. Karst and A. van den Berg, *Analytical Chemistry*, 2015, **87** (3), 1527-1535
239. H. Wei, J.-J. Sun, Y. Xie, C.-G. Lin, Y.-M. Wang, W.-H. Yin and G.-N. Chen,

Analytica Chimica Acta, 2007, **588** (2), 297-303.
240. R. P. W. Scott, *Liquid chromatography detector,* ELSEVIER, USA, 1st edn., 1986, p 120.
241. M. Noel and P. N. Anantharaman, *Analyst,* 1985, **110** (9), 1095-1103.
242. S. Watt, The element of silver, Marshall, USA, 1st edn., 2003, p 13.
243. D. G. Rethwisch., W. D. Callister, *Fundamentals of material sciences and engineering: An integrated approach*, Wiley, USA, 4th edn., 2011, p. 59.
244. M. E. Spahr, *Lithium-ion batteries: Science and technologies.* A. Kozawa, R. J. Brodd and M. Yoshio, Springer, USA, 1st edn., 2009, p 127.
245. J. Wang, *Electroanalytical chemistry: A series of advances*, ed. A. Bard, Marcell, USA, 1st edn., 1989, p. 5.
246. H. Kaeshe, *Corrosion of metals: physiochemical principles and current problems*, Springer, Germany, 1st edn., 2003, p. 154.
247. D. T. Fagan, I. F. Hu and T. Kuwana, *Analytical Chemistry,* 1985, **57** (14), 2759-2763.
248. B. W. Allen and C. A. Piantadosi, *Nitric Oxide-Biology and Chemistry,* 2003, **8** (4), 243-252.
249. M. Chikasou, T. Hirabayashi, T. Nakamura and T. Hinoue, *Analytical Sciences,* 2004, **20** (8), 1171-1177
250. A. D. Bott, *Current separations,* 1997, **16**, 79.
251. M. Monk, *Fundamentals of electro-Analytical chemistry*, Wiley, UK, 1st edn., 2001, p. 277.
252. Watts, W. Gattrell and T. Wirth, *Beilstein Journal of Organic Chemistry*, 2011, **7.**
253. M. Pravda, C. O'Meara and G. G. Guilbault, *Talanta,* 2001, **54** (5), 887-892.
254. J. Wang, M. Pedrero, H. Sakslund, O. Hammerich and J. Pingarron, Electrochemical activation of screen-printed carbon strips. *Analyst* 1996, **121** (3), 345-350.
255. C. M. Thompson, J. H. Capdevila and H. W. Strobel, *Journal of Pharmacology and Experimental Therapeutics*, 2000, **294** (3), 1120-1130.
256. L. N. Yu, H. Liu, W. K. Li, F. G. Zhang, C. Luckie, R. B. van Breemen, G. R. J. Thatcher and J. L. Bolton, *Chemical Research in Toxicology,* 2004, **17** (7), 879-888.
257. P. Munoz, S. Huenchuguala, I. Paris and J. Segura-Aguilar, *Parkinson's Disease,* 2012. DOI.
258. F. Zoccarato, P. Toscano and A. Alexandre, *Journal of Biological Chemistry*, 2005, **280** (16), 15587-15594.
259. M. Zahid, M. Saeed, L. Yang, C. Beseler, E. Rogan and E. L. Cavalieri, *Iubmb Life,* 2011, **63** (12), 1087-1093.
260. A. Bagheri and H. Hosseini, *Bioelectrochemistry,* 2012, **88,** 164-170.
261. U. Ullah, A. Rauf, U. A. Rana, R. Qureshi, M. N. Ashiq, H. Hussain, H.-B Kraatz, A. Badshah and A. Shah, *Journal of the Electrochemical Society*, 2015, **162** (3), H157-H163.
262. S. Horvath, L. E. Fernandez, A. M. Appel and S. Hammes-Schiffer, *Inorganic Chemistry,* 2013, **52** (7), 3643-3652.
263. C. A. Martinez-Huitle, M. Cerro-Lopez and M. Antonio Quiroz, *Materials Research-Ibero-American Journal of Materials*, 2009, **12** (4), 375-384.
264. C.-y. Liu, Z.-y.; Liu, R. Peng, Z.-c. Zhong, *Journal of Analytical Methods in Chemistry*, 2014. DOI.
265. P. M. Dangili, R. A. Olowu, S. N. Mailu, R. F. Ngece, A. Jijana, A. Williams, F. Iftikhar, P. G. L. Baker and E. I. Iwuoha, *International Journal of Electrochemical Science,*

2011, **6** (5), 1438-1453.
266. J. G. Manjunatha, B. E. K. Swamy, G. P. Mamatha, U. Chandra, E. Niranjana and B. S. Sherigara, *International Journal of Electrochemical Science*, 2009, **4** (2), 187-196.
267. D.-Q. Huang, C. Chen, Y.-M Wu, H. Zhang, L.-Q. Sheng, H.-J. Xu and Z.-D. Liu, *International Journal of Electrochemical Science*, 2012, **7** (6), 5510-5520.
268. R. Z. Shervedani and H. A. Alinajafi-Najafabadi, *International journal of electrochemistry*, 2011, **2011**, 1-11.
269. N. Gonzalez-Dieguez, A. Colina, J. Lopez-Palacios and A. Heras, *Analytical Chemistry*, 2012, **84** (21), 9146-9153
270. N. J. Ke, S.-S. Lu, and S.-H. Cheng, *Electrochemistry Communications*, 2006, **8** (9), 1514-1520.
271. H. L. Martin and P. Teismann, *Faseb Journal*, 2009, **23** (10), 3263-3272.
272. S. S. Kalanur and J. Seetharamappa, *Sensor Letters*, 2011, **9** (4), 1403-1409.
273. M. M. Ghoneim, A. M. Hassanein, N. A. Salahuddin, H. S. El-Desoky and M. N. Elfiky, *Journal of the Brazilian Chemical Society*, 2012, **23** (9), 1594-1605.
274. J. L. Bolton, *Current Organic Chemistry*, 2014, **18** (1), 61-69.
275. B. M. VandenBrink, J. A. Davis, J. T. Pearson, R. S. Foti, L. C. Wienkers and D. A. Rock, *Molecular Pharmacology*, 2012, **82** (5), 835-842.
276. C. D. Moore, C. A. Reilly and G. S. Yost, *Biochemistry*, 2010, **49** (21), 4466-4475.
277. X.-Q. Li, J.-B. He, L. Liu and T. Cui, *Electrochimica Acta*, 2013, **96** 74-81.
278. H. Liu, Z. Qin, G. R. J. Thatcher and J. L. Bolton, *Chemical Research in Toxicology*, 2007, **20** (11), 1676-1684.
279. G. P. Kamatou, I. Vermaak and A. M. Viljoen, *Molecules*, 2012, **17** (6), 6953-6981.
280. S. Zhang, X. Liu, T. Bawa-Khalfe, L. S. Lu, Y. L. Lyu, L. F. Liu and E. T. H. Yeh, *Nature Medicine*, 2012, **18** (11), 1639-1642.
281. M. Takeyoshi, S. Noda, S. Yamazaki, H. Kakishima, K. Yamasaki and I. Kimber, *Journal of Applied Toxicology*, 2004, **24** (1), 77-81.
282. D. Thompson, K. Norbeck, L. I. Olsson, D. Constantinteodosiu, J. Vanderzee and P. Moldeus, *Journal of Biological Chemistry*, 1989, **264** (2), 1016-1021.
283. F. Bertrand, D. A. Basketter, D. W. Roberts and J. P. Lepoittevin, *Chemical Research in Toxicology*, 1997, **10** (3), 335-343.
284. J. L. Bolton and J. A. Thompson, *Quinone methides*, ed. S. E. Rokita. Wiley, USA, 1st edn., 2009, p. 341.
285. B. K. Shinha and R. P. Mason, *Journal of drug metabolism and toxicology*, 2015, **6** (3), 1-8.
286. N. Willmott, *Microspheres and regional cancer therapy*, ed. N. Willmott and J. M. Daly, CRC, USA, 1st edn., 1994, p. 132.
287. C. H. Frith and C. L. Alden, *Handbook of toxicologic pathology*, ed. W. M. Haschek and C. G. Rousseaux, Academic press, USA, 1st edn., 1991, pp. 330-331.
288. S. Benger and D. Sicker, *Isolation and structure elucidation of natural products*, Wiley, Germany, 1st edn., 2009, p. 145.
289. E. S. Gil, and R. O. Couto, *Revista Brasileira De Farmacognosia-Brazilian Journal of Pharmacognosy* **2013,** *23* (3), 542-558.
290. Author names, *Journal of Analytical Chemistry*, 2014, **69** (10), 990-997.
291. J. F. Arteaga, M. Ruiz-Montoya, A. Palma, G. Alonso-Garrido, S. Pintado and J. M. Rodriguez-Mellado, *Molecules*, 2012, **17** (5), 5126-5138.

292. B. G. Kim, J. Y. Kim, Y. Yi and Y. Lim, *Journal of the Korean Society for Applied Biological Chemistry*, 2012, **55** (5), 677-680.
293. D. Melles, T. Vielhaber, A. Baumann, R. Zazzeroni and U. Karst, *Journal of Chromatography B-Analytical Technologies in the Biomedical and Life Sciences*, 2013, **913,** 106-112.
294. ANTEC Technical report. FlexCell™ The most versatile flow cell for LC-ECD a. 2014_productflyer flexcell.
295. A. M. Oliveira-Brett, J. A. P. Piedade and A. M. Chiorcea, *Journal of Electroanalytical Chemistry*, 2002, **538**, 267-276.
296. P. S. Guin and S. Das, *International journal of electrochemistry*, 2014, **2014**, 1-8.
297. P. S. Guin, S. Das and P. C. Mandal, *International Journal of Electrochemical Science*, 2008, **3** (9), 1016-1028.
298. C. Molinierjumel, B. Malfoy, J. A. Reynaud and G. Aubelsadron, *Biochemical and Biophysical Research Communications*, 1978, **88** (2), 441-449.
299. Y. H. Hahn and H. Y. Lee, *Archives of Pharmacal Research*, 2004, **27** (1), 31-34.
300. J. Vacek, L. Havran, M. Fojta, *Electroanalysis*, 2009, **21** (19), 2139-2144.
301. D. P. Wasalathanthri, V. Mani, C. K. Tang and J. F. Rusling, *Analytical Chemistry*, 2011, **83** (24), 9499-9506.
302. D. P. Wasalathanthri, R. C. Faria, S. Malla, A. A. Joshi, J. B. Schenkman and J. F. Rusling, *Analyst*, 2013, **138** (1), 171-178.
303. Ong, S.E.; Zhang, S.; Du, H.; Fu, Y., Fundamental principles and applications of microfluidic systems. Frontiers in Bioscience 2008, 13, 2757-2773.
304. A. R. Kopf-Sill, A. W. Chow, L. Bouse, L. and C. B. Cohen, *Creating a lab on chip with microfluidic technologies*, ed. Guttman, A., Heller, M.J., Marcel Dekker, USA, 1st edn., 2002, p. 44.

Presentations and publications

CONFERENCES

1) **R. Vasiliadou,** S. Lambert and K.J. Welham. Towards an online system for mimicking human drug metabolism. Annual analytical chemistry conference, July 8-10, 2013, University of Hertfordshire, UK (Poster).

2) **R. Vasiliadou**, S. Lambert, K.J. Welham. EC/MS: An alternative approach in drug metabolism. Redwood award event, November 26, 2013, University of Hull, UK (poster).

3) **R. Vasiliadou** and K.J. Welham. Electrogenerated metabolites identified by mass spectrometry. Postgraduate research colloquium, June 18-19, 2014, University of Hull, UK (Oral).

4) **R. Vasiliadou** and K.J. Welham. Generation of metabolite-glutathione adducts. Postgraduate research colloquium, June 18-19, 2014, University of Hull, UK (poster).

5) **R. Vasiliadou** and K.J. Welham. Reactive drug metabolites generated by EC/MS. Postgraduate conference, June 23, 2014, University of Hull and graduate school, UK (Oral).

6) **R. Vasiliadou** and K.J. Welham. Electrochemical synthesis of Quinone-Glutathione adducts. 2nd annual international conference on chemistry, July 21-24, Athens, 2014, Greece (Oral).

7) **R. Vasiliadou** and K.J. Welham. Metabolic reactions mimicked by electrochemistry/mass spectrometry. PhD experience conference, April 7-8, 2015, University of Hull, UK (Oral).

JOURNALS

1) **R. Vasiliadou,** M.M. Nasr-Esfahani**,** N.J. Brown and K.J. Welham. A disposable microfluidic device connected to ESI/MS for studying phase II metabolism. In preparation for submission.